AN ABSTRACT OF THE DISSERTATION OF

Barry Alan Walker, Jr. for the degree of Doctor of Philosophy in Geology presented on July 20, 2011.

Title: The Geochemical Evolution of the Aucanquilcha Volcanic Cluster: Prolonged Magmatism and its Crustal Consequences

Abstract approved:

_____

Anita L. Grunder

The interaction of magma with continental crust at convergent margins is fundamental to understanding if and how continents grow. Isotopic and elemental data constrain the progressive stages of development of the magmatic underpinnings of the long-lived Aucanquilcha Volcanic Cluster (AVC), situated atop the thick continental crust of the central Andes in northern Chile. Whole rock data are used in conjunction with mineral compositions to infer processes that gave rise to eleven million years of intermediate, dominantly dacite, arc volcanism. A pulse of volcanic activity at the AVC between ~5 and 2 Ma is bracketed by more sluggish rates. We document chemical changes in the lavas that accompany this eruptive evolution. Trace element data suggest that crystal fractionation and magma mixing were the dominant mechanisms generating the diversity observed in the AVC whole rock data. Fractionation was dominant during early and waning stages of magmatism, and magma mixing was an important process during the high flux period. Peak thermal maturity of the AVC underpinnings coincided with the high magma flux and likely promoted open system processes during this time. Mineral

compositions from zircon, amphibole, pyroxene, and Fe-Ti oxides confirm the importance of material recycling in the production of evolved AVC rocks. Various geothermometers were employed to calculate the pre-eruptive conditions of AVC magma using mineral compositions. Pressure estimates from amphibole and two-pyroxene barometry indicate crystallization depths of 1 – 5 kb and 4 – 6 kb, respectively. Temperature estimates from zircon, Fe-Ti oxides, amphiboles, and pyroxenes indicate temperatures ranging from ~700°C to 1100°C. Zircon temperatures are always the lowest (700°C - 950°C), and pyroxene temperatures are always the highest (1000°C - 1100°C), with Fe-Ti oxide and amphiboles temperatures falling in between. U-Pb ages from zircons and thermometry from individual samples evidence the thermal maturation and consolidation of the underpinnings below the AVC, presumably culminating in a large, crystal-rich mush zone where magmas were trapped and processed. It is in these middle to upper crustal zones where magmatic diversity is attenuated and giant, relatively homogeneous batholiths are formed. Isotopes of AVC lavas are similar to values observed from other central Andes volcanic centers. Lead isotopes are consistent with the AVC's location within a Pb isotope transition zone between the Antofalla and Arequipa basement terranes. Oxygen and Sr isotopic ratios are high and Nd isotopic ratios low with respect to a depleted mantle. Through time, $^{87}Sr/^{86}Sr$ values of AVC lavas progressively increase from lows of ~0.70507 to ~0.70579 (upper values of 0.70526 to 0.70680), and ε_{Nd} values decrease from highs of -1.0 to -4.6 (lows of -1.6 to -7.3). Similarly, O isotopes ($\delta^{18}O$) show a slight increase in base level through time from lows of 6.5‰ to 7.0‰ (highs of 6.75‰ – 7.5‰). Dy/Yb and Sm/Yb ratios also increased systematically from highs of 2.11 to 3.45, and 2.76 to 6.67, respectively. Despite the temporal isotopic variation, there is little isotopic variation with indices of fractionation, suggesting this signal is the consequence of deep magmatic processing, here attributed to an expanding zone of melting, assimilation, storage, and homogenization (MASH) of mantle-derived magma in the deep crust. Upward expansion brought the MASH zone into contact with rocks that were increasingly evolved with respect to Sr and Nd isotopes, explaining the isotopic shifts. Downward expansion of the MASH zone enhanced garnet stability during basalt fractionation, explaining the increased Dy/Yb and Sm/Yb ratios.

Mass balance calculations involving Sr, Nd, and O isotope modeling are consistent with a crustal component making up 10 - 30% of AVC lavas, implying that although the history of central Andean magmatism is replete with large scale crustal recycling, the current phase is largely a crust formation event.

The Geochemical Evolution of the Aucanquilcha Volcanic Cluster: Prolonged Magmatism and its Crustal Consequences

by

Barry Alan Walker, Jr.

A DISSERTATION

Submitted to

Oregon State University

in partial fulfillment of
the requirement for the
degree of

Doctor of Philosophy

Presented July 20, 2011
Commencement June 2012

Doctor of Philosophy dissertation of Barry Alan Walker, Jr. presented on July 20, 2011.

APPROVED:

Major Professor, representing Geology

Chair of the Department of Geosciences

Dean of the Graduate School

I understand that my dissertation will become part of the permanent collection of Oregon State University libraries. My signature below authorizes release of my dissertation to any reader upon request.

Barry Alan Walker, Jr., Author

ACKNOWLEDGEMENTS

My scholarship up to this point has been a long and tortuous path, though not necessarily, or at least not always, torturous (har har). For quite some time, I reckoned I'd been pulling the wool over the eyes of my colleagues and mentors, inasmuch as they allowed me to continue my academic journey alongside them without objection. At some point I realized that the very bright people around me were indeed too bright to be fooled by me, at least for such a long time. Of course, realizing one's own potential and developing a sense of self-worth is important and all, but then I also know the fate of the seed that fell among thorns. Yes, the days of the one-man-show being over, if indeed they ever existed as romanticized, many acknowledgements are due here, and they'll come quick.

First mention goes to the Stone Mountain pluton, outside of Atlanta, GA. I visited this granite (*sensu lato*) dome as a child and experienced a geological awakening—in particular my awe of magma, the earth, and the hugeness of it all. Just ask my sisters about it, or my parents. They, my family, and in particular my parents, get second mention. To my mother, Elaine Walker and my father, Barry Walker, I will be forever grateful. Their love, support, and enthusiasm and interest in my interests and success have been full, always. I am blessed to have such loving people as my parents. I dedicate this dissertation to them both. I thank the rest of my family, as well, in particular Bud Gore and Mickey Walker, my uncles, for many interesting and encouraging discussions about all things, ranging from the perils of graduate school to the rewards of a diurnal lifestyle. And, certainly, thanks to 'Daddy' John Walker, my eldest living forebear. He is truly a singularity: as playful and genuine a man as there ever was, and whom I love very much.

The National Science Foundation funded all of this research (EAR 0610114), and I say thankya. While working on this dissertation for the past five years, Anita Grunder has been my guide, God bless her. Her intellect, class, humor, generosity, and spontaneity are unmatched in my life. She's the one I want on my team at all times. Thank you

Anita, you are the queen of decency. Calvin Miller, ditto. He taught me in more ways than he will ever know. The good cheer and creativity he sparks and spreads do not go unnoticed. The members of my committee here at Oregon State, including John Dilles, Adam Kent, and Frank Tepley, have been top-notch. You all have provided me with critical instruction and guidance. In particular, thank you John Dilles for your insistence on excellence, your encouragement, and your friendship. Thanks to the other coauthors of this dissertation: Joe Wooden, Erik Klemetti and Denise Giles. Thanks to Steve "Shavedawg" Shaver and Bran Potter, my undergraduate advisors at Sewanee, who fanned my geological flames and taught me many, many things about geology, teaching, and uncluttered living. Other geologists that have been critical to my development as a scientist include Jonathan Miller, Shan de Silva, Lily Claiborne, Guil Gualda, Isabelle Chambefort, Olivier Bachmann, George Bergantz, Chad Deering, Juan Otamendi, Bob Wiebe, and Andrew Meigs. For help in various labs throughout my time, I'd like to thank Dale Burns, Frank Mazdab, Rick Conrey, Adam Kent, Lang Farmer, Emily Verplank, and Allison Weinsteiger.

To my fellow students here at OSU, I bow my head. Morgan Salisbury has been my colleague and friend for five years now, and I thank him for his companionship, knowledge, and vibe. Thanks to Federico Cernuschi, my friend and Spanish instructor, for his endless energy and his unique life-flavor. Thanks also to OSU-related geologists past and present, including, but not limited to: Rob Lee, Jed Roberts, Dave Trench, Nate Edem, Emily Underwood, Mark Ford, Ashley Hatfield, Chris Folkes, Alison Koleszar, Ashley Bromley, Erin and Rocco Lieuallen, Dale Burns, Stephanie Grocke, Julia Cohen, Luc Farmer, Darrick Boschmann, Jack Zunka, Bob Peckyno, Amy Lange. Thank you to the Coalition of Graduate Employees, in particular Dennis Dugan, John Osborne, Rob Hess for their tireless work. The Union makes us strong.

I spend a lot of my time playing music, and many people of note in my life are associated with this wholly honorable enterprise. While most are not directly involved with the geological sciences, they deserve mention. First of all, I thank my fellow Tanks, the

space country warriors. The Tanks, both collectively and individually, have been a cornerstone in my life over the past two years. The songs had a slow and murky beginning, but Bobby Babra encouraged me, played with me and even wrote with me, and for that, among many other things, I thank him. Jawsh Holmes and Julia Rosen, two of the finest people I know, have also blessed me with their talent and life-zest, in pursuits both musical and heady. To Travis Witmer, the original Tank, I bequeath a man-hug and a kiss on his giant beard. You've taught me a lot, Travis. I thank Rob Smith, my country brother from our days back in Oklabama, drinking from rain gutters and poaching golf balls out of the river. I love you too! We'll meet again someday, Rude Dude. Thanks to Justin Niedermeyer. You hit the spot, my man. Off and on, I was also involved in a dusty blues outfit called the Taint Brothers, including the aforementioned Babra, and the legendary Shane Hayden, the Pacific Northwest's own Jack of Diamonds. Shane challenged me on many occasions to be the best I could be. Thank you brother Shane.

There are several others. Valerie Osterberg is a genius mystical flower orphan. She communes with the lightning. She talks to snails, and she breathes for the dead orchards. "Uncle" Levi Fredrikson is my righteous brother from the Weirdland Realm. I'll see you when I see you, Levi, we'll leg wrestle on-sight. Jeannie Holiday: bustling bundle of beauty and badness! I cannot fail to mention: Lanier Brandau (the stalwart protector), Becky Olson, Ashlee Claire, Silvina de Brum, Bevan-Frost, Lisa Willot, Ron Jon, Rosalie Bienik, Stavros Calos, Emily Vollmer, Thomas Dieter, Chris Konieczka, Cody Buckman, Morelia Chapin, Erin Madeen, Tammy Winfield, Amy Garrett, Lummi Island, Adrian Haskins, Kara Brausen, Steve Hunter, Ditch Projects, the flame, oak groves, Leo and Zoe Dilles, etc. etc. etc. Thankya thankya.

"Your wisdom will be when you say, 'I do not know.'" -Sun Ra

CONTRIBUTIONS OF AUTHORS

Anita Grunder spearheaded this project and her ideas and discussions with me were a major inspiration for these papers. Joe Wooden helped perform the analyses presented in chapter 2, and provided insight into the interpreting the analytical data presented there. Erik Klemetti collected about half of the radiogenic isotope data presented in chapter 3, many amphibole analyses presented in Chapter 4, and also discussed much of this data with me. Denise Giles also provided many amphibole analyses presented in Chapter 4 and discussed ideas concerning AVC magmatic processes with me. John Dilles added extremely valuable insight and interpretation with respect to the mineral data presented in Chapter 4. Frank Tepley helped acquire much of the electron microprobe data presented in chapter 4. His discussions were also valuable.

TABLE OF CONTENTS

TABLE OF CONTENTS (Continued)

Page

TABLE OF CONTENTS (Continued)

Page

LIST OF FIGURES

Figure

Page

LIST OF FIGURES (Continued)

Figure

Page

LIST OF TABLES

Table

Page

LIST OF CD-ROM APPENDICES (Pocket)

Supplementary data and figures for chapter 2

Supplementary data and figures for chapter 3

Supplementary data and figures for chapter 4

The Geochemical evolution of the Aucanquilcha Volcanic Cluster: prolonged magmatism and its crustal consequences

CHAPTER 1
General Introduction

Argument

Magmatism is manifested on the earth's surface in two fundamentally different ways. Plutons are physical "fossil" specimens of magmatic systems, sometimes providing many hundreds of square kilometers of exposed igneous rock. Such exposed intrusions provide a time-integrated, spatial perspective that has greatly contributed to the understanding of the operative processes of crustal magmatism. Exhumed by time and tectonics, they offer a window into the depths of frozen magmatic systems. The view they afford, however, is subtlety skewed. Their mineral assemblages, radiometric ages, and textures reflect crystallization, volatile loss, and cooling histories. Their shapes, structure and volumes are the result of piecemeal accumulation and overprinting, the averaging of long duration processes.

Volcanic rocks, on the other hand, represent intermittent samplings of magma systems. Silicic to intermediate eruptives, in particular, are generally recognized as mixtures of variable proportions of crystals and frozen liquid. Once erupted, this material cools relatively abruptly, sometimes preserving mineral compositions in equilibrium with the active magmatic conditions from which they emerged. It is these pre-eruptive conditions of an active magma system—locked into erupted crystals—that are lacking in plutonic rocks.

There has been a push in recent years to bridge what is a sort of philosophical gap in the volcanic and plutonic literature (Hildreth, 1981; Hildreth and Moorbath, 1988; Dilles and Wright, 1988; Riciputi et al., 1995; Miller and Wooden, 2004; Grunder et al., 2006;

Lipman, 2007; de Silva and Gosnold, 2007; Bachmann et al., 2007; Claiborne et al., 2010 among many others). There is converging opinion that volcanic rocks might not represent simply a molten version of plutonic material. Rather, the two might be physically complimentary in a sense that a pluton might represent an accumulation of crystals from which a large portion of liquid was expelled (Hildreth, 2004; Bachmann and Bergantz, 2004; Deering and Bachmann, 2010). Alternatively, it is also argued that many plutons do represent frozen magma compositions and that cumulates may be rare (Glazner et al., 2004; Bartley et al., 2007). Constraining crystallization ages, depths and temperatures of crystals in volcanic rocks is critical to understanding the processes, mechanics, and architecture of active magmatic systems which produce volcanic eruptions but also may give rise to incrementally constructed batholiths at depth. Long-lived volcanic provinces, sometimes encompassing millions of years worth of successive eruptions, are wholistic samples of this process, providing a time-transgressive perspective on the evolution and organization of such dynamic systems.

Tectonic context of the Aucanquilcha volcanic cluster

The Aucanquilcha Volcanic Cluster (AVC) is situated at ~ 21° S in northern Chile, within the Central Volcanic Zone of the Andean arc (**Figure 1.1**). Subduction magmatism along the western coast of South America has been ongoing nearly continuously since at least the late Precambrian (Lucassen et al., 2001). The basement of the central Andes comprises the Arequipa-Antofalla block, a tectonic terrane with multiple domains, that grew incrementally southward from ~2 to 0.4 Ga (Lowey et al., 2004). The northern portion of this basement block is called the Arequipa domain, and is identified by 2 – 1.8 Ga juvenile magmatism and metamorphism. The Arequipa domain was apparently accreted to South America during the Sunsas orogeny, 1.2 – 0.9 Ga (Loewy et al., 2004). The next decipherable tectonomagmatic event occurred during the early Paleozoic, when the southern portion of the Arequipa block was heavily reworked by erosion, magmatism and metamorphism of Pampean (~550 – 500 Ma) and Famatinian age (~495 – 400 Ma), essentially generating a new crustal domain known as the Antofalla

block. The segmented nature of the central Andean crust is demonstrated by sparse outcrops of basement rocks (e.g., Lucassen et al., 2000; Lucassen et al., 2001), and also by detailed Pb isotope studies of available igneous rocks (volcanic, plutonic, gneisses, ores). Importantly, the boundary between the Arequipa and Antofalla domains is detectable with respect to $^{206}Pb/^{204}Pb$, with a transition zone at ~20 - 22°S between older, rigid, low $^{206}Pb/^{204}Pb$ rocks of the Arequipa domain and the younger/reworked, higher $^{206}Pb/^{204}Pb$ rocks of the Antofalla domain (Mcfarlane et al., 1990; Wörner et al., 1992, Aitcheson et al., 1995; Mamani et al., 2008, 2010). The AVC is situated atop, and was magmatically processed through, this crustal transition zone.

After an apparent pause, magmatism began again around 300 Ma and has continued intermittently until the present. A major tectonic reorganization apparently occurred, beginning in the early Triassic, with a shift to an extensional to transtensional regime (Lucassen et al., 2006; Coney and Evenchick, 1994). Notably, Jurassic magmatism from around 200 to 160 Ma was dominantly mafic with isotopically primitive compositions (Miller and Harris, 1989). A return to a compressional environment began around 90 Ma, as evidenced by foreland sedimentation in the Altiplano-Puna (Sempere et al., 1997). Since the Tertiary, compositions have been dominantly andesitic to dacitic. Another major tectonic reorganization apparently began in the central Andes around 30 - 25 Ma. Based on structural data in the foreland, and a conspicuous gap in volcanism, workers believe that the crust began to significantly thicken, a process that continued for possibly 10 – 15 million years (Allmendinger et al., 1997; McQuarrie et al., 2005). Geochemical arguments have also been made for a thickened crust since ~25 Ma lavas (Haschke et al., 2002; Mamani et al., 2010). Post ~15 Ma structural data (e.g. Kennan et al., 1997) and GPS surveys (e.g. Kendrick et al., 2001; Bevis et al., 1999) provide evidence for modern back arc deformation, suggesting the central Andes continue to be shortened, although at a modest rate (~9 mm/yr).

Since ~25 Ma, no primitive basalts have erupted in the CVZ. Also, widespread, voluminous behind-arc volcanism has occurred up to 300 km east of the arc, including the ignimbrites and lavas of the Altiplano-Puna Volcanic complex (de Silva et al., 1989;

Salisbury et al., 2011), and farther south (Siebel et al., 2001; Schurr et al., 2007), along with other behind-arc centers such as Los Frailes (Kay and Coira, 2009), the Intersalar Volcanic Field (Salisbury, 2011) and various monogenetic fields (Davidson and de Silva, 1995; Hoke and Lamb, 2007).

Geophysical considerations for the central volcanic zone of the Andes

The crust of the central Andes at the latitude of the AVC (**Figure 1.2**) has been the subject of a suite of geophysical studies. Most importantly, the crust is very thick, in excess of 70 km in some places (Wigger et al., 1994; Beck et al., 1996; Schmitz et al., 1997; Giese et al., 1999) and mostly felsic (Zandt et al., 1996; Beck and Zandt, 2002). The lower crust beneath the arc is interpreted to be 20 to 25 km thick (Graber and Asch, 1999) and has velocities and densities consistent with mafic to ultramafic compositions (Schmitz et al., 1997; Yuan et al., 2002). This lower crust appears to correspond to a "blurred" Moho beneath the central Andes at the latitude of the AVC, and is represented by seismic velocities that are transitional between lower crust and mantle from ~50 – 80 km (Giese et al., 1999). The means of crustal thickening in the central Andes remains unresolved, though it is generally accepted that tectonic shortening is the main cause (Isacks, 1988; Beck et al., 1996; Almendinger et al., 1997; Baby et al., 1997; Giese et al., 1999; Hascke and Gunther, 2003; McQuarrie et al., 2005). The crustal thickness is attributable to a combination of a long-term compressional setting, the rigid backstop of the Brazilian craton, a lithosphere weakened by magmatism, and the magmatic addition itself.

Another observation gleaned from the geophysical studies is that the CVZ arc crust is ripe with low seismic velocity anomalies, which are interpreted to be zones of partial melt. A widespread low velocity zone in the crust has been observed beginning at ~18 km (ANCORP working group, 1996; Scheuber and Giese, 1999; Chmielowski et al., 1999; Beck and Zandt, 2002; Leidig and Zandt, 2003; Zandt et al., 2004; Heit et al., 2008). The thickness of this low velocity zone is not well constrained, though it may be

only a few kms (Chmielowski et al., 1999; Leidig and Zandt, 2003; Zandt et al., 2004). The pronounced upper to mid crustal low velocity zone extends widely beneath the Altiplano-Puna Volcanic Complex (APVC), a giant caldera and ignimbrite province that has been active for about 10 m.y. (de Silva and Gosnold, 2007; Salisbury et al., 2011). Under the APVC, the top of the low velocity zone is well defined and coincides with a zone of high electrical conductivity (Scheuber and Giese, 1997; Schilling et al., 1996). This top zone is inferred to be a high degree of melt and (or) the brine rich top of a 15-20% partial melt zone that extends to uncertain depth (Chmielowski et al., 1999; Zandt et al., 2003; Schilling et al., 2006). The AVC lies at the northwestern edge of this Altiplano-Puna magma body, which is the best example of what is interpreted to be an extensive, modern batholith.

The Aucanquilcha volcanic cluster

Volcanoes of the AVC comprise 340 $\pm$ 20 km^3 of basaltic andesite to dacite lavas clustered over an area of ~700 km^2. The volcanoes number ~20 with an eruptive history spanning the last 11 million years (**Figure 1.3, 1.4, & 1.5**). Grunder and others (2006) identify four main phases of AVC volcanism: the Alconcha group (11 – 8 Ma), the Gordo Group (~6 – 4 Ma), the Polan Group (~4 – 2.5 Ma), and the Aucanquilcha Group (~1 Ma to present). Two relatively small ignimbrites, the Ujina (~9.6 Ma) and the Carcote (5.5 Ma), are possibly the product of AVC magmatism, though their exact provenance is uncertain (Grunder et al., 2006; Baker and Francis, 1978). After these main phases of volcanism, several small basaltic andesite scoria cones erupted, including the eroded edifices of Poruñita and Luna de Tierra, defining a field located just to the east of the AVC (**Figure 1.6**). Basaltic andesite to andesite lavas of the AVC are generally crystal-poor (<10%) and fine-grained, with plagioclase, clinopyroxene, orthopyroxene, and olivine phenocrysts. Dacites are generally crystal-rich (>20%) and coarse-grained, with plagioclase, clinopyroxene, amphibole, orthopyroxene, and biotite. Minor and accessory minerals, common in dacites but less common in andesites, include magnetite, ilmenite, apatite, and zircon. Rare quartz, likely to be xeno- or auto-crystic, is also found in

several flows. Three main temporal trends are observed in the volcanic cluster. First, relatively diverse lavas (basaltic andesites to andesites and dacites) give way to more compositionally restricted (dacite) lavas. Second, the locus of volcanism shifts from broadly distributed or peripheral to restricted and central. And third, early lavas contain mainly anhydrous mafic minerals (pyroxene dominant), whereas later lavas contain dominantly hydrous mafic minerals (amphibole, biotite). Eruption rates in the AVC increased sharply after about six million years of activity (**Figure 1.7**), coincident with more central distribution of vents, more homogeneous composition of lavas, and the onset of extensive hydrothermal activity. Since about 2.5 Ma, the eruption rate has declined, consistent with a waning system. These observations, combined with the longevity of the system and the underlying zone of partial melt, suggest that the AVC is the surface representation of a incrementally assembled, patchwork batholith at depth. Furthermore, the AVC has been active for the same time interval as the Altiplano-Puna Volcanic Complex (cf. Salisbury et al., 2011) and shares a higher volcanic eruption rate between 5 to 2 Ma. The lava-dominated AVC is less silicic and less voluminous than the Altiplano-puna system and appears to be a peripheral, on-arc manifestation of a broader thermal and magmatic signal (Grunder and de Silva, 2007).

Directions

The second chapter of this thesis examines the zircon history of the AVC. Zircons from dacites from throughout the history of the AVC were probed to examine the age distribution and crystallization temperatures of crystal populations within individual lavas. The third chapter explores the petrologic history of the AVC by examining the variation observed in the trace elements and Sr, Nd, Pb, and O isotopes of the lavas. By modeling magmatic differentiation, we place mass balance constraints on the material componentry of AVC lavas through time. The fourth chapter summarizes the findings of four different geothermobarometers, employed to constrain the temperatures and pressures at which phases in AVC lavas were crystallizing. These data supply estimates of pre-eruptive conditions of crystal populations within erupted lavas from the AVC.

References

Aitcheson, S.J., Harmon, R.S., Moorbath, S., Schneider, A., Soler, P., Soria-Escalante, E., Steele, G., Swainbank, I., Wörner, G., 1995, Pb isotopes define basement domains of the Altiplano, central Andes. *Geology* 23 (6), 555-558.

Almendinger, R.W., Jordan, T.E., Kay, S.M., Isacks, B.L., 1997, The evolution of the Altiplano-Puna plateau of the central Andes. *Annual Review of Earth and Planetary Sciences* 25, 139-174.

Baby, P., Rochat, P., Mascle, G., Hérail, G., 1997, Neogene shortening contribution to crustal thickening in the back arc of the central Andes. *Geology* 25 (10), 883-886.

Baker, M.C.W., Francis, P.W., 1978, Upper Cenozoic volcanism in the central Andes – ages and volumes. *Earth and Planetary Science Letters* 41, 175-187.

Beck, S.L., Zandt, G., Myers, S.C., Wallace, T.C., Silver, P.G., Drake, L., 1996, Crustal-thickness variations in the central Andes: Geology, v. 24, p. 407-410.

Beck, S.L., Zandt, G., 2002, The nature of the orogenic crust in the central Andes. Journal of Geophysical Research 107 (B10), doi:10.1029/2000JB000124

Bevis, M., E. C. Kendrick, R. Smalley Jr., T. Herring, J. Godoy, and F. Galban (1999), Crustal motion north and south of the Arica deflection: Comparing recent geodetic results from the central Andes, *Geochem. Geophys. Geosyst.*, *1*(12), 1005, doi:10.1029/1999GC000011.

Chmielowski, J., Zandt, G., and Haberland, C., 1999, The central Andean Altiplano-Puna magma body: *Geophysical Research Letters*, v. 26, p. 783-786.

Coney, P., Evenchick, C., 1994, Consolidation of the American Cordilleras. *Journal of South American Earth Science* 7, 241–262, 1994.

Davidson, J.P., and de Silva, S.L., 1995, Late Cenezoic magmatism of the Bolivian Altiplano. *Contributions to Mineralogy and Petrology* 119, 387-408.

de Silva, S.L., 1989, Altiplano-Puna volcanic complex of the central Andes: Geology, v. 17, p. 1102-1106.

de Silva, S.L., Francis, P.W., 1989, *Volcanoes of the Central Andes*. Springer-Verlag, 216 p.

Dilles, J.H., Wright, J.E., 1988, The chronology of early Mesozoic arc magmatism in the Yerington district of western Nevada and its regional implications. GSA Bulletin 11 (5), p. 644-652.

Isacks, B.L., 1988, Uplift of the central Andean plateau and bending of the Bolivian orocline. *Journal of Geophysical Research* 93 (B4), 3211-3231.

Giese, P., Scheuber, E., Schilling, F.R., Schmitz, M. and Wigger, P., 1999. Crustal thickening processes in the Central Andes and the different natures of the Moho-discontinuity. *Journal of South American Earth Sciences* 12: 201-220.

Graeber, F.M., Asch, G., 1999, Three-dimensional models of *P* wave velocity and *P*-to-*S* velocity ratio in the southern central Andes by simultaneous inversion of local earthquake data. *Journal of Geophysical Research* 194 (B9), 20,237-20,256.

Grunder, A. L. 1997. Report on the Miocene to Recent volcanic rocks from the eastern margin of the project area. *In* Tomlinson, A. *et al*. (eds) *Proyecto de Estudio Geológico de la Franja Longitudinal entre Quebrada Blanca y Chuquicamata, Fase I*. SERNAGEOMIN de Chile report to Coldelco.

Grunder, A.L., Klemetti, E.W., Feeley, T.C., and McKee, C.M., 2006, Eleven million years of arc volcanism at the Aucanquilcha Volcanic Cluster, Northern Chilean Andes: implications for the life span and emplacement of plutons: Transactions of the Royal Society of Edinburgh-Earth Sciences, v. 97, p. 415-436.

Grunder, A.L., de Silva, S.L., 2007, Patterns in Long-lived Continental Magmatism; Crustal Modulation of Mantle-Derived Input, *Eos Trans. AGU*, 88 (52), Fall Meet. Suppl., Abstract V41F-05.

Haschke, M., Gunther, A., 2003, Balancing crustal thickening in arcs by tectonic vs. magmatic means. *Geology* 31 (11), 933-936.

Heit, B., Sodoudi, F., Yuan, X., Bianchi, M., Kind, R., 2007, An S receiver function analysis of the lithospheric structure in South America. American Geophysical Research Letters 34, L14307. 5 p., doi:10.1029/2007GL030317.

Hoke, L., Lamb, S., 2007, Cenozoic behind-arc volcanism in the Bolivian Andes, South America: implications for mantle melt generation and lithospheric structure. *Journal of the Geological Society of London* 164, 795-814.

Kay, S.M., and Coira, B.L., 2009, Shallowing and steepening subduction zones, continental lithospheric loss, magmatism, and crustal flow under the Central Andean Altiplano-Puna plateau, in Kay, S.M., Ramos, V.A., and Dickinson, W.R., eds., Backbone of the Americas: Shallow Subduction, Plateau Uplift, and Ridge and Terrane Collision: Geological Society of America Memoir 204, p. 229–259.

Kendrick, E., Bevis, M., Smalley, R., Brooks, B., 2001, An integrated crustal velocity field for the central Andes, Geochemistry Geophysics Geosystems 2, 11 p, DOI: 10.1029/2001GC000191

Kennan, L., Lamb, S.H., Hoke, L., 1997, High-altitude paleosurfaces in the Bolivian Andes: evidence for late Cenozoic surface uplift, *in Palaeosurfaces: Reconstruction and Palaeoenvironmental Interpretation,* ed. Widdowson, M.*,* Geological Society Special Publications No. 120, 307 – 323.

Klemetti, E.W., and Grunder, A.L., 2008, Volcanic evolution of Volcán Aucanquilcha: a long-lived dacite volcano in the Central Andes of northern Chile. *Bulletin of Volcanology*, v. 70, p. 633-650.

Leidig, M., Zandt,G., 2003, Modeling of highly anisotropic crust and application to the Altiplano-Puna volcanic complex of the central Andes. Journal of Geophysical Research 108 (B1) doi:10.1029/2001JB000649.

Loewy, S.L., Connelly, J.N., Dalziel, I.W.D., 2004, An orphaned basement block: The Arequipa-Antofalla Basement of the central Andean margin of South America, *GSA Bulletin* 116 (1/2), pp. 171-187.

Lucassen, F., Becchio, R., Wilke, H. G., Franz, G., Thirlwall, M. F., Viramonte, J., Wemmer, K., 2000, Proterozoic-Paleozoic development of the basement of the Central Andes (18-26 degrees S)- a mobile belt of the South American craton, *Journal of South American Earth* Sciences 13 (8), 697-715.

Lucassen, F., Becchio, R., Harmon, R.S., Kasemann, S., Franz, G., Trunbull, R., Wilke, H.G., Romer, R.L., Dulski, P., 2001, Composition and density model of the continental crust at an active continental margin—the Central Andes between 21° and 27°S. *Tectonophysics* 341, 195-223.

Lucassen, F., Kramer, W., Bartsch, V., Wilke, H., Franz, G., Romer, R.L., Dulski, P., 2006, Nd, Pb, and Sr isotope composition of juvenile magmatism in the Mesozoic large magmatic province of northern Chile (18 – 27 °S): indications for a uniform subarc mantle. Contributions to Mineralogy and Petrology 152, p. 571-589.

Macfarlane, A.W., Marcet, P., LeHuray, A.P., and Petersen, U., 1990, Lead isotope provinces of the Central Andes inferred from ores and crustal rocks. *Economic Geology* 85 (8), p. 1857-1880.

Mamani, M., Tassara, A., and Woerner, G., 2008, Composition and structural control of crustal domains in the central Andes: *Geochemistry Geophysics Geosystems*, v. 9.

Mamani, M., Worner, G., and Sempere, T., 2010, Geochemical variations in igneous rocks of the Central Andean orocline (13ºS to 18ºS): Tracing crustal thickening and magma generation through time and space, *GSA Bulletin*, v. 122, no. 1/2, p. 162-182.

McKee, C. M. 2001, Volcanology and petrology of Volcán Miño,; Andean central volcanic zone‘. Master’s Thesis, Oregon State University, USA.

McQuarrie, N., Horton, B.K., Zandt, G., Beck, S., DeCelles, P.G., 2005, Lithospheric evolution of the Andean fold-thurst belt, Bolivia, and the origin of the central Andean plateau. *Tectonophysics* 399, p. 15-37.

Miller, J.F., Harris, N.B.W., 1989, Evolution of continental crust in the Central Andes; constraints from Nd isotope systematics. *Geology* 17, p. 615 – 617.

Salisbury, M.J. Jicha, B.R., de Silva, S.L., Singer, B.S., Jiménez, N.C., and Ort, M.H., 2011, $^{40}Ar/^{39}Ar$ chronostratigraphy of Altiplano-Puna volcanic complex ignimbrites reveals the development of a major magmatic province: *GSA Bulletin*, v. 123, no. 5-6, p. 821-840.

Salisbury, M.J., 2011, Convergent margin magmatism in the central Andes and its near antipodes in western Indonesia: spatiotemporal and geochemical considerations. Ph.D. dissertation. 147p.

Scheuber, E., Giese, P., 1999, Architecture of the Central Andes—a compilation of geoscientific data along a transect at 21°S. *Journal of South American Earth Sciences* 12, p. 103-107.

Schilling, F.R., Partzsch, G.M., Brasse, H., Schwarz, G., 1997, Partial melting below the magmatic arc in the central Andes deduced from geoelectromagnetic field experiments and laboratory data. *Physics Earth Planet. Interiors* 103, p. 17-31.

Scmitz, M., Heinsohn, W.D. and Schilling, F.R., 1997. Seismic, graviy and petrological evidence for partial melt beneath the thickened Central Andean crust (21-23S). *Tectonophysics*, 270: 313-326.

Schnurr, W.B.W., Trumbull, R.B., Clavero, J., Hahne, K., Sibel, W., Gardeweg, M., 2007, Twenty-five million years of silicic volcanism in the southern central volcanic zone of the Andes: Geochemistry and magma genesis of ignimbrites from 25 to 27 °S, 67 to 72 °W, *Journal of Volcanology and Geothermal Reasearch* 166, pp. 17-46.

Sempere, T., Butler, R.F., Richards, D.R., Marshall, L.G., Sharp, W., Swisher, C.C., 1997, Stratigraphy and chronology of late Cretaceous-early Miocene major tectonic crisis and related basins in Bolivia and northern Argentina. *Geological Society of America Bulletin* 109, p. 709-727.

Siebel, W., Schnurr, W., Hahne, K., Kraemer, B., Trumbull, R.B., van den Bogaard, P., Emmermann, R., 2001, Geochemistry and isotope systematics of small- to medium-volume Neogene-Quaternary ignimbrites in the southern central Andes: evidence for derivation from andesitic magma sources. *Chemical Geology* 171 (3-4), p. 213-237.

Wigger et al., Schmitz, M., Asch, G., Baldzuhn, S., Giese, P., Heinsohn, W., Martinez, E., Ricaldi, E., Röwer, P., Viramonte, J., 1994. In: Reutter, K, J., Scheuber, E., Wigger, P.J. (Eds.), Variation of the crustal structure of the southern central Andes deduced from seismic refraction investigations, Tectonics of the southern central Andes. Springer-Verlag, New york, pp. 23-48.

Wörner, G., Moorbath, S., Harmon, R.S., 1992a, Andean Cenozoic volcanic centers reflect basement isotopic domains: Geology, v.20, p.1103-1106.

Yuan, X., Sobolev, S.V., and Kind, R., 2002, Moho topography in the central Andes and its geodynamic implications: Earth and Planetary Science Letters, v. 199, p. 389-402.

Zandt, G., Leidig, M., Chmielowski, J., Baumont, D., and Yuan, X.H., 2003, Seismic detection and characterization of the Altiplano-Puna magma body, central Andes: Pure and Applied Geophysics, v. 160, p. 789-807.

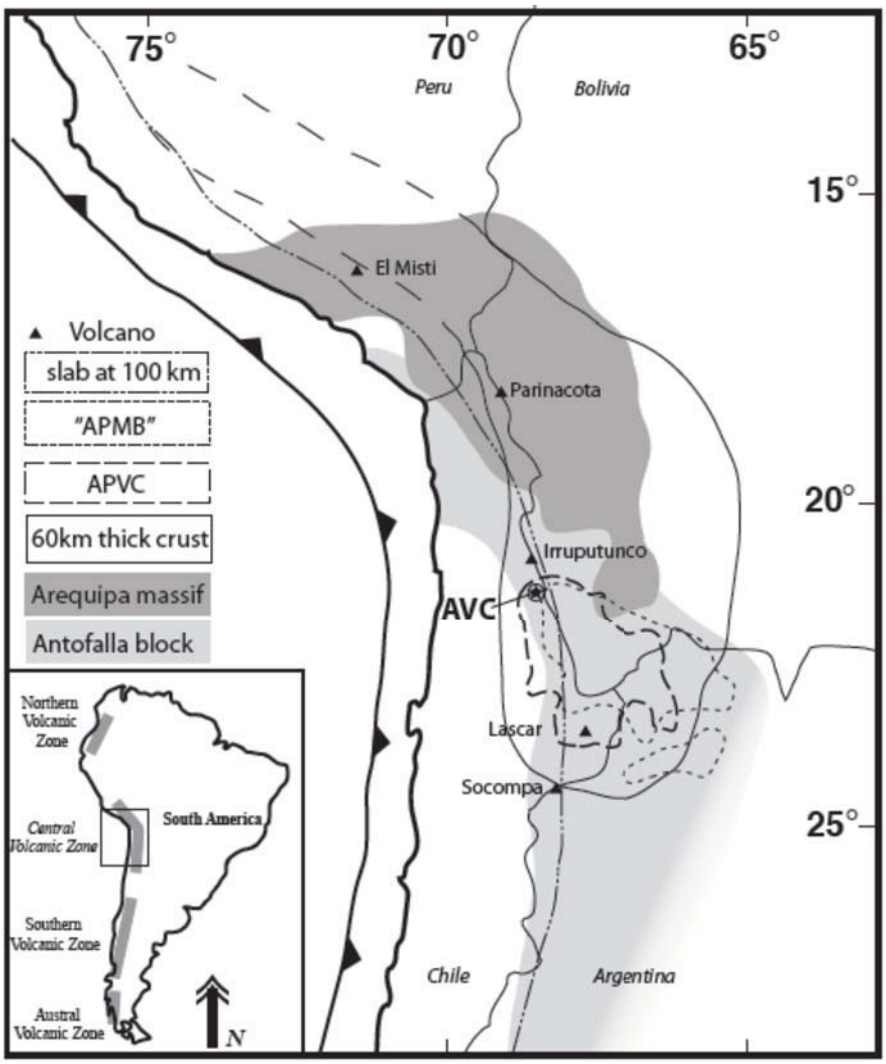

Figure 1.1: Location map of the Aucanqulicha Volcanic Cluster within the central Andean Volcanic zone. APVC = Altiplano-Puna volcanic complex (extent from Salibury et al., 2011). APMB=Altiplano-Puna magma body (Zandt et al., 2003). Arequipa massif, as defined by Pb isotopes (Loewy et al., 2004; Mamani et al., 2010). Antofalla basement from Mamani and others (2010) and Lucassen and others (2001). Slab depth from Cahill and Isacks (1992). Crustal thickness isopleth from Allmendinger and others (1997).

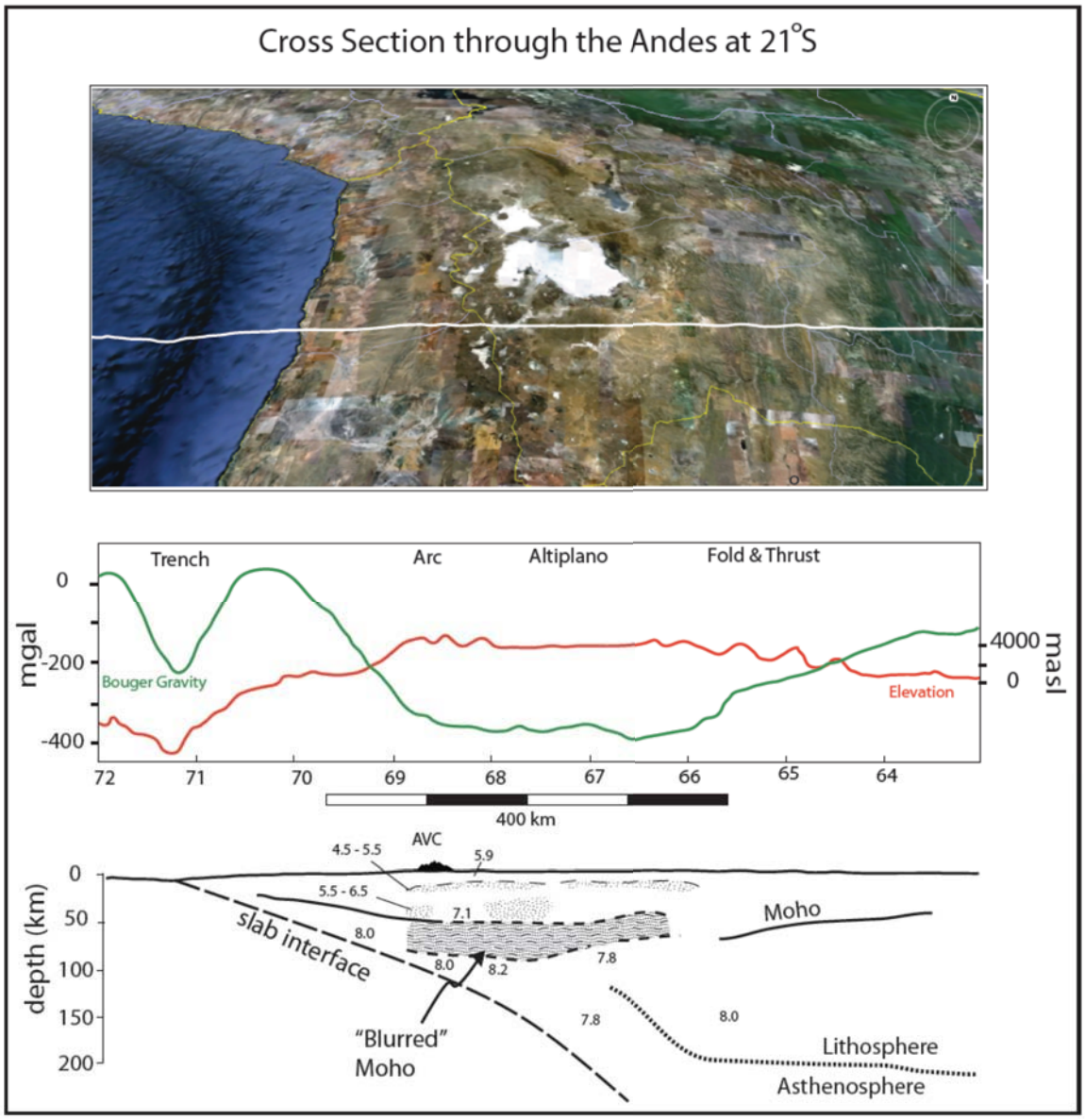

Figure 1.2: Summary of the geophysical characteristics of the central Andean crust at ~21°S. Stippled areas represent the low velocity zones, with numbers indicating *P*-wave velocities, km/s (Wigger et al., 1994, Giese et al., 1999). Mantle *P*-wave velocities (km/s) from Meyers and others (1998) Moho discontinuity (including "blurred" region) from Giese and others (1999). Slab interface from Cahill and Isacks (1992). Gravity and elevation curve from Scheuber and Giese (1999). Lithosphere-asthenosphere boundary after Heit and others (2007). Image from Google Earth.

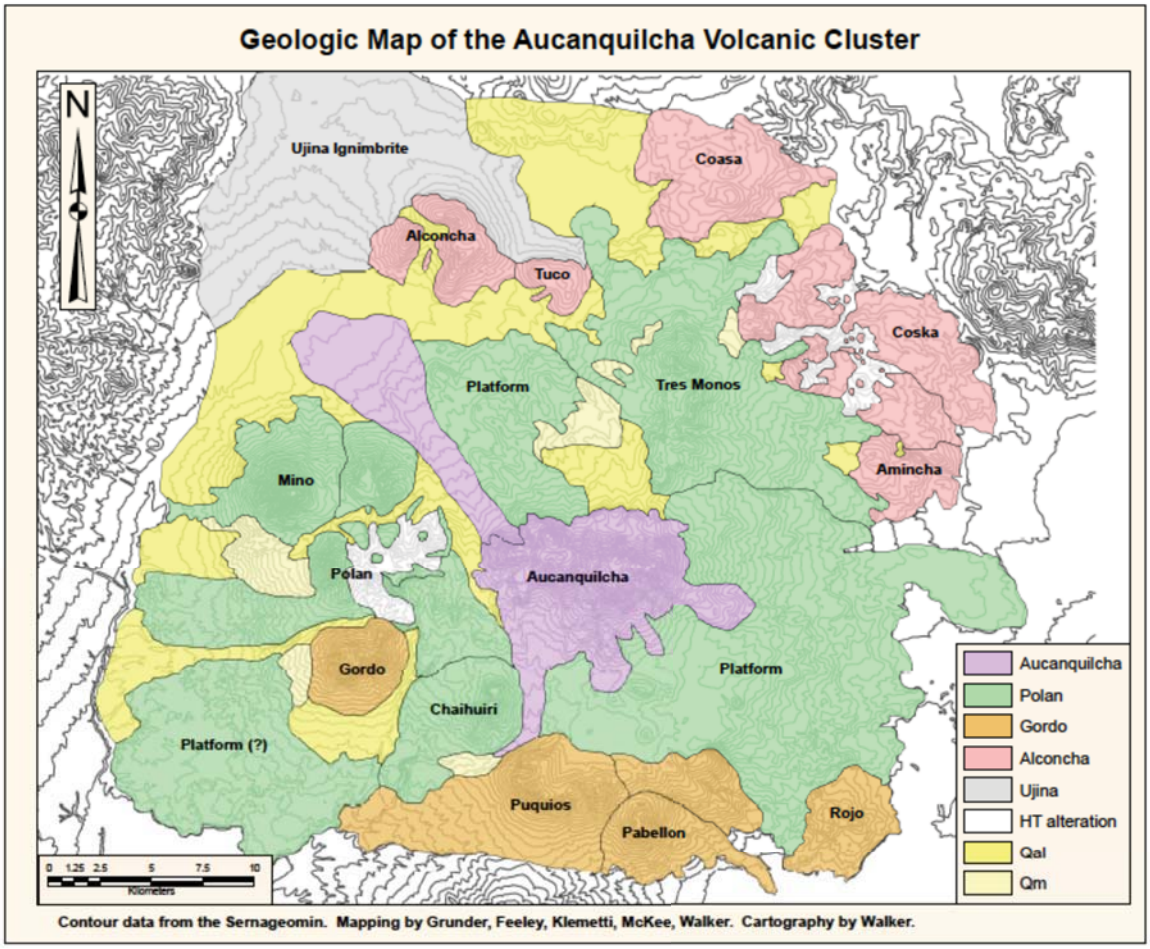

Figure 1.3: Geologic Map of the Aucanquilcha Volcanic cluster, broken out by temporal units. Eruptive groups: Alconcha = 11 - 8 Ma; Ujina = 9.6 Ma Ujina ignimbrite; Gordo = 6 - 4 Ma; Polan = 4 – 2 Ma; Aucanquilcha = ~1 Ma - present; HT alteration = hydrothermally altered rock; Qal = alluvium; Qm = moraines.

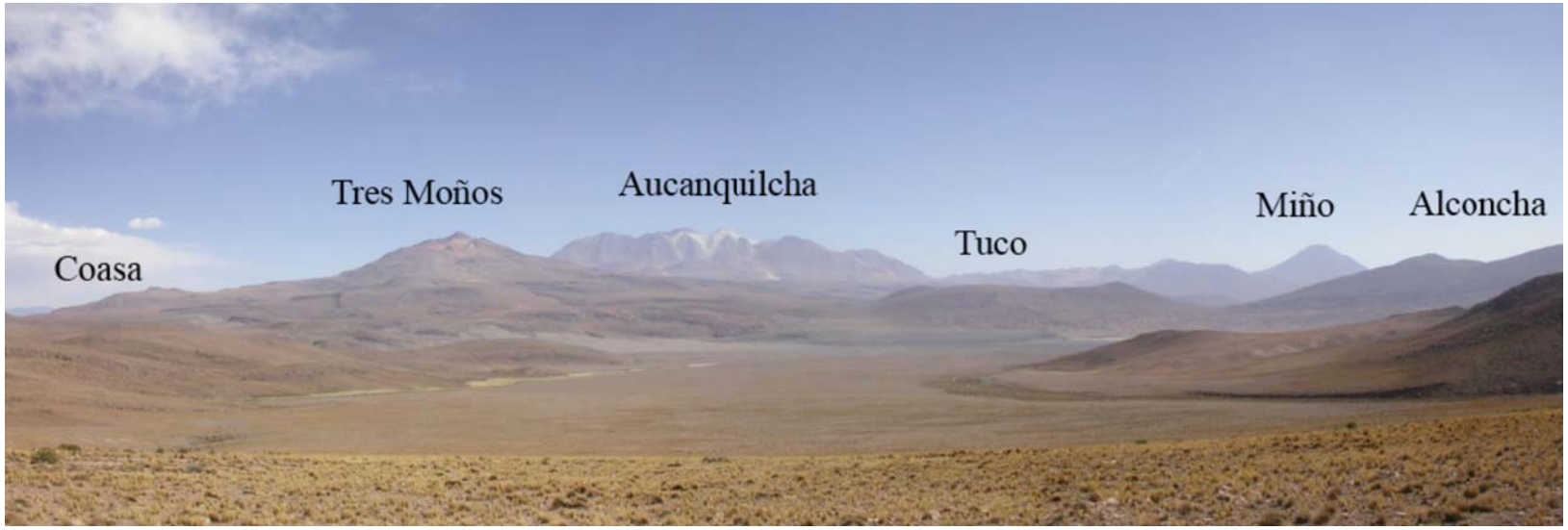

Figure 1.4: The Aucanquilcha volcanic cluster from the north.

Figure 1.5: The Aucanquilcha volcanic cluster from the southeast.

Figure 1.6: Looking east from the AVC at Volcán Ollagüe and the basaltic andesite scoria cones Poruñita and Luna de Tierra. Note also the hummocky topography of the Ollagüe debris avalanche.

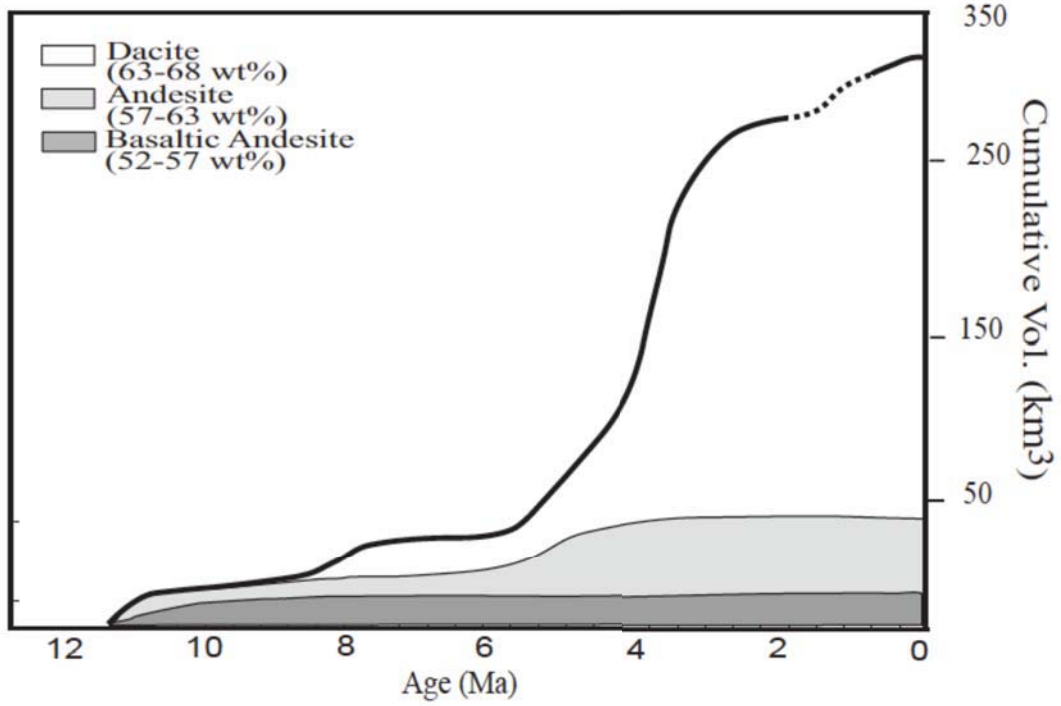

Figure 1.7: Eruptive Volume through time for the AVC. Note the dramatic increase in output beginning ~ 5Ma, coincident with compositional homogenization.

Table 1.1: Summary of age, volume, and basic compositional information regarding the eruptive groups of the Aucanquilcha Volcanic cluster. Ignimbrites (*). The Ujina and Carcote ignimbrites and the cinder cone field may not be directly related to AVC magmatism, but their timing and proximity warrant their inclusion here. Data sources: 1. Grunder, 1997; 2) McKee, 2002; 3) Grunder et al., 2006; 4) Mattioli et al., 2006; 5) Klemetti et al., 2008; 6) Walker et al., 2010; 7) this study; 8) Baker and Francis, 1978.

Eruptive Group	Age range (Ma)	Vol. (km3)	wt% SiO2 range	Mineral assemblages	Ref.
Alconcha (1)	11 - 7.5	25	57 - 68	<15% xls plag>cpx>opx>amph +/- olv	3,7
Alconcha (2)	~9 - 7.5	25	59 - 66	25-35% xls plag>cpx>opx>amph> bio +/- olv	3, 6, 7
Ujina*	9.4	2	64 - 65	15-20% xls. plag>cpx>amph>bio> kspar	1,7
Carcote*	5.6	~100	76	2.5% xls (bulk) 15-20% xls (welded) plag>bio>Fe-Ti oxides	1, 7, 8
Gordo	5.8 - 4	100	56 - 68	<15% (andesites) 25-35% (dacites) plag>cpx>opx>amph +/- olv	3, 6, 7
Polán	4 - 2.2	135	56 - 66	<15% (andesites) 25-35% (dacites) plag>cpx>amph>opx +/- bio, olv	3, 6, 7
Miño	3.3 - 3	15	58 - 61	<15% xls. plag>opx>cpx>amph +/- olv	2,3
Aucanquilcha	1 - present	50	62 - 67 (59-60 for 3 inclusions)	25-35% xls. plag>amph>bio>cpx> opx	3,5,6,7
Scoria cones	<0.5 Ma	<1	56 - 58	<10% xls. Plag=cpx>opx>olv	4,7

CHAPTER 2

Organization and thermal maturation of long-lived arc systems: evidence from zircons at the Aucanquilcha Volcanic cluster, northern Chile

Barry A. Walker Jr.
Anita L. Grunder
Joseph L. Wooden

Geology
3300 Penrose Place, Boulder, Colorado, USA
November 2010; v. 38; no. 11; p. 1007-1010

Abstract

Age and trace element data from zircons constrain the progressive stages of development of the magmatic underpinnings of the long-lived, dacite dominant Aucanquilcha Volcanic Cluster (AVC), in northern Chile . Large U/Pb age spectra (<2 my) are observed in the samples from the beginning and waning stages of the AVC, which are times characterized by low eruption rates. In contrast, small age spectra (<500 ky) are typical of samples from the middle stage of the AVC, a time characterized by high eruptive output. The preservation of precursor crystals is interpreted to reflect the thermal maturity of the AVC magmatic system; the middle stage is a time of homogenization and increased volumetric output rate and corresponds to a time of substantial resetting of the zircon ages, presumably through pervasive dissolution and crystallization. Crystallization temperatures for AVC zircons, calculated using the Ti-in-zircon thermometer, range from 690 – 920°C, with typically ~100°C variation in single samples. Higher concentrations of Ti, and thus hotter zircon crystallization temperatures, are recorded in samples that correspond to the eruptive flare-up. The timing of plutonic and volcanic events correspond based on correlation of peaks in zircon spot ages with eruptive episodes.

Introduction

In silicic to intermediate magmas, zircons are resilient repositories that can survive magmatic reentrainment and still reflect their initial time and condition of formation. Zircon studies have thus yielded salient information on magmatic incubation, crystal recycling, magmatic temperatures, differentiation histories, and batholith construction (e.g., Vazquez and Reid, 2002; Miller and Wooden, 2004; Bacon and Lowenstern, 2005; Watson and Harrison, 2005; Claiborne et al., 2006; Matzel et al., 2006; Walker et al., 2007). In particular, age studies of zircons have led to controversy over lifetimes of felsic magmas (Simon and Reid, 2005; Crowley et al., 2007) and whether plutons assemble fitfully or gradually (e.g., Coleman et al., 2004; Miller et al., 2007).

We here exploit the archive of age and temperature information available through SHRIMP-RG microanalysis of zircon spots from successively erupted dacite lavas to assess crystal recycling and thermal maturation over the ~10 million year history of the Aucanquilcha Volcanic Cluster (AVC) with inferences for the development of the subjacent plutonic complex. The age and compositional data from these zircons help reveal the evolution and self-organization of the AVC underpinnings, which appear to reflect an on-arc, local focusing of a thermal pulse associated with the magmatic flare-up of the Altiplano-Puna Volcanic Complex.

Geologic Setting

The Aucanquilcha Volcanic Cluster (AVC) is situated at ~ 21° S in northern Chile, within the Central Andes (**Figure 2.1**) where the crust is ~70 km thick (Beck et al., 1996). Volcanoes of the AVC number ~20 and comprise 340 ± 20 km^3 of high-K andesites and dacites with an eruptive history spanning the last 11 million years (Grunder et al., 2008). Dominant plagioclase is accompanied by subordinate clino- and orthopyroxene ± amphibole or by amphibole + biotite with minor pyroxene. Magnetite, ilmenite, apatite and zircon are present. Like many intermediate suites, textural evidence for magma mingling, mixing and self-mixing is abundant (ibid; Klemetti et al, 2008; Giles, 2009). Eruption rates in the AVC increased sharply after about 6 m.y. of activity (**Figure 2.2**), coincident with more central distribution of vents, more homogeneous composition of lavas, and the onset of extensive hydrothermal activity. Since about 2 Ma, the eruption rate has declined, consistent with a waning system.

The AVC lies at the northwestern edge of the Altiplano-Puna Volcanic Complex (de Silva and Gosnold, 2007), a giant ignimbrite province that overlies a large seismic attenuation zone extending from ~20 km to uncertain depth (Chmielowski et al, 1999). Zandt et al. (2003) infer ~15-25 % partial melt in this region of the crust. Although much less voluminous than ignimbrite eruptions of the APVC, the proximity of the

Aucanqulicha Volcanic Cluster and its similar ~ 10 m.y. lifespan support that it is a peripheral, dampened manifestation of a broad magmatic signal.

Methods

For U/Pb dating of zircon, we focused on 13 dacite lavas (62.0 - 67.2 % SiO_2—see supp. data) spanning the eruptive history and spatial distribution of the AVC. We imaged zircons (typically ~100-300 μm in length) with cathodoluminescence (see representative grains in the suppl data) and found complex zoning and resorption surfaces in grains from every sample. Spots were chosen in order to represent cores, interiors, rims, and regions of distinct CL intensity. Between 16 and 24 spots (~25 μm) were analyzed per sample with an O^{2-} beam current of ~5nA using the USGS/Stanford Sensitive High Resolution Ion Microprobe-Reverse Geometry (SHRIMP-RG). Zircon standards R33 (419 Ma) and MAD (see suppl. data) were used as U-Pb isotopic and trace element concentration standards, respectively. We used Isoplot (Ludwig 2003) for data reduction and rely on ^{207}Pb-corrected ^{206}Pb/^{238}U for our age data (see suppl. data). The Unmix algorithm (Sambridge and Compston, 1994) along with peaks and shoulders on the probability density function (PDF) identify separate age populations (cf. Walker et al., 2007).

Analyses on ten samples (10-15 spots at 10-15 μm) allow for the application of the Ti-in-zircon thermometer (Watson and Harrison, 2005). Beam current was 3 nA, and MAD the standard. Ti-in-zircon crystallization temperatures (T_{Ti}^{zir}) were calculated after Ferry and Watson (2007). We report larger uncertainty in the T_{Ti}^{zir} than the analytical error of ~1-1.2% (2σ) because we estimate α_{SiO2} and α_{TiO2} (see suppl. data) to be 0.9 and 0.5, respectively—both plausible estimates for crystal-rich intermediate to silicic rocks with Ti-bearing minerals (in this case ilmenite) (Hayden and Watson, 2007). Fe and Ca were monitored to identify contamination from inclusions or metasomatic alteration (cf. Claiborne et al., 2006). Samples with abnormally high Fe or Ca contents (~10 ppm) were discarded.

Controversy surrounds this thermometer (Ferry and Watson, 2007; Hofmann et al., 2009; Ferriss et al., 2008; Claiborne et al., 2006; Fu et al., 2008). The extrapolation to quartz and rutile undersaturated conditions adds not fully quantified uncertainty. Potential for nonequilibrium or coupled substitution has been pointed out by Hoffman and others (2009) working on Archean zircons. Because our zircons come from restricted lava compositions, are young and minimally damaged by radiation, and have been carefully screened for inclusions, the relative if not absolute values should be robust.

Results

U-Pb Age Data

Stacked analyses of U/Pb age are fitted with weighted probability density functions (**Figure 2.2**, also **electronic Appendix 1**), where individual peaks may not have absolute age significance, but differences in age spectra between samples are interpreted as real differences in crystal cargo inheritance. All samples have a spectrum of U-Pb zircon ages and most have more than one age population of zircon. We distinguish an age *spectrum* as a *relatively continuous age distribution* with no large time gaps between individual analyses in a single sample. We note the following patterns:

1. Excluding xenocrysts (that predate AVC activity), the range of zircon ages overall is ~12.5 m.y, and coincides well with the life span of the AVC as constrained by ^{40}Ar-^{39}Ar dating (Grunder et al., 2008, Klemetti et al., 2008).
2. Six xenocrysts were found only in the Aucanquilcha Group, with ages of 36, 223, 241, 245, 252, and 312 Ma.
3. Continuous age spectra for individual samples range from 0.5 to ~2 m.y., and span more time among samples of the oldest (Alconcha) and youngest (Aucanquilcha) group. In contrast, samples from the eruptive flare-up (~6 - 3 Ma) have restricted spectra.
4. Four samples contain single grains which predate their age spectra by >2 m.y. Two of these grains date back to the inception of AVC volcanism (~12.5 Ma).

Ti-in-Zircon

Crystallization temperatures (T_{Ti}^{zir}) of AVC zircons (excluding xenocrysts) range from 690°C to 920°C ± ~20°C (see supp. data) and decrease systematically with Hf concentration (**Figure 2.3**), which is a fractionation proxy (Claiborne et al., 2006). T_{Ti}^{zir} spectra preserved in individual samples are typically ~100 °C but range from ~50°C to ~230°C. A majority of zircons from the flare-up period have T_{Ti}^{zir} of > 780 °C, while samples from the beginning and ending phases of volcanism have T_{Ti}^{zir} that cluster between ~690 °C – 800°C. Data from Volcán Aucanquilcha lie on a trend ~parallel to the other samples on a T vs. Hf plot, but are offset to lower temperatures by ~80°C (**Figure 2.3**). Multiple analyses on single grains yield cases of both lower and higher Ti cores than in rims.

Discussion

Precursor Representation

Patterns in the AVC age spectra and populations help to reconstruct the evolution of the plutonic underpinnings. Where ^{40}Ar-^{39}Ar data are not available, we interpret the youngest peaks of any given sample to lie within ~200 ky of the age of the erupting pulse of magma. Older peaks are thought to represent antecrysts—grains that were entrained from precursor plutonic material or crystal mush (cf. Bacon and Lowenstern, 2005; Walker et al., 2007; Miller et al., 2007). We can identify crystal populations that span from ~0.5 to 8 m.y. older than the eruption age that are reasonably antecrystic in the scheme of the AVC magmatic system. We reserve the term “xenocrystic” for clearly foreign crystals (e.g., the Mesozoic grains of which there are remarkably few).

The age range of recycled material is generally greatest during beginning and waning phases of magmatism when volumetric output rates were low. In this scenario, magma pods are smaller as thermal contrast between magma and ambient crust is sharp and individual pulses of magma would not necessarily affect large portions of the plutonic mass, but rather remobilize and recycle only neighboring material. This would allow for

the preservation of chronologically discrete plutonic sectors as well as enhance the chances of an ascending magma batch to encounter such distinct sectors (see **Figure 2.4**).

In contrast, the samples from the "flare-up" period lack such large zircon age spectra. This time of increased volumetric output rate at the AVC corresponds to a time of substantial resetting of the zircon ages in the system, presumably through pervasive dissolution and crystallization of new grains as the magma system became homogenized. Samples with small age spectra likely reflect a series of magma chambers in which crystal cargo had largely been equilibrated with more recent magmatic events (see **Figure 2.4**). A crystal mush network was sustained during these times and perhaps hovered around zircon saturation.

Magmatic Temperatures

Zircons from the AVC record a wide range in T_{Ti}^{zir}, typically ~100°C, but as much as ~230°C, in one sample. These temperature spectra probably reflect the typical saturation range for intermediate magmas (cf. Harrison et al., 2007), though large spectra are, in part, attributable to recycling of precursor zircon into erupting magma batches. High temperature zircon occurs as either core or rim, demonstrating that individual zircons record distinct thermal histories amassed from disparate parts of the plumbing system just prior to eruption. Zircons that were grown and erupted during the flare up in eruptive activity record T_{Ti}^{zir} as much as 100 °C greater than in samples from the beginning and end phases of AVC activity (**Figure 2.3**). Zircons from Volcán Aucanquilcha record much lower temperatures (~690—750ºC), which together with the antecryst-rich nature of V. Aucanquilcha samples suggests that many of these grains plausibly grew from a near-solidus mush. Subsequently, they were likely entrained and flushed out of the plutonic system by magma batches that either erupted rapidly enough to limit dissolution, or were already saturated with zircon.

Though we acknowledge the limitations and uncertainties of the Ti-thermometry component of our study, the calculated temperatures are reasonably consistent with

patterns from independent temperature estimates from amphibole-plagioclase pairs from AVC lavas (Giles, 2009). Calculated temperatures for amphiboles from flare-up are ~800-900°C, while temperatures for the birth and death period get appreciably lower (~750-850°C and ~725-890°C, respectively).

Volcanic-Plutonic Connection

The range of zircon ages closely corresponds to the eruptive history of the AVC, as constrained by ^{40}Ar-^{39}Ar dating (Grunder et al., 2008). The oldest zircon ages *just* predate the initiation of eruptive activity at the AVC (~12 Ma) and no zircons analyzed hail from the time gap in AVC volcanism (from ~7.5 - 6 Ma), indicating a period of *both* magmatic and volcanic quiescence during this gap in eruptive activity.

Old, outlying *antecrystic* grains (Figure 2) illustrate the assimilation of older plutonic sectors throughout the AVC flare-up. These sectors were apparently not accessible to the magma in the final, most centralized time of volcanism at V. Aucanquilcha. This is consistent with pervasive dissolution of antecrystic zircon in the main plexus during the thermal peak, thus erasing the zircon record of plutonic precursors with progressive mush development and system organization. Also, the inclusion of xenocrystic material indicates the late magma had access to wall rock, which suggests that the magma locus moved to levels not armored by previous plutonic episodes. The masking of the magmatic record via thermal and organizational overprinting may be a common occurrence and would promote underestimates of the lifespans of large, silicic to intermediate plutonic or volcanic igneous systems, particularly those that are not well-exposed.

Conclusion

Erupted zircons were extensively derived from the evolving plutonic plexus of the AVC and are broadly cognate crystal cargo at the multi million-year scale. The plutonic underpinnings were episodically active in concert with the volcanic pulses. Most zircon

recycling involved grains only a few hundred thousand years older than the eruption age. We take this to reflect the timescale of plutonic episodes. Antecrysts of older vintage document the magmatic cannibalism associated with batholith assembly—that is, the blending of discrete plutons into a patchwork body.

The system went through waxing, climactic, and waning stages as indicated by large zircon age spectra in old and young samples and restricted age spectra from flare-up samples. Lavas erupted subsequent to the flare-up have very few antecrysts that *predate* the flare-up, suggesting wide scale eradication and regrowth of zircons during the thermal maturation. A thermal climax is supported by Ti-in-zircon thermometry, as hotter $T_{\mathrm{Ti}}^{\mathrm{zir}}$ are observed in grains from the eruptive flare-up.

Finally, the zircon age ranges observed in AVC lavas stand in contrast to large, explosive systems such as Long Valley, Taupo, and Yellowstone, which lack such antiquity (exception: the Timber Mountain Complex; Bindeman et al. 2006). Instead, the AVC zircon record is more analogous to plutonic systems (Tuolumne, Spirit Mountain, Tatoosh). The relatively small volume and long-lived nature of the AVC may be more indicative of typical effluent of batholith building systems.

Acknowledgments

Funding provided by NSR EAR 0610114 to A. Grunder and F. Tepley. We'd like to thank Frank Mazdab for help in the SHRIMP lab, Frank Tepley for help in the field, and the VIPER group at OSU for their banter. For helpful insights and comments we thank Jonathan Miller and David Hawkins as well as Mary Reid, Olivier Bachmann and an anonymous reviewer regarding an earlier version of this paper.

References

Bacon, C.R., and Lowenstern, J.B., 2005, Late Pleistocene granodiorite source for

recycled zircon and phenocrysts in rhyodacite lava at Crater Lake, Oregon: Earth and Planetary Science Letters, v. 233, p. 277-293.

Beck, S.L., Zandt, G., Myers, S.C., Wallace, T.C., Silver, P.G., and Drake, L., 1996, Crustal-thickness variations in the central Andes: Geology, v. 24, p. 407-410.

Bindeman, I.N., Schmitt, A.K., Valley, J.W., 2006, U-Pb zircon geochronology of silicic tuffs from the Timber Mountain/Oasis Valley caldera complex, Nevada: rapid generation of large volume magmas by shallow-level remelting: Contributions to Mineral Petrol, v.152, n.6.

Chmielowski, J., Zandt, G., and Haberland, C., 1999, The central Andean Altiplano-Puna magma body: Geophysical Research Letters, v. 26, p. 783-786.

Claiborne, L.L., Miller, C.F., Walker, B.A., Wooden, J.L., Mazdab, F.K., and Bea, F., 2006, Tracking magmatic processes through Zr/Hf ratios in rocks and Hf and Ti zoning in zircons: An example from the Spirit Mountain batholith, Nevada: Mineralogical Magazine, v. 70, p. 517-543.

Coleman, D.S., Gray, W., and Glazner, A.F., 2004, Rethinking the emplacement and evolution of zoned plutons: Geochronologic evidence for incremental assembly of the Tuolumne Intrusive Suite, California: Geology, v. 32, p. 433-436.

Crowley, J.L., Schoene, B., and Bowring, S.A., 2007, U-Pb dating of zircon in the Bishop Tuff at the millennial scale: Geology, v. 35, p. 1123-1126.

de Silva, S.L., and Gosnold, W.D., 2007, Episodic construction of batholiths: Insights from the spatiotemporal development of an ignimbrite flare-up: Journal of Volcanology and Geothermal Research, v. 167, p. 320-335.

Ferriss, E.D.A., Essene, E.J., Becker, U., 2008, Computational study of the effect of pressure on the Ti-in-zircon geothermometer; European Journal of Mineralogy, v. 20, p. 745-755.

Ferry, J.M., and Watson, E.B., 2007, New thermodynamic models and revised calibrations for the Ti-in-zircon and Zr-in-rutile thermometers: Contributions to Mineralogy and Petrology, v. 154, p. 429-437.

Fu, B., Page, Z., Cavosie, A.J., Fournelle, J., Kita, N.T., Lackey, J.S., Wilde, S.A., Valley, J.W., 2008, Ti-in-zircon thermometry: applications and limitations:

Contributions to Mineralogy and Petrology, v. 156, p. 197-215.

Giles, D., 2009, Dynamics of a long-lived magmatic system as indicated by variations in amphibole composition and textures in dacites erupted over 11 m.y. at the Aucanquilcha Volcanic Cluster, Central Andes, Chile. MS thesis.

Grunder, A.L., Klemetti, E.W., Feeley, T.C., and McKee, C.M., 2008 (for 2006), Eleven million years of arc volcanism at the Aucanquilcha Volcanic Cluster, Northern Chilean Andes: implications for the life span and emplacement of plutons: Transactions of the Royal Society of Edinburgh-Earth Sciences, v. 97, p. 415-436.

Harrison, T.M., Watson, E.B., and Aikman, A.B., 2007, Temperature spectra of zircon crystallization in plutonic rocks: Geology, v. 35, p. 635-638.

Hayden, L.A., and Watson, E.B., 2007, Rutile saturation in hydrous siliceous melts and its bearing on Ti-thermometry of quartz and zircon: Earth and Planetary Science Letters, v. 258, p. 561-568.

Hofmann, A.E., Valley, J.W., Watson, E.B., Cavosie, A.J., and Eiler, J.M., 2009, Sub-micron scale distributions of trace elements in ziron: Contributions to Mineralogy and Petrology, v.158, n.3, 317-335.

Klemetti, E.W., and Grunder, A.L., 2008, Volcanic evolution of Volcan Aucanquilcha: a long-lived dacite volcano in the Central Andes of northern Chile: Bulletin of Volcanology, v. 70, p. 633-650.

Ludwig, K.R., 2003. Isoplot 3.00: A geochronological toolkit for Microsoft Excel. Berkeley, CA: Berkeley Chronological Center.

Matzel, J., Bowring, S., Miller, R., 2006, Time scales of pluton construction at differing crustal levels: Examples from the Mount Stuart and Tenpeak intrusions, North Cascades, WA, GSA Bulletin, v. 118, p. 1412 - 1430

Miller, C.F., McDowell, S.M., and Mapes, R.W., 2003, Hot and cold granites? Implications of zircon saturation temperatures and preservation of inheritance: Geology, v. 31, p. 529-532.

Miller, J.S., Matzel, J.E.P., Miller, C.F., Burgess, S.D., and Miller, R.B., 2007, Zircon growth and recycling during the assembly of large, composite arc plutons: Journal of Volcanology and Geothermal Research, v. 167, p. 282-299.

Miller, J.S., and Wooden, J.L., 2004, Residence, resorption and recycling of zircons in Devils Kitchen rhyolite, Coso Volcanic field, California: Journal of Petrology, v. 45, p. 2155-2170.

Sambridge, M.S., and Compston, W., 1994, Mixture Modeling of Multicomponent Data Sets with Application to Ion-Probe Zircon Ages: Earth and Planetary Science Letters, v. 128, p. 373-390.

Simon, J.I., and Reid, M.R., 2005, The pace of rhyolite differentiation and storage in an 'archetypical' silicic magma system, Long Valley, California: Earth and Planetary Science Letters, v. 235, p. 123-140.

Vazquez, J.A., and Reid, M.R., 2002, Time scales of magma storage and differentiation of voluminous high-silica rhyolites at Yellowstone caldera, Wyoming: Contributions to Mineralogy and Petrology, v. 144, p. 274-285.

Walker, B.A., Miller, C.F., Claiborne, L.L., Wooden, J.L., and Miller, J.S., 2007, Geology and geochronology of the Spirit Mountain batholith, southern Nevada: Implications for timescales and physical processes of batholith construction: Journal of Volcanology and Geothermal Research, v. 167, p. 239-262.

Watson, E.B., and Harrison, T.M., 1983, Zircon Saturation Revisited - Temperature and Composition Effects in a Variety of Crustal Magma Types: Earth and Planetary Science Letters, v. 64, p. 295-304.

Watson, E.B., and Harrison, T.M., 2005, Zircon thermometer reveals minimum melting conditions on earliest Earth: Science, v. 308, p. 841-844.

Zandt, G., Leidig, M., Chmielowski, J., Baumont, D., and Yuan, X.H., 2003, Seismic detection and characterization of the Altiplano-Puna magma body, central Andes: Pure and Applied Geophysics, v. 160, p. 789-807.

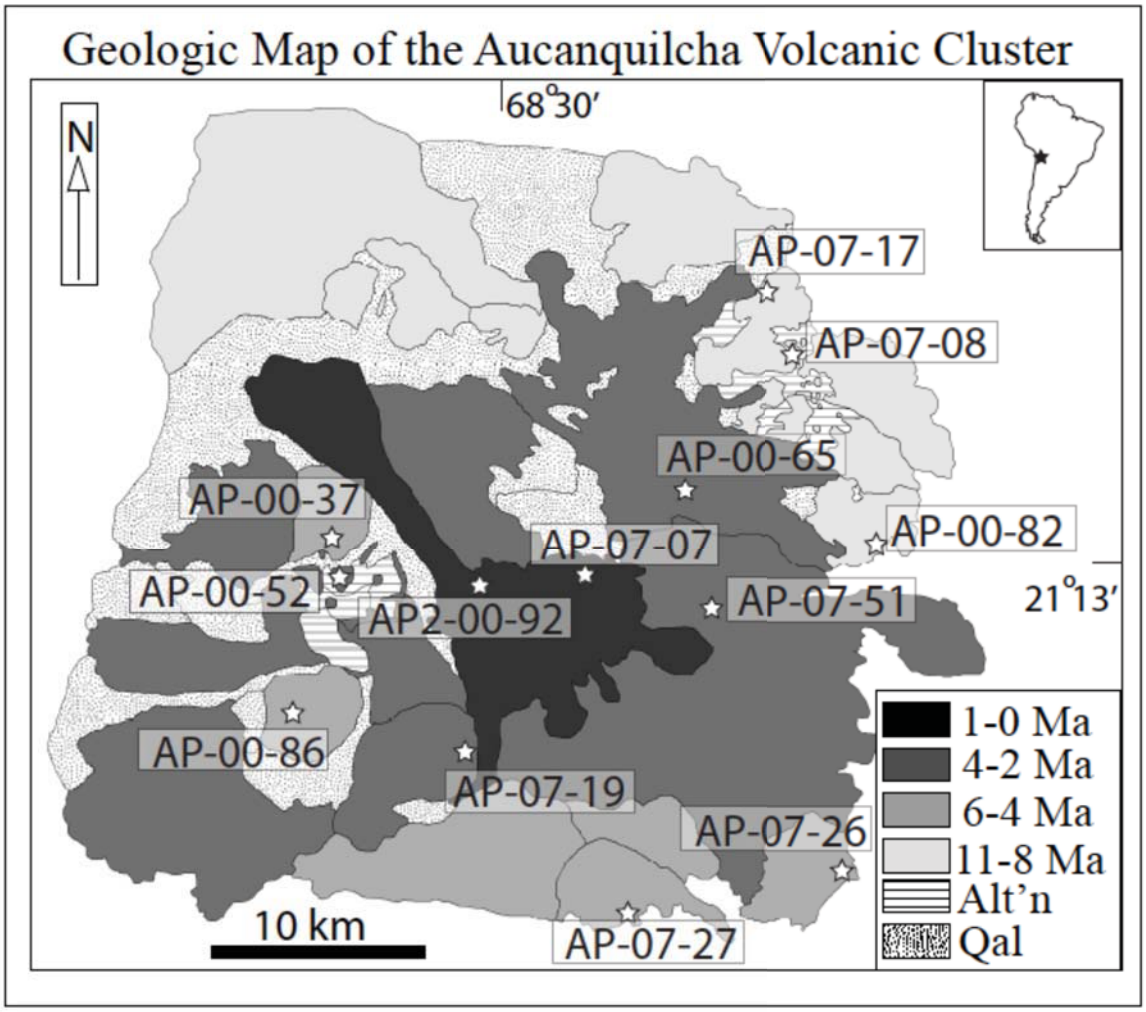

Figure 2.1: Generalized geologic map of the Aucanquilcha Volcanic Cluster, showing units broken out by time. Eruptive groups: Alconcha = 11 - 8 Ma; Gordo = 6 - 4 Ma; Polan = 4 – 2 Ma; Aucanquilcha = ~1 Ma - present; Alt'n = hydrothermally altered rock. Zircon sample locations starred.

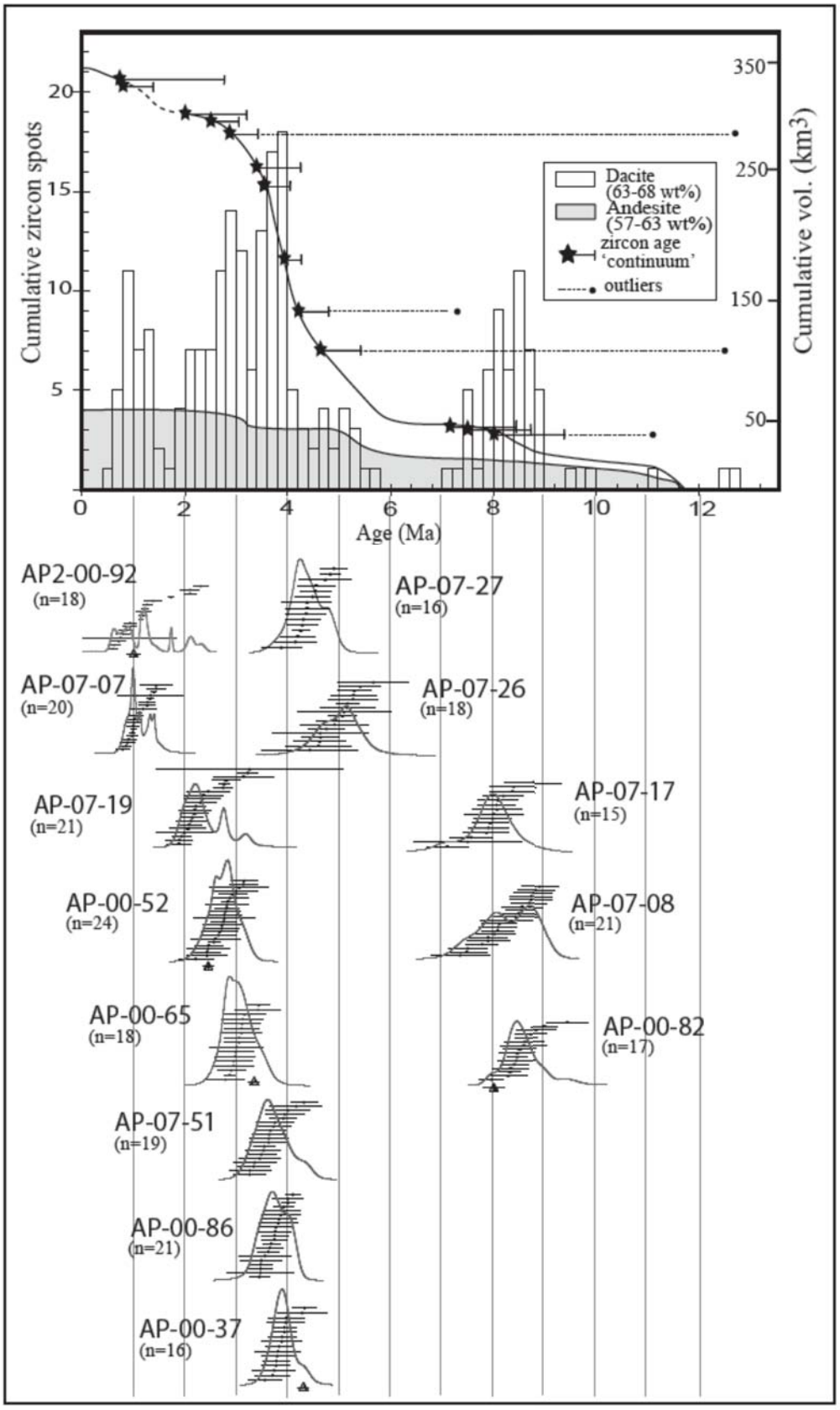
Cumulative zircon spots
Cumulative vol. (km3)
Age (Ma)
Dacite (63-68 wt%)
Andesite (57-63 wt%)
zircon age 'continuum'
outliers
AP2-00-92 (n=18)
AP-07-27 (n=16)
AP-07-07 (n=20)
AP-07-26 (n=18)
AP-07-19 (n=21)
AP-07-17 (n=15)
AP-00-52 (n=24)
AP-07-08 (n=21)
AP-00-65 (n=18)
AP-00-82 (n=17)
AP-07-51 (n=19)
AP-00-86 (n=21)
AP-00-37 (n=16)

Figure 2.2 (previous page): Summary of zircon age data for the AVC plotted with cumulative volume and time. Spot analyses (2σ errors) are shown with probability density functions (PDFs) for individual samples. Age *spectra* (see text) for individual samples are shown with a star corresponding to the youngest peak/shoulder on the PDF for that sample, with a tail extending to the oldest peak in the *continuum* of the age spectrum. Note the generally shorter age spectra for the samples from ~5 to 2.5 Ma, which correspond to the eruptive flare-up at the AVC. Available Ar-Ar ages are shown as triangles (w/ error bars) at the base of each sample. Cumulative volume and compositional proportions updated from Grunder et al., 2008.

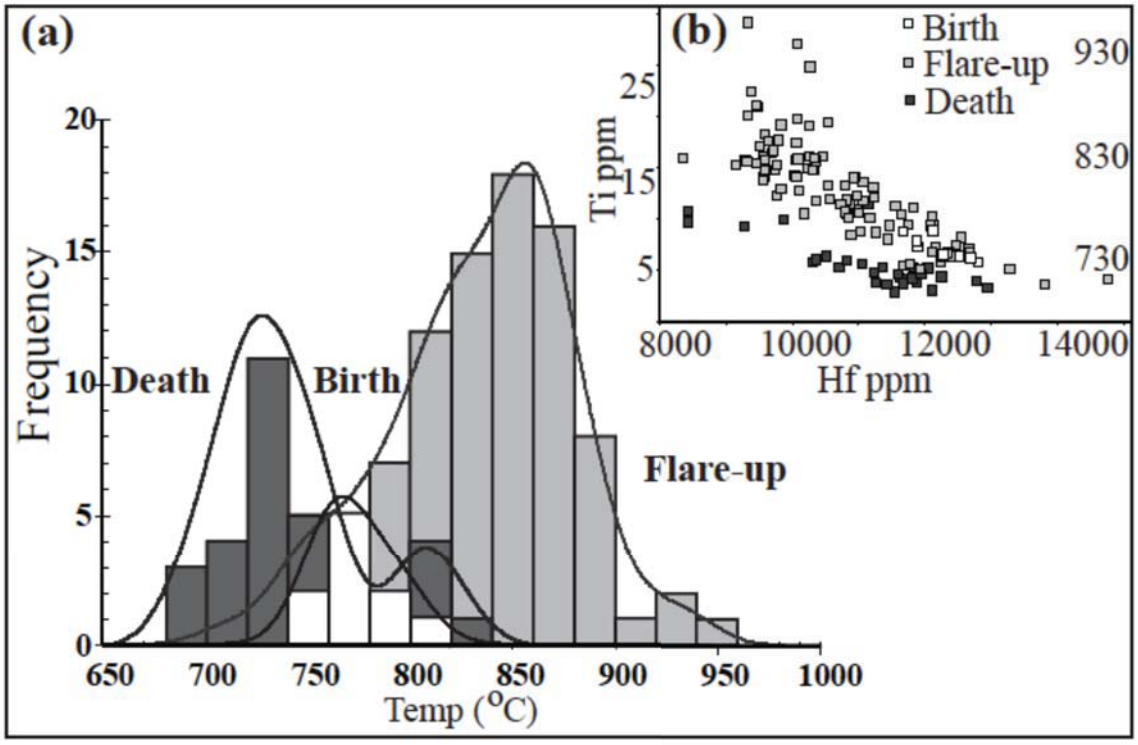

Figure 2.3: Ti concentrations and corresponding crystallization temperatures for AVC zircons as calculated from the Ti-in-zircon thermometer (Ferry and Watson, 2007; see methods section for calculation parameters). Data separated by eruptive pulse and plotted (a) as probability density functions and (b) against Hf concentration. Note the higher temperatures recorded during the flare-up period, as compared with the birth and death of the system.

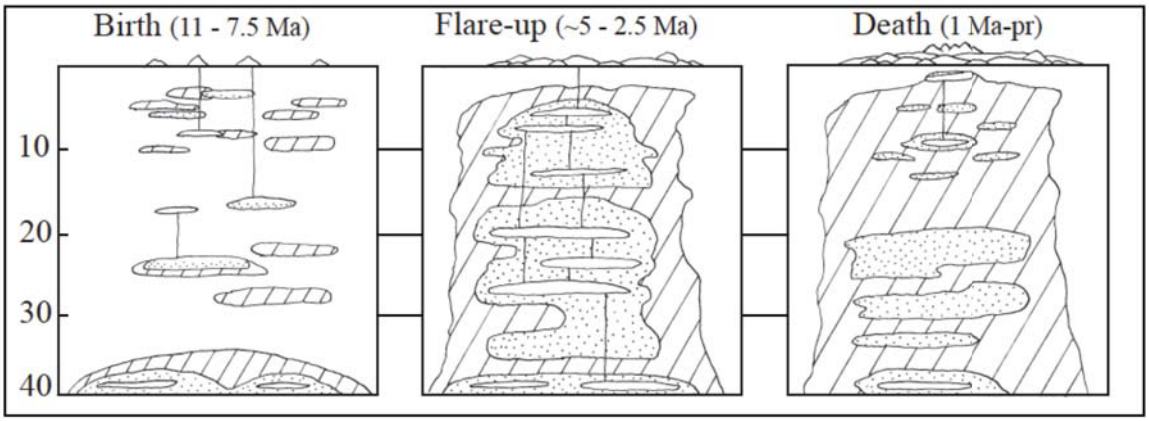

Figure 2.4: Generalized cartoon illustrating the assembly of the AVC plutonic underpinnings. Depth in km. Plain white pods = liquid-rich magma; stippled pods = crystal-rich mush; striped = totally solidified magma and/or remnant country rock. Isolated sectors of magmatism (birth) gave way to a more extensive, thermally mature magma plexus during the eruptive flare-up. The final stage (death) is again marked by smaller, more isolated magma chambers as the system cools from its flare-up. See discussion for details.

CHAPTER 3

Crustal Growth and changing magmatic processes during an eleven million year magmatic pulse at the Aucanquilcha volcanic cluster: isotopic and trace element constraints

Barry A. Walker, Jr.
Anita L. Grunder
Erik W. Klemetti

In preparation for submission to:
Journal of Petrology

Introduction

Studies of long-term continental subduction have revealed a pulsatory history of magmatism. The "steady state" subduction signal is punctuated by periods of increased activity separated by periods of relative quiescence, the fluctuations of which have been attributed to major reorganizations of convergent margin tectonics (Decelles et al., 2009; Haschke et al., 2002). While the existence of magmatic cycling is acknowledged, the eruptive histories and magmatic evolution of such cycles are not well documented. Long-lived volcanic provinces afford a unique perspective on these magmatic cycles as their successive products reveal a long duration account of the processing experienced by magma en route from its source. Conversely, such magma systems undoubtedly affect the crust through which they pass.

Assessing the effect of sustained magmatism on the crust has proven to be a complicated undertaking. Studies of the Southern Rocky Mountain Volcanic Field (SRMVF) (Lipman 2007; Riciputi et al., 1995; Johnson et al., 1990) have demonstrated that prolonged voluminous magmatism has resulted in appreciable temporal shifting of isotopic signatures toward mantle values (low $^{87}Sr/^{86}Sr$, high εNd). This is attributed to the addition of significant amounts of mantle material during magmatism. Conversely, Ducea and Barton (2007) find that εNd values from plutons of the North American Cordillera strongly correlate with the Nd model ages of the local basement rock. This correlation suggests that the main component in North American Cordilleran magma was crustal melt, and that voluminous continental arc magmatism primarily involves a reorganization of the crustal mass rather than a significant addition of mantle material into the crust (Ducea and Barton, 2007). For the central Andes, Lucassen and others (2001) similarly conclude that recycling is the principal process of crustal evolution, coincident with Phanerozoic magmatism.

The Central Volcanic Zone of the Andes is the archetypal continental subduction margin. Magmatism here has been the subject of hundreds of studies, in large part because it is

the only case of active subduction zone magmatism where there is thick continental crust. The 1970s and 1980s were a prolific decade for isotopic and geochemical studies on central Andean magmatism (James et al., 1976; Tilton, 1978; Thorpe and Francis, 1979; Francis et al., 1980; Harmon et al., 1981; Hawkesworth et al., 1982; Davidson et al., 1990). During the 1990s and 2000s, geophysical studies (Potsdam, COCORP) revealed seismically inferred glimpses of sub-arc structure, yielding insight into the lithospheric architecture above subduction zones. Also, recent high-resolution geochronological studies are providing precise age control on magmatic processes (Hora et al., 2007; Salisbury et al., 2011). Several studies have explored along-arc and across-arc compositional and/or structural variation as related to magmagenesis (Hildreth and Moorbath, 1988; Rogers and Hawkesworth, 1989; Wörner et al., 1994; Giese et al, 1999; Mamani et al., 2010), providing evidence that difference in crustal composition and thickness are critical in producing the variability observed in arc intermediates.

Within this geological setting, we look to the Aucanquilcha Volcanic Cluster (AVC), a long-lived, on-arc volcanic complex. The AVC is an arc node that has persisted for eleven million years, and its lavas are time-transgressive samplings of its magmatic system at depth. The ~10 m.y. timespan of the AVC is a typical life cycle for major crustal magmatic systems expressed either as volcanism or plutonism (Grunder et al, 2006) and is also reflected in the duration of the neighboring Altiplano-Puna Volcanic Complex (Salisbury et al., 2011; Grunder and de Silva, 2007). Using trace element and isotope geochemistry, we explore the processes that contributed to produce the erupted lavas and, by inference, the plutonic dregs, as viewed from an evolutionary perspective relevant to the development of batholiths.

The Aucanquilcha Volcanic Cluster

The AVC makes up a geomorphologically distinct cluster of ~20 volcano centers that break into four broad groups based on timing (cf. Grunder et al., 2006; **Figure 3.1**; see also **Figure 1.3**, from Chapter 1). Erupting first, from 11 to ~7.5 Ma, was the Alconcha

group, comprising about seven centers and cropping out in the northwest. We break the Alconcha group into two distinct subgroups based on timing, crystal content. The first subgroup (Alconcha 1) is early (~11-10 Ma) and relatively crystal poor (<15 vol% crystals). The second subgroup (Alconcha 2) erupted later (~8 – 7.5 Ma) and is relatively crystal-rich (>25 vol% crystals). The Ujina ignimbrite, a small (~2 km^3) dacitic ash flow tuff, erupted at ~9.4 Ma, and is also considered part of the Alconcha group due to its timing and proximity, though its vent area is uncertain. The second main eruptive phase was the Gordo group, which erupted from ~6 to 4 Ma, and consists of six identified centers, distributed around the southern and western AVC. The third main eruptive phase was the Polán group, active from ~ 4 to 2 Ma, comprising around ten volcanoes that are widely, but more centrally, distributed. Volcán Miño erupted during this period, at ~3 Ma, but we break out separately this large andesite volcano on the western edge of the AVC (McKee, 2002). The fourth and last is the Aucanquilcha group, consisting of Volcán Aucanquilcha itself, which erupted from ~ 1 Ma to recently (Klemetti et al., 2008) and lies in the center of the AVC. Aucanquilcha comprises six or more overlapping domes that form an east-west ridge.

The systematic development of the AVC from peripheral or widely distributed to centrally distributed corresponds to the evolution from compositionally diverse, mafic andesite to dacite, to relatively homogeneous dacite concurrent with a dramatic increase in eruptive output (see **Figure 1.4** from Chapter 1) and the broad transition from early anhydrous mafic silicate assemblages (pyroxenes) to later hydrous phases (amphibole and biotite) (Grunder et al., 2006). This general evolutionary pattern is echoed in the Altiplano-Puna Volcanic Complex, in the San Juan Volcanic Field, Colorado, USA, the Yanacocha gold District, Peru, and in the Tuolumne Intrusive series of the Sierra Nevada Batholith among others (Longo et al., 2010; Lipman, 2007; Grunder et al., 2006).

Just to the east of the long-lived, dacite-dominated arc node expressed as the AVC is a small field of Quaternary monogenetic andesitic scoria cones that includes the eroded

edifices of Poruñita and Luna de Tierra. Like La Poruña, 80 km to the south, such centers are the only record of ambient mafic flux.

Methods

Samples representing the geographic, age, and compositional range of the AVC were selected, crushed to pea gravel, and powdered in a tungsten carbide vessel using a shatter-box. Preference was given to fresh samples without oxidation. Sample sizes were typically ~0.5 to 1 kg of material, crushed and split. In addition to the data from previous AVC work (Grunder, 1997; McKee, 2002; Grunder et al., 2006; Klemetti et al., 2008; Walker et al., 2010), 42 new analyses are presented here. Major and trace elements were analyzed by X-ray fluorescence (ThermoARL) at the GeoAnalytical lab at Washington State University (methods of Johnson et al., 1999). Rare earth and select trace elements were analyzed by inductively coupled plasma mass spectrometry (ICP-MS; Agilent 7700, quadrupole mass spectrometer) at Washington State University. Whole rock powders were then taken to the University of Colorado for determination of Sr, Nd, and Pb isotopes using thermal ionization mass spectrometry (TIMS). Isotopic compositions were obtained using techniques and standardization of Farmer and others (1991). Plagioclase separates were prepared by magnetic separation and hand-picking, and were analyzed at the University of Oregon for oxygen isotopic compositions, reported as $\delta^{18}O$ on the VSMOW scale. One mg aliquots of unaltered, inclusion-free plagioclase crystals (and quartz for two samples where it was present in appreciable quantities) were analyzed with CO_2 laser fluorination and mass spectrometry following the techniques of Bindeman and others (2004).

Results

Major and trace elements

The major element compositions of Aucanquilcha Volcanic Cluster lavas have been described previously by Grunder and others (2006) and Klemetti and others (2008), but a

brief description here is warranted. As is true of the entire modern Central Andean arc, no true basalts are found in the AVC. Lavas from the AVC are medium to high-K (~1 – 4 wt% K_2O) and span the range from basaltic andesite to dacite (**Figure 3.2; Table 1**). As with most calc-alkaline suites, Al_2O_3, TiO_2, FeO*, MnO, CaO, MgO, all decrease with SiO_2 whereas K_2O, and Na_2O (broadly) increase (**Figure 3.3**).

Although the AVC data, in total, make a diffuse cloud in variation diagrams, there are several distinctions to note. The least evolved compositions are represented throughout the AVC history by basaltic andesite to andesite lavas and andesitic magmatic inclusions in dacite. Samples from the peripheral scoria cones overlap in composition with the more mafic lavas of the AVC (**Figure 3.2**). Most lavas, however, are dacites, with a paucity of compositions between ~ 60 – 61 wt% SiO_2. Notably, there are two different trends within the Alconcha (first group) suite, warranting their separate notation (Alconcha 1 and Alconcha 2). Alconcha 1 samples have <15% crystals, have pyroxenes as the main mafic silicates and are mainly from the oldest centers. The lavas that comprise the Alconcha 2 subgroup are more crystal-rich (>25%) and contain large, conspicuous *family Bibles* of biotite. The Alconcha 2 subgroup lies within the main trend of the AVC, whereas the Alconcha 1 group commonly delimits one boundary of the AVC compositional distribution, such as high Al_2O_3, MnO and low TiO_2 as well as high Zr and low Dy/Yb with respect to SiO_2 (**Figures 3.3, 3.5**). Notably, one lava (AP-07-10B) is of Alconcha 2 type, but a mafic inclusion (AP-07-10A) within it is of Alconcha 1 type.

In contrast to the Alconcha 1 subgroup, the Aucanquilcha group is the most silicic overall, and defines the uppermost range of TiO_2 values and the lowermost K_2O and MnO values for the AVC suite with respect to SiO_2 and also low Zr and high Dy/Yb. Thus, when the AVC data cloud is taken together, the Alconcha 1 group defines the general limit on one side and Aucanquilcha the other side with temporally intermediate samples making up the data cloud in between with respect to many elements. Through time, the general trend is toward more homogeneous compositions; andesites through dacites were common in the earlier stages of AVC volcanism, giving way to relatively

homogeneous dacites during the period of high eruptive output. The last stage of AVC volcanism produced Volcán Aucanquilcha itself, which is compositionally restricted to dacites, excepting inclusions.

The trace element compositions of AVC lavas (**Table 3.1**) broadly overlap with other central Andean arc lavas and are remarkable for their similar patterns through time (**Figure 3.4**). Large ion lithophile elements show positive spikes and high field strength elements negative spikes, consistent with their arc origin. Chromium and Ni contents are low (less than 150 and 50 ppm, respectively) and decrease with SiO_2, suggesting early removal of ferromagnesian phases such as olivine and pyroxene. Elements such as Sr, Sc, and the middle and heavy rare earth elements (MREEs, HREEs) decrease with SiO_2 (**Figure 3.5**), consistent with their compatibility with the major arc lava phases such as plagioclase, clinopyroxene, amphibole and garnet, respectively. Overall, Dy/Yb ratios decrease with increasing SiO_2, broadly consistent with amphibole fractionation (cf. Davidson et al., 2007), although Dy/Yb ratios increase in the suite overall with time (**Figure 3.6**). Elements incompatible with the major phases, such as Ba, Rb, Zr, U, Th, Pb, Ta, and the light rare earth elements (LREEs) all increase with SiO_2. There is a subtle Rb, U, Cs, and Ta depletion and slight Ba enrichment in the Alconcha 1 subgroup lavas. Several elements, such as Nd and Nb, do not systematically vary with SiO_2. Interestingly, a few andesite lavas, including two scoria cone samples, are enriched in elements such as the LREEs, Zr, Hf, Nb, Ba, Ti, and K. When Ba is plotted against Rb/Sr (**Figure 3.7**), the data diverge at more silicic compositions, with one extreme toward higher Ba at lower Rb/Sr, and the other toward higher Rb/Sr at slightly lower Ba. Specifically, the Alconcha 1 subgroup along with the Aucanquilcha group and a scattering of other AVC samples, fall on the high-Ba, low-Rb/Sr trend. Compositions from the Alconcha 2 fall along the low-Ba trajectory. Gordo and Polán groups are scattered mainly along the low-Ba trend and between the two trends.

With respect to temporal variations in trace elements, the most obvious feature is that the lavas from Volcán Aucanquilcha are slightly offset from the main trend defined by the

rest of the AVC data. Aucanquilcha lavas are enriched in Ba, Sr, Eu/Eu* (small Eu anomaly), and are depleted in Rb, U, Y (see **Table 3.1**), at given SiO_2. The MREE/HREE ratios of AVC lavas increase appreciably through time (**Figure 3.6**). At any given time, andesites form both baseline and high values. Dy/Yb ratios range from ~2 in the earliest lavas to ~2.5 – 3.5 in Aucanquilcha lavas. Sm/Yb ranges from 2.25 – 3 in early lavas to 4 – 6.25 in Aucanquilcha lavas. Similarly high MREE/HREE ratios are observed in lavas from other central Andean volcanoes (Mamani et al., 2010).

Isotopes

Initial $^{87}Sr/^{86}Sr$ ratios from lavas from the AVC range from 0.70507 to 0.70680, in keeping with the elevated values characteristic of the central Andes. $^{87}Sr/^{86}Sr$ of the AVC has no systematic variation with SiO_2 or Rb/Sr, but increases overall through time (**Figure 3.8, 3.9, 3.10, Table 3.2**). The Alconcha group has little variation in $^{87}Sr/^{86}Sr$ values, ranging from 0.7051 – 0.7055. Gordo andesites are relatively diverse (~0.7054 – 0.7065) with respect to Gordo dacites (~0.7057 – 0.7061). The Polán group, representing the most voluminous period of volcanism, has the narrowest range of values (0.7056 – 0.7059). The Aucanquilcha group has the highest $^{87}Sr/^{86}Sr$ values (0.70580 – 0.70680). Two andesitic enclaves from Aucanquilcha display high values with respect to the Aucanquilcha dacites. Three samples from the recently erupted monogenetic field to the east of the AVC also have elevated $^{87}Sr/^{86}Sr$ 0.70635 - 0.70683). Through time, andesites generally define the baseline $^{87}Sr/^{86}Sr$, but they also contain some of the highest values in the sample suite.

Trends observed in εNd more or less mirror those of the $^{87}Sr/^{86}Sr$ system (**Figure 3.8; Figure 3.11; Table 3.2**). εNd broadly decreases through time from -1 to -7.3, with the lowest values observed in lavas from Aucanquilcha (-4.5 to -7.3). Unlike for $^{87}Sr/^{86}Sr$, the largest range of εNd (-1.0 to -4.7) is observed in the earliest eruptive group, with a conspicuous lack of samples falling in the εNd range of -1.6 to -3.3. Lavas from the Gordo group range from -3.0 to -6.3. Similar to $^{87}Sr/^{86}Sr$, lavas from 4 – 2.5 Ma, the

peak AVC eruptive period, have restricted values (-3.8 to -4.9). The lavas from the monogenetic field have rather low εNd values (-6.1 to -6.6). As with the Sr isotopes, there is no correlation between Nd or SiO_2 and εNd. Additionally, andesites form the 'baseline' signature (the highest values in the case of εNd) only for the earliest eruptive group.

Lead isotopes of the AVC vary little: $^{206}Pb/^{204}Pb$ ranges from 18.47 to 18.70; $^{207}Pb/^{204}Pb$ ranges from 15.58 to 15.66; and $^{208}Pb/^{204}Pb$ ranges from 38.24 to 38.73 (**Figure 3.12, Table 3.2**). There is, however, subtle variation in $^{206}Pb/^{204}Pb$ through time with the lowest values found in the Alconcha group and the highest values in the Aucanquilcha group. With respect to basement Pb isotopic signatures, the AVC is situated on a basement transition zone between the older, less radiogenic Arequipa block to the north, and the younger, more radiogenic Antofalla block to the south. $^{206}Pb/^{204}Pb$ values for AVC lavas are, indeed, intermediate between the two basement blocks, but are consistent with a dominant Antofalla-block influence (**Figure 3.13**).

Oxygen isotopes from the AVC vary little, ranging from ~6.5 to 7.5‰ (**Figure 3.8, Table 3.2**) and are at the low end of the range for the central Andes (~5 to ~14 ‰; **Figure 3.14**). The earliest erupted lavas from the Alconcha group have the lowest $\delta^{18}O$ values and the least variation, ranging from ~6.5 to 6.75‰. After ~8 Ma, the lowest $\delta^{18}O$ values AVC lavas increase to ~6.8‰ during Gordo time (excluding one 6.5‰ value for sample AP-07-29). During Polán time, $\delta^{18}O$ values slightly increase further to ~7.0‰. From ~8 to 3 Ma, the highest $\delta^{18}O$ values are ~7.3 – 7.5‰. Lavas from Volcán Aucanquilcha have fairly restricted $\delta^{18}O$ values, ranging from 7 to 7.3‰, and although more felsic, have $\delta^{18}O$ lower than some older dacites. Plagioclase from the eroded scoria cone, Luna de Tierra, yielded a value of 7.1‰, similar to the rest of the AVC lavas. Plagioclase from the scoria cone Poruñita, however, yielded a much higher value of 9‰.

Discussion

Many studies have applied petrogenetic modeling to central Andean volcanic systems, and they all tell a broadly similar story: data suites define trends which can be interpreted as being the result of combined fractional crystallization and assimilation (AFC) (e.g., James, 1982; Davidson et al., 1990; Feeley and Davidson, 1994; Delacour et al., 2007). Such petrologic models have mass consequences and allow for the calculation of 1) the mass left behind due to crystallization 2) the amount of basalt needed to materially drive the system, and 3) the amount of crust assimilated. The inescapable problem with these models is the uncertainty associated with virtually every variable (e.g. the compositions of the parent magma and contaminant, the crystallizing assemblage, the efficiency of the assimilation process, the processes by which assimilation occurs). These problems are magnified when modeling modern central Andean systems, as the magmas were processed through very thick crust, probably at multiple levels with multiple contaminants. Despite these obstacles, it is probably not coincidental that many petrogenetic studies have arrived at similar numbers (15 – 20%) with respect to the amount of crustal component typical of evolved, modern central Andean arc lavas (eg., James, 1982; Davidson et al., 1990). As the AVC is time transgressive, we are in a unique position to investigate the petrogenetic *evolution* of this arc node over an eleven million year period.

We modeled variations in Cr, Rb, Sr, Ba, $^{87}Sr/^{86}Sr$, and ε_{Nd}, and $\delta^{18}O$ to gain insight into the processes producing data trends of AVC lavas, and in particular, individual eruptive groups. As variation in AVC trace element data is consistent with a component of fractional crystallization, and isotopic compositions implicate a crustal contribution, we present a set of AFC models to explain the compositional variation observed in erupted AVC lavas. Despite the variable and moderately "crustal" isotopic compositions overall, there is no correlation between isotopic composition and SiO_2, and lavas within all eruptive phases are isotopically very similar (see **Figure 3.9**). There is, however, an appreciable increase in $^{87}Sr/^{86}Sr$ and decrease in ε_{Nd} with time (see **Figure 3.11**).

Therefore, our models can be broken into two parts (see **Table 3.3** for distribution coefficients used in each model). First, we address the variation in the trace element data, which we explain by variable degrees of fractional crystallization from a basaltic andesite and mixing with a (cognate) granodiorite. Secondly, we address the varying crustal contribution as indicated by temporal changes in isotopic values. For lack of primitive rocks in the central Andes, we use a relatively primitive basalt from Puyehue volcano (southern Andes; Gerlach et al., 1988) as a surrogate parent composition, and gneisses from Chile and northern Argentina (Lucassen et al., 2001) as assimilants. Before presenting the models in detail, a few caveats warrant discussion. We first consider the nature of the parental magma, and the concept of the liquid line of descent, as it relates to our data suite.

Petrogenetic caveats

There are many ways that are proposed, and likely plausible, for the generation of intermediate arc magmas. Leading hypotheses are fractional crystallization from basalt (Ownby et al., 2010), crustal melting of a mafic protolith (Rapp and Watson, 1995), contamination of a mantle-derived basalt by partially melting crustal material (Mattioli et al., 2006), reaction of a basalt with crustal material (Patiño Douce, 1995) and mixing of basaltic magma with some more felsic component, be that a granitic mush or magma (Reubi and Blundy, 2009). A compelling case has also been made for the generation of primary andesite magmas (Baker et al., 1994, though see Streck et al., 2007). The reigning paradigm seems to be the "MASH" hypothesis (and its cousin, the "hot zone" model): a zone of melting, assimilation, storage, and homogenization in the lower crust where, perhaps, a combination of the above processes gives rise to hybrid intermediate magmas consisting of basalt derivatives, partially melted precursor basalts and cumulates, and crustal melts (Hildreth and Moorbath, 1988; cf. Dufek and Bergantz, 2005; Annen et al., 2006). However, petrologic work on basaltic arc volcanism has spotlighted the complexity researchers are up against when trying to unravel the sources of even the most primitive rocks (Leeman et al., 1990; Hart et al., 2003; Dungan and Davidson, 2004; Schmidt et al., 2008; Jicha et al., 2009; Schmidt et al., 2011). Melting of distinct mantle

domains and varying melting processes beneath a single volcano can produce isotopic and trace element variability from the outset of magma evolution (Reiners and Nelson, 1998), signals which are further obscured by MASH processes.

The nature of primitive magmas in the modern central Andes is the subject of much debate. The fundamental observation is that the most mafic of erupted lavas are basaltic andesites, which have high $^{87}Sr/^{86}Sr$ and $\delta^{18}O$, low εNd and enriched in some trace elements (e.g. Sr and Ba). These characteristics are generally considered to be signatures of crustal contamination of melts from a mantle that has a more or less constant isotopic composition ($^{87}Sr/^{86}Sr = 0.7035$, $\varepsilon Nd = 6$, $\delta^{18}O = 5.8$). Any deviation from these values is attributable to contamination by material in the crustal column through which the magma travels before eruption. High concentrations of incompatible elements such as Ba and Sr can be attributed to basaltic recharge in a deep crustal MASH zone.

Alternatively, the enriched signatures involve a heterogeneous (or "polluted") mantle, which varies in isotopic composition, thereby producing isotopically variable basalts when melted. Proposed mechanisms for mantle variability include subduction erosion (Stern, 1991; Kay et al., 2005) and removal of the lower crust through delamination (Kay and Kay, 1993; Lackey et al., 2005; Drew et al., 2009), both of which would produce an enriched subcontinental lithospheric mantle (Rogers and Hawkesworth, 1989; Lackey et al., 2005; Drew et al., 2009). Additionally, the influx of enriched (OIB-like) asthenosphere, which perhaps not coincidentally would likely accompany delamination, could also produce the proposed mantle variability (Hoke and Lamb, 2007). Relevant to this argument is the ~23 Ma basaltic sill at Chiar Kkollu, ~200 km northeast of the AVC in the Bolivian Altiplano, which preserves relatively primitive isotopic signature ($^{87}Sr/^{86}Sr = 0.70405$, $\varepsilon Nd = 3.2$) and suggests that a non-enriched mantle does, or did, exist beneath the CVZ (cf. Davidson and de Silva, 1992; Davidson and de Silva, 1993; Lamb et al., 1993; Hoke and Lamb, 2007). For the second part of our modeling—dealing with the production of intermediate magmas from a mafic source—we use parental basalt a composition consistent with derivation from a subarc mantle that is not anomalously

enriched (see below). If the mantle below the CVZ is indeed polluted, less intracrustal assimilation is implicated than our model predicts.

Liquid Lines of Descent

It is important to point out that the suite of data presented here does not represent a strict liquid line of descent (cf., Eichelberger et al., 2006). The spatial and temporal patterns of the AVC suite indicate an overall relationship, even if not strict consanguinity, and invite consideration of the processes that acted through time. Trace element and isotopic diversity of the basaltic andesites to andesites sampled at the AVC evidences the breadth of intricacies that crustal processing is capable of producing, as well as the potential diversity of basaltic parents. This variability among potential mafic parental magmas, however, gives way to a suite of dacites that are broadly similar at each successive stage, suggesting that crustal processes are efficient at attenuating input diversity, and are highly repeatable. The general decrease of compatible elements with SiO_2 indicates a substantial role for crystal fractionation. Linear arrays within the AVC data cloud and the abundance of crystals in many lavas as well as the textural and compositional diversity of minerals are evidence for mixing and self-mixing. The isotopic compositions and temporal trends implicate significant involvement of crustal material, the amount and (or) composition of which changes with time.

Petrogenetic modeling of observed variation within AVC lavas

Fractional crystallization

With respect to Rb, Sr, Ba, and Cr, we show crystal fractionation models to account for varying influences of different minerals (**Figure 3.15; Table 3.3**). Taken together, crystal fractionation appears to have been a dominant process at the very outset of the AVC history (Alconcha 1 subgroup) and at the end (Aucanquilcha group) with an increasing role of amphibole with time. Volcan Miño, on the periphery of the AVC also has a strong record of fractionation.

The first fractionation model is consistent with an andesitic crystallizing assemblage: 72% plag, 12% opx, 10% opx, 6% magnetite (FCpx). A second fractionation model shows the effect of a dacitic crystallizing assemblage: 68% plagioclase, 9% clinopyroxene, 9% amphibole, ~4.5% each of orthopyroxene, biotite, and magnetite (FCam). These assemblages were chosen based on observed crystal contents in AVC lavas. We chose the most mafic Mino andesite as a starting composition (VM99-16; McKee, 2002) for models FCpx and FCam. The fractionation trends drive a strong depletion in Cr coupled with a steep increase in Rb after about 25% crystal removal. This path reasonably describes the distribution of Alconcha 1 samples and the Mino Group with, up to ~ 60% crystallization of the pyroxene-dominated assemblage, which in turn is consistent with little variation in Dy/Yb for these subsuites (**Figure 3.5**).
Lavas from Volcán Aucanquilcha have a trajectory with respect to Ba versus Rb/Sr as well as Rb versus Cr that is parallel to the amphibole-bearing fractionation trend, but emanates from a more evolved parental andesite (**Figure 3.15**). We show a second set of fractionation trajectories (FCpx2, FCam2) that account for much of the variation in the Aucanquicha group (**Figure 3.16**). The overall decrease in Dy/Yb within the Aucanquilcha group with SiO2 is consistent with a significant role for amphibole fractionation.

Most samples of the AVC are not consistent with such a fractionation trends. To reproduce the high-Rb/Sr, low-Ba trend through fractional crystallization alone, unrealistic distribution coefficients and unreasonable amounts of crystallization (>90%) would have to be called upon. Most samples are too high in Rb relative to Cr to be described by fractionation model. Therefore, we consider the effects of magma mixing or high degrees of assimilation relative to fractionation to account for the compositional variability of AVC lavas.

Magma mixing

Magma mixing has been invoked, with mounting frequency, as an important process in the production of evolved arc lavas (e.g. Eichelberger, 1975; Bacon, 1986). In particular, crystal scale studies have shown again and again that open system processes such as magma mixing, crystal recycling and crustal contamination are prevalently recorded in volcanic rocks (Nakamura, 1995; Tepley et al., 2000; Humphreys et al., 2006; Ruprecht and Wörner, 2007; Streck, 2008; Salisbury et al., 2008; Francalanci et al., 2011). Extensive crystal recycling within AVC lavas has been demonstrated by zircon age data (Walker et al., 2010) and amphibole, pyroxene, and Fe-Ti oxide compositions (Giles, 2009; see also Chapter 4). However, because crystal recycling at the AVC likely involves the same minerals as are fractionating, the two processes mutually obscure trace element distributions and cannot be distinguished with respect to major elements. The trace element variability of most AVC lavas and the temporal increase in crustal isotopic signatures cannot be adequately explained by fractional crystallization alone.

The production of an intermediate magma from mixing of a mafic parent with a felsic component obviously requires that the felsic component exist, be it a product of fractional crystallization and(or) melting of pre-existing crust. Elemental and isotopic variation of eruptive suites thought to arise from magma mixing provide constraints on the nature and origin of the end-members. At the AVC, isotopic variation with SiO_2 (and other fractionation indices) within eruptive suites is minimal (see **Figures 3.9, 3.10**), suggesting the silicic end-member is isotopically similar to the mafic end-member, albeit both are changing in time. We postulate that the silicic end-member is genetically related crystal-laden magma and (or) plutonic material.

Cognate plutonic blocks are common in lavas (i.e., Conrad et al., 1983; Watts et al., 1999; Leonard et al., 2002; Bacon and Lanphere, 2006), sometimes preserving textures of partial melting (Bacon, 1992). Near the AVC, at the Cerro Chascon-Runtu Jarita dome complex (within the Altiplano-Puna ignimbrite field), Watts and others (1999) observed biotite-granodiorite clasts in a small pyroclastic eruption (sample CC17 from Watts et al., 1999). While not genetically related to the AVC magmas, the clasts represent an evolved

granodiorite composition in the local crust and are an analog for the product of dacite crystallization. These granodiorite clasts have relatively low Ba contents (~600 ppm) with respect to AVC lavas, likely owing to alkali feldspar fractionation. (Alkali feldspar is very rarely observed in AVC lavas). This is important in that many AVC dacites trend toward low Ba values at high Rb/Sr consistent with mixing with a cogenetic granodiorite or granodioritic mush composition similar to that reported by Watts and others (1999). Up to 50% mixing is implicated on chords between potential mafic parents on the fractionation trend and a proposed range of felsic end-members that was cogenetic, cognate plutonic material, which would be isotopically the same as the lavas. We envision the silicic end-member to comprise a mixture of dissolved crystals (such as quartz, alkali feldspar, and biotite) and crystals that survive and are re-entrained (such as plagioclase, amphibole, zircon, etc.). Essentially, this is mush remobilization (cf., Bacon and Lowenstern, 2005).

The mixing signal is strongest for dacites of the Alconcha 2, Gordo, and Polán groups (**Figure 3.15**). The Gordo and Polán groups, in particular, are times characterized by more voluminous volcanism and presumably plutonism as well—the thermal maximum for the AVC system. These data suggest these times of increased activity were also associated with mixing and homogenization of magmas, likely in the upper crust based on their mineral assemblages (see Chapter 4). During this time of homogenization and mixing, we envision an upper crustal patchwork plutonic network consisting of melt-rich domains (magma chambers) within a matrix of totally solid rock to crystal-rich magma mush. The thermal maturity of the plutonic system—with a low thermal contrast between magma and host rock—would promote an environment where fresh magmatic invasions are more likely to remobilize surrounding plutonic material, ultimately leading to the eruption of mixed magmas. In contrast, dacites from the Alconcha 1 and Aucanquilcha groups are dominated by a fractionation signal. These lavas erupted during times of low volcanic output, and presumably when the AVC was thermally either immature or waning. The fractionation-dominant nature of these lavas evidence their derivation from a system where mixing was at a minimum, envisioned here as a series of

discrete magma chambers where little interaction between magma and host rock occurred. Lavas from Volcán Miño are also fractionation dominant. Although Miño was active during the high flux period of the AVC, it is peripherally located. Magma chambers feeding eruptions to Volcán Miño are therefore likely to have been relatively autonomous with respect to the main magmatic plexus.

Mass balance of the fractional crystallization/magma-mixing model

Basic mass balance constraints can be placed on the amount of crystal residue is left behind during fractionation and magma mixing accompanying the evolution of AVC magmas (see **Table 3.4**). AVC andesites that fall on the crystal fractionation trend indicate up to ~40% fractionation from the Miño basaltic andesite, while dacites indicate ~60% fractionation (~50% for Volcán Aucanquilcha lavas). With respect to these fractionation trends, the mixing clouds emanate from a range in compositional space, coincident with F-values of ~1 – 0.6 (0 – 40% crystallization). We use an F-value of 0.8 to represent the average amount of fractionation experienced by the mixed magmas *before* they were mixed. Based on these observations, and assuming a total eruptive volume for the AVC of 350 km^3, ~175 km^3 of cumulate residue from fractional crystallization is implicated (see **Table 3.4**). Materially, then, ~525 km^3 of magma, similar in composition to the Miño basaltic andesite starting composition, was required to produce the 350 km^3 of erupted AVC lavas. This estimate is almost certainly a minimum, as the silicic mixing end-member, comprising ~125 km^3 of material, is likely the result of a fractionation-dominated process as well.

Petrogenetic modeling of basalt differentiation: the missing link

Time-transgressive isotopic variation

Isotopic variation within individual eruptive phases is small and not correlated with a fractionation index. In fact, as much or more isotopic variability is observed within the andesites of any given eruptive period, as in the entire compositional spectrum. This tendency for the mafic end members to display more isotopic variability has been

recognized before (Feeley et al., 1993; Barnes et al., 2005; Jicha et al., 2009), and likely illustrates two things. One is the homogenization effect that comes with crustal processing, involving the confluence and compositional averaging of a large amount of material (see Grunder and Mahood, 1988; Ruprecht and Wörner, 2007). Second is susceptibility of mafic magmas to isotopic (Nd, Sr, Pb) contamination through assimilation of small degrees of wet crustal melts that can lower the liquidus of the ascending magma (Reiners et al., 1995; Bohrson and Spera, 2001). Regardless, temporal isotopic shifts with system evolution are undeniable at the AVC, and this trend can be explained two ways. First, it could represent the tapping of a progressively polluted mantle. Second, it could represent the addition of either *more* or *different* crustal components to AVC magmas as time and system evolution progressed.

No basalts—primitive or otherwise—have erupted in central Andes in the past 20 million years. Basaltic andesite to andesite lavas provide the baseline composition at every eruptive center in the central Andes, whereas andesites and dacites are the dominant rock type. We have shown that bulk rock compositional variation within eruptive suites at the AVC is likely attributable to crystal fractionation and magma mixing, with little evidence for isotopic contamination (see **Figures 3.9, 3.10,** and **3.15**). There are, however, isotopic shifts through time. Because these isotopic shifts occur concurrently with the development of such a long-lived magmatic system as the AVC, we do not find it necessary to invoke a changing mantle source as the cause. Rather, these isotopic signatures can be feasibly acquired in a deep crustal MASH zone, and accompany the chemical evolution from basalt to andesite. This evolution, however, is simply not preserved in the form of a liquid line of descent (real or perceived)—it is a petrological missing link. To put basic constraints on magma production at the AVC, we cautiously model this missing link using hypothetical parent and assimilant compositions. We do not think all mantle-derived basalts are the same. We nevertheless choose a single non-enriched mantle source from the southern Andes where crustal overprinting is not so prevalent.

Crustal contamination constraint from $\delta^{18}O$

When considering crustal contamination, oxygen isotopes ($\delta^{18}O$) are more robust than the Sr and Nd systems, as oxygen makes up roughly 50% (mass) of silicate magma, rather than trace concentrations of Sr and Nd. Putative end member compositions can be better estimated. Based on a worldwide compilation, Harmon and others (1995) demonstrate that MORBs have a uniform $\delta^{18}O$ composition of ~5.7‰, though basalts from other tectonic settings are more variable. They suggest, however, that the slight $\delta^{18}O$ enrichment seen in continental arc basalts is due to interaction with crustal material. We choose a value of ~6‰ for primitive basalts beneath the CVZ. There are very few $\delta^{18}O$ data available for the central Andean basement rocks; values range from ~7 – 12 (Wörner, pers. comm.). This roughly coincides with the $\delta^{18}O$ values of nearby lavas which, near the latitude of the AVC, range from ~6 to 14 ‰ (**Figure 3.14**).

Throughout the eruptive history of the AVC, $\delta^{18}O$ compositions of the lavas vary little, with a total range over eleven million years of 6.5 – 7.5 ‰—values that are low relative to the CVZ overall. Nearby CVZ volcanoes display as much or more variation over a few 100,000 years: Ollagüe lavas range from 7.1 to 8.1 ‰ (Feeley and Sharp, 1995), and Parinacota from 6.8 to 8.4 ‰ (Davidson et al., 1990). Unlike with the Sr and Nd isotopic systems, we do not observe an appreciable shift in $\delta^{18}O$ with time (see **Figure 3.8**). In fact, $\delta^{18}O$ values for Volcán Aucanquilcha are actually lower than the highest values from earlier AVC lavas. This narrow range of relatively low values of $\delta^{18}O$ may be attributable to the homogenization effect of prolonged magmatism. Progressive construction and consolidation of the AVC plutonic system would armor the magma plexus in such a way as to restrict access to crustal rocks, promoting precursor recycling and system homogenization. Alternatively, or perhaps attendant to this homogenization, the low range of $\delta^{18}O$ may be attributable to the assimilation of hydrothermally altered rocks, particularly for the Aucanquilcha group (cf. Friedman et al., 1974; Grunder, 1987; Feeley and Sharp, 1995; Bindeman and Valley, 2001). With the long duration of the Aucanquilcha system, it is likely that a hydrothermal system developed above and around main magma plexus. Pervasive alteration of various AVC edifices (Aucanquilcha, Polán,

Tres Moños, Koska) confirms this at the surface. If hydrothermal upper portions of the magma plexus were involved, Sr and Nd isotopes indicate such material added to AVC magmas in the upper crust was similar to the magmas with respect to these isotopes.

Assuming, that shifting of $\delta^{18}O$ by hydrothermal material is fairly minimal, except for the Aucanquilcha group, mixing calculations suggest that there was no considerable contribution of high $\delta^{18}O$ crust to produce AVC lavas (**Table 3.5**). Fractionation from basalt to andesite would increase the $\delta^{18}O$ by ~0.5‰ (cf. Taylor and Sheppard, 1986). However, even with slight enrichment through crystal fractionation, δ18O values are too high to be caused by fractionation alone. If the contaminant has a $\delta^{18}O$ of 10‰, ~ 30% crustal addition is required to generate the highest $\delta^{18}O$ (~7.5‰) observed in AVC lavas. If the contaminant's $\delta^{18}O$ is lower than 10‰, more crust would be required (**Table 3.5**).

AFC model using Sr and Nd isotopes

Reconciling the Sr, Nd, and O data requires a broad approach. We here employ AFC equations (DePaolo, 1981) to provide constraints on minimum amounts of crustal involvement through time. We also address the shift in baseline isotopic signature of the AVC data array with respect to O, Sr, and Nd isotopes. By baseline, we mean those samples that are most primitive with respect to the given isotopic system (low $^{87}Sr/^{86}Sr$ and $\delta^{18}O$; high ε_{Nd}). As a hypothetical parental magma, we use a relatively primitive lava from the Southern Volcanic Zone in Chile (from Puyehue volcano [sample IB-7 from Gerlach et al., 1988]). For an assimilant, we tested a variety of compositions from basement rocks exposed in the central Andes (Lucassen et al., 2001). In particular, we focused on gneisses from Chile and northern Argentina. While it is uncertain that exposed gneisses represent the rocks at depth, Pb isotopes permit that several Chilean and Argentinian gneisses are plausible contaminant compositions. These basement rocks, however, are highly variable in their isotopic compositions, with $^{87}Sr/^{86}Sr$ ranging from ~0.7033 – 0.8399 (Sr ppm ranging from ~10 to ~1,400) and εNd from +5 to -13 (Nd ppm ranging from ~5 to 65) (**Figure 3.13**). Rocks with the highest $^{87}Sr/^{86}Sr$ have the lower Sr concentrations, limiting their leverage on the magma composition (e.g. almost all

basement rocks with $^{87}Sr/^{86}Sr$ >0.720 have Sr contents of <250 ppm). Nd isotopic variability is still appreciable, though less dramatic than $^{87}Sr/^{86}Sr$. From broad this array, we narrowed our choice of contaminant to a subset of these rocks that overlap AVC Pb isotope compositions, though this subset still varies considerably with respect to isotopes (**Figure 3.16**).

Accounting for the diversity observed in the basement rocks, we provide three examples of AFC calculations, using three different contaminants that represent a wide range of isotopic and elemental compositions (**Figures 3.17, 3.18**). From the hypothetical parent basalt, we modeled the assimilation and fractional crystallization necessary to produce a daughter magma with εNd of -6 and $^{87}Sr/^{86}Sr$ of 0.706. These isotopic compositions represent average values for AVC lavas and, as such, should approximate average amounts of assimilation necessary for production of AVC lavas. In this way, basic constraints are put on the petrogenetic processes. Additionally, we tested a range of R-values (assimilation rate/crystallization rate), and note that in acceptable models—those that adequately account for the variation of all modeled elements and isotopic ratios—increasing the R-value results in higher F- values, indicating less crystallization (see **Figure 3.19** and **Tables 3.6 & 3.7**). This has significant mass balance consequences when considering the generation of an appropriate volume of basaltic andesite (~500 km^3), implicated by the trace element fractionation model discussed above, from the surrogate parental basalt. Our Sr and Nd isotope modeling suggests that, for R = 0.3, between ~700 km^3 and ~2700 km^3 of cumulate residue is required, depending on the assimilant. For R = 0.7, ~100 – 300 km^3 of crystals are required (**Figure 3.20** and **Table 3.7**). Based on the overall fit for both $^{87}Sr/^{86}Sr$ and ε_{Nd}, we think an R-value of ~0.5 is reasonable, yielding ~250 – 1000 km^3 of unerupted crystals during the evolution from basalt to basaltic andesite. Despite this large estimate range for cumulate crystal volume, the contaminant contribution estimate does not dramatically vary with a changing R-value (cf., Grunder, 1992; see **Figure 3.19 & Table 3.6**). As such, no model requires more than ~35% crust in AVC lavas (**Figure 3.19**). These figures are consistent with feasible crustal percentages according to $\delta^{18}O$ values (**Table 3.5**).

If a single AFC model—with a single contaminant—were used to describe the temporal variation of the AVC data, it would suggest that crustal contamination became a progressively more important process through time. However, we consider it unlikely that the least voluminous volcanic period would involve the most crustal assimilation in its magma genesis. Peak assimilation rates more plausibly would accompany the time of peak power in a magma system, as the digestion of crustal rocks by magma requires significant thermal addition (eg. Bohrson and Spera, 2001). We therefore think it probable that as the AVC magma system evolved, the nature of the assimilated crust changed; throughout its evolution, the magma system encountered crust that was progressively higher with respect to $^{87}Sr/^{86}Sr$ and lower with respect to ε_{Nd} through time. The relatively similar $\delta^{18}O$ values through time indicate the crustal rocks may be more uniform with respect to oxygen isotopes.

An Expanding MASH Zone

Hildreth and Moorbath (1988) postulated that one might expect to see a gradual increase in base-level $^{87}Sr/^{86}Sr$ values at long-lived centers, in the case of an expanding MASH zone. We think the base-level increase in $^{87}Sr/^{86}Sr$ and $\delta^{18}O$ in conjunction with the decrease in ε_{Nd} of AVC lavas is consistent with such a hypothesis. We thus envision the result of an eleven million year history of basaltic underplating to be an upwardly migrating MASH zone. Concurrent downward expansion of the MASH zone is predicted, as well, as successive batches of underplating basalt are trapped and stored. As such a zone expanded upward, it would no doubt reconstitute the crust, depleting fusible materials and/or bulk assimilating, possibility via a reactive process (Patiño Douce, 1995; Beard et al., 2005). The isotopic shifts observed at the AVC, then, can be explained by the assimilation of isotopically more evolved rocks as the MASH zone accessed higher levels in the crust.

Lead isotopes bear on this problem as well. The AVC is located in a transition zone between the Arequipa and Antofalla crustal provinces, demarcated by Pb isotopes. Based on Pb isotopic compositions of lavas erupted along the arc in this transition zone, Wörner and others (1992), proposed in a simple model that the central Andean crust is stratified with respect to age and isotopic composition. In particular, they show that the Antofalla block (relatively high $^{206}Pb/^{204}Pb$) dominates the middle and upper crust, while rocks of the Arequipa block (relatively low $^{206}Pb/^{204}Pb$) are present at depth. The subtle temporal variation in Pb isotopes from AVC lavas (**Figure 3.12**) support this; $^{206}Pb/^{204}Pb$ values from Alconcha group lavas are, in general, the lowest while $^{206}Pb/^{204}Pb$ of Aucanquilcha lavas are the highest. A MASH zone migrating through such a crustal stratigraphy as proposed by Wörner and others (1992) would produce the Pb isotopic variation observed at the AVC.

The garnet signature

It has been recognized by various workers that there is a correlation with crustal thickness and REE fractionation in igneous rocks that are processed through a thickened crust (Hildreth and Moorbath, 1988; Davidson et al., 1991; McMillan et al., 1993; Kay et al., 1999; Haschke et al., 2002; Mamani et al., 2010). Heavy REEs (HREEs) are fractionationed with respect to middle REEs (MREES) by the partial melting of rock in which garnet is residual and/or the crystallization of garnet, as garnet prefers the HREEs to the MREEs. Mamani and others (2010) showed that central Andean rocks have had elevated MREE/HREE (Dy/Yb and Sm/Yb) ratios since ~30 Ma, corresponding to stabilization of garnet owing to crustal thickening. They note the increase of maximum values of MREE/HREE in central Andean lavas erupted since ~3 Ma, which we also observe in AVC lavas (see **Figure 3.5**). In general, we agree with their conclusions that this signal is related to increased garnet fractionation during magmatic differentiation.

At >60 km deep, the base of the central Andean crust is deep enough to stabilize garnet in a basaltic magma, even at elevated water contents (Green, 1982). Experiments by

Müntener and others (2001) and Müntener and Ulmer (2006) also demonstrate copious garnet crystallization from a basaltic andesite at high pressure. Natural examples of garnet residua from arc basalt crystallization include garnet-bearing xenoliths from the Sierra Nevada (Ducea and Saleeby, 2008; Ducea, 2002; Lee et al., 2006) and lower crustal (near Moho) sections from the Kohistan arc (Jagoutz et al., 2006; though see also Garrido et al., 2006).

At the AVC, the pronounced increase in Dy/Yb through time tracks the shift observed in Sr, Nd, and O isotopes. Time-integrated basaltic underplating would likely produce a thick, hot region at the base of a thickened crust, which would, in turn, intercept successive basalt injections, promoting the downward growth of the MASH zone. We envision prodigious garnet crystallization to occur here. With repeated basalt injection and the thickening of the MASH zone through time, it is also expected that garnet would form as a melting residuum from precursor basalt (cf. Ratajeski et al., 2005). Finally, preexisting crustal material incorporated into the MASH zone at such great pressures would most likely have residual garnet, further increasing the garnet signature. Intriguingly, the end result of such a process would be a large, refractory, and probably gravitationally unstable mass at the base of the crust, such as that currently imaged at the latitude of the AVC (Giese et al., 1999; Schmitz et al., 1997; Yuan et al., 2002).

System architecture

There is a preference amongst the volcanological community for a two-tiered conceptual model of arc magmatism whereby basaltic magma intrudes the base of the crust and (1) undergoes a vigorous MASH and/or AFC process, presumably with a high assimilation component, the compositionally intermediate product of which ascends to the upper crust where (2) further differentiation occurs, dominantly through crystal fractionation (c.f. Feeley and Davidson, 1994; Hart et al., 2003; Annen et al., 2006; Ownby et al., 2010). Exhumed exposures of deep arc crust—natural examples of this process— are rare. However, several relatively continuous exposures that preserve middle crustal depths

such as the north Cascades (Miller et al., 2009), the Salinian block (Kidder et al., 2003; Saleeby et al., 2003), and the Valle Fértil complex in northern Argentina (Otamendi et al., 2009) demonstrate igneous rocks are present as deep as exposure permits a view. Crustal exposures from Kohistan (Bard et al., 1980; Garrido et al., 2006) and Talkeetna (Debari and Coleman, 1989; Greene et al., 2006; Rioux et al., 2007) mafic complexes confirm this in the lower crustal setting as well. In north Cascades exposure of Cretaceous arc crust, Miller and others (2009) conclude that plutonic rocks are volumetrically significant at all levels, and highlight that, with increasing paleo-depth, a greater percentage of rocks are igneous (from ~37% at ~5 km to ~65% at ~30 km). They observe that shallow level plutonism is characterized by large batholiths (with few unfocused, discrete bodies), indicating the upper crust is a site of pluton consolidation and magma homogenization. Lower crustal exposures, though, also contain batholith-scale bodies, albeit with a greater amount of small-sized intrusions as well. Field data from the Ordovician Valle Fértil complex in Argentina support this idea of a continuous magmatic section. There, exposures reveal a gradational batholith ranging from gabbros to tonalites to granodiorites, with pressure estimates ranging from ~8 kbar to ~4 kbar (Otamendi et al., 2009; Otamendi et al., in press).

While plutonic sections are time-integrated documents of magmatism, likely with *in situ* homogenization and overprinting giving rise to an emergent architecture (Walker et al., 2007), their relevance to the crustal consequences of arc magmatism is unequivocal. When considering the underpinnings of the Aucanquilcha Volcanic cluster, then, we interpret our geochemical data with deference to such crustal exposures, where crustal reconstitution appears to be the general observation. The volcanic record at the AVC is essentially a broad pulse, with its most voluminous period occurring about half way through its lifetime. Whatever the cause for this volcanic pulse, the erupted material is likely to be but the icing on the cake—the surface expression of a complex magmatic miasma that assembled incrementally over eleven million years. Throughout that time, we envision the crust beneath the AVC to have experienced significant magmatism, with plutonic bodies forming at all levels throughout the crustal column (**Figure 3.21**). As

magmatism progressed, smaller bodies likely merged to form larger ones, and heterogeneities were mixed or erased to a certain extent. The lavas erupted during the volume peak of the pulse likely drained a patchwork mush network at depth—a system at its peak power that was accompanied by a thermal regime whereby there was a relatively low thermal contrast between intruding magma batches and their wall rock, be it plutonic precursors or not.

Magmatic Pulsing

Over the last ten million years or so, central Andean volcanism has been broadly distributed and extremely voluminous, giving rise to the Altiplano-Puna "ignimbrite flare-up" and other moderate- to large-volume arc to behind-arc volcanic centers. The high-resolution geochronological breakdown of the Altiplano-Puna ignimbrites (Salisbury et al., 2011) demonstrates a pulsatory history of volcanism, with major pulses at ~8.4 Ma, ~5.6 Ma, 4 Ma, ~3 Ma. Geochronological data from the Aucanquilcha cluster, although more sparse, indicates a clear eruptive pulse from ~5.5 to ~2 Ma (Grunder et al., 2006; Klemetti et al., 2008), coinciding with the three largest pulses of the Altiplano-Puna ignimbrite field. Aside from the steady state subduction that is likely to be at play along the main arc, this regional-scale pulsing is suggestive of some larger, common process. For the magmatic pulses at the Sierra Nevada Batholith, Ducea and Barton (2007) suggest massive crustal reorganization events, involving mostly crustal material. Conversely, for the Southern Rocky Mountain Volcanic Zone, Johnson and others (1990) and Riciputi and others (1995) interpret the magmatic pulse to represent a significant mantle addition to the crust. For the Timber Mountain complex in southern Nevada, Farmer and others (1991) come to a similar conclusion—namely, that the crust becomes more mantle-like with prolonged magmatism.

The eruptive history at the AVC, and in particular its eruptive flare-up from ~5 – 2 Ma, provides another perspective on this argument. If the AVC magmatic pulse was largely due to crustal reorganization, or more specifically, the introduction of large amounts of

crustal melt into the magma system, a correlative departure to crustal isotopic values (high $^{87}Sr/^{86}Sr$ and $\delta^{18}O$; low ε_{Nd}) would be expected, especially during the time of the eruptive flare-up. Granted, the AVC isotopes are relatively contaminated with respect to what is considered primitive mantle, and there is a systematic isotopic shift to contaminated values. However, we do not observe a dramatic shift in isotopic values that temporally coincides with the eruptive flare-up. Instead, we observe a rather narrow range of Sr and Nd isotopic compositions from that time (**Figure 3.8**). These isotopic trends suggest that the dramatic increase in eruptive output was not the result of peak rates of crustal addition, but rather the result of peak rates of mantle delivery and thermal modulation in the crust accompanied by modest crustal input. Therefore, at the AVC, it appears that crustal formation, rather than crustal recycling is the dominant process of the modern eruptive pulse.

Conclusions

Erupted lavas at the Aucanquilcha Volcanic Cluster document eleven million years of stationary and relatively continuous arc volcanism in the central Andes. Bulk compositional trends of AVC lavas indicate that fractional crystallization and recycling of precursor magmas (magma mixing) are the most important processes generating compositional diversity observed in any given eruptive phase. Time transgressive trends suggest that the high flux period of AVC volcanism (5 – 2 Ma) was characterized by magma mixing and mush remobilization, likely leading to the development and homogenization of a large, upper crustal batholith. Lavas from the beginning and waning phases of AVC volcanism lack this strong mixing signal, suggesting these low-flux times were characterized by disparate, physically isolated magmatism.

All AVC lavas are isotopically contaminated (high $^{87}Sr/^{86}Sr$ and $\delta^{18}O$, low εNd) with respect to primitive mantle and have pronounced garnet signatures (elevated Dy/Yb ratios). Though bulk compositions do not change appreciably, the baseline isotopic

signature and the Dy/Yb ratios of AVC lavas increase through time, suggesting the site of the isotopic contamination and acquisition of garnet signature was likely the middle to deep crust where higher temperatures and pressures promote fusion of crustal material and/or reactions between crust and basaltic magma. Time-integrated basaltic underplating and an expanding zone of melting, assimilation, homogenization, and storage (MASH) likely influence, to a first order, this progressive evolution. With prolonged magmatism, successive basalt injections into such an expanding MASH zone would be increasingly intercepted, where prodigious crystallization of garnet is likely to occur. The large, blurred MOHO from ~50 – 80 km beneath the AVC is probably the result of such protracted MASH expansion. Incorporation of crustal material with residual garnet likely enhances the garnet signal.

The eruptive flare-up from ~5 – 2 Ma at the AVC is characterized by a focusing of Sr and Nd isotopes, suggesting that the increased system power was mantle derived, and not a feedback from crustal incubation and melting. Sr, Nd, and O isotopes are consistent with a crustal component making up 10 - 30% of AVC lavas, implying that although the history of central Andean magmatism is replete with large scale crustal recycling, the current phase is largely a crust formation event.

References

Annen, C., Blundy, J. D., Sparks, R. S. J., 2006, The genesis of intermediate and silicic magmas in deep crustal hot zones, *Journal of Petrology* 47 (3), 505-539.

Bacon, C.R., 1992, Partially melted granodiorite and related rocks ejected from Crater Lake caldera, Oregon. *Transactions of the Royal Society of Edinburgh, Earth Science* 83, p. 27-47.

Bindeman, I.N., Valley, J.W., 2001, Low-$\delta^{18}O$ rhyolites from Yellowstone: Magmatic evolution based on analyses of zircons and individual phenocrysts. *Journal of Petrology* 42 (8), p. 1491-1517.

Bindeman, I.N., Ponomareva, V.V., Bailey, J.C., Valley, J.W., 2004, Volcanic arc of Kamchatka: a province with high-δ18O magma sources and large-scale 18O/16O depletion of the upper crust. *Geochimica et Cosmochimica Acta* 68, 841–865.

Bohrson,, W.A., Spera, F.J., 2001, Energy-constrained open-system magmatic processes II: Application of Energy-Constrained Assimilation-Fractional Crystallization (EC-AFC) model to magmatic systems. *Journal of Petrology* 42 (5), p. 1019-1041.

Conrad, W.K., Kay, S.M., Kay, R.W., 1983, Magma mixing in the Aleutian arc: evidence from cognate inclusions and composite xenoliths. *Journal of Volcanology and Geothermal Research* 18 (1-4), p. 279-295.

Davidson, J.P., McMillan, N.J., Moorbath, S., Wörner, G., Harmon, R.S., Lopez-Escobar, L., 1990, The Nevados de Payachata volcanic region (18°S/69°W Chile) II. Evidence for widespread crustal involvement in Andean magmatism. *Contributions to Mineralogy and Petrology* 105, p. 412-432.

Davidson, J.P. , Harmon, R.S, and Worner, G., 1991. The source of central Andean magmas: Some considerations. In: Andean Magmatism and its Tectonic Setting, eds. R.S. Harmon and C.W. Rapella, *GSA Special Paper* 265; 233-244

de Silva, S.L., 1989, Altiplano-Puna volcanic complex of the central Andes: Geology, v. 17, p 1102-1106.

de Silva, S.L., and Gosnold, W.D., 2007, Episodic construction of batholiths: Insights from the spatiotemporal development of an ignimbrite flare-up: Journal of Volcanology and Geothermal Research, v. 167, p. 320-335.

DeCelles, P.G., Ducea, M.N., Kapp, P., Zandt, G., 2009, Cyclicity in Cordilleran orogenic systems. *Nature Geoscienes* 2, 251 -257.

Delacour, A., Gerbe, M.C., Thouret, J.C., Wörner, G., Paquereau-Lebti, P., 2007, Magma evolution of Quaternary minor volcanic centres in southern Peru, central Andes. *Bulletin of Volcanology* 69, p. 581-608.

DePaolo, D.J., 1981, Trace element and isotopic effects of combined wallrock assimilation and fractional crystallization. *Earth and Planetary Science Letters* 53 (2), p. 189-202.

Ducea, M.N., Barton, M.D., 2007, Igniting flare-up events in Cordilleran arcs, *Geology* 35 (11), 1047-1050.

Dufek, J., and Bergantz, G.W., 2005, Lower crustal magma genesis and preservation: a stochiastic framework for the evaluation of basalt – crust interaction, Journal of Petrology 46 (11), 2167-2195.

Farmer, G.L., Broxton, D.E., Warren, R.G., Pickthorn, W., 1991, Nd, Sr, and O isotopic variations in metaluminous ashflow tuffs and related volcanic rocks at the Timber Mountain/Oasis Valley Caldera Complex, SW Nevada: implications for the origin and evolution of large-volume silicic magma bodies, *Contrib. Mineral. Petrol.* 109, 53-68.

Feeley, T.C., Sharp, Z.D., $^{18}O/^{16}O$ isotope geochemistry of silicic lava flows erupted from Volcán Ollagüe, Andean Central Volcanic Zone, *Earth and Planetary Science Letters* 133 (3-4), ps. 239 – 254.

Feeley, T.C., Davidson, J.P., and Armendia, A., 1993. The volcanic and magmatic evolution of Volcan Ollague, a high-K, late Quaternary stratovolcano in the Andean Central Volcani Zone.. *J. of Volcanology and Geothermal Res*., v. 54, p. 221-245.

Feeley, T.C., and Davidson, J.P., 1994. Petrology of calcalkaline lavas at Volcan Ollague and the origin of compositional diversity at the Central Andean stratovolcanoes. *J. Petrol.* V. 53(5), p. 1295-1340.

Francis, P.W., Thorpe, R.S., Moorbath, S., Kretzschmar, G.A., Hammill, M., 1980, Strontium isotope evidence for crustal contamination of calc-alkaline volcanic rocks from Cerro Galan, northwest Argentina. *Earth and Planetary Science Letter* 48, p. 257-267.

Friedman, I., Lipman, P.W., Obradovich, J.D., Gleason, J.D., Christiansen, R.L., 1974, Meteoric water in magmas. *Science* 184 (4141), p. 1069-1072.

Giese, P., Scheuber, E., Schilling, F.R., Schmitz, M. and Wigger, P., 1999. Crustal thickening processes in the Central Andes and the different natures of the Moho-discontinuity. Journal of South American Earth Sciences, 12: 201-220.

Grunder, A.L., 1987, Low $\delta^{18}O$ silicic volcanic rocks at the Calabozos caldera complex, southern Andes. *Contributions to Mineralogy and Petrology* 95 (1), p. 71-81.

Grunder, A.L., Mahood, G.A., 1988, Physical and chemical models of zoned silicic magmas: the Loma Seca Tuff and Calabozos Caldera, southern Andes. *Journal of Petrology* 29 (4), p. 831-867.

Grunder, A.L., 1992, Two-stage contamination during crustal assimilation: isotopic evidence from volcanic rocks in eastern Nevada. *Contributions to Mineralogy and Petrology* 112 (2-3), p. 219-229.

Grunder, A.L., 1995, Material and thermal roles of basalt in crustal magmatism: case study from eastern Nevada. *Geology*, 23:952-956.

Grunder, A.L., Klemetti, E.W., Feeley, T.C., and McKee, C.M., 2006, Eleven million years of arc volcanism at the Aucanquilcha Volcanic Cluster, Northern Chilean Andes: implications for the life span and emplacement of plutons: *Transactions of the Royal Society of Edinburgh-Earth Sciences*, v. 97, p. 415-436.

Hawkesworth, C.J., Hammill, M., Gledhill, A.R., van Calsteren, P., Rogers, G., 1982, Isotope and trace element evidence for late-stage intra-crustal melting in the High Andes. *Earth and Planetary Science Letter* 58, p. 240-254.

Harmon, R.S., Thorpe, R.S., Francis, P.W., 1981, Petrogenesis of Andean andesites from combined O-Sr isotope relationships. *Nature* 290, p. 396-399.

Harmon, R.S., Hoefs, J., 1995, Oxygen isotope heterogeneity of the mantle deduced from global 18O systematics of basalts from different geotectonic settings. *Contributions to Mineralogy and Petrology* 120 (1), p. 95-114.

Haschke, M., Siebel, W., Günther, A., Scheuber, E., 2002, Repeated crustal thickening and recycling during the Andean orogeny in north Chile (21° -26° S). Journal of Geophysical Reearch 107 (B1),

Hildreth, W., and Moorbath, S., 1988, Crustal contributions to arc magmatism in the Andes of Central Chile, *Contributions to Mineralogy and Petrology* 98, 455-489.

Hora, J.M., Singer, B.S., and Wörner, G., 2007, Volcano evolution and eruptive flux on the thick crust of the Andean Central Volcanic Zone: $^{40}Ar/^{39}Ar$ constraints from Volcán Parinacota, Chile: GSA Bulletin, v. 119, no. 3-4, p. 343-362.

James, D.E., Brooks, C., Cuyubamba, A., 1976, Andean Cenozoic volcanism: Magma genesis in the light of strontium isotopic composition and trace-element geochemistry. *GSA Bulletin* 87, p. 592-600.

James, D.E., 1982, A combined O, Sr, Nd, and Pb isotopic and trace element study of crustal contamination in central Andean lavas, I. Local geochemical variations. *Earth and Planetary Science Letters* 57, p. 47-62.

Johnson, C.M., Lipman, P.W., Czamankse, G.K., 1990, H, O, Sr, Nd, and Pg isotope geochemistry of the Latir volcanic field and cogenetic intrusions, New Mexico, and relations between evolution of a continental magmatic center and modifications of the lithosphere. *Contributions to Mineralogy and Petrology* 104, p. 99-124.

Johnson, D.M., Hooper, P.R., and Conrey, R.M., 1999, XRF analysis of rocks and minerals for major and trace elements on a single low-dilution Li-tetraborate fused bead: Advances in X-Ray Analysis, v. 41, p. 117–132.

Karlstrom, L., Dufek, J., Manga, M., 2009, Organization of volcanic plumbing through magmatic lensing by magma chambers and volcanic loads. *Journal of Geophysical Research* 114, 16p.

Karlstrom., L., Dufek, J., Manga, M., 2010, Magma chamber stability in arc and continental crust. *Journal of Volcanology and Geothermal Research* 190 (3-4), p. 249-270.

Kay, R.M., and Kay, S.M., 1993, Delamination and delamination magmatism: Tectonophysics, v. 219, no. 1–3, p. 177–189.

Kay, S.M., Mpodozis, C., Coira, B., 1999, Neogene magmatism, tectonism, and mineral deposits of the central Andes (22° to 33°S Latitude), *in* Skinner, B.J., ed., Geology and Ore Deposits of the Central Andes: *Society of Economic Geology Special Publication* 7, p. 27-59.

Kay, S.M., Godoy, E., Kurtz, A., 2005, Episodic arc migration, crustal thickening, subduction erosion, and magmatism in the south-central Andes. *GSA Bulletin* 117 (1/2), p. 67-88.

Klemetti, E.W., and Grunder, A.L., 2008, Volcanic evolution of Volcan Aucanquilcha: a

long-lived dacite volcano in the Central Andes of northern Chile: *Bulletin of Volcanology*, v. 70, p. 633-650.

Leonard, G.S., Cole, J.W., Nairn, I.A., Self, S., 2002, Basalt triggering of the c. AD 1305 Kaharoa rhyolite eruption, Tarawera Volcanic Complex, New Zealand. *Journal of Volcanology and Geothermal Research* 115 (3-4), p. 461-486.

Lipman, P.W., 2007, Incremental assembly and prolonged consolidation of Cordilleran magma chambers: Evidence from the Southern Rocky Mountain volcanic field: *Geosphere*, v. 3, p. 42-70.

Lucassen, F., Becchio, R., Harmon, R.S., Kasemann, S., Franz, G., Trunbull, R., Wilke, H.G., Romer, R.L., Dulski, P., 2001, Composition and density model of the continental crust at an active continental margin—the Central Andes between 21° and 27°S. *Tectonophysics* 341, 195-223.

Macfarlane, A.W., Marcet, P., LeHuray, A.P., and Petersen, U., 1990, Lead isotope provinces of the Central Andes inferred from ores and crustal rocks. *Economic Geology* 85 (8), p. 1857-1880.

Mamani, M., Worner, G., and Sempere, T., 2010, Geochemical variations in igneous rocks of the Central Andean orocline (13ºS to 18ºS): Tracing crustal thickening and magma generation through time and space, *GSA Bulletin* 122 (1/2), p. 162-182.

Nakamura, M., 1995, Continuous mixing of crystal mush and replenished magma in the ongoing Unzen eruption. *Geology* 23 (9), p. 807-910.

Reiners, P.W., Nelson, B.K., Ghiorso, M.S., 1995, Assimilation of felsic crust by basaltic magma: Thermal limits and extents of crustal contamination of mantle-derived magmas. *Geology* 23 (6), p. 563-566.

Reiners, P.W., Nelson, B.K., 1998, Temporal-compositional-isotopic trends in rejuvenated-stage magmas of Kauai, Hawaii, and implications for mantle melting processes. *Geochimica et Cosmochimica Acta* 62 (13), p. 2,347-2,368.

Reubi, O., Blundy, J., 2009, A dearth of intermediate melts at subduction zone volcanoes and the petrogenesis of arc andesites. *Nature* 461, p. 1269 – 1273.

Riciputi, L.R., Johnson, C. M., Sawyer, D. A., Lipman, P. W., 1995, Crustal and magmatic evolution in a large multicyclic caldera complex: isotopic evidence from the central San Juan volcanic field, *Journal of Volcanology and Geothermal Research* 67, 1-28.

Rogers, G., Hawkesworth, C.J., 1989, A geochemical traverse across the north Chilean Andes: evidence for crust generation from the mantle wedge. *Earth and Planetary Science Letters* 91, p. 271-285.

Scmitz, M. et al., 1999. The crustal structure beneath the Central Andean forearc and magmatic arc as derived from seismic studies--the PISCO 94 experiment in northern Chile (21-23S). *Journal of South American Earth Sciences* 12: 237-260.

Scmitz, M., Heinsohn, W.D. and Schilling, F.R., 1997. Seismic, graviy and petrological evidence for partial melt beneath the thickened Central Andean crust (21-23S). Tectonophysics, 270: 313-326.

Streck, M.J., 2008, Mineral textures and zoning as evidence for open system processes. In: *Minerals, Inclusions, and Volcanic Processes, Reviews of Mineralogy & Geochemistry*, 69: 595-619

Tepley, F. J., III, Davidson, J. P., Tilling, R. I. & Arth, J. G. (2000). Magma mixing, recharge, and eruption histories recorded in plagioclase phenocrysts from El Chichón Volcano, Mexico. *Journal of Petrology*, 41, 1397-1411.

Thorpe, R.S., Francis, P.W., 1979, Variations in Andean andesite compositions and their petrogenetic significance. *Tectonophysics* 57 (1), p. 53-70.

Tilton, G.R., 1979, Isotopic studies of Cenozoic Andean calc-alkaline rocks. *Carnegie Institution of Washigton Yearbook* 78, p. 298-304.

Wörner, G., Moorbath, S., Horn, S., Entenmann, J., Harmon, R.S., Davidson, J.P., Lopez-Escobar, L., 1994. Large- and fine-scale variations along the Andean arc of Northern Chile (17.5° - 22°S). In: Reutter, K.J., Scheuber, E., Wigger, P.J. (Eds.). Tectonics of the Southern Central Andes. Springer, Heidelberg, Germany, pp. 77-92.

Figure 3.1: Google Earth image of the Aucanquilcha volcanic cluster, with its extent outlined in white. Also shown are the scoria cone field to the east of the AVC, and Volcán Ollagúe.

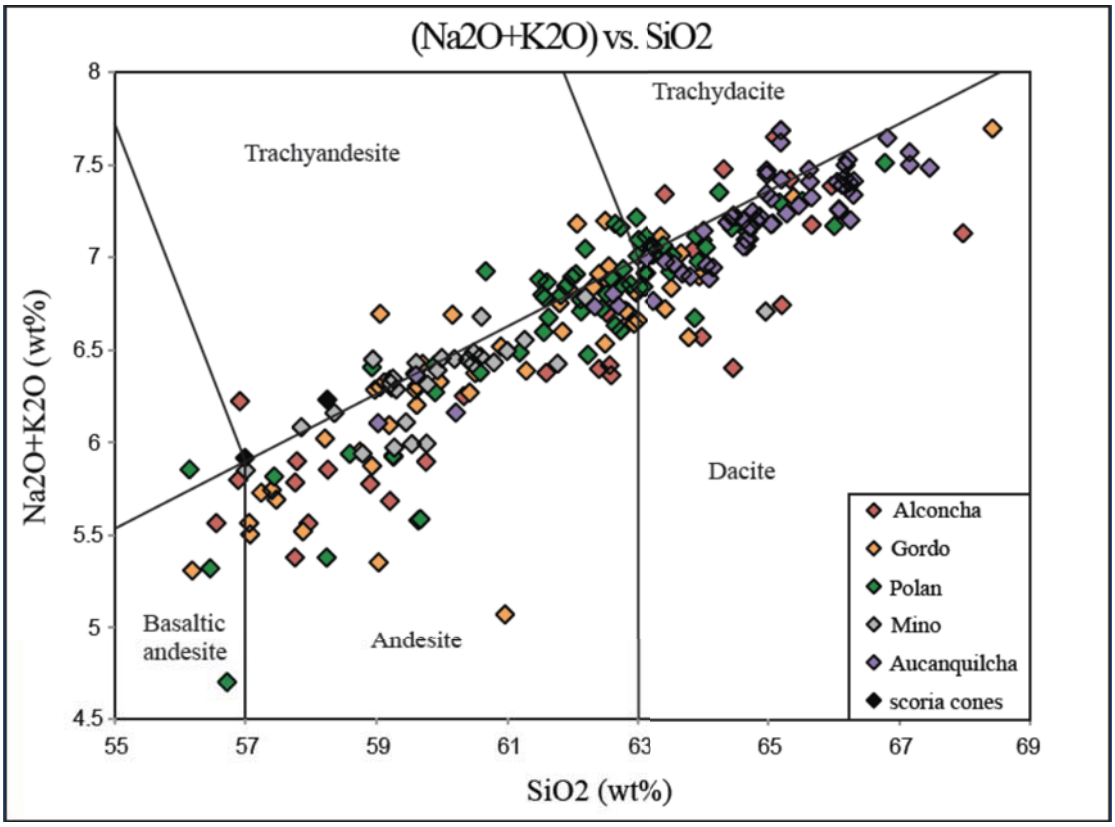

Figure 3.2: Total Alkali vs. Silica for AVC lavas. AVC lavas range in composition from basaltic andesite to dacite, with lavas from Volcán Aucanquilcha being slightly more evolved.

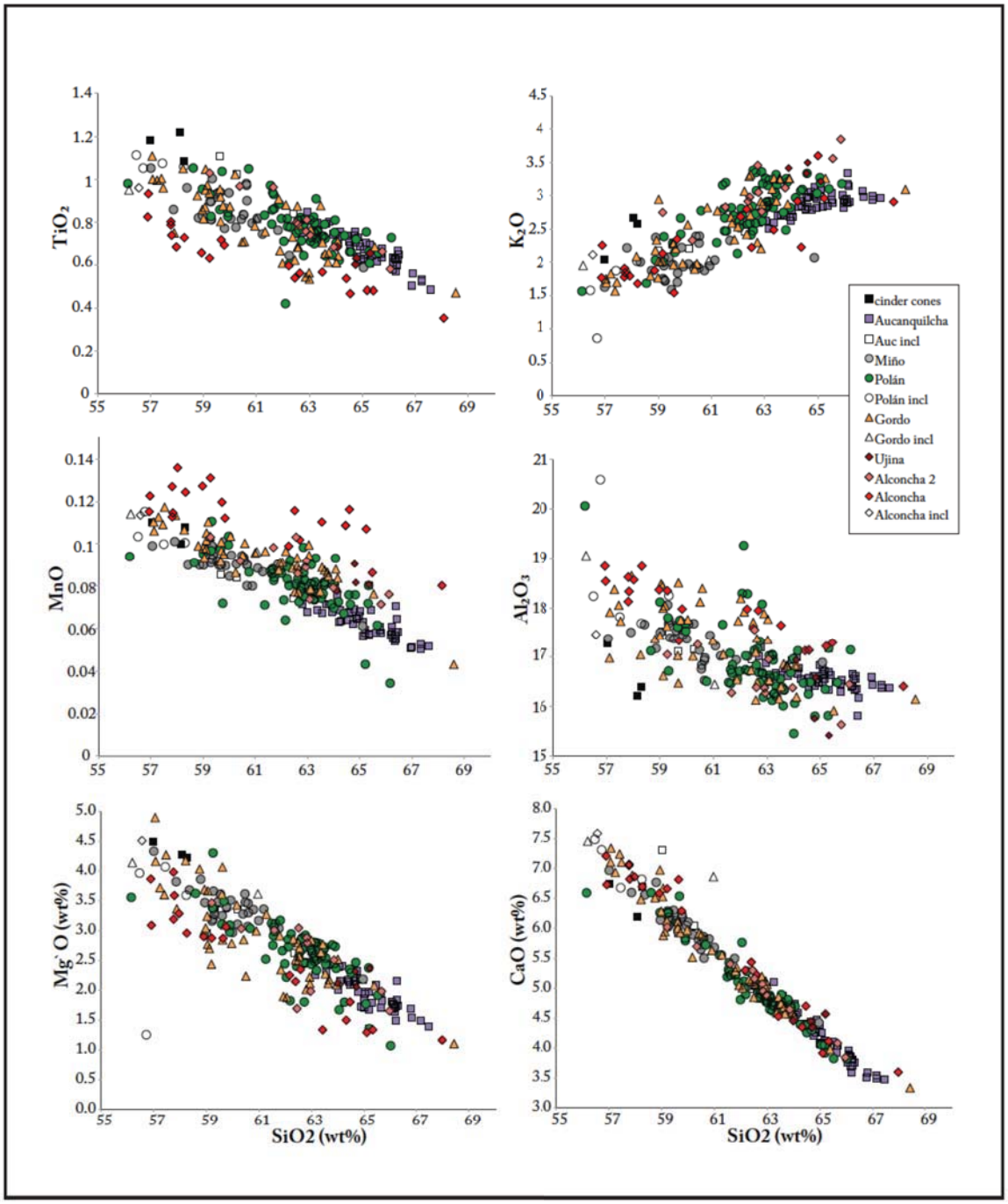

Figure 3.3: Major element variation of AVC lavas, broken out by eruptive group. Inclusions are also discriminated, with clear symbols.

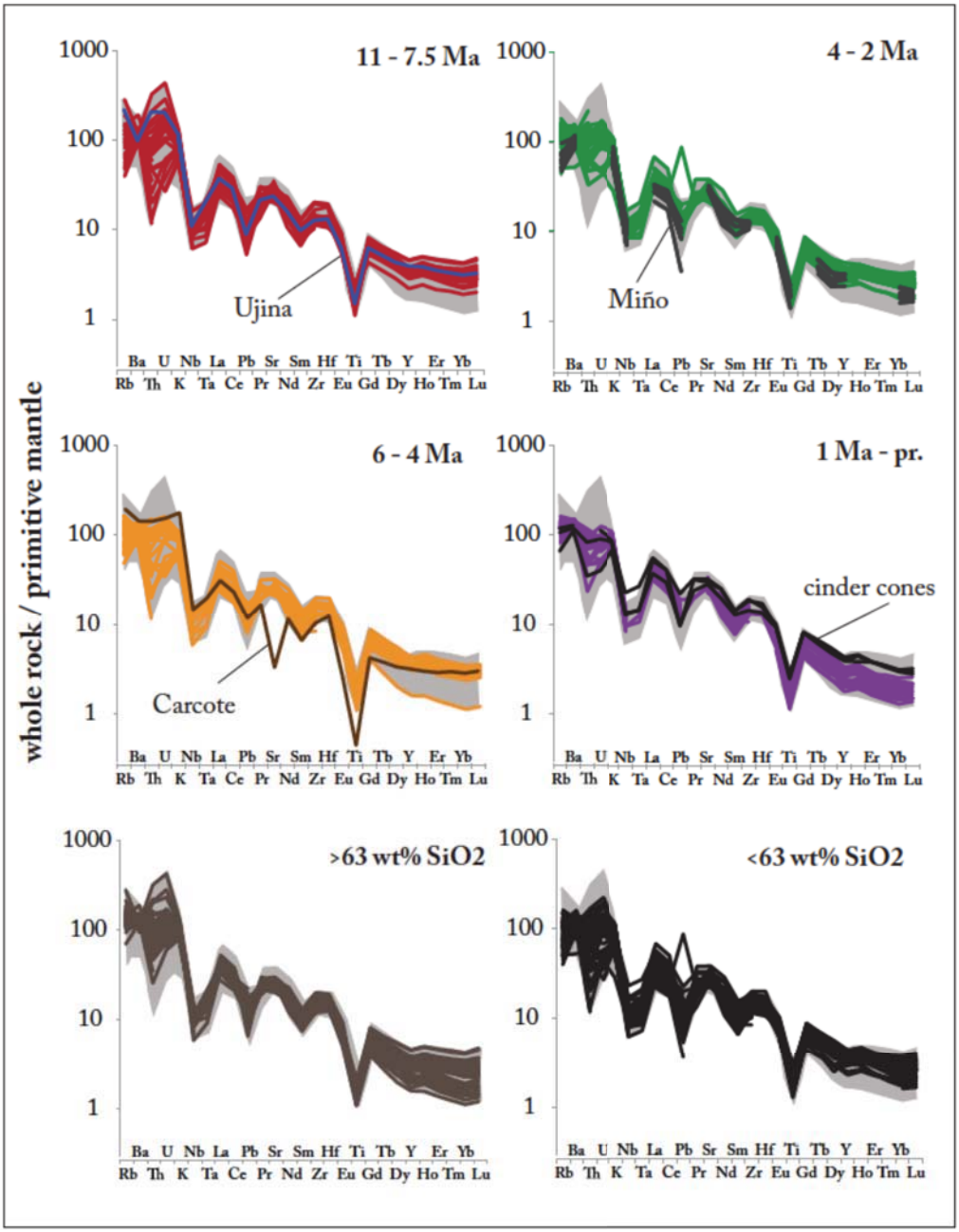

Figure 3.4: Spidergraph showing the trace element patterns of AVC lavas normalized to primitive mantle values. Note the enrichment in fluid mobile elements such as U, Th, K, Ba, Rb, and the depletion in high field strength elements such as Nb, Ta and Ti, which is typical of subduction zone magmas. The gray field represents the entire range of the AVC for reference. The lowest two panels illustrate the enrichment in LILs and reduced diversity of elements of moderate incompatibility in dacites relative to andesites. Conversely, it also illustrates the reduced diversity of HREEs in andesites with respect to dacites. The Carcote ignimbrite is shown, as it crops out near the AVC. It is a rhyolite and is of uncertain source.

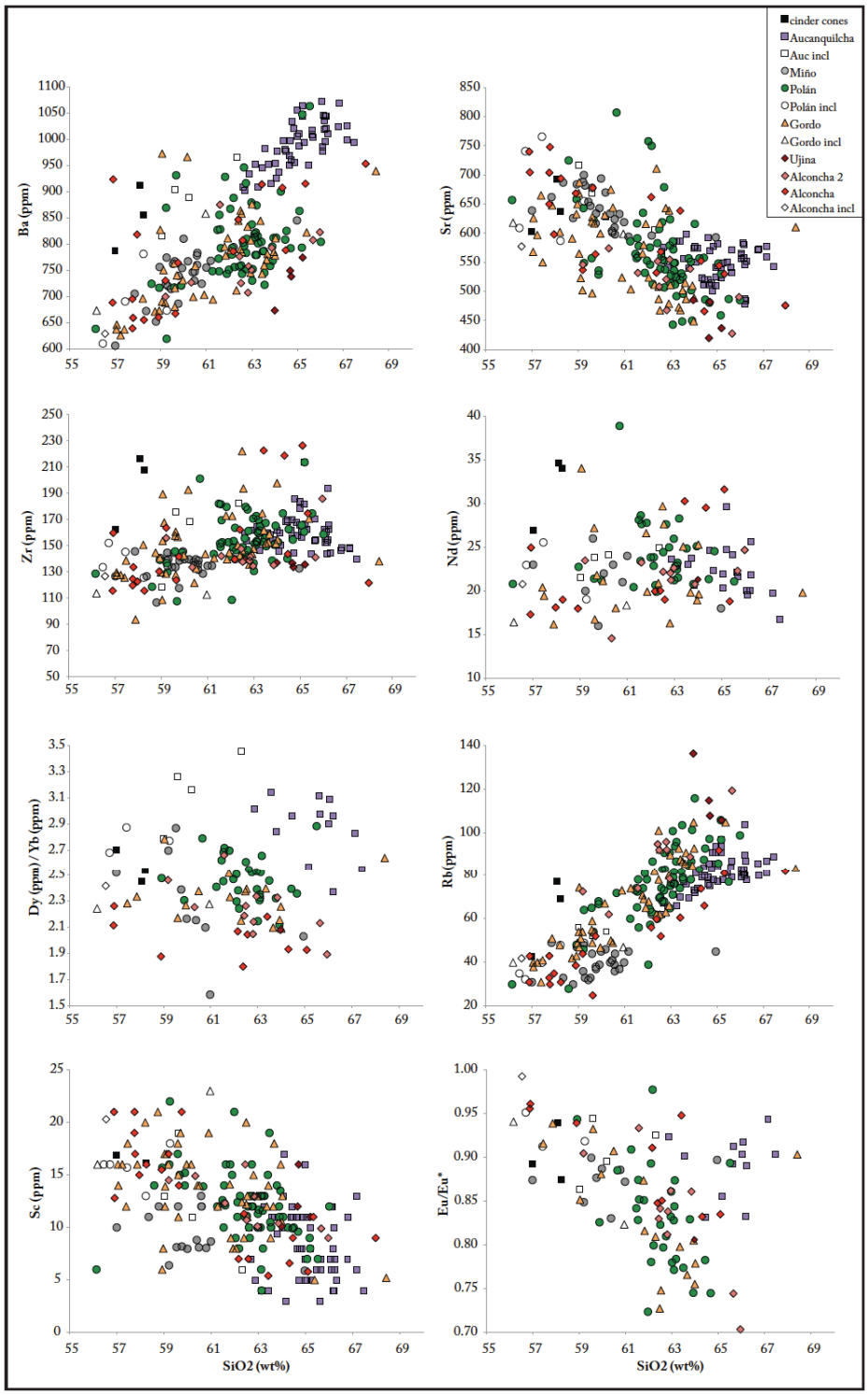

Figure 3.5: Trace element variation observed in AVC lavas, broken out by eruptive group. Inclusions are also discriminated, with clear symbols.

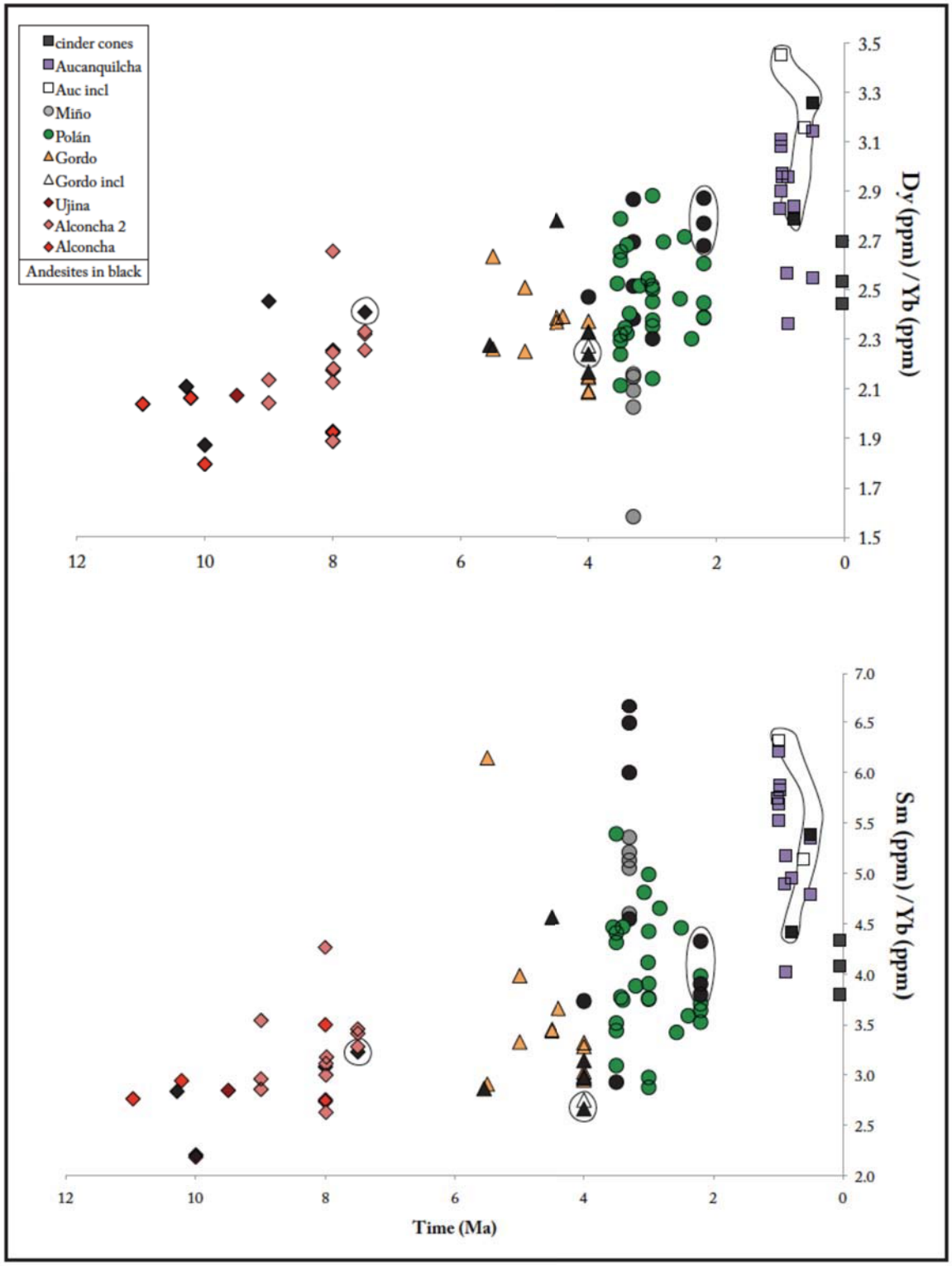

Figure 3.6: Dy/Yb and Sm/Yb (all in ppm) increases through time, consistent with other CVZ lavas. Lavas with < 60 wt% SiO_2 are black symbols. Inclusions are circled.

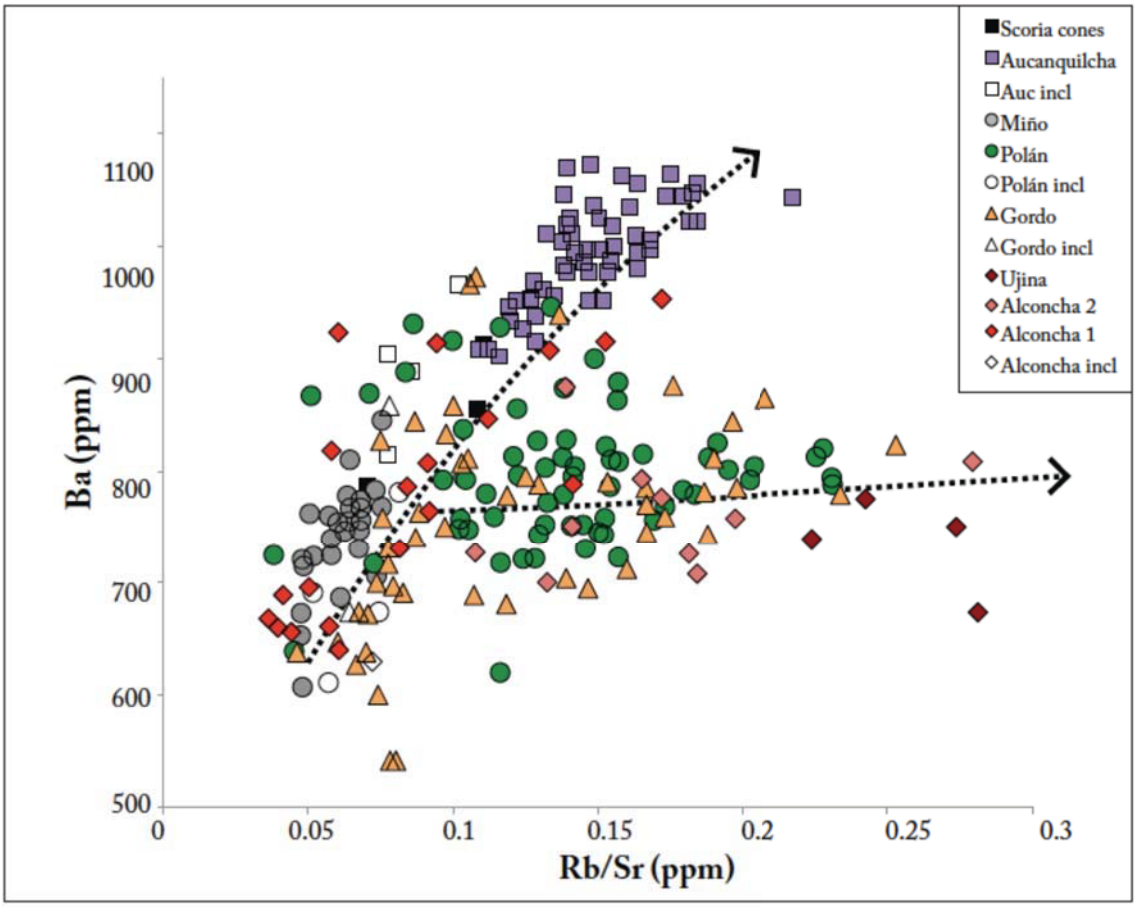

Figure 3.7: Ba vs. Rb/Sr for AVC lavas. Note the two trends, indicating two different processes controlling trace element distribution. Note that the Alconcha 2 group falls entirely on the lower trend, while the Alconcha 1 groups falls on the upper trend. Samples from V. Aucanquilcha are enriched with Ba with respect to most of the AVC.

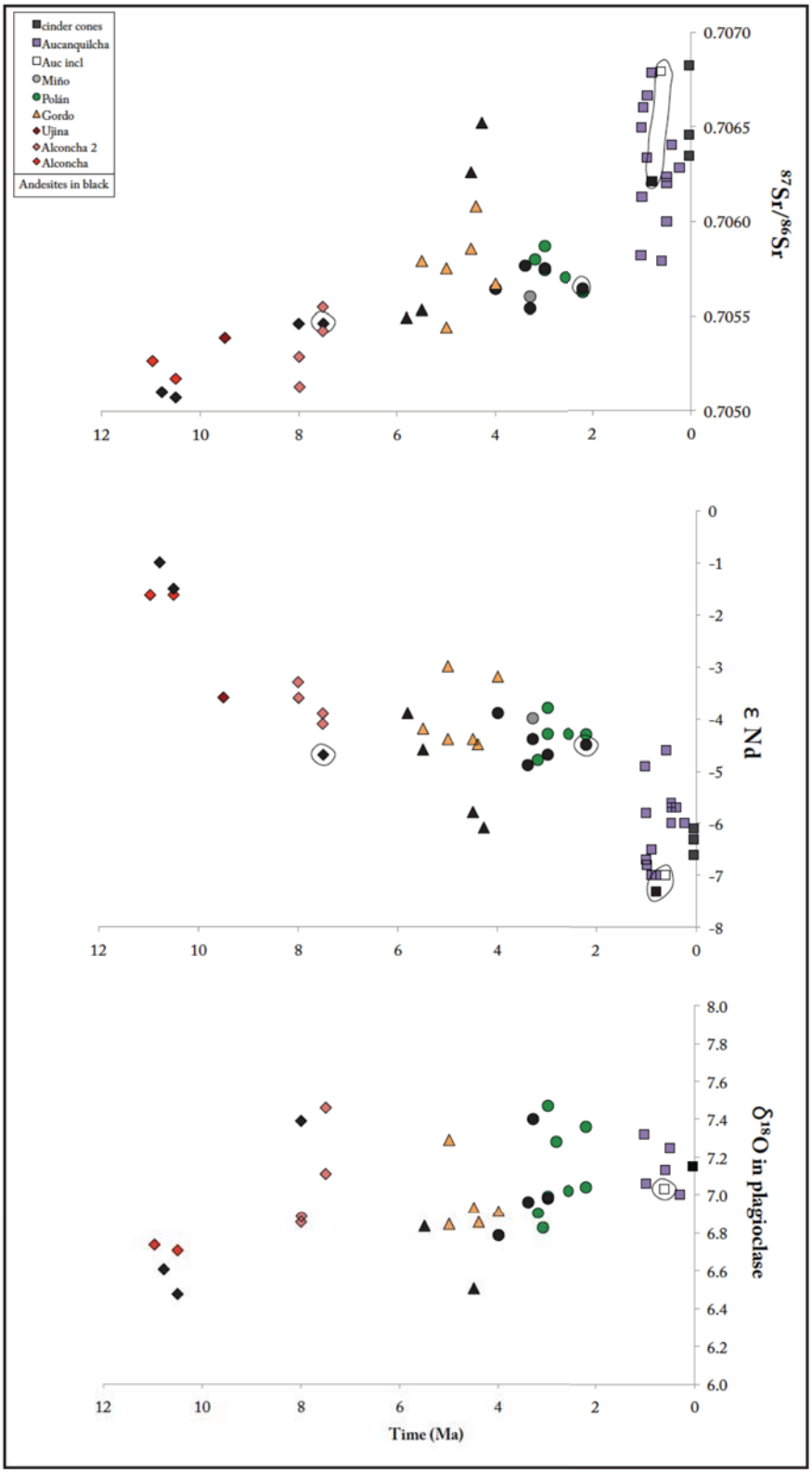

Figure 3.8: Temporal isotopic variation at the AVC. Note the increase in $^{87}Sr/^{86}Sr$, decrease in ε_{Nd}, and slight increase in $\delta^{18}O$ base level through time.

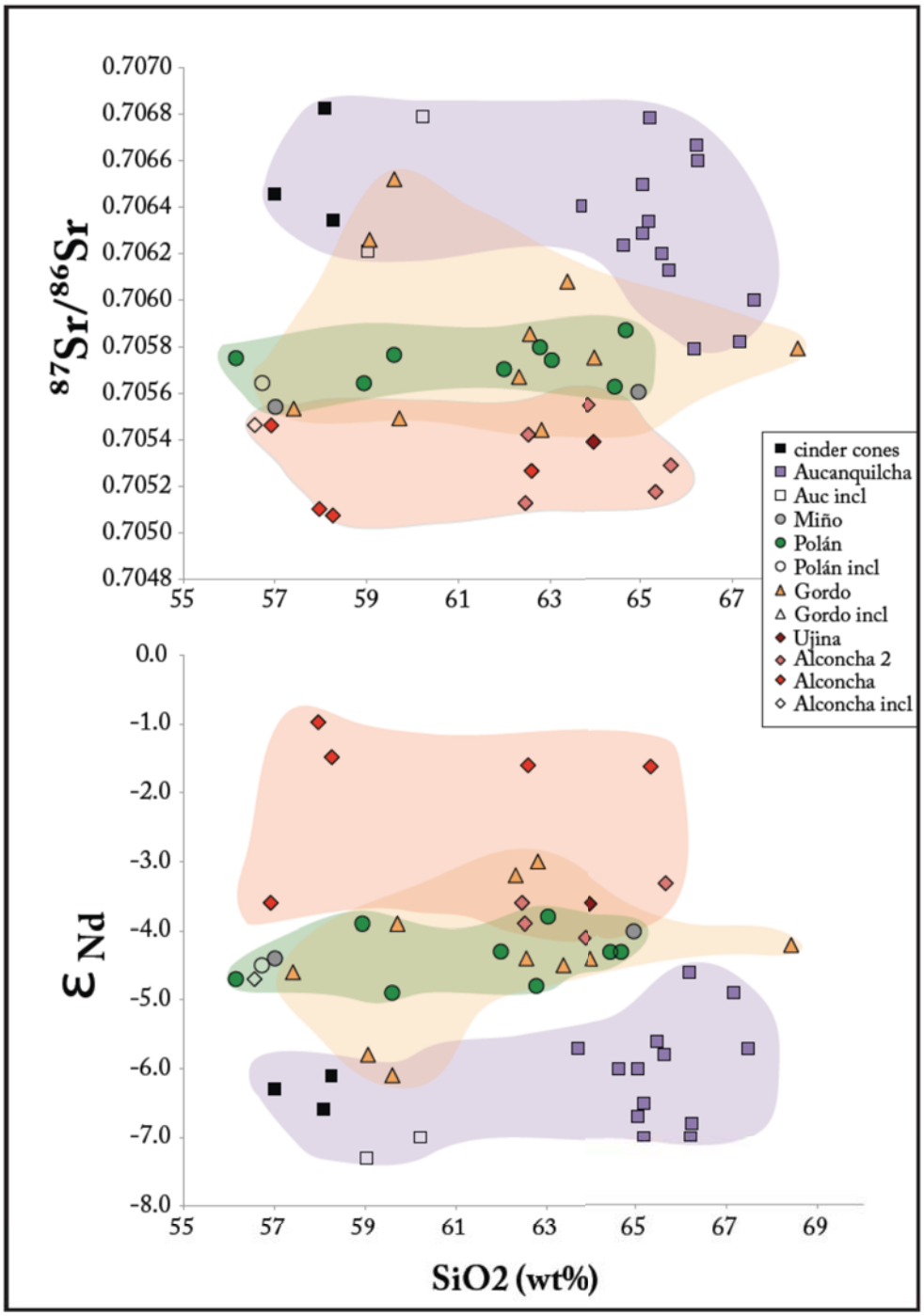

Figure 3.9: Variations of Sr and Nd isotopes against SiO_2 for AVC lavas. Note that there is not significant variation with SiO_2, indicating it is unlikely that crustal contamination with old, radiogenic crust played a role generating in this diversity.

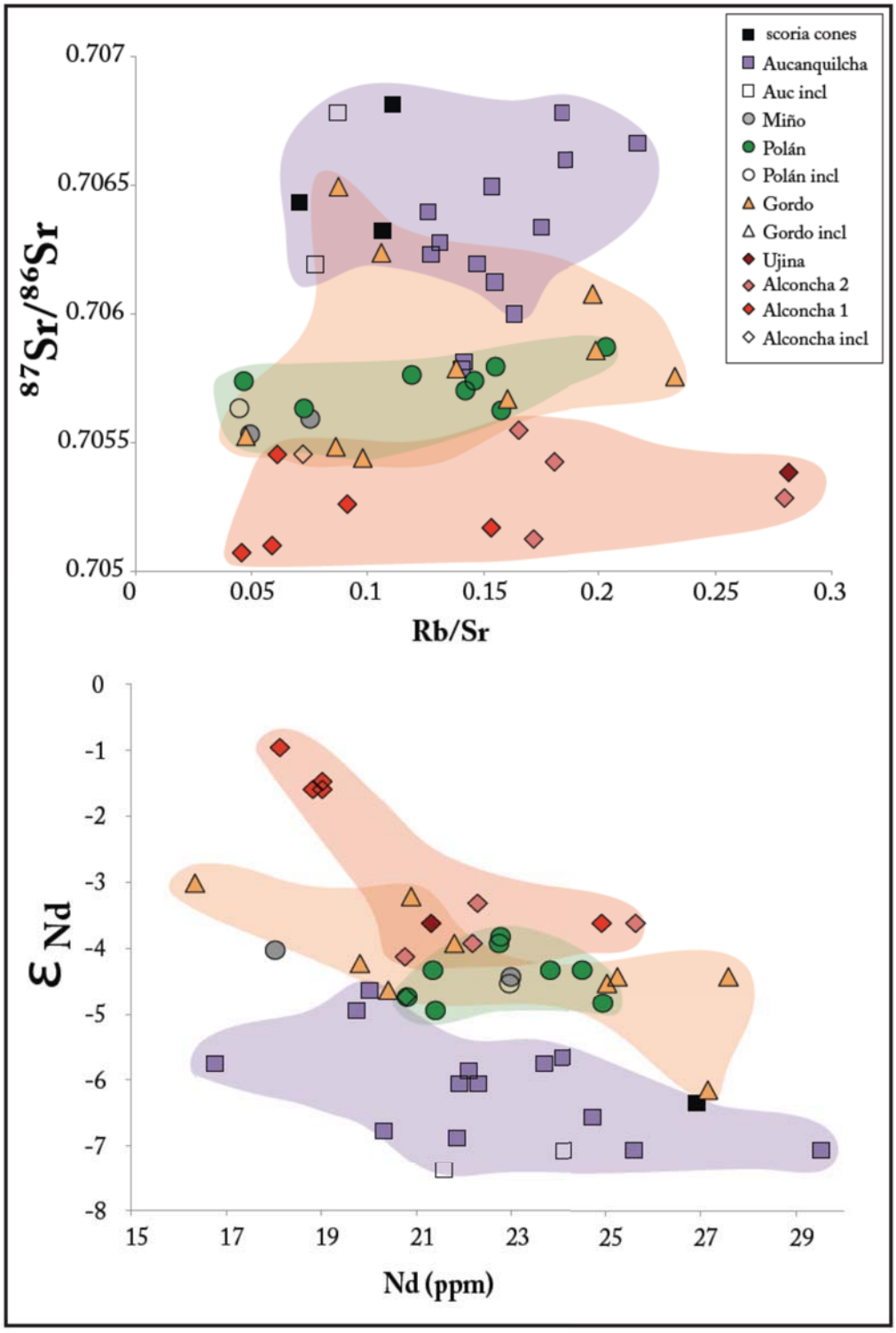

Figure 3.10: Isotopic variation ($^{87}Sr/^{86}Sr$ and ε_{Nd}) with the respective elemental concentration. Like SiO_2, the correlation between isotopic and elemental variation is minimal, suggesting that isotopic variation is not related to fractionation.

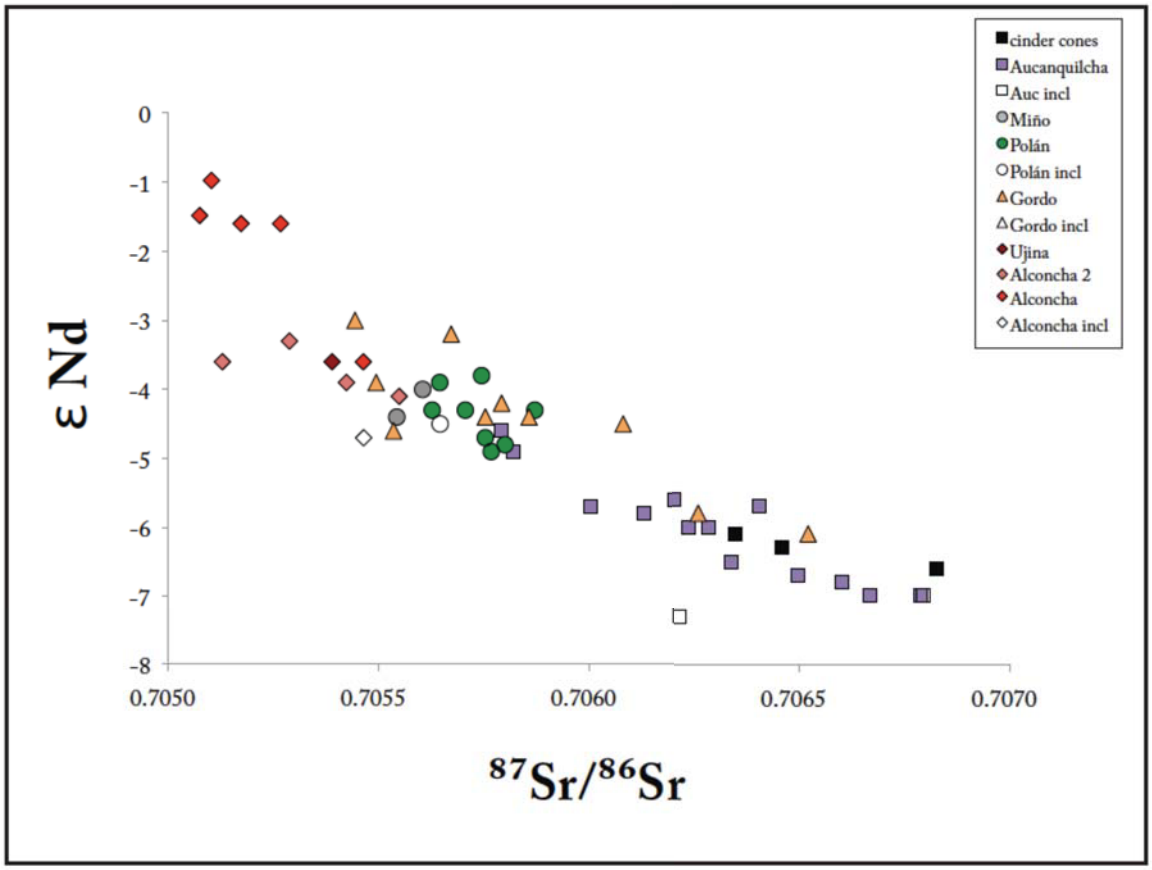

Figure 3.11: Sr vs. Nd isotopic variation for the AVC. The two systems track each other fairly well. There is, however, a distinct lack of samples with ε_{Nd} from -2 to -3.

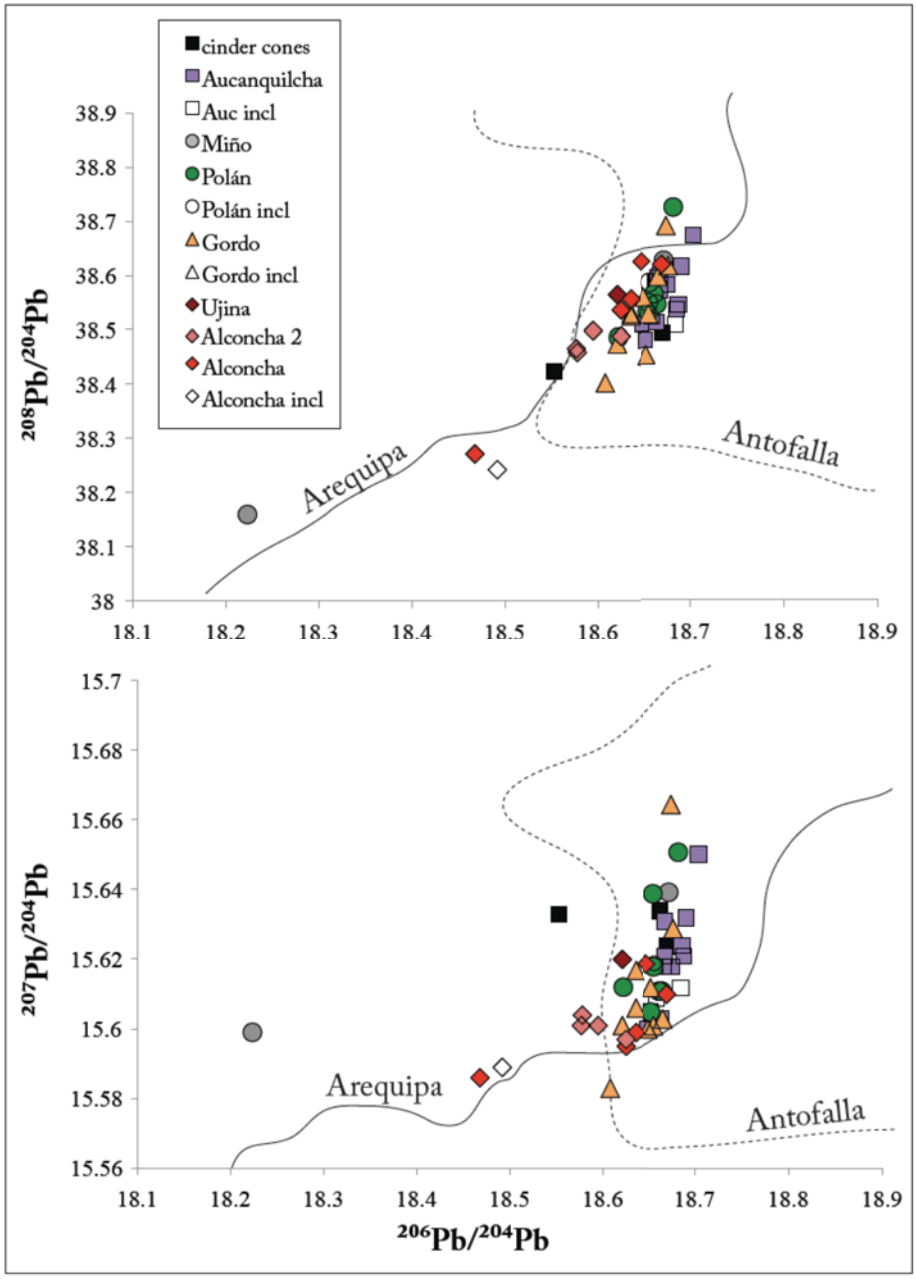

Figure 3.12: Pb isotopes of the AVC show little variability, with the exception of a few outlying points. There is, however, a subtle shift to higher values of $^{206}Pb/^{204}Pb$ through time. The fields for the Arequipa and Antofalla basement domains are shown for reference (the labels fall on the side of the line occupied by the corresponding data field). Note that AVC Pb isotopes are in the zone of compositional overlap for the two basement domains, consistent with its situation in the transition zone between these two domains.

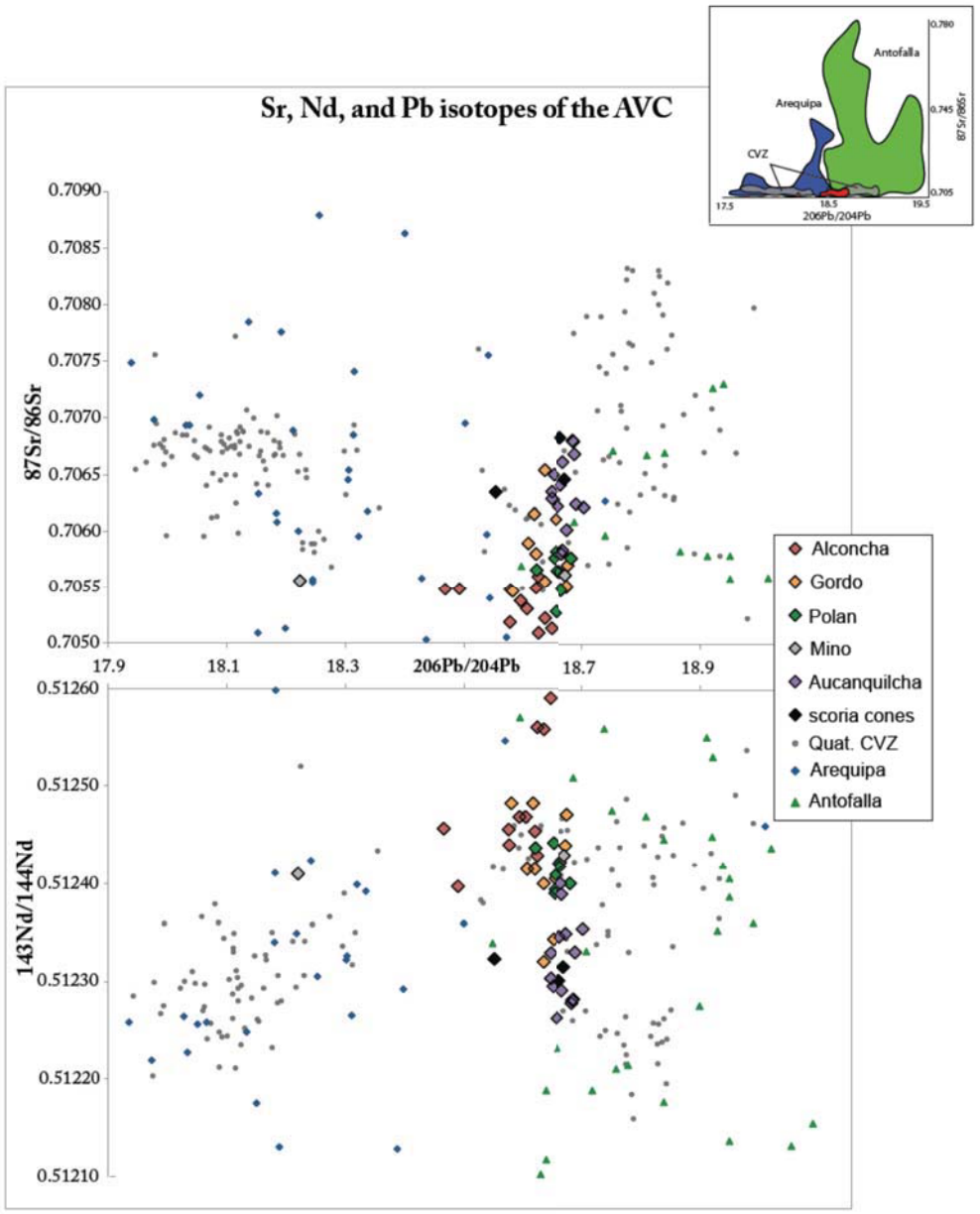

Figure 3.13 Sr, Nd, Pb isotopes of the AVC, in comparison to compositions from other CVZ volcanoes and basement. Note the two different trends in Quaternary CVZ rocks (one to lower $^{206}Pb/^{204}Pb$, and one to higher $^{206}Pb/^{204}Pb$), which mirrors the trends of basement rocks (cf. Mamani et al., 2010). The AVC trends toward Antofalla compositions, though a few lavas display affinities for Arequipa rocks. This is likely attributable to the AVC's situation at the transition zone between these two basement provinces. However, based on these trends, an average contaminant for the AVC is likely to be a composition from the Antofalla domain.

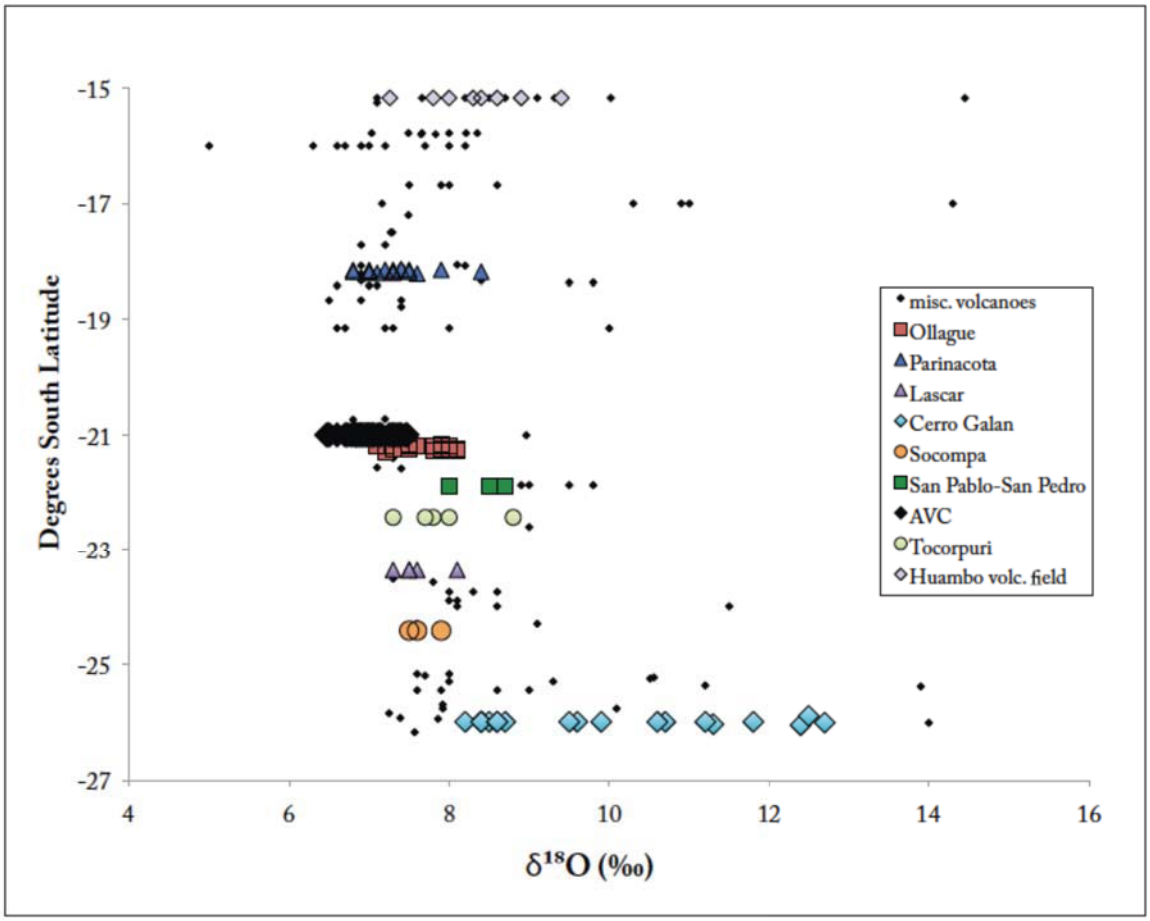

Figure 3.14: Oxygen isotope values for central Andean volcanic rocks, ranging from roughly ~5‰ to ~14‰. Note that $\delta^{18}O$ values for AVC lavas (6.5 – 7.5‰) are near the low end of this range. Central Andean data culled from many data sources through a GEOROC search.

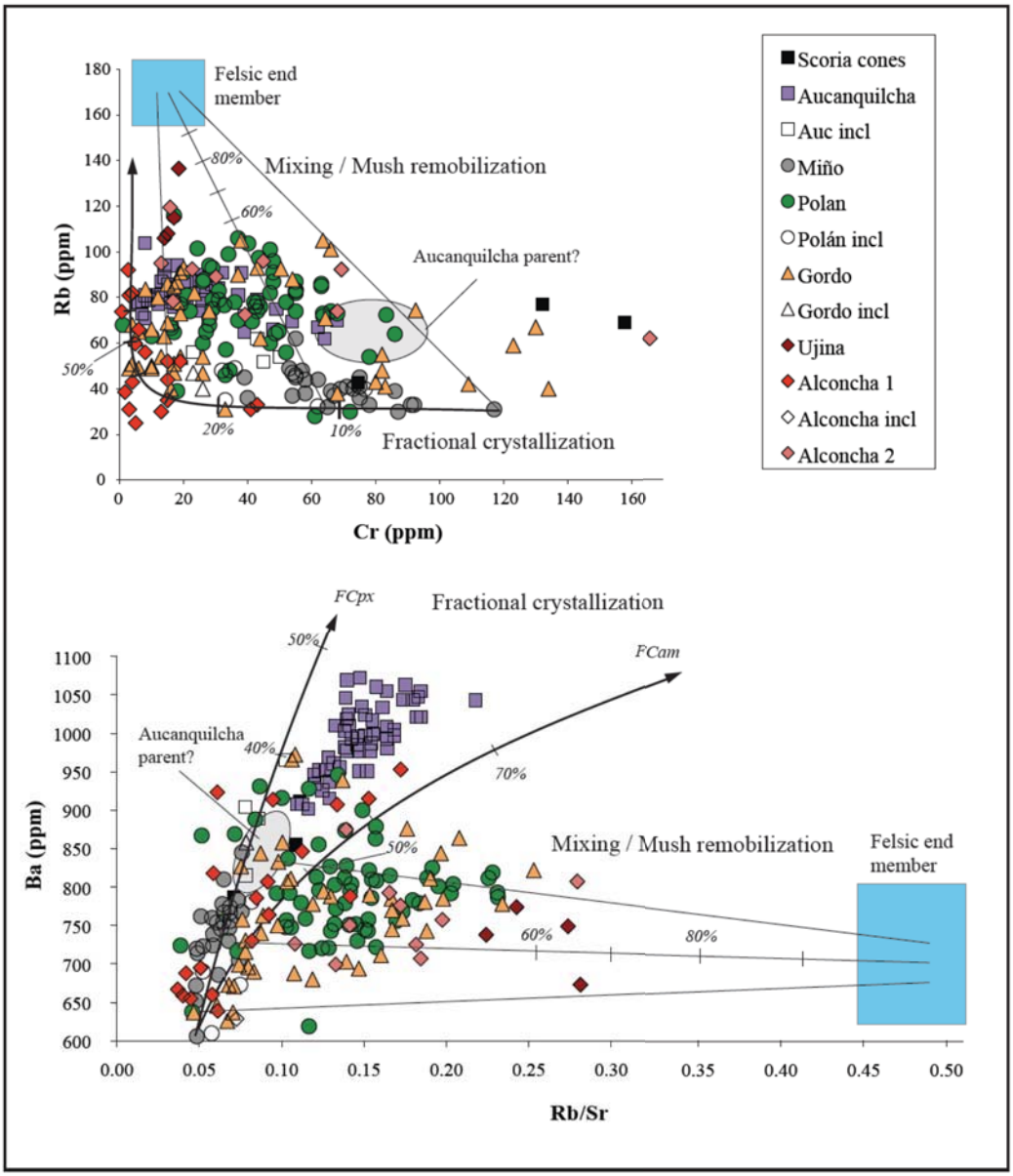

Figure 3.15: Fractional crystallization curves and mixing lines for Rb/Sr vs. Ba and Rb vs. Cr of AVC lavas. Two fractionation curves shown in order to portray the effects of a varying mineral assemblage (mt=magnetite, amph=amphibole, bio=biotite). For the Cr vs. Rb plot, the two fractionation curves are almost identical, owing to the similar incompatibility of Cr in both assemblages. Most andesites fall in between these two curves. Magma mixing lines are shown originating from various points along the fractionation curve. The "felsic end-member" field approximates the composition of the proposed end-member of magma mixing. Owing to the more evolved nature of Aucanquilcha groups lavas, separate fields showing possible parent compositions are shown. The variation observed in the AVC data are adequately explained by a combination of up to ~50% fractional crystallization and the mixing in of up to ~60% felsic end-member (likely to be precursor fractionates—see text for discussion).

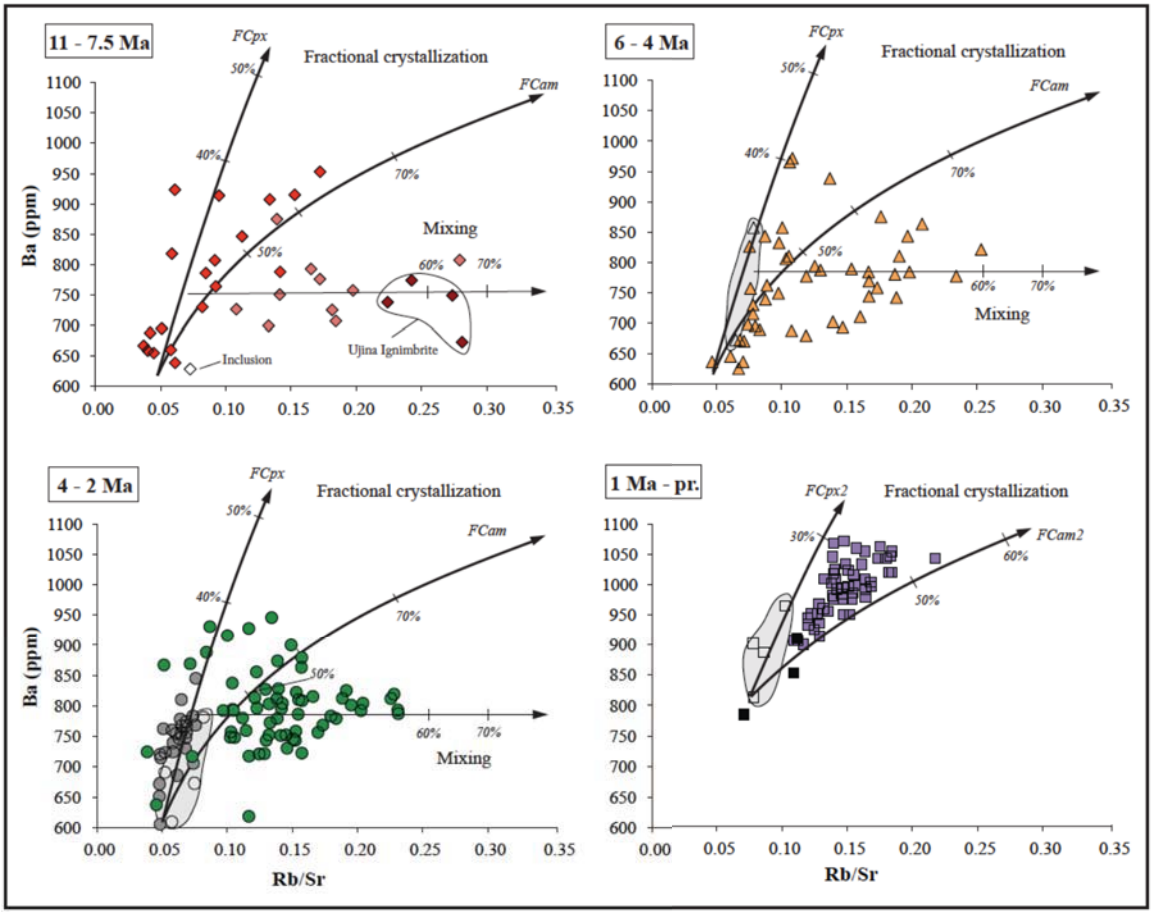

Figure 3.16: Ba vs. Rb/Sr for AVC lavas, broken out by eruptive phase. Shown here are two fractionation curves, corresponding to two different mineral assemblages, and a mixing line to a hypothetical felsic end-member (see **Figure 3.15**). For the Aucanquilcha group (1 Ma to present), a different starting composition was used due to the groups more evolved nature. Symbols the same as in previous figures. Inclusions circled in grey fields. Note that the inclusions, Alconcha1, Miño and Aucanquilcha groups are dominated by fractionation, while Alconcha 2, Gordo, Polán groups are dominated by a mixing signal.

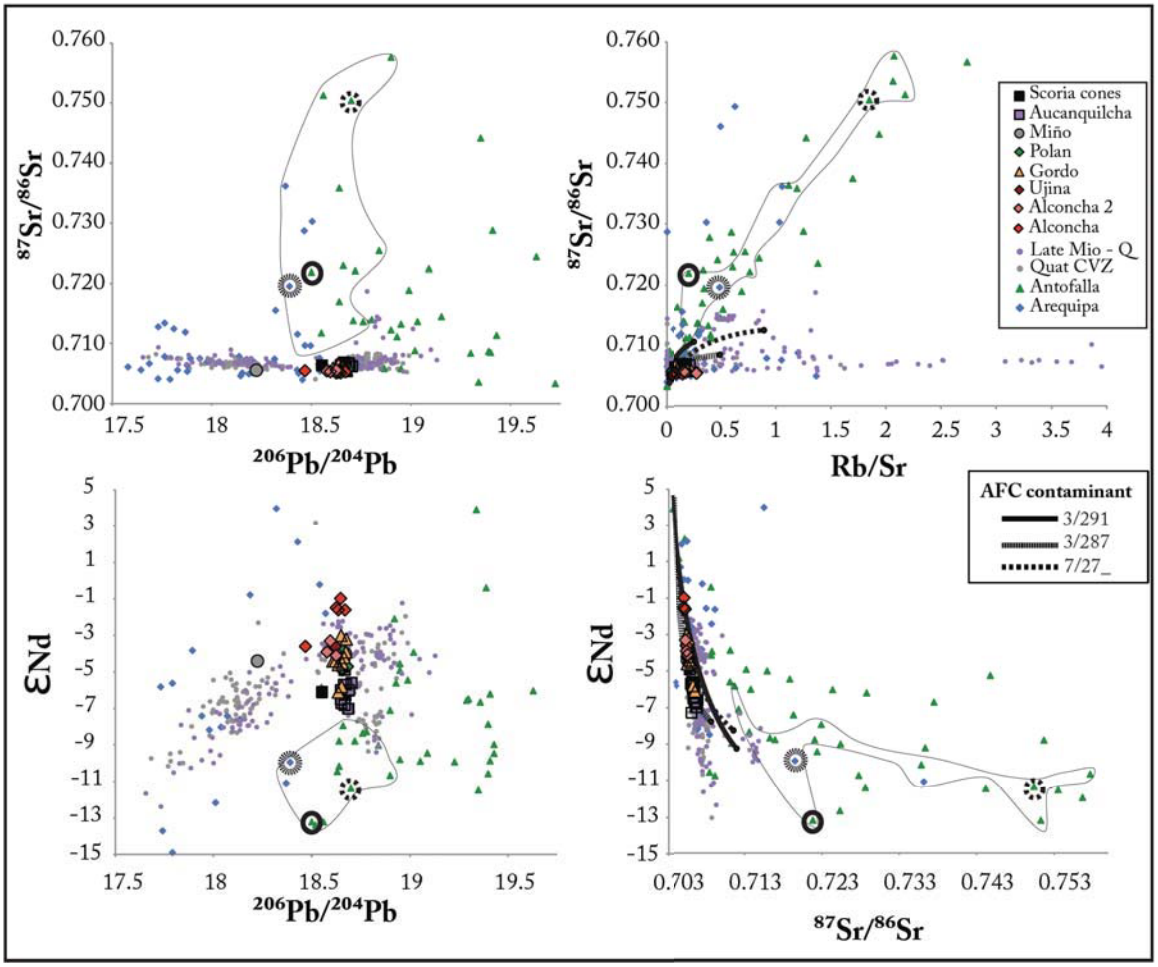

Figure 3.17: Sr, Nd, and Pb isotopes and Rb/Sr of AVC lavas compared with other central Andean rocks, with three AFC models shown. Quaternary central Andean lavas and late Miocene – Quaternary lavas are shown for reference, as they are AVC contemporaries. Basement rocks from the Arequipa and Antofalla terranes are shown; these are the best estimates for crustal contaminants for the AVC (and other central Andean lavas). The enclosed data field comprises basement rocks with similar Pb isotopic compositions to the AVC. AVC model curves for three unique contaminants are shown with different line patterns; the corresponding assimilant composition for each curve is individually circled with the same line pattern. The R-value (assimilation rate /crystallization rate) is 0.4 for each model.

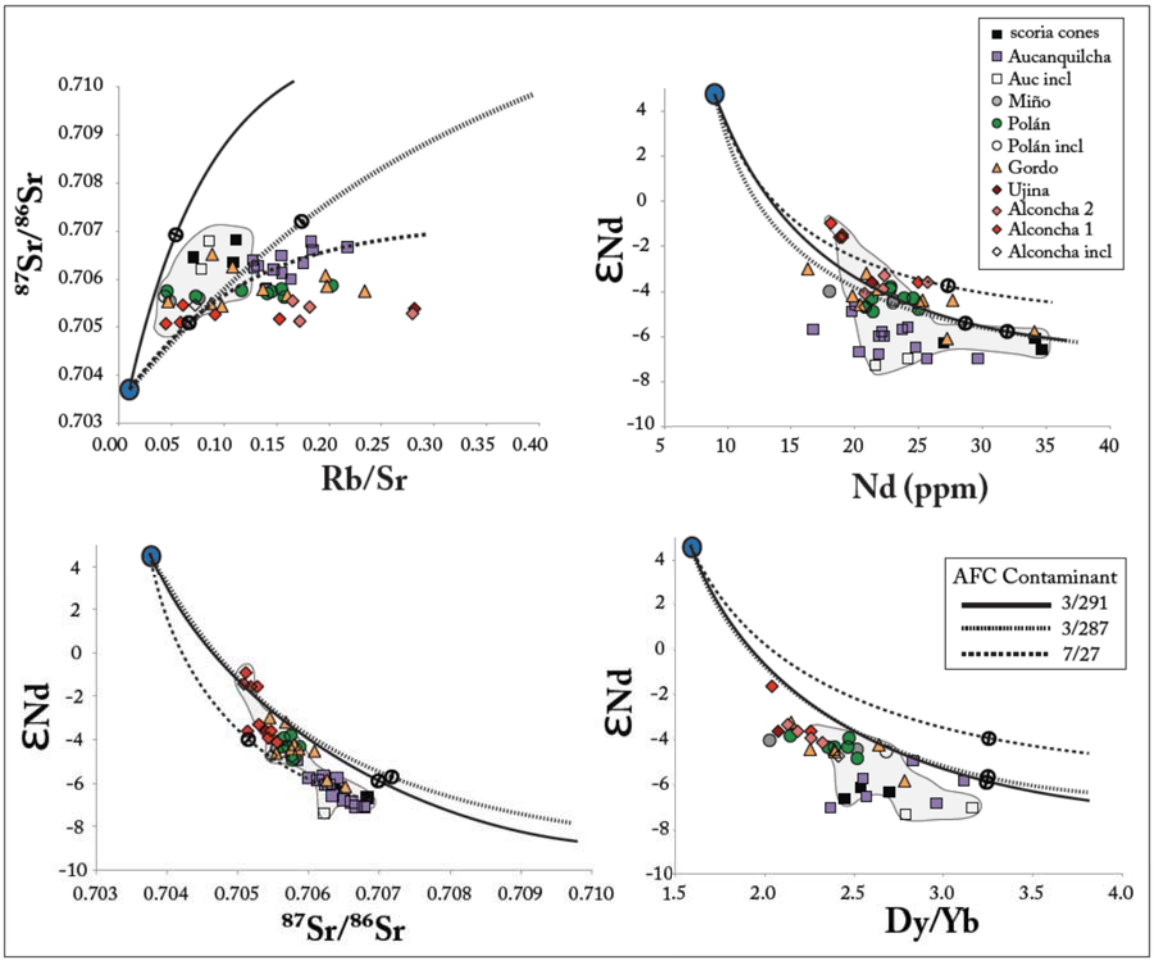

Figure 3.18: Sr and Nd isotopes, and Dy/Yb, with three AFC curves, calculated using three different contaminants (DePaolo, 1981; see also **Figure 3.17**). The encircled crosses on the curves represent the point at which F (liquid remaining) equals 0.5. AVC andesites in gray field. The parent rock (blue circle) is a relatively primitive basalt from Puyehue volcano (Gerlach et al., 1988). Contaminants are Chilean and Argentine gneisses (Lucassen et al., 2001). See **Table 3.6** for more information on the models, and **Table 3.5** for mass balance information.

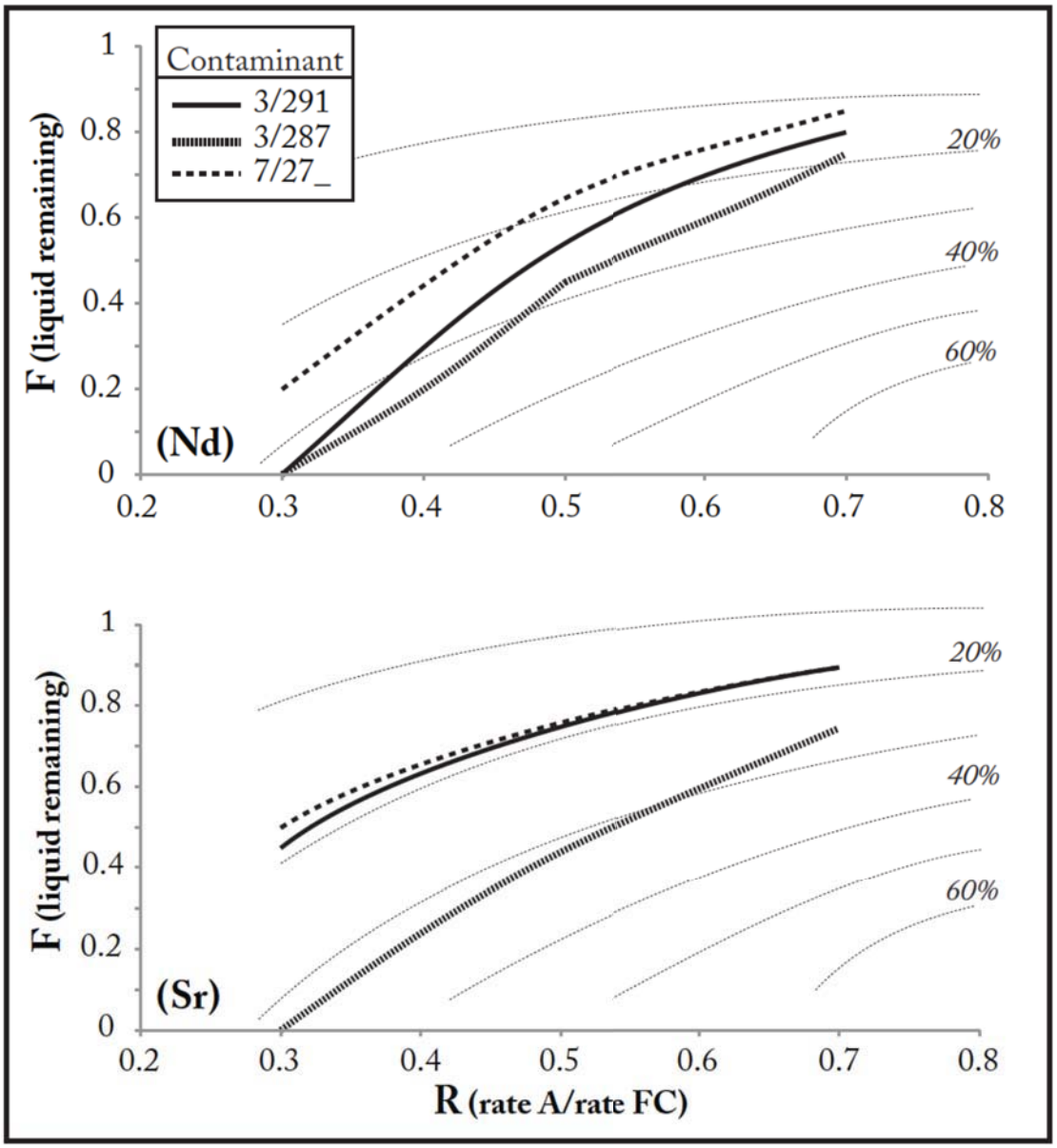

Figure 3.19: Consequences of AFC model parameter variation for the ε_{Nd} (top) and $^{87}Sr/^{86}Sr$ (bottom) systems, contoured for percent contaminant implicated. Three different AFC models, each with a different contaminant (see text), were employed to describe the hypothetical differentiation of a parental basalt ($^{87}Sr/^{86}Sr = 0.7038$; $\varepsilon_{Nd} = +4$. Plotted above are the F values (liquid remaining) necessary to achieve an ε_{Nd} of -6 (top), and a $^{87}Sr/^{86}Sr$ (bottom) of 0.706, as they vary with changing R (assimilation rate/crystallization rate). These isotopic compositions are ~average values for AVC lavas and, as such, should approximate average amounts of assimilation necessary for production of AVC lavas. The plot is contoured for the percentage of the contaminant the final magma will contain, given the F and R value (cf., DePaolo, 1981). Note that even with significant change in R-value, the amount of contaminant implicated remains very similar. All three models suggests AVC lavas contain ~10-30% crust.

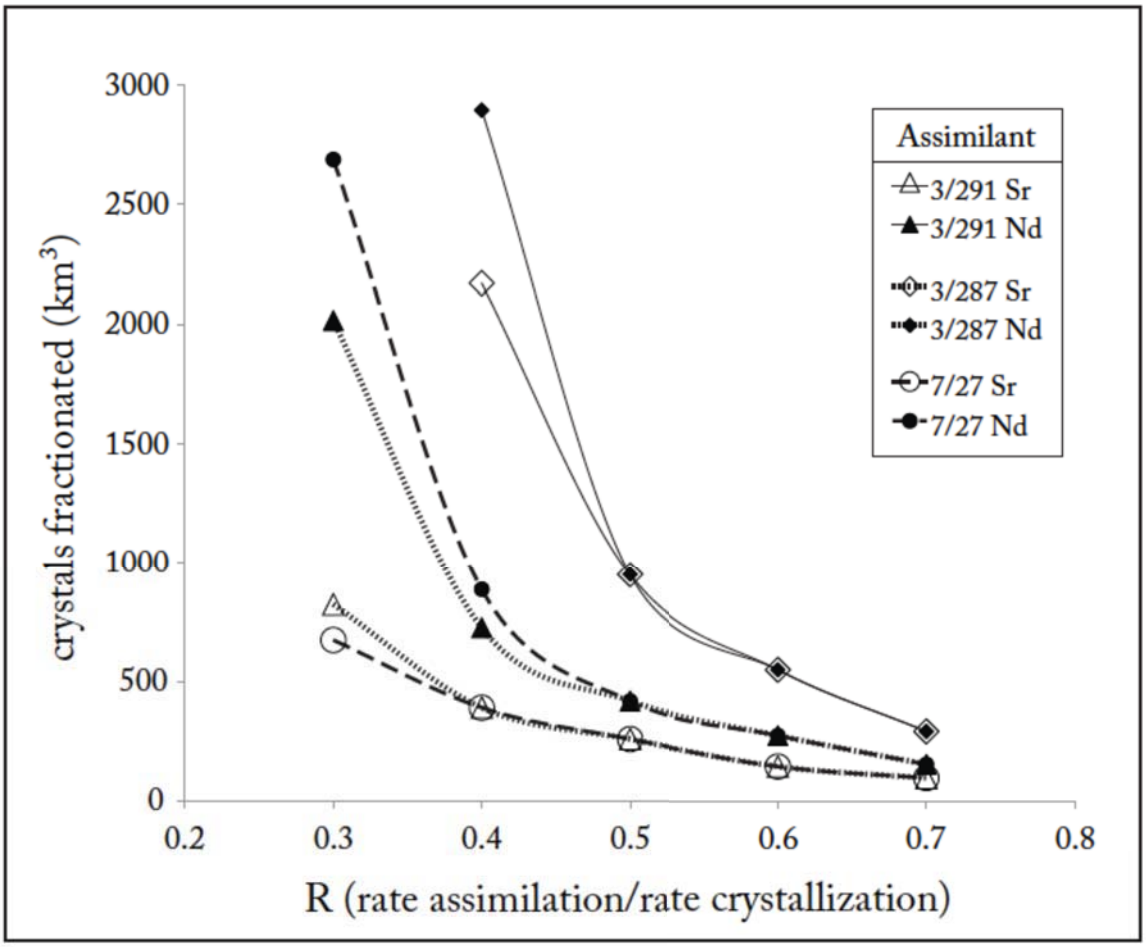

Figure 3.20: Mass balance consequences of changing the R-value (rate assimilation/rate crystallization), calculated with AFC equations (DePaolo, 1981). With increasing R-value, the volume of cumulate crystals required increases. Solutions for both $^{87}Sr/^{86}Sr$ and ε_{Nd} are shown for three different assimilants (see text, and **Tables 3.7 & 3.8**). Despite large variations in crystal volume estimates with changing R, calculated crustal additions do not vary significantly (see **Figure 3.19**).

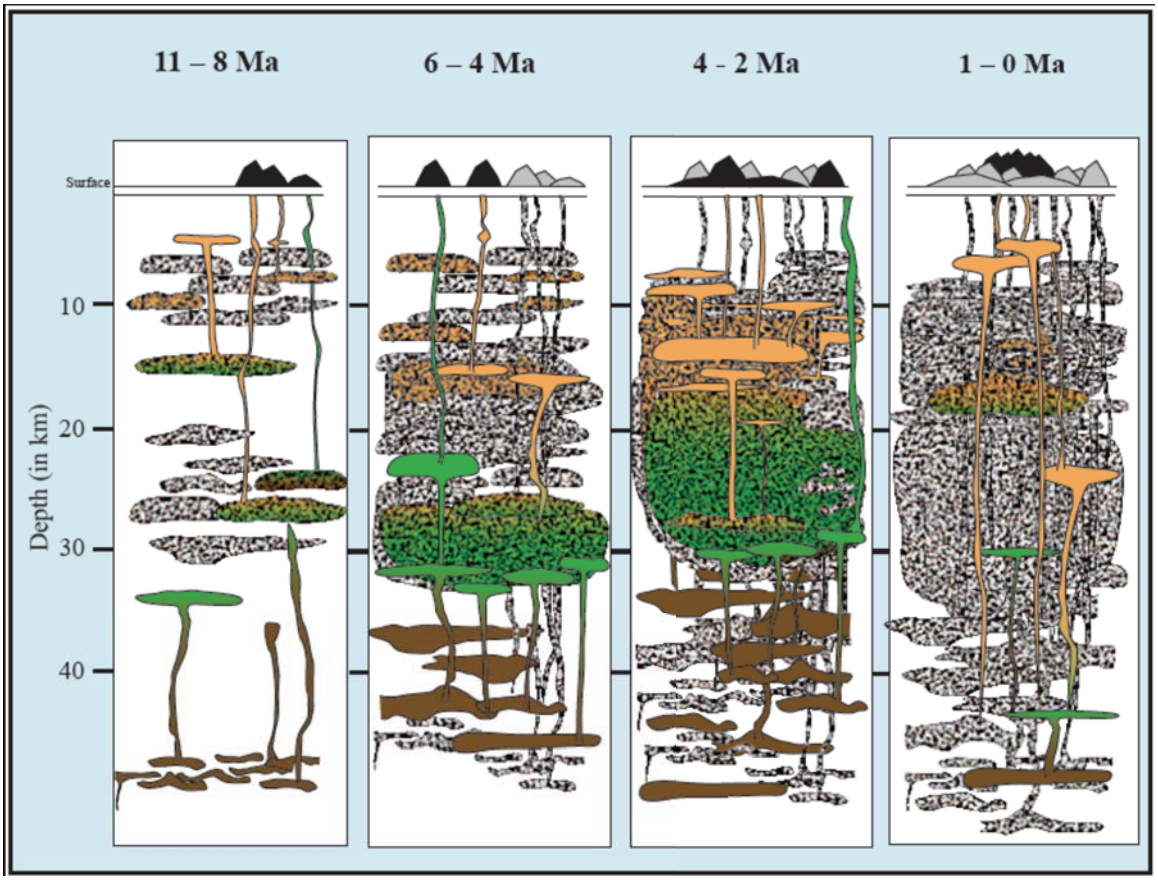

Figure 3.21: Cartoon for the underpinnings of the AVC. See text for discussion.

Tables

(captions for Tables 3.1 and 3.2)

Table 3.1: Representative whole rock compositions of the AVC. Major elements expressed in wt %, and are normalized to 100% volatile free. Trace elements expressed in ppm. Major and trace elements (Ni through Zn) analyzed at Washington State University by XRF. Elements La through Cs (including the REEs) were analyzed by ICP-MS at Washington State University. FeO* is total Fe. Ages in italics are estimates based on stratigraphic relation to previous age data (Grunder et al., 2006; Klemetti et al., 2008). Non-italicized ages from zircon dating (Walker et al., 2010).

Table 3.2: Isotope data for the AVC. $^{87}Sr/^{86}Sr$ and $^{143}Nd/^{144}Nd$ are age corrected. Sr and Nd in ppm. $\delta^{18}O$ values in per mil (‰). Errors for Sr and Nd isotopes is the number in the parentheses in the last reported decimal place. Radiogenic isotopes were analyzed by TIMS at the University of Colorado. $\delta^{18}O$ was analyzed by CO_2 laser fluorination and mass spectrometry at the University of Oregon. Age data: (a) Ar-Ar (Grunder et al., 2006; Klemetti et al., 2008); (k) K-Ar (Grunder, 1997; Baker and Francis, 1978); (z) zircon. Ages in italics are estimates based on stratigraphic relation to previous age data.

Table 3.1:

Sample	AP-07-10A	AP-07-03	AP-07-04	AP-07-73	AP-07-74	AP-07-75	AP-07-91	AP-07-08	AP-07-10B	AP-07-13	AP-07-16	AP-07-17	AP-07-70	AP-07-81	AP-07-84	AP-07-87
Age (Ma)	*7.5*	*10*	*10*	*8*	*8*	*8*	*8*	*7.5*	*7.5*	*7.5*	*8*	*8*	*8*	*9*	*8*	*9*
Eruptive gp.	Alconcha	Alconcha	Alconcha	Alconcha	Alconcha	Alconcha	Alconcha	Alconcha 2	Alconcha 2	Alconcha 2	Alconcha 2	Alconcha 2	Alconcha 2	Alconcha 2	Alconcha 2	Alconcha 2
Latitude	-21.12634	-21.09396	-21.09087	-21.18604	-21.18163	-21.16960	-21.17968	-21.12238	-21.12453	-21.12275	-21.07820	-21.07913	-21.11372	-21.00979	-21.12561	-21.05383
Longitude	-68.35943	-68.55986	-68.56707	-68.32598	-68.32301	-68.33231	-68.31157	-68.36030	-68.36083	-68.37257	-68.35965	-68.36530	-68.40573	-68.39778	-68.30178	-68.37597
volcano	Quenal	Alconcha	Alconcha	Amincha	Amincha	Amincha	Co. Inca Ridge	Koska	Quenal	Quenal	Coscalito	Coscalito	Coscalito	Coasa	Koska	Coasa east
SiO2	56.6	62.4	58.9	56.9	64.3	63.4	65.1	62.5	63.9	63.0	61.6	65.7	60.3	59.2	66.0	62.8
Al2O3	17.5	17.6	18.4	18.5	17.1	17.6	17.2	16.4	16.4	16.9	16.3	15.6	17.2	17.0	16.4	16.4
TiO2	0.96	0.54	0.66	0.93	0.54	0.57	0.48	0.79	0.68	0.74	0.96	0.66	0.97	1.03	0.58	0.76
FeO*	7.02	5.14	6.45	7.12	4.28	4.65	3.96	5.13	4.63	5.35	6.03	4.56	6.10	6.53	3.90	5.17
MnO	0.11	0.12	0.13	0.12	0.11	0.11	0.11	0.09	0.08	0.07	0.10	0.07	0.09	0.10	0.08	0.09
CaO	7.59	5.44	6.59	6.73	4.35	4.53	3.92	5.17	4.65	4.89	5.41	4.09	5.70	6.02	3.85	5.08
MgO	4.51	2.14	2.90	3.09	1.50	1.33	1.29	3.04	2.51	1.98	3.01	1.98	3.03	3.47	1.65	2.88
K2O	2.11	2.80	1.87	2.25	2.92	2.48	3.60	2.98	3.12	2.76	2.83	3.56	2.33	2.75	3.85	3.46
Na2O	3.46	3.60	3.90	3.97	4.56	4.86	4.05	3.72	3.92	4.05	3.55	3.61	3.92	3.59	3.53	3.18
P2O5	0.23	0.24	0.23	0.33	0.31	0.40	0.28	0.20	0.19	0.24	0.25	0.18	0.27	0.26	0.16	0.21
Pre-norm Total	97.29	97.71	99.13	99.00	98.46	97.93	97.62	98.44	98.09	98.10	98.47	97.99	97.85	98.36	97.39	97.71
Ni	28	2	2					18	6	7	15	4	47	14	2	12
Cr	73	5	2		1		3	69	30	17	68	16	166	39	10	45
Sc	20	11	16	13	7	5	6	11	10	10	12	10	15	15	9	13
V	181	97	145	143	48	48	39	128	117	125	133	103	144	161	89	132
Ba	629	846	660	923	907	914	1324	725	793	751	875	807	726	699	822	707
Rb	42	60	39	43	74	61	92	92	89	78	74	120	62	73	178	96
Sr	577	532	668	705	552	639	544	508	539	555	532	428	574	546	491	521
Zr	127	163	131	160	219	223	227	138	136	135	142	141	134	156	186	139
Ga	19	16	18	19	19	18	18	17	18	17	17	17	18	19	18	17
Cu	42	41	60	26	9	13	4	28	49	47	44	59	24	51	25	50
Zn	96	74	80	93	83	88	82	100	74	91	89	77	96	90	58	77
La	20.8	23.1	18.5	25.1	33.8	32.9	36.5	25.0	24.0	24.5	24.3	26.5	16.5	24.4	30.8	25.0
Ce	41.3	44.4	37.1	49.9	66.3	66.1	68.4	49.0	47.0	48.3	48.1	52.4	31.2	48.5	59.2	48.7
Pr	5.2	5.4	4.6	6.3	7.9	8.0	8.4	5.8	5.5	5.9	6.0	6.1	3.7	6.0	6.9	5.9
Nd	20.8	20.0	18.0	25.0	29.5	30.3	31.6	22.2	20.8	22.6	23.3	22.3	14.6	23.5	24.7	22.0
Sm	4.3	4.0	3.7	5.0	5.7	5.6	5.8	4.3	3.9	4.5	4.7	4.2	2.9	4.8	4.6	4.4
Eu	1.3	1.0	1.1	1.5	1.4	1.6	1.4	1.1	1.0	1.2	1.3	1.0	1.2	1.3	1.0	1.1
Gd	3.7	3.4	3.3	4.4		4.4	4.9	3.7	3.2	3.7	4.1	3.6	2.6	4.0	3.6	3.6
Tb	0.6	0.5	0.5	0.7	0.7	0.6	0.7	0.5	0.5	0.5	0.6	0.5	0.4	0.6	0.6	0.5
Dy	3.2	3.3	3.2	3.7	4.0	3.5	4.1	3.0	2.7	3.0	2.9	3.0	2.1	3.3	3.3	3.1
Ho	0.6	0.7	0.7	0.7	0.8	0.7	0.8	0.6	0.5	0.6	0.5	0.6	0.4	0.6	0.7	0.6
Er	1.6	1.8	1.8	1.9	2.2	1.8	2.2	1.5	1.4	1.5	1.3	1.5	1.0	1.6	1.9	1.6
Tm	0.2	0.3	0.3	0.3	0.3	0.3	0.3	0.2	0.2	0.2	0.2	0.2	0.2	0.2	0.3	0.2
Yb	1.3	1.8	1.7	1.6	2.1	1.6	2.1	1.3	1.2	1.3	1.1	1.4	0.9	1.4	1.7	1.5
Lu	0.2	0.3	0.3	0.3	0.3	0.3	0.4	0.2	0.2	0.2	0.2	0.2	0.1	0.2	0.3	0.2
Th	4.4	4.3	3.1	3.7	9.1	5.8	8.4	13.8	11.1	11.6	10.5	22.1	9.3	10.5	31.2	13.6
Nb	5.6	6.6	4.9	7.3	9.7	9.0	9.7	7.4	6.9	7.4	7.6	9.0	7.2	7.7	9.6	7.3
Y	15.9	17.7	16.8	18.9	21.2	17.3	22.2	15.3	13.4	14.7	14.6	15.4	10.5	15.9	17.5	16.5
Hf	3.3	4.2	3.5	4.2	5.7	5.6	6.0	3.9	3.9	3.8	4.0	4.1	3.8	4.2	5.5	4.1
Ta	0.3	0.5	0.3	0.4	0.7	0.6	0.6	0.6	0.6	0.6	0.6	0.9	0.6	0.6	0.9	0.6
U	1.2	1.0	0.6	0.8	2.2	1.3	2.1	3.9	3.2	3.6	3.1	6.0	2.8	2.9	9.0	3.8
Pb	7.4	11.9	9.2	6.7	11.7	8.7	11.8	12.4	13.1	10.2	10.6	14.9	10.1	10.3	17.7	12.6
Cs	1.7	1.9	1.1	0.9	2.3	1.0	2.8	6.0	4.9	3.5	6.0	13.2	3.8	4.7	17.2	7.2
Rb/Sr	0.07	0.11	0.06	0.06	0.13	0.09	0.17	0.18	0.17	0.14	0.14	0.28	0.11	0.13	0.36	0.18
dy/yb	2.4	1.8	1.9	2.3	1.9	2.2	1.9	2.3	2.3	2.3	2.7	2.1	2.2	2.5	1.9	2.0
sm/yb	3.2	2.2	2.2	3.1	2.8	3.5	2.7	3.3	3.4	3.5	4.3	3.0	3.1	3.5	2.6	2.9
Sr/Y	35.9	31.5	41.5	40.7	26.7	37.8	25.9	34.4	41.5	39.3	39.4	28.9	56.8	35.5	29.0	33.2
Eu/Eu*	0.99	0.85	0.94	0.96	0.83	0.95	0.84	0.84	0.86	0.86	0.93	0.74	1.29	0.90	0.70	0.81

Table 3.1, continued:

Sample	AP-07-22	AP-07-36	AP-07-43	AP-07-46	AP-07-51	AP-07-53	AP-07-54	AP-07-55	AP-07-62A	AP-07-65A	AP-07-71	AP-07-78	AP-07-86	AP-07-07	AP-07-23A	AP-07-83
Age (Ma)	*2.5*	*3.5*	*3*	*3*	3	*3.5*	*3.5*	*3.4*	*2.2*	*2.2*	*3*	*3.2*	*4*	0.8	*0.05*	*0.05*
Eruptive gp.	Polan	Polan	Polan	Polan	Polan	Polan	Polan	Polan	Polan	Polan	Polan	Polan	Polan	Aucanquilcha	cinder cone	cinder cone
Latitude	-21.28241	-21.16373	-21.32659	-21.33304	-21.23761	-21.27763	-21.27782	-21.28339	-21.26735	-21.29289	-21.11941	-21.12705	-21.20359	-21.20219	-21.30626	-21.31749
Longitude	-68.33218	-68.39050	-68.59420	-68.63110	-68.39913	-68.40983	-68.41276	-68.43315	-68.54340	-68.55653	-68.41846	-68.54084	-68.37442	-68.46605	-68.33126	-68.29290
volcano	SE platform	Central Monos	SW lava field	SW lava field	South plat	CampOguan	CampOguan	Camp/S plat	Chaihuiri	Chaihuiri	Tres Monos	N Platform	E Platform	Aucanquilcha	Luna de Tierra	Poruñita
SiO2	61.6	60.7	62.1	63.0	64.7	63.9	61.5	61.6	62.5	61.6	59.9	62.8	58.9	63.8	58.3	57.0
Al2O3	16.7	16.5	16.7	16.6	15.8	16.1	16.5	16.4	16.8	16.7	17.5	16.2	18.1	16.9	16.4	17.3
TiO2	0.93	1.05	0.82	0.73	0.72	0.70	0.97	0.94	0.81	0.86	0.84	0.81	0.95	0.74	1.09	1.18
FeO*	5.41	5.65	5.30	5.14	4.62	5.12	5.53	5.59	5.07	5.59	6.25	5.18	6.08	4.34	6.69	7.06
MnO	0.08	0.09	0.08	0.09	0.08	0.09	0.09	0.09	0.08	0.09	0.10	0.08	0.10	0.07	0.11	0.11
CaO	5.23	5.73	5.12	4.80	4.30	4.57	5.20	5.28	5.11	5.43	5.80	4.91	6.26	4.56	6.70	6.74
MgO	2.98	3.04	2.85	2.63	2.47	2.36	3.12	3.05	2.56	2.91	3.09	2.92	2.91	2.44	4.23	4.49
K2O	3.20	2.77	2.52	2.74	3.34	3.21	3.16	2.66	2.59	2.47	2.42	3.08	2.03	2.70	2.58	2.03
Na2O	3.67	4.15	4.25	4.10	3.80	3.77	3.72	4.12	4.21	4.13	3.85	3.86	4.38	4.19	3.65	3.88
P2O5	0.24	0.36	0.21	0.21	0.20	0.18	0.25	0.26	0.22	0.23	0.21	0.21	0.24	0.21	0.34	0.25
Pre-norm Total	98.08	99.02	99.31	99.29	97.37	99.26	98.43	100.15	98.80	99.18	99.05	98.64	97.85	98.73	97.74	99.41
Ni	14	14	12	14	12	4	12	14	9	13	9	9	29	7	27	17
Cr	52	64	49	33	44	24	64	83	41	50	16	55	34	54	158	74
Sc	12	14	11	12	10	14	13	12	11	14	15	12	16	9	16	17
V	137	141	138	129	115	118	141	140	137	149	153	128	156	106	165	193
Ba	828	1102	780	752	792	812	827	856	759	748	721	810	716	916	855	786
Rb	78	72	64	77	97	102	73	72	70	65	67	83	48	70	69	43
Sr	560	807	576	528	481	450	564	591	607	617	536	538	658	539	637	603
Zr	170	202	149	152	155	166	182	182	149	149	145	162	140	155	208	163
Ga	20	20	18	19	18	17	18	17	20	19	19	17	20	18	19	20
Cu	34	43	47	45	53	34	38	43	35	38	33	45	52	26	30	23
Zn	98	94	86	84	80	76	93	91	88	91	93	82	92	86	97	114
La	29.4	46.6	24.0	24.8	27.7	29.2	29.8	30.6	27.1	24.6	22.0	27.0	23.4	24.0	36.0	26.0
Ce	58.9	88.8	48.6	49.1	53.6	57.8	59.8	61.6	53.7	50.1	44.9	53.6	46.0	46.5	73.5	53.2
Pr	7.2	10.5	5.9	6.0	6.6	6.9	7.3	7.5	6.5	6.1	5.5	6.6	5.8	5.5	8.9	6.7
Nd	27.6	38.9	22.9	22.8	24.5	25.1	28.1	28.6	24.4	23.4	21.2	25.0	22.7	20.6	34.1	27.0
Sm	5.5	6.9	4.5	4.5	4.7	4.8	5.5	5.5	4.8	4.7	4.5	4.9	4.6	4.0	6.4	5.8
Eu	1.4	1.7	1.2	1.1	1.0	1.1	1.4	1.4	1.2	1.2	1.1	1.2	1.3	1.2	1.6	1.6
Gd	4.3	5.1	3.6	3.8	3.8	3.9	4.4	4.4	3.8	3.9	3.9	4.0	3.8	3.1	4.9	5.0
Tb	0.6	0.7	0.5	0.6	0.5	0.6	0.6	0.6	0.6	0.6	0.6	0.6	0.6	0.4	0.7	0.7
Dy	3.4	3.6	2.9	3.3	3.0	3.5	3.3	3.3	3.2	3.1	3.6	3.2	3.1	2.3	3.9	4.1
Ho	0.6	0.6	0.5	0.6	0.5	0.7	0.6	0.6	0.6	0.6	0.7	0.6	0.6	0.4	0.7	0.8
Er	1.5	1.6	1.4	1.7	1.4	1.8	1.5	1.5	1.5	1.5	1.8	1.5	1.5	1.0	1.9	1.9
Tm	0.2	0.2	0.2	0.2	0.2	0.3	0.2	0.2	0.2	0.2	0.3	0.2	0.2	0.1	0.3	0.3
Yb	1.2	1.3	1.2	1.5	1.3	1.6	1.3	1.2	1.2	1.3	1.6	1.3	1.2	0.8	1.6	1.5
Lu	0.2	0.2	0.2	0.2	0.2	0.3	0.2	0.2	0.2	0.2	0.2	0.2	0.2	0.1	0.2	0.2
Th	8.2	8.1	8.0	10.3	12.6	13.1	9.4	8.6	9.2	8.4	8.6	11.1	4.4	6.3	7.7	3.5
Nb	8.9	12.7	7.1	7.3	7.9	8.5	10.0	8.8	8.6	8.1	7.1	7.9	5.8	7.6	9.9	9.1
Y	15.6	17.8	13.7	16.8	14.4	17.7	15.8	15.6	15.1	15.6	17.7	15.0	15.2	10.1	18.7	19.3
Hf	4.6	5.2	4.2	4.2	4.4	4.7	4.9	4.8	4.1	4.1	4.1	4.5	3.7	4.3	5.4	4.2
Ta	0.7	0.9	0.5	0.6	0.6	0.7	0.7	0.6	0.7	0.6	0.5	0.6	0.3	0.5	0.6	0.6
U	2.5	1.9	2.1	2.7	3.4	3.6	2.3	2.1	2.5	2.3	2.2	3.0	1.1	1.8	1.9	0.9
Pb	12.2	10.0	11.8	12.5	13.9	13.4	11.8	11.2	11.7	10.9	10.9	12.8	9.4	11.8	10.5	9.0
Cs	3.1	1.9	2.8	3.6	5.0	3.4	3.1	1.9	1.7	2.3	2.9	4.1	1.4	2.3	25.1	0.8
Rb/Sr	0.14	0.09	0.11	0.15	0.20	0.23	0.13	0.12	0.11	0.11	0.12	0.15	0.07	0.13	0.11	0.07
dy/yb	2.7	2.8	2.5	2.1	2.4	2.1	2.6	2.7	2.6	2.4	2.3	2.5	2.5	2.8	2.5	2.7
sm/yb	4.5	5.4	3.9	3.0	3.8	2.9	4.3	4.5	4.0	3.7	2.9	3.9	3.7	5.0	4.1	3.8
Sr/Y	35.4	47.8	40.8	31.4	36.1	25.7	38.9	39.4	40.5	42.5	31.2	35.8	41.4	58.0	34.8	30.3
Eu/Eu*	0.85	0.89	0.89	0.78	0.74	0.75	0.84	0.87	0.82	0.83	0.83	0.81	0.94	1.05	0.88	0.89

Table 3.1, continued:

Sample	AP-07-90	AP-07-88A	AP-07-72	AP-07-24	AP-07-26	AP-07-27	AP-07-28	AP-07-29	AP-07-30	AP-07-40	AP-07-41	AP-07-62C	AP-07-65B	AP-07-37	AP-07-19	AP-07-20
Age (Ma)	*9*	*9.5*	*5.5*	*4.5*	4.5	4	*5*	*4.5*	*5*	*5.5*	*5.5*	*2.2*	*2.2*	*3.5*	2.2	*2.2*
Eruptive gp.	Alconcha 2	Ujina	Carcote	Gordo	Gordo	Gordo	Gordo	Gordo	Gordo	Gordo	Gordo	Polan	Polan	Polan	Polan	Polan
Latitude	-21.04678	-21.06433	-21.18784	-21.33081	-21.34910	-21.35446	-21.33551	-21.33440	-21.32224	-21.33363	-21.33098	-21.26735	-21.29289	-21.14974	-21.27444	-21.27578
Longitude	-68.35262	-68.37579	-68.32483	-68.33718	-68.37756	-68.39689	-68.40138	-68.40048	-68.40098	-68.55437	-68.58903	-68.54340	-68.55653	-68.38685	-68.50732	-68.51475
volcano	Coasa far E	Ujina	Carcote Ign	Rojo	Rojo	Pabellon	Las Bolitas	Rojo	Las Bolitas	Puquios	Iconas	Chaihuiri	Chaihuiri	Tres Monos	Chaihuiri	Chaihuiri
SiO2	62.8	64.0	76.1	62.5	62.5	62.3	64.0	59.1	61.8	60.0	68.4	56.7	57.4	63.2	64.5	63.0
Al2O3	16.3	16.9	13.1	16.1	16.5	16.7	16.2	16.6	16.5	17.8	16.1	20.6	17.8	16.3	16.2	17.0
TiO2	0.81	0.68	0.19	0.87	0.79	0.73	0.71	1.05	0.91	0.87	0.47	1.05	1.07	0.91	0.66	0.71
FeO*	5.34	4.98	0.97	5.36	5.16	5.11	4.68	6.61	5.47	5.96	2.62	8.00	6.73	5.29	4.48	4.68
MnO	0.09	0.08	0.08	0.09	0.09	0.09	0.08	0.11	0.09	0.10	0.04	0.12	0.10	0.09	0.08	0.08
CaO	4.96	4.46	0.62	4.85	5.07	5.15	4.54	5.89	5.29	5.98	3.34	7.31	6.68	4.63	4.38	4.87
MgO	2.79	2.11	0.20	2.79	2.71	2.86	2.52	3.66	2.91	2.78	1.10	1.25	4.07	2.33	2.35	2.44
K2O	3.05	3.42	5.47	3.29	3.32	3.07	3.26	2.95	2.67	1.98	3.09	0.86	1.87	2.85	3.07	2.62
Na2O	3.65	3.15	3.14	3.90	3.63	3.77	3.83	3.75	4.08	4.35	4.60	3.84	3.95	4.19	4.08	4.39
P2O5	0.20	0.20	0.05	0.23	0.21	0.19	0.20	0.32	0.25	0.25	0.17	0.27	0.27	0.25	0.20	0.22
Pre-norm Total	99.23	96.42	94.61	98.46	97.44	98.27	98.06	98.79	98.21	98.93	97.40	97.55	97.68	98.86	98.24	98.49
Ni	14	8		13	14	11	19	18	16	14	1	28	17	9	4	4
Cr	23	19	2	66	50	23	64	93	64	26	8	62	77	42	26	17
Sc	13	10	3	12	11	12	11	14	14	16	5	16	16	12	10	11
V	131	111	8	130	115	133	109	158	137	154	69	142	176	128	118	127
Ba	757	673	1026	864	785	711	778	972	795	731	939	363	690	874	808	837
Rb	92	137	127	101	93	82	105	74	71	47	84	32	40	76	88	65
Sr	468	485	69	487	468	512	449	688	565	599	610	741	766	549	558	624
Zr	142	137	115	223	194	151	198	190	173	143	139	152	146	170	141	137
Ga	18	19	14	16	18	18	19	19	19	19	20	22	20	19	18	18
Cu	52	22	7	40	63	47	38	27	49	63	44	55	48	60	54	53
Zn	70	69	27	84	80	74	78	103	85	83	60	322	110	99	74	75
La	24.3	24.7	21.5	30.4	30.8	22.6	27.8	35.3	28.5	20.7	24.5	21.9	24.0	28.9	24.0	23.3
Ce	47.9	49.2	41.2	63.3	57.2	45.6	56.2	72.0	57.2	42.5	47.1	45.6	50.4	57.6	47.7	46.0
Pr	5.7	5.7	4.6	7.7	7.3	5.4	6.7	8.8	6.9	5.3	5.4	5.8	6.4	7.3	5.6	5.6
Nd	21.2	21.3	15.6	29.7	27.6	20.9	25.3	34.0	26.6	21.1	19.8	23.0	25.6	28.3	21.3	21.2
Sm	4.2	4.2	2.9	5.9	5.4	4.2	5.0	6.5	5.2	4.4	3.4	4.8	5.2	5.6	4.2	4.1
Eu	1.1	1.0	0.4	1.3	1.2	1.0	1.1	1.6	1.3	1.2	0.8	1.4	1.4	1.3	1.0	1.0
Gd	3.4	3.6	2.5	4.9	4.5	3.5	4.1	5.2	4.3	3.9	2.4	4.1	4.4	4.7	3.3	3.3
Tb	0.5	0.5	0.4	0.7	0.7	0.5	0.6	0.7	0.6	0.6	0.3	0.6	0.6	0.6	0.5	0.5
Dy	3.0	3.1	2.4	4.0	3.7	3.1	3.4	4.0	3.3	3.5	1.5	3.3	3.5	3.4	2.7	2.7
Ho	0.6	0.6	0.5	0.8	0.7	0.6	0.6	0.7	0.6	0.7	0.3	0.6	0.6	0.6	0.5	0.5
Er	1.6	1.6	1.4	1.9	1.8	1.6	1.7	1.7	1.6	1.7	0.7	1.5	1.6	1.6	1.3	1.4
Tm	0.2	0.2	0.2	0.3	0.3	0.2	0.2	0.2	0.2	0.2	0.1	0.2	0.2	0.2	0.2	0.2
Yb	1.4	1.5	1.4	1.7	1.6	1.4	1.5	1.4	1.3	1.5	0.6	1.2	1.2	1.3	1.1	1.2
Lu	0.2	0.2	0.2	0.3	0.2	0.2	0.2	0.2	0.2	0.3	0.1	0.2	0.2	0.2	0.2	0.2
Th	15.5	18.5	11.0	11.1	9.7	10.1	12.3	6.8	9.2	4.6	7.4	5.1	3.8	9.2	10.1	7.0
Nb	8.2	8.4	10.4	10.3	8.3	6.8	8.6	11.9	9.4	6.1	5.3	6.5	8.0	8.6	6.9	6.2
Y	15.4	16.6	14.0	19.5	18.6	15.1	17.2	18.0	16.0	17.2	7.0	15.4	16.4	17.1	13.1	13.5
Hf	4.2	3.9	3.8	6.2	5.3	4.2	5.3	5.1	4.6	3.8	3.9	3.9	3.9	4.7	4.0	3.8
Ta	0.7	0.8	0.8	0.7	0.6	0.5	0.7	0.7	0.7	0.4	0.4	0.4	0.5	0.6	0.6	0.5
U	4.1	4.9	3.3	3.1	2.6	2.8	3.4	2.0	2.3	1.2	1.8	1.0	0.9	2.6	2.8	1.9
Pb	12.9	9.4	11.2	14.0	12.6	11.7	13.2	11.3	9.8	10.0	14.4	76.4	10.6	12.5	13.2	12.4
Cs	6.0	10.8	6.6	5.3	4.3	4.2	5.6	2.2	1.6	0.9	2.7	21.2	1.3	3.0	4.4	3.3
Rb/Sr	0.20	0.28	1.84	0.21	0.20	0.16	0.23	0.11	0.13	0.08	0.14	0.04	0.05	0.14	0.16	0.10
dy/yb	2.1	2.1	1.8	2.4	2.4	2.1	2.3	2.8	2.5	2.3	2.6	2.7	2.9	2.7	2.4	2.4
sm/yb	3.0	2.8	2.1	3.4	3.5	3.0	3.3	4.6	4.0	2.9	6.2	3.9	4.3	4.4	3.6	3.5
Sr/Y	30.8	28.2	4.8	25.4	24.9	35.3	26.4	39.3	36.7	35.3	83.6	49.1	48.8	31.6	45.7	46.2
Eu/Eu*	0.84	0.81	0.48	0.73	0.75	0.81	0.76	0.85	0.87	0.88	0.90	0.95	0.91	0.78	0.78	0.86

Table 3.2:

Sample	Age	$d^{18}O$	Sr	$^{87}Rb/^{86}Sr$	$^{87}Sr/^{86}Sri$	Nd	$^{147}Sm/^{144}Nd$	$^{143}Nd/^{144}Ndi$	End	$^{208}Pb/^{204}Pb$	$^{207}Pb/^{204}Pb$	$^{206}Pb/^{204}Pb$
AP-07-23a	*0.05*	7.15 (8.82)	604	0.296	0.70635(1)	31.5	0.1071	0.51232(1)	-6.1	38.424	15.633	18.553
AP-07-83	*0.05*	8.96	570	0.194	0.70646(1)	25.0	0.1234	0.51231(2)	-6.3	38.494	15.624	18.671
AP2-00-57	0.24 (a)		544	0.379	0.70629(2)	21.9	0.1081	0.51233(2)	-6.0	38.525	15.603	18.652
AP2-00-49	*0.3*	7.00										
AP2-00-75	*0.4*		549	0.354	0.70640(2)	23.7	0.1133	0.51234(1)	-5.7	38.522	15.607	18.668
AP2-00-61	*0.5*		514	0.461	0.70600(1)	15.7	0.1072	0.51235(1)	-5.7	38.597	15.621	18.679
AP2-00-79	*0.5*	7.25	561	0.367	0.70624(1)	22.3	0.1116	0.51233(2)	-6.0	38.630	15.635	18.695
AP2-00-92	0.5 (z)	7.32	542	0.387	0.70582(2)	18.8	0.1041	0.51239(2)	-4.9	38.614	15.624	18.672
AP2-00-96	*0.5*		633	0.423	0.706202(7)	24.1	0.1091	0.51235(2)	-5.6	38.687	15.654	18.708
AP2-00-91	*0.6*	7.13	526	0.418	0.705791(8)	20.0	0.1075	0.51240(2)	-4.6	38.604	15.622	18.670
AP2-00-77	0.62 (a)	7.03	591	0.247	0.70679(2)	25.9	0.1193	0.51228(2)	-7.0	38.518	15.616	18.689
AP2-00-98	*0.8*		512	0.428	0.70679(1)	29.6	0.0938	0.512277(9)	-7.0	38.537	15.624	18.686
AP2-00-71	*0.8*		663	0.223	0.706212(8)	22.3	0.1183	0.51226(3)	-7.3	38.537	15.612	18.663
AP2-00-100	0.89 (a)		453	0.615	0.70667(1)	26.7	0.1034	0.51228(3)	-7.0	38.560	15.624	18.692
AP2-00-70	*0.9*		499	0.494	0.70634(1)	25.5	0.0994	0.51230(2)	-6.5	38.525	15.603	18.652
AP-00-54	0.98 (a)	7.06	396	0.661	0.706602(8)	24.9	0.1057	0.51229(1)	-6.8	38.582	15.635	18.672
AP2-00-47	*1*		530	0.413	0.706129(9)	23.3	0.0973	0.51234(1)	-5.8	38.574	15.626	18.678
AP2-00-64	1.01 (a)	7.28	505	0.449	0.706497(9)	20.3	0.1087	0.51229(2)	-6.7	38.489	15.609	18.656
AP-07-19	2.2 (z)	7.36 (7.88)	533	0.431	0.705627(9)	19.6	0.1096	0.51242(3)	-4.2	38.566	15.611	18.662
AP-07-62a	*2.2*	7.04										
AP-07-62c	*2.2*		702	0.118	0.70565(1)	21.2	0.1192	0.51241(2)	-4.4	38.587	15.619	18.657
AP-00-52	2.57 (a)	7.02	538	0.379	0.705705(9)	22.8	0.1081	0.51242(3)	-4.2	38.949	15.689	19.459
AP-00-30	*3*	6.99	635	0.127	0.705753(9)	20.8	0.1094	0.51239(1)	-4.7	38.726	15.651	18.682
AP-07-45	*3*	6.98	494	0.403	0.70574(1)	20.9	0.1153	0.51244(1)	-3.8	38.534	15.605	18.653
AP-07-51	3	7.47	453	0.534	0.70587(1)	22.6	0.1102	0.51242(1)	-4.3	38.547	15.611	18.665
AP-00-45	*3.1*	6.82										
AP-07-78	*3.2*	6.90	510	0.429	0.70580(2)	22.9	0.1142	0.51239(1)	-4.7	38.550	15.618	18.656
VM99-16	*3.3*	7.40	617	0.437	0.705543(8)	19.7	0.1154	0.5124(2)	-4.4	38.160	15.599	18.223
VM99-52	3.3 (a)		613	0.192	0.70560(1)	16.0	0.1030	0.512432(5)	-3.9	38.627	15.639	18.672
AP-00-62	*3.4*	6.96	543	0.316	0.705767(9)	21.4	0.1089	0.51239(1)	-4.8	38.529	15.639	18.655
AP-07-27	4 (z)	6.91	483	0.445	0.70567(1)	18.8	0.1152	0.51247(1)	-3.2	38.618	15.629	18.677
AP-07-86	*4*	6.78	624	0.201	0.70564(1)	20.8	0.1113	0.51243(2)	-3.9	38.487	15.612	18.622
AP-00-38	4.28 (a)		603	0.252	0.70652(1)	27.2	0.1023	0.51232(2)	-6.1	38.529	15.606	18.684
AP-00-37	4.4 (z)	6.85	456	0.387	0.70608(1)	23.1	0.1134	0.51240(2)	-4.5	38.529	15.601	18.656
AP-07-26	4.5 (z)	6.93	445	0.555	0.70586(1)	25.3	0.1118	0.51241(2)	-4.3	38.403	15.583	18.608
AP-07-29	*4.5*	6.50	656	0.301	0.70626(1)	31.4	0.1092	0.51234(1)	-5.7	38.453	15.612	18.653
AP-07-28	*5*	7.29	422	0.652	0.70575(1)	23.6	0.1128	0.51241(3)	-4.3	38.475	15.601	18.621
AP-00-72	*5*	6.84	619	0.262	0.70544(1)	16.3	0.1087	0.51248(1)	-3.0	38.564	15.599	18.648
AP-00-83	*5.5*	6.83	648	0.131	0.70553(1)	20.4	0.1135	0.51240(1)	-4.5	38.525	15.617	18.636
AP-07-41	*5.5*		576	0.379	0.70579(1)	18.2	0.0994	0.512419(9)	-4.1	38.598	15.603	18.666
AP-07-72b	5.6 (k)		63.7	5.157	0.70575(1)	13.3	0.1098	0.512446(1)	-3.6	38.499	15.611	18.618
AP-00-92	5.81 (a)		599	0.237	0.70549(1)	21.8	0.1071	0.51243(2)	-3.9	38.691	15.665	18.675
AP-07-08	7.5 (z)	7.46	483	0.507	0.70542(1)	20.2	0.1140	0.51243(1)	-3.8	38.459	15.604	18.578
AP-07-10a	*7.5*		547	0.197	0.70546(1)	19.4	0.1203	0.51239(1)	-4.6	38.243	15.589	18.492
AP-07-10b	*7.5*	7.11	512	0.459	0.70555(1)	18.9	0.1103	0.51242(2)	-4.0	38.489	15.597	18.625
AP-00-82	7.99 (a)	6.88	517	0.508	0.70512(1)	24.1	0.1199	0.51245(3)	-3.5	38.466	15.601	18.577
AP-07-17	8 (z)	6.85	407	0.777	0.705288(7)	20.5	0.1103	0.512462(8)	-3.2	38.499	15.601	18.595
AP-07-73	*8*	7.39	672	0.167	0.70546(1)	23.1	0.1173	0.51245(1)	-3.5	38.272	15.586	18.468
AP-07-88a	9.4 (k)		460	0.763	0.70539(1)	19.5	0.1136	0.51245(2)	-3.5	38.565	15.620	18.621
AP-00-03	*10*	6.70	486	0.338	0.70517(1)	18.8	0.1070	0.51255(2)	-1.4	38.557	15.599	18.636
AP-00-11	*10.5*	6.47	669	0.131	0.70507(1)	19.0	0.1085	0.51255(2)	-1.4	38.536	15.595	18.625
AP-00-04	10.78 (a)	6.60	583	0.166	0.70510(1)	18.1	0.1127	0.51258(2)	-0.9	38.625	15.619	18.648
AP-00-17	10.97 (a)	6.73	555	0.247	0.70527(1)	18.5	0.1137	0.51255(1)	-1.5	38.619	15.606	18.672

Table 3.3: Distribution coefficients used for the FC and AFC models in this study. Bulk K_Ds were calculated for the following assemblages. "Dacite FC": 68% plagioclase, 9% clinopyroxene, 9% amphibole, ~4.5% orthopyroxene, ~4.5% biotitte, and ~4.5% magnetite; "Andesite FC": 72% plag, 12% opx, 10% opx, 6% magnetite. Basalt K_Ds were used in modeling the baseline change in Sr and Nd isotopes and the Dy/Yb through time. K_D values for this model were calculated for the assemblage: 30% plagioclase, 30% clinopyroxene, 22% garnet, 16% orthopyroxene. Mineral K_D values were mined from the Geochemical Earth Reference Model (GERM).

Model type	Rb	Sr	Ba	Cr	Nd
FCpx	0.04	1.5	0.22	7	
FCam	0.15	1.5	0.7	10	
Basalt AFC	0.02	0.4	0.1		0.2

Table 3.4: Mass balance calculations for the observed compositional variation of AVC lavas. Individual eruptive groups are shown, broken out into two calculations: those samples interpreted to have experienced fractional crystallization (FC) only; and those interpreted to have experienced both FC and magma-mixing. The FC groups are broken out into andesites and dacites, as FC to these two general compositions involve different amount of crystallization. All mixed magmas are generalized to have experienced 20% crystallization. Volumes are in km^3. Terms: F is the liquid remaining; % xl is the percentage of the starting magma that crystallized; xl mass is the volume of crystals; mass (total) is the combined erupted and crystallized volumes; % mix is the percentage of the rock which is the silicic mixing end-member, 50% in all cases; mix mass is the mass of the silicic mixing end-member. The total volumes are shown at the end of the table.

Alconcha (total eruptive volume = 50)

FC vol.	25					
composition	%	vol	F	% xls	xl mass	mass (total)
andesite	0.5	12.5	0.7	0.3	5.36	17.86
dacite	0.5	12.5	0.4	0.6	18.75	31.25
				Total	24	49

	vol	F	% xls	xl mass	mass (total)	% mix	mix mass
Mix vol.	25	0.8	0.2	6.25	31.25	0.5	15.63

Total volume	80

Gordo (total eruptive volume = 100)

FC vol.	30					
composition	%	vol	F	% xls	xl mass	mass (total)
andesite	0.7	21	0.7	0.3	9	30
dacite	0.3	9	0.5	0.5	9	18
				Total	18	48

	vol	F	% xls	xl mass	mass (total)	% mix	mix mass
Mix vol.	70	0.8	0.2	17.5	87.5	0.5	43.75

Total volume	136

Table 3.4 continued:

Polan (total eruptive volume = 135)

FC vol. 27

composition	%	vol	F	% xls	xl mass	mass (total)
andesite	0.05	1.35	0.6	0.4	0.9	2.25
dacite	0.95	25.65	0.5	0.5	25.65	51.3
				Total	27	54

	vol	F	% xls	xl mass	mass (total)	% mix	mix mass
Mix vol.	108	0.8	0.2	27	135	0.5	67.5

Total volume 189

Mino (total eruptive volume = 15)

FC vol. 15

composition	%	vol	F	% xls	xl mass	mass (total)
andesite	1	15	0.7	0.3	6.43	21.43
dacite	0	0	1	0	0	0
				Total volume	6	21

Aucanq. (total eruptive volume = 50)

FC vol. 50

composition	%	vol	F	% xls	xl mass	mass (total)
andesite	0.05	2.5	0.7	0.3	1.07	3.57
dacite	0.95	47.5	0.5	0.5	47.5	95
				Total volume	49	99

FC and Mixing Mass balance volumes

	Total	cumulate	xls mixed
Alconcha	80	30	15.63
Gordo	136	36	43.75
Polán	189	54	67.5
Miño	21	6	0
Aucanquilcha	99	49	0
total	524	174	127

Table 3.5: Oxygen isotope mixing matrix demonstrating various assimilant $\delta^{18}O$ compositions (top), mixed with a parental magma (bottom). As oxygen makes up ~50% of most silicate magmas and rocks, assimilation can be modeled by mixing. The $\delta^{18}O$ of the parent magma is set at 6.3‰ and 6.5‰, assuming a mantle value of ~5.8‰, and a 0.5 – 0.7‰ increase in $\delta^{18}O$ with differentiation from basalt to andesite. The % assimilant column shows the effect of mixing the given percentage of assimilant with the parent magma.

	$\delta^{18}O$ of the assimilant					
% assimilant	8	10	12	8	10	12
50	7.15	8.15	9.15	7.25	8.25	9.25
45	7.07	7.97	8.87	7.18	8.08	8.98
40	6.98	7.78	8.58	7.10	7.90	8.70
35	6.90	7.60	8.29	7.03	7.73	8.42
30	6.81	7.41	8.01	6.95	7.55	8.15
25	6.73	7.23	7.72	6.88	7.38	7.87
20	6.64	7.04	7.44	6.80	7.20	7.60
15	6.56	6.86	7.15	6.73	7.03	7.32
10	6.47	6.67	6.87	6.65	6.85	7.05
5	6.39	6.49	6.58	6.58	6.68	6.77
0	6.3	6.3	6.3	6.5	6.5	6.5

Table 3.6: Mass balance matrix calculations as R (assimilation rate/crystallization rate) and F (liquid remaining) vary. All numbers are relative to M(erupted), which is the mass erupted. M(o) is original mass, and is equal to M*(erupted)/F. M(loss) is the amount of the original mass lost during differentiation, and is equal to M(o) – M(erupted). Mass (xl) is the mass crystallized during differentiation, and is equal to F*(1+R). M(assim) is the mass assimilated, and equals M(loss)*R. % assim. equals M(assim)/M(o).

M(erupted)	R	F	M(o)	M(loss)	mass(xl)	M(assim)	% assim.
0.2	0.3	0.2	1	0.8	1.04	0.24	0.24
0.3	0.3	0.3	1	0.7	0.91	0.21	0.21
0.4	0.3	0.4	1	0.6	0.78	0.18	0.18
0.5	0.3	0.5	1	0.5	0.65	0.15	0.15
0.6	0.3	0.6	1	0.4	0.52	0.12	0.12
0.7	0.3	0.7	1	0.3	0.39	0.09	0.09
0.8	0.3	0.8	1	0.2	0.26	0.06	0.06
0.9	0.3	0.9	1	0.1	0.13	0.03	0.03

M(erupted)	R	F	M(o)	M(loss)	mass(xl)	M(assim)	% assim.
0.2	0.4	0.2	1	0.8	1.12	0.32	0.32
0.3	0.4	0.3	1	0.7	0.98	0.28	0.28
0.4	0.4	0.4	1	0.6	0.84	0.24	0.24
0.5	0.4	0.5	1	0.5	0.7	0.2	0.2
0.6	0.4	0.6	1	0.4	0.56	0.16	0.16
0.7	0.4	0.7	1	0.3	0.42	0.12	0.12
0.8	0.4	0.8	1	0.2	0.28	0.08	0.08
0.9	0.4	0.9	1	0.1	0.14	0.04	0.04

M(erupted)	R	F	M(o)	M(loss)	mass(xl)	M(assim)	% assim.
0.2	0.5	0.2	1	0.8	1.2	0.4	0.4
0.3	0.5	0.3	1	0.7	1.05	0.35	0.35
0.4	0.5	0.4	1	0.6	0.9	0.3	0.3
0.5	0.5	0.5	1	0.5	0.75	0.25	0.25
0.6	0.5	0.6	1	0.4	0.6	0.2	0.2
0.7	0.5	0.7	1	0.3	0.45	0.15	0.15
0.8	0.5	0.8	1	0.2	0.3	0.1	0.1
0.9	0.5	0.9	1	0.1	0.15	0.05	0.05

M(erupted)	R	F	M(o)	M(loss)	mass(xl)	M(assim)	% assim.
0.2	0.6	0.2	1	0.8	1.28	0.48	0.48
0.3	0.6	0.3	1	0.7	1.12	0.42	0.42
0.4	0.6	0.4	1	0.6	0.96	0.36	0.36
0.5	0.6	0.5	1	0.5	0.8	0.3	0.3
0.6	0.6	0.6	1	0.4	0.64	0.24	0.24
0.7	0.6	0.7	1	0.3	0.48	0.18	0.18
0.8	0.6	0.8	1	0.2	0.32	0.12	0.12
0.9	0.6	0.9	1	0.1	0.16	0.06	0.06

Table 3.7: Comparison of three AFC models for generating AVC andesites from a primitive basalt (from Gerlach et al., 1988). In particular, we show the variation in F (liquid remaining) as R (assimilation rate/crystallization rate) is changed. We show the F values calculated for satisfactory models for both the Sr and Nd isotopic systems. All models indicate ~10 -30 % crust for AVC lavas. Contaminants are all from Lucassen and others (2001). See **Figure 3.19** for a graphical representation.

Assimilant				
3/291	**Sri**	**Rb/Sr**	**Eps Nd**	**Nd (ppm)**
Sierra de Moreno	**0.7218**	**0.21**	**-13.2**	**35**
Chilean gneiss				
	R	**F (Sr)**	**F (Nd)**	**% crust**
	0.3	0.45	0.25	16 - 23
	0.4	0.65	0.5	14 - 20
	0.5	0.75	0.65	12 - 18
	0.6	0.85	0.75	10 - 16
	0.7	0.9	0.85	7 - 14

3/287	**Sri**	**Rb/Sr**	**Eps Nd**	**Nd (ppm)**
Sierra de Moreno	**0.719**	**0.5**	**-9.9**	**35**
Chilean gneiss				
	R	**F (Sr)**	**F (Nd)**	**% crust**
	0.3	0	0	
	0.4	0.25	0.2	30 - 32
	0.5	0.45	0.45	28
	0.6	0.6	0.6	24
	0.7	0.75	0.75	17

7/27	**Sri**	**Rb/Sr**	**Eps Nd**	**Nd (ppm)**
Sierra de Quilmes	**0.75**	**1.8**	**-11.5**	**43**
Argentine paragneiss				
	R	**F (Sr)**	**F (Nd)**	**% crust**
	0.3	0.5	0.2	15 - 24
	0.4	0.65	0.45	14 - 22
	0.5	0.75	0.65	12 - 18
	0.6	0.85	0.75	9 - 15
	0.7	0.9	0.85	7 - 10

Table 3.8: Mass balance calculations for the evolution from a hypothetical parent basalt (Puyehüe; from Gerlach, 1988) to basaltic andesite, as constrained by modeling the Sr and Nd isotopic systems (see **Figure 3.17 & 3.18, Table 3.7**). Models using three different assimilants, representing the diverse central Andean crust, are shown here. Presented here are only those models deemed acceptable—in that they adequately account for the variation of all modeled elements and isotopic—for the given contaminant. Note that F (liquid remaining) increases with R (assimilation rate/crystallization rate) (see **Figure 3.20**), yet crustal contribution does not vary dramatically (see **Figure 3.19**). M is the mass of the basaltic andesite calculated to be necessary to produce the compositional variation observed in the trace element data (see **Table 3.4**). See **Table 3.6** for other term definitions.

Assimilant	isotope	M	R	F	M(o)	M(loss)	mass(xl)	M(assim)	% assim.
3/291	**Sr**	525	0.3	0.45	1167	642	834	193	0.17
		525	0.4	0.65	808	283	396	113	0.14
		525	0.5	0.75	700	175	263	88	0.13
		525	0.6	0.85	618	93	148	56	0.09
		525	0.7	0.9	583	58	99	41	0.07
	Nd	525	0.3	0.25	2100	1575	2048	473	0.23
		525	0.4	0.5	1050	525	735	210	0.20
		525	0.5	0.65	808	283	424	141	0.18
		525	0.6	0.75	700	175	280	105	0.15
		525	0.7	0.85	618	93	158	65	0.11

	isotope	M	R	F	M(o)	M(loss)	mass(xl)	M(assim)	% assim.
3/287	**Sr**	525	0.4	0.25	2100	1575	2205	630	0.30
		525	0.5	0.45	1167	642	963	321	0.28
		525	0.6	0.6	875	350	560	210	0.24
		525	0.7	0.75	700	175	298	123	0.18
	Nd	525	0.4	0.2	2625	2100	2940	840	0.32
		525	0.5	0.45	1167	642	963	321	0.28
		525	0.6	0.6	875	350	560	210	0.24
		525	0.7	0.75	700	175	298	123	0.18

	isotope	M	R	F	M(o)	M(loss)	mass(xl)	M(assim)	% assim.
7/27	**Sr**	525	0.3	0.5	1050	525	683	158	0.15
		525	0.4	0.65	808	283	396	113	0.14
		525	0.5	0.75	700	175	263	88	0.13
		525	0.6	0.85	618	93	148	56	0.09
		525	0.7	0.9	583	58	99	41	0.07
	Nd	525	0.3	0.2	2625	2100	2730	630	0.24
		525	0.4	0.45	1167	642	898	257	0.22
		525	0.5	0.65	808	283	424	141	0.18
		525	0.6	0.75	700	175	280	105	0.15
		525	0.7	0.85	618	93	158	65	0.11

CHAPTER 4

Assembly, maturation and waning of an eleven million year crustal magma cycle: thermobarometry of the Aucanquilcha Volcanic cluster

Barry A. Walker, Jr.
Erik W. Klemetti
Anita L. Grunder
John H. Dilles
Frank J. Tepley
Denise Giles

For submission to *Earth and Planetary Science Letters*
Marquis One, 245 Peachtree Center Avenue, Suite 1900, Atlanta, GA 30303

Introduction

There has been a push in recent years to bridge a philosophical gap in the volcanic and plutonic literature volcanic rocks might not represent simply a molten version of plutonic material. Rather, the two might be physically complementary in that a pluton might represent variable degrees of accumulation of crystals in a magma from which a liquid-rich portion was expelled (Hildreth, 1981, 2004; Hildreth and Moorbath, 1988; Riciputi et al., 1995; Miller and Wooden, 2004; Grunder, 1995; Lipman, 2007; Bachmann and Bergantz, 2004; Bachmann et al., 2007; Deering and Bachmann, 2010;Claiborne et al., 2010; among many others). Alternatively, it is also argued that many plutons do represent frozen magma compositions and that cumulates may be rare (Glazner et al., 2004; Bartley et al., 2006). Constraining crystallization ages, depths and temperatures of crystals in volcanic rocks is critical to understanding the processes, mechanics, and architecture of active magmatic systems which produce volcanic eruptions but also may give rise to incrementally constructed batholiths at depth. Long-lived volcanic provinces, sometimes encompassing millions of years worth of successive eruptions, are holistic samples of this process, providing a time-transgressive perspective on the evolution and organization of such dynamic systems.

We have probed selected mineral compositions of thirty-nine samples in order to constrain the pressures and temperatures of equilibration of minerals from andesites and dacites lavas from throughout the eleven million year eruptive history of the Aucanquilcha Volcanic cluster (AVC). Previous work on mineral chemistry (Giles, 2009; Klemetti, 2005; Walker et al., 2010) has demonstrated that AVC lavas contain mixed populations of crystals, and that magma mixing and(or) crystal recycling has played a dominant role in generating the observed variation of lava chemistry (see Chapter 3). We have employed compositions of amphiboles, orthopyroxene, clinopyroxene, magnetite and ilmenite to estimate temperatures and pressures and oxygen fugacity of crystallization and thereby the crustal residence history of erupted magmas. We pair these intensive parameters with previously published crystallization temperatures, calculated using the Ti-in-zircon thermometer. We compare these

thermometers and barometers in order to determine the provenance of the crystal cargo of AVC lavas and to glean a greater understanding of the magmatic processes operating beneath a long-lived, intermediate arc system.

The Aucanquilcha Volcanic Cluster

The AVC makes up a geomorphologically distinct cluster of ~20 volcanic centers that span from ~11 Ma to the Recent Volcan Aucanquilcha that lies at the center of the cluster. The volcanoes break into four broad groups based on timing: the Alconcha group (11-~7.5 Ma); the Gordo group (~6-4 Ma); the Polan group (~ 4 to 2 Ma) and the Aucanquilcha group (~ 1 Ma to recent; cf. Grunder et al., 2006; see also **Figure 1.3**, from Chapter 1).

The Alconcha group comprises about seven centers, which crop out in the northwest sector of the cluster. We break it out into two distinct groups based on age and mineral mode. The first subgroup (Alconcha 1) is the oldest record of AVC activity from ~11-10 Ma and lavas are relatively crystal poor (<15 vol% crystals) and lack biotite. The second subgroup (Alconcha 2) erupted later (~8 – 7.5 Ma) and comprises more crystal-rich (>25 vol% crystals) lavas that commonly include biotite. The Ujina ignimbrite, a small (~2 km^3) dacitic ignimbrite, erupted at ~9.4 Ma (Grunder, 1997), and is also considered part of the Alconcha group due to its age and proximity, though its source remains uncertain.

A hiatus of as much as 1.5 million years separates the Alconcha group for the Gordo group, which is made up of around six centers, distributed around the southern and western AVC. The Gordo group was quickly immediately by the third and main eruptive phase, the Polán group, which comprises around ten volcanoes, that are widely distributed within the halo of the older groups. Erupting during this time (~3 Ma), but broken out separately is Volcán Miño, a large andesite volcano on the western edge of the AVC. The last main stage of volcanism is Volcán Aucanquilcha, erupting from ~ 1 Ma to recent (Klemetti et al., 2008). Aucanquilcha comprises around six overlapping

eruptive vents, giving the volcano a ridge-like appearance. After these main phases of volcanism, several small basaltic andesite scoria cones erupted, including the eroded edifices of Poruñita and Luna de Tierra, defining a field located just to the east of the AVC (see **Figure 3.1** from Chapter 3).

The systematic development of the AVC from peripherally to centrally distributed, the evolution from compositionally diverse (basaltic andesite to dacite) to relatively homogeneous (dacite) concurrent with a dramatic increase in eruptive output from ~5 to 2 Ma (see **Figure 1.4** from Chapter 1), and the broad transition from early anhydrous mafic silicate (pyroxenes) assemblages to later hydrous phases (amphibole and biotite) are the basis for treating the AVC as the volcanic sampling of a long-lived magmatic locus comparable to other long-lived continental magmatic systems (Grunder et al., 2006).

We emphasize that textures and previous work clearly indicate that many crystals in the AVC lavas are not in equilibrium with each other nor with the quenched host melt. Crystals range from xenocrysts, meaning entrained wall rock material unrelated to the host melt, to phenocrysts representing the last stage of crystal-melt equilibration; many are variably cognate crystal cargo carrying glimpses into the magma history.

Methods

Polished thin sections were made from samples representing the temporal, spatial, and compositional spectrum of AVC lavas (**Table 4.1**) to the purpose of chemical analysis for use in calculations of intensive parameters. Preference was given to samples with fresh, unoxidized, and unaltered phases. All new compositional data presented here were collected at Oregon State University on the CAMECA SX-100 electron microprobe.

We analyzed titanomagnetite and ilmenite pairs that appeared to be in equilibrium. This included touching crystals, groundmass crystals near each other, and when nothing else

was available, grains comprising either titanomagnetite or ilmenite as lamellae inside the other phase—the result of thermal exsolution and also of oxidation exsolution (**Figure 4.1, Table 4.2**). Magnetite-ilmenite equilibrium was tested by comparing the Mg/Mn ratio in the magnetite and ilmenite, using the method of Bacon and Hirschmann (1988). Only pairs whose 2σ errors overlap with the envelope defined by Bacon and Hirschmann (1988) were used (**Figure 4.2**). Data reduction was performed using the ILMAT spreadsheet (LePage, 2003), which calculates crystallization temperatures and oxygen fugacity of Fe-Ti oxide pairs using a variety of published thermometers. We compare Fe-Ti oxide equilibrium temperatures and oxygen barometry calculated from the formulations of Andersen and Lindsley (1985) and Ghiorso and Evans (2008). We also utilized the formulation of Ghiorso and Evans (2008) to estimate the $a_{(TiO2)}$ of the magma in equilibrium with the Fe-Ti oxide pair.

For amphibole compositions, we compare the parameters calculated from two independent calibrations. First is the solution model of Holland and Blundy (1994), used for geothermometry, relying on the formulation that does not require quartz saturation. We iterated the temperature solution with the plagioclase-amphibole geobarometer of Anderson and Smith (1995) to solve for pressure and temperature for amphibole/plagioclase pairs. Only grains were selected that appeared to be in equilibrium—touching pairs, plagioclase inclusions in amphibole, and cores of adjacent, relatively large grains (**Figure 4.3**). Errors are likely to be ± 30°C for temperatures and ± 0.5 kb for pressure (cf., Anderson and Smith, 1995; Bachmann and Dungan, 2002). Here, we present new data along with existing temperatures and pressures from amphibole/plagioclase pairs calculated by Giles (2009).

The second amphibole thermobarometer used is from Ridolfi and others (2010), which estimates intensive parameters based on amphibole composition alone. This model was formulated based on natural and experimental compositions, screened by texture and mineral chemistry. The assumptions in its application are that amphibole crystallized in equilibrium with a calc-alkaline melt crystallizing primarily at conditions near the

amphibole upper temperature stability limit, and that even small changes in temperature and/or pressure will trigger destabilization or reequilibration.

For two-pyroxene thermobarometry, we analyzed touching clinopyroxene-orthopyroxene pairs (**Figure 4.4, Table 4.3**) from eleven samples from AVC lavas (three andesite, seven dacites, one andesitic magmatic inclusion in a host dacite). We use revised calibrations (Putirka, 2008), based on previous thermometry calculations by Brey and Köhler (1990) and barometry calculations by Mercier and others (1984). Equilibrium was tested using a method similar to that proposed by Roeder and Emslie (1970), which compares the Fe-Mg exchange coefficient in clinopyroxene and orthopyroxene of the samples with exchange coefficients determined to be in equilibrium based on experimental work. We screened our pyroxene pairs based on this equilibrium test, rejecting pairs whose Fe-Mg exchange coefficient fall outside of the putative equilibrium value of 1.09 ± 0.14 (cf. Putirka, 2008).

Results

Fe-Ti oxides

Very commonly, Fe-Ti oxides are petrographically associated with apatite and clinopyroxene (see **Figure 4.1**) and often occur in crystal clusters with these phases. Ilmenite was difficult to locate in many AVC samples. Though autonomous crystals of ilmenite were present, the most common occurrence observed in thin section was in resorbed, composite grains with titanomagnetite. Many times, ilmenite was observed in lamellae in magnetite grains, the product of oxidation exsolution (cf. Haggerty, 1991). Conversely, there were many large ilmenite grains with magnetite exsolution lamellae, as well. Many of the exsolution pairs appear to be in equilibrium based on their Mg/Mn ratios, despite Bacon and Hirschmann's (1988) observation that exsolved pairs commonly fell outside their acceptable window of equilibrium on log (Mg/Mn) plots.

Magnetite and ilmenite pairs yielded temperatures ranging from 700 - 1080 °C (though most temperatures are < 980 °C; **Figure 4.5, Table 4.2**), and oxygen fugacities ranging from NNO to NNO+2 (**Figure 4.6**, **Table 4.2**). Fe-Ti oxide equilibration temperatures from the early Alconcha group and Volcán Aucanquilcha are the lowest (<900°C), with samples from the Polán, Gordo, and later Alconcha group (<9Ma), yielding temperatures above 900°C. In general, calculated temperatures range widely, even within individual samples (>100°C), suggesting that flows were not erupted from a homogeneous, thermally equilibrated batch of magma.

Generally, the equilibrium temperatures calculated from the two different geothermometers of Andersen and Lindsley (1985) and Ghiorso and Evans (2008) are very similar. There is no systematic offset with either thermometer, though the temperatures calculated from Ghiorso and Evans' thermometer are more variable for individual samples. When all the Fe-Ti oxide pairs are considered, the average difference in calculated temperatures of individual pairs is 13 °C (n = 73; s.d. = 46) with the Ghiorso and Evans thermometer yielding the higher temperatures.

Activity of TiO_2 estimated from Fe-Ti oxides—effect on Ti-in-zircon temperatures

The activity of TiO_2 calculated from Fe-Ti oxide pairs, using the formulation of Ghiorso and Evans (2008) ranges from 0.50 to 0.82 (**Table 4.2**), though most pairs fall between 0.60 and 0.75 (average of 0.67, one standard deviation of 0.05 for all pairs). The Ti-in-zircon thermometer is particularly sensitive to the activities chosen for SiO_2 and TiO_2, which, when unconstrained, adds uncertainty that is not easily quantifiable. Walker and others (2010) reported Ti-in-zircon temperatures calculated using a a_{TiO2} estimate of 0.5. The a_{TiO2} estimates presented here are thus applied to the Ti-in-zircon calculations (Watson and Harrison, 2005; Ferry and Watson, 2007) and used to modify the temperatures reported by Walker and others (2010). Observing no appreciable change in a_{TiO2} through time, we set the a_{TiO2} to equal 0.65, an increase of 0.15, resulting in a decrease in the temperature estimate by ~25°C. The corrected Ti-in-zircon temperatures are ~670 - 900 °C.

Pyroxenes

Clinopyroxene is more common in andesites than in dacites, and in more mafic lavas may be accompanied by olivine. Clinopyroxenes compositions from AVC lavas vary little, and define a relatively tight cluster in the pyroxene quadrilateral (**Figure 4.7, Table 4.3**). Orthopyroxenes from AVC lavas (including from V. Aucanquilcha) are more compositionally variable and many lavas have bimodal populations. Modes are centered at ~En_{78} and ~En_{68} with the total range in orthopyroxene from En_{81} to En_{61}. Both normal and reverse zoning are observed within individual pyroxene crystals, though the compositional spectra are rather limited, and the two compositional populations of orothopyroxene are not observed in single grains. Orthopyroxene compositions from the three andesite lavas analyzed tend to cluster in the gap observed in the dacite orthopyroxene data. One andesite sample (AP-00-11) from the earliest eruptive phase of the AVC trends toward a more Fe-rich composition, but also has a population in the dacite gap.

Clinopyroxene-orthopyroxene pairs yielded temperatures ranging from 986 – 1115 °C, though individual samples have relatively small variability (~50°C; see **Table 4.3**). Temperature estimates from dacites and andesites do not appreciably differ, and variability through time is insignificant. Pressure estimates presented here are averaged from two different equations in the model by Putirka (2008; equations 38 and 39) as suggested by the author (personal communication). Using this average, crystallization pressures range from 3.8 to 7.6 kb, with a total data average of ~5 to 6 kb. Like temperature estimates, pressure estimates for andesites and dacites do not differ, and variation through time is not significant.

Error is difficult to estimate for this thermobarometer (Putirka, 2008). If all of the temperature data are considered, two standard deviations is ±50°C. For individual samples, single standard deviations range from ~11°C to 50°C. Variability is greater for the pressure data. For the pressure estimates using equation 38, two standard deviations

for all the data are 2 kb; for the pressure estimates using equation 39, two standard deviations are 1.2 kb. For pressures reported here, averaged from equations 38 and 39, two standard deviations are 1.2 kb.

Amphiboles

Giles (2009) and Klemetti (2005) provide a detailed discussion of AVC amphibole compositions and textures. Generally, amphibole is sparse in AVC lavas, comprising less than ~5 volume % of any given rock. Amphibole is present throughout the AVC eruptive history, but becomes more common in the later eruptive suites. It is ubiquitous in lavas from Volcán Aucanquilcha. Amphibole is also present, though sparse, in lavas from Volcán Miño. Variably thick reaction rims are common on amphiboles, though thin (~1μm) rims are the prevalent texture. In Volcán Aucanquilcha itself, euhedral, reaction-free grains are the dominant texture. Amphiboles from AVC lavas have considerable compositional variability (**Table 4.4 & 4.5**), ranging from magnesiohornblende to tschermakite and into the pargasite field (amphibole nomenclature after Leake et al., 1997). Both Klemetti (2005) and Giles (2009) recognized that compositional variability, in particular Al-content, is greatest in amphiboles from the beginning and ending phases of volcanism (Alconcha and Aucanquilcha), and lesser during the time of peak volcanism (Gordo and Polán).

Using the thermobarometer from Ridolfi and others (2010) (hereafter: "Ridolfi model"), the overall range of amphibole temperature and pressure estimates is 768 - 1007 °C and 0.8 -5.4 kb (**Figure 4.8, Table 4.4 & 4.5**). Individual samples contain amphibole populations yielding up to ~200°C temperature range and ~4 kb pressure range. Consistent with compositional observations, the early and late periods of volcanism yield more variable temperatures and pressures than do the middle period. Problematically, temperature and pressure estimates using the Ridolfi model do not correspond very well with those obtained using amphibole-plagioclase pairs (Anderson and Smith, 1995; Holland and Blundy, 1994; see **Table 4.5**). When the two different temperature estimates (an amphibole/plag pair versus just the amphibole analysis) are directly compared, values

for the Ridolfi model are consistently higher, though they do appear to converge to some extent at the highest temperatures (**Figure 4.9**). Pressure estimates from the two different models are more consistent, though again, the Ridolfi model yields higher pressure estimates for much of the data. When the two pressure/temperature models are compared, side-by-side, though, they are disturbingly anti-correlated (**Figure 4.10**). For the Ridolfi model, there is a smooth positive correlation of pressure with temperature. For the amphibole-plagioclase pair solution, there are two trends: one in which pressure and temperature are negatively correlated, and one in which pressure varies little with an increase in temperature. We discuss the implications of this below.

Discussion

Equilibrium considerations

The application of geothermobarometry predicates that the phases be in equilibrium. With some systems, and with some rocks, such demonstration of equilibrium does not appear to be such a dire problem (e.g., Blundy and Cashman, 2008, and references therein). However, with crystal-rich volcanic rocks, juxtaposition of crystals with different provenance is very common (Davidson et al., 2005), making identification of an equilibrium pair extremely difficult. Amphibole-plagioclase thermobarometry starkly illustrates this problem. Both plagioclase and amphibole grains are commonly complexly zoned, and an erroneous pairing will yield an errant but seemingly realistic temperature and pressure estimate. This is likely the cause of some of the perplexing pressure-temperature estimate trend observed in our amphibole-plagioclase pairs.

Our Fe-Ti oxide temperatures also indicate disequilibrium with the host magma. Though all samples were screened for the Mg/Mn chemical equilibrium test, many pairs yield relatively low temperatures (<850°C) compared to the temperature estimates of other phases. Furthermore, many samples have pairs that yield a range (50 - 150°C) of equilibrium temperatures. These diverse Fe-Ti oxide temperatures, in conjunction with their sometimes rather large size (>200 μm; see **Figure 4.1**), may stem from

remobilization of crystals, a consequence of mixing and reheating by magma recharge (cf. Venezky and Rutherford, 1999). Large, coarsely exsolved pairs are likely yielding information on a cognate, plutonic precursor rather than on the erupting magma.

The pyroxene pairs presented here have Fe-Mg concentrations and proportions consistent with equilibrium crystallization, though this does not ensure the grains grew in equilibrium with the host (quenched) melt. Individual samples yield fairly self-consistent temperatures +/- 50°C, close to the ~30°C error of the thermometer (Putirka, 2008). The diverse pressures recorded in some AVC pyroxene pairs are quite likely real, as these pressure estimates result from averaging two different thermometers. In the case of outlying, high-pressure grains, each thermometer independently yielded a high pressure.

The Ridolfi thermobarometer

Pressures and temperatures of AVC amphiboles calculated using the Ridolfi model yield values within the range of other intermediate magmas (Ridolfi et al., 2010), but many fall outside of amphibole stability with respect to andesitic (Eggler and Burnham, 1973; Green, 1982) and dacitic (Rutherford and Devine, 2003; Holtz et al., 2005; Rutherford and Devine, 2008) magmas (**Figure 4.11**). Because the Ridolfi model only uses a single phase, it must make assumptions that limit the degrees of freedom if pressure, temperature, and water pressure are to be deduced. Under the assumptions of the Ridolfi model, all amphibole pressures and temperatures derived from this formulation will lie near the upper temperature limit of amphibole stability. This model will thus not yield realistic pressures and temperatures of an amphibole grown well inside its stability field (such as might result through crystallization with variable decreasing temperatures at the same pressure). At the AVC, and at many other volcanic centers, pluton and/or crystal mush remobilization has been invoked as a process to account for the diversity observed in mineral compositions and ages (cf. Watts et al., 1999; Bacon et al., 2005; Giles, 2009; Walker et al., 2010; see also Chapter 3). Specifically, coexistence of distinct disequilibrium textures and variable compositions among amphiboles at the AVC suggest that erupted lavas collected crystals from distinct magma batches before eruption (Giles,

2009). The presence of such mixtures implies that amphibole crystals—reaction rims aside—can survive magma mixing and/or remobilization with their composition intact.

In particular, the Al-content in the amphiboles alone corroborates the inference that lavas contain multiple populations of amphibole that grew at disparate pressures and temperatures (Klemetti et al., 2008; Giles, 2009; Longo et al, 2010). Perhaps lending credence to its utility, Ridolfi and other (2010), using their thermobarometer, report similar pressures (~1 – 5 kb, with correspondingly high temperatures) for Soufriere Hills volcano. Mt. Hood andesites also contain amphiboles ranging in pressure from ~1-5 kb (Koleszar et al., 2010). In general then, and perhaps for the most part, the Ridolfi model and its assumptions are probably valid. It does not, however, precisely account for amphibole that crystallizes at pressures and temperatures inside its stability field—conditions at which amphibole also crystallizes.

Comparison of the thermobarometers

Geothermometers considered here employ four different phases and (or) phase pairs (orthopyroxene-clinopyroxene, amphibole, magnetite-ilmenite, and zircon). No single sample we analyzed contained the phases necessary to employ all four thermometers. Only one sample contained amphibole and two pyroxenes (AP2-00-77, an inclusion from Volcán Aucanquilcha). Three samples yielded two-pyroxene, zircon, and Fe-Ti oxide temperatures, and four yielded amphibole, zircon, and Fe-Ti oxides temperatures. We have many thermobarometric estimates for amphibole, which we treat with the caveats above.

Some variation in the calculated crystallization temperatures is expected as these phases do not all crystallize at the same temperature and have different rates of reequilibration. Reequilibration rates for pyroxene in intermediate to mafic magmas are calculated to be on the order of hundreds to tens of thousands of years (Brady and McCallister, 1983). For Fe-Ti oxides, magmatic reequilibration is much more rapid, on the scale of days to weeks (Venezky and Rutherford, 1997). Amphibole breakdown is relatively rapid—also

on the order days to weeks—during water or volatile loss of the host magma (Rutherford and Hill, 1993), but chemical reequilibration is much more sluggish if magmatic water content remains relatively constant (Cherniak and Dimanov, 2010). Reequilibration in zircon via chemical diffusion is extremely slow, and does not have an appreciable effect on zircon chemistry at magmatic temperatures at the hundred thousand year timescale (Cherniak and Watson, 2003). Therefore, inter-thermometer variation can yield insight into the provenance of different crystal populations that were amassed in the pre-eruptive chambers. We furthermore compare temperatures calculated from the pyroxene, Fe-Ti oxide, and amphibole thermometers with Ti-in-zircon temperatures from the AVC (modified from Walker et al., 2010). As there is a certain amount of skepticism with regard to the Ti-in-zircon thermometer (Fu et al., 2008; Hofmann et al., 2009; Reid et al., 2011), it is appropriate to examine its agreement with the thermometers presented here.

Within samples, and for the dataset as a whole, pyroxenes always yielded the highest temperatures of ~1000-1100 °C, with little variation within each sample. Zircon always yielded the lowest temperatures of ~700 - 900°C, with ~100°C variation typical for individual samples. Amphibole temperatures and Fe-Ti oxide temperatures fall in between (**Figure 4.12, Figure 4.13**). Pressures and temperatures from high-Al amphibole overlap with the coolest, shallowest P/T estimates from pyroxenes (~1,000°C, ~5kb). The coolest Fe-Ti oxide temperatures overlap with the hottest Ti-in-zircon temperatures (~850°C). The pyroxenes temperatures and pressures likely represent the last equilibrium conditions of the basaltic andesite parent to the upper crustal system. Conversely, the lower temperatures recorded by zircons are likely representative of re-entrained, near solidus autocrysts. Zircons may also be phenocrystic, in which case their temperatures would represent crystallization in the erupting batch of magma. Given the speed at which Fe-Ti oxides reequilibrate, their equilibrium temperatures probably most closely approximate the eruption temperature of AVC lavas. Amphibole temperature variation, while probably not precise, demonstrates the disparate conditions from which crystals—and by inference magma—were amassed to generate an eruptible batch of magma. The preservation of such significant ranges in temperature, then, can be most

plausibly interpreted to represent magma mixing, whereby a relatively mafic magma containing phenocrysts that grew at relatively hot, deep conditions invades the upper crust and intercepts a higher level (and presumably cooler) magma reservoir containing crystals that reflect those conditions. Samples that contain multiple analyzed phases such as pyroxene, zircon, and Fe-Ti oxides, likely have distinct crystal populations that document the conditions of a) the invading, mafic end-member of magma mixing, b) the silicic end-member, and c) the mixed magma.

Variations through time

Walker and others (2010) observed that the maximum zircon crystallization temperatures were from lavas erupted during the most voluminous period of AVC volcanism, with lower temperatures calculated for lavas erupted during the less voluminous beginning and waning phases of volcanism. Temperatures calculated from Fe-Ti oxide pairs grossly support this, as the lowest temperatures observed are from lavas erupted during the beginning and waning stages of AVC magmatism. Amphibole temperatures and pressures from this time period are considerably variable, suggestive of incomplete mixing and hybridization of melts. These relatively cool Fe-Ti oxide and zircon temperatures paired with variable amphibole temperatures likely results from small, and perhaps scattered and unconnected magma chambers at depth.

Relatively higher zircon and Fe-Ti oxide temperatures and reduction in range of amphibole temperatures and pressures characterize the most volcanically active period in the AVC eruptive history. Peak volcanic output corresponds to peak thermal maturity of the evolving plutonic system. With long duration, progressive magmatism came the development and evolution of an extensive batholith. Through time, as various magma chambers grew and expired, the central magma plexus became armored with magmatic precursors in a piecemeal fashion. This process would lead to an increase of the ambient wall-rock temperatures, serving to thermally buffer the active magma chambers (Grunder et al., 2006; Walker et al., 2010). Pressure estimates from amphiboles from this thermally mature stage of AVC volcanism suggest a consolidation of magma processing

to a range of ~2 – 4 kb (7 - 14 km; **Figure 4.14**). This processing is interpreted to have taken place in a plutonic network consisting of a substantial, variably interconnected crystal mush zone. Such a system would, in turn, act as an effective trap and processing reservoir for incoming magmas (cf. Karlstrom et al., 2010).

Pyroxene pressures indicate magmatic staging areas with significant crystallization extend to deeper levels at ~5 – 7 kb (16 – 24 km) (**Figure 4.15**). These two pyroxene-bearing andesites are evidence that magma batches were, at least intermittently, able to penetrate the more shallow, amphibole-dominated storage zone relatively unmodified, probably via a dike-sill network. Through time, in a melt-poor regime, clinopyroxene-bearing magmas would be likely to pierce the upper storage zone relatively unaffected. In a more melt-rich regime, ascending magmas are more likely to be trapped and more thorough mixing will probably lead to pyroxene destabilization and homogenization during replenishment.

Conclusions

The phenocryst assemblages of AVC lavas have been probed for various intensive parameters. Crystallization is documented for over 7 kb (~24 km) of pressure and ~1150 - 750°C in these lavas. The diversity of crystallization temperatures and pressures recorded by phases in individual AVC lavas suggests erupting magma batches accumulate phases from disparate levels within the upper crust. Intensive parameters of AVC phases indicate a spatial focusing of the upper crustal subvolcanic system that accompanying increased volcanic output, and presumably system power. Many crystals in AVC lavas are likely to be true phenocrysts, but eruptions also extensively recycled crystals from the possibly multi-tiered, evolving reservoir. If intensive parameters of erupted crystals are indicative of those left behind at similar conditions of formation, they imply the existence of a large, zoned batholith, ranging from at least ~3 to 25 km depth.

References

Andersen, D.J., Lindsley, D.H., (1985). New (and final!) models for the Ti-magnetite/ilmenite geothermometer and oxygen barometer. Abstract AGU 1985 Spring Meeting Eos Transactions. *American Geophysical Union 66* (18), 416.

Anderson, J.L. and Smith, D.R. 1995. The effects of temperature and f (sub O2) on the Al-in-hornblende barometer. *American Mineralogist,* Issue 5-6, pp.559-549.

Anderson, J.L., Barth, A.P., Wooden, J.L, Mazdab, F., 2008, Thermometers and thermobarometers in granitic systems. Reviews in Mineralogy and Geochemistry 69, 121 – 142.

Bachmann, O., and Bergantz, G.W., 2004. On the origin of crystal-poor rhyolites: extracted from batholithic crystal mushes. *Journal of Petrology* 45 (8), 1565-1582.

Bachmann, O. B., L.A. Charlier and J.B. Lowenstern (2007) Zircon crystallization and recycling in the magma chamber of the rhyolitic Kos Plateau Tuff (Aegean arc): *Geology*, vol. 35, no. 1, pp. 73-76.

Bachmann, O. and Dungan, M., 2002. Temperature-induced Al-zoning in hornblendes of the Fish Canyon magma, Colorado. *American Mineralogist* 87 (8-9), pp. 1062-1076.

Bacon, C. R., Hirschmann, M. M., (1988). Mg/Mn partinitioning as a test for equilibrium between coestisting Fe-Ti oxides. *American Mineralogist 73*(1), 57-61.

Bacon, C.R., and Lowenstern, J.B., 2005, Late Pleistocene granodiorite source for recycled zircon and phenocrysts in rhyodacite lava at Crater Lake, Oregon: *Earth and Planetary Science Letters*, v. 233, p. 277-293.

Blundy, J., Cashman, K., 2008, Petrologic reconstruction of magmatic systems variables and processes, Reviews in Mineralogy and Geochemistry 69, p. 179-239.

Bartley, J.M., Coleman, D.S., Glazner, A.F., 2006, Incremental pluton emplacement by magmatic crack-seal. *Earth and Environmental Transactions of the Royal Society of Edinburgh* 97, p. 383-396.

Brady, J.B., McCallister, R.H., 1983, Diffusion data for clinopyroxenes from

homogenization and self-diffusion experiments. *American Mineralogist* 68, p. 95-105.

Brey, G.P., Kohler, T., 1990, Geothermobarometry in four-phase lherzolites II. New thermobarometers, and practical assessment of existing thermobarometers. *Journal of Petrology* 31, p. 1,353-1,378.

Cherniak, D.J., Watson, E.B., 2003, Diffusion in zircon, *in* Hanchar, J.M., Hoskin, P.W.O., (eds.) Zircon. *Reviews in Mineralogy and Geochemistry* 53, p. 113-143.

Cherniak, D.J., Dimanov, A., 2010, Diffusion in Pyroxene, Mica and Amphibole, *in* Zhang, Y., Cherniak, D.J., (eds.), Diffusion in minerals and melts. *Reviews in Mineralogy and Geochemistry* 72, p. 641-690.

Claiborne, L.L., Miller, C.F., Flanagan, D.M., Clynne, M.A., Wooden, J.L., 2010, Zircon reveals protracted magma storage and recycling beneath Mount St. Helens, *Geology* 38 (11), p. 1011-1014.

Davidson, J.P., Hora, J.M., Garrison, J.M., Dungan, M.A., 2005, Crustal forensics in arc magmas. *Journal of Volcanology and Geothermal Research* 140, pp. 157-170.

Deering, C.D., Bachmann, O., 2010, Trace element indicators of crystal accumulation in silicic rocks. *Earth and Planetary Science Letters* 297, p. 324-331.

Eggler, D.H., Burnham, C.W., 1973, Crystallization and fractionation trends in the system Andesite-H_2O-CO_2-O_2 at Pressures to 10 Kb. *GSA Bulletin* 84 (8), p. 2517-2532.

Ferry, J.M., and Watson, E.B., 2007, New thermodynamic models and revised calibrations for the Ti-in-zircon and Zr-in-rutile thermometers: Contributions to Mineralogy and Petrology, v. 154, p. 429-437.

Fu B, Page FZ, Cavosie AJ, Fournelle J, Kita NK, Lackey JS, Wilde SA, Valley JW (2008) Ti-in-zircon thermometry: applications and limitations. *Contrib Mineral Petrol* 156:197–215. doi: 10.1007/s00410-008-0281-5

Ghiorso, M.S., Evans B.W., 2008, Thermodynamics of Rhombohedral Oxide Solid Solutions and a Revision of the Fe-Ti Two-oxide Geothermometer and Oxygen-barometer. *American Journal of Science* 308, p. 957-1039.

Giles, D., 2009, Dynamics of a long-lived magmatic system as indicated by variations in

amphibole composition and textures in dacites erupted over 11 m.y. at the Aucanquilcha Volcanic Cluster, Central Andes, Chile. MS thesis.

Glazner, A.F., J.M. Bartley, D.S. Coleman, W. Gray and R.Z. Taylor (2004) Are plutons assembled over millions of years by amalgamation from small magma chambers? *GSA Today*, v. 14, no. 4-5, p. 4-11.

Green, T.H., 1982, Anatexis of mafic crust and high pressure crystallization of andesite. *In* R.S. Thorpe, ed., *Andesites*. John Wiley & Sons, p. 465-487.

Grunder, A. L. 1997. Report on the Miocene to Recent volcanic rocks from the eastern margin of the project area. *In* Tomlinson, A. *et al*. (eds) *Proyecto de Estudio Geológico de la Franja Longitudinal entre Quebrada Blanca y Chuquicamata, Fase I*. SERNAGEOMIN de Chile report to Coldelco.

Grunder, A.L., Klemetti, E.W., Feeley, T.C., and McKee, C.M., 2006, Eleven million years of arc volcanism at the Aucanquilcha Volcanic Cluster, Northern Chilean Andes: implications for the life span and emplacement of plutons: *Transactions of the Royal Society of Edinburgh-Earth Sciences*, v. 97, p. 415-436.

Haggerty, S.E., 1991, Oxide Textures – A Mini-atlas. In D.H. Lindsley, *Ed.*, Oxide Minerals: Petrologic and Magnetic Significance. *Mineralogical Society of America*, vol. 25, p. 129-219.

Hildreth, W., 1981, Gradients in silicic magma chambers: implications for lithospheric magmatism. *Journal of Geophysical Research* 86 (B11), p. 10,153 – 10,192.

Hildreth, W., and Moorbath, S., 1988, Crustal contributions to arc magmatism in the Andes of Central Chile, *Contributions to Mineralogy and Petrology* 98, 455-489.

Hildreth, W., 2004, Volcanological perspectives on Long Valley, Mammoth Mountain and Mono Craters: several contiguous but discreet systems. *Journal of Volcanology and Geothermal Research* 136, 169-198.

Hofmann, AE, Valley, JW, Watson, EB, Cavosie, AJ, Eiler, JM, 2009, Sub-micron scale distributions of trace elements in zircon, *Contributions to Mineralogy and Petrology*. DOI: 10.1007/s00410-009-0385-6

Holland, T.J.B. and Blundy, J.D., 1994. Non-ideal interactions in calcic amphiboles and their bearing on amphibole-plagioclase thermometry. *Contributions to*

Mineralogy and Petrology, v.116, pp.433-447.

Holtz, F., Sato, H., Lewis, J., Behrens, H., Nakada, S., 2005, Experimental petrology of the 1991-1995 Unzen dacite, Japan. Part I: Phase relations, phase composition and pre-eruptive conditions. *Journal of Petrology* 46 (2), p. 319-337.

Karlstrom., L., Dufek, J., Manga, M., 2010, Magma chamber stability in arc and continental crust. *Journal of Volcanology and Geothermal Research* 190 (3-4), p. 249-270.

Klemetti, E.W., 2005, Constraining the magmatic evolution of the Andean arc at 21°S using the volcanic and petrologic history of Volcán Aucanquilcha, Central Volcanic Zone, northern Chile. Ph.D. Thesis.

Klemetti, E.W., and Grunder, A.L., 2008, Volcanic evolution of Volcan Aucanquilcha: a long-lived dacite volcano in the Central Andes of northern Chile: Bulletin of Volcanology, v. 70, p. 633-650.

Koleszar, A.M., Kent, A.J., Cooper, K.M., Eppich, G.R., 2010, Conditions of magma mixing as recorded in amphiboles from Mount Hood, Oregon. *American Geophysical Union*, Fall Meeting 2010, abstract #V43C2387

Leake, B.E., Woolley, A.R., Arps, C.E.S., Birch, W.D., Gilbert, M.C., Grice J.D., Hawthorne, F.C., Katio, A., Kisch, H.J., Krivovichev, V.G., Linthout, K., Laird, J., Mandarino, J.A., Maresch, W.V., Nickel, E.H., Rock, N.M.S., Schumacher, J.C., Smith, D.C., Stephenson, N.C.N., Ungaretti, L., Whittaker, E.J.W., Youzhi, G. 1997. Nomenclature of amphiboles: report of the subcommittee on amphiboles of the International Mineralogical Association, Commission on new minerals and mineral names. *The Canadian Mineralogist,* v. 35, pp. 219-246.

LePage, L.D., 2003, ILMAT: an excel worksheet for ilmenite-magnetite geothermotery and barometry. *Computers & Geosciences* 29 (5), pp. 673-678. doi: 10.1016/S0098-3004(03)00042-6

Lipman, P.W., 2007, Incremental assembly and prolonged consolidation of Cordilleran magma chambers: Evidence from the Southern Rocky Mountain volcanic field: *Geosphere*, v. 3, p. 42-70.

Longo, A.A., Dilles, J.H., Grunder, A.L., Duncan, R., 2010, Evolution of Calc-alkaline

volcanism and associated hydrothermal gold deposits at Yanacocha, Peru. *Economic Geology* 105 (7), p. 1191-1241.

Mercier, J-C., Beoit, V., Girardeau, J., 1984, Equilibrium state of diopside-bearing harzburgites from ophiolites: geobarometric and geodynamic implications. *Contributions to Mineralogy and Petrology* 85, p. 391-403.

Miller, J.S., and Wooden, J.L., 2004, Residence, resorption and recycling of zircons in Devils Kitchen rhyolite, Coso Volcanic field, California: *Journal of Petrology*, v. 45, p. 2155-2170.

Putirka, K.D., 2008, Thermometers and barometers for volcanic systems. *Reviews of Mineralogy and Geochemistry* 69. P. 61-120.

Reid, M.R., Vazquez, J.A., Schmitt, A.K., 2011, Zircon-scale insights in the history of a Supervolcano, Bishop Tuff, Long Valley, California, with implications for the Ti-in zircon geothermometer. *Contributions to Mineralogy and Petrology* 161, p. 293-311.

Riciputi, L.R., Johnson, C. M., Sawyer, D. A., Lipman, P. W., 1995, Crustal and magmatic evolution in a large multicyclic caldera complex: isotopic evidence from the central San Juan volcanic field, *Journal of Volcanology and Geothermal Research* 67, p. 1-28.

Ridolfi, F., Renzulli, A., Puerini, M., 2010, Stability and chemical equilibrium of amphibole in calc-alkaline magmas: an overview, new thermobarometric forumulations and application to subduction-related volcanoes, *Contributions to Mineralogy and Petrology* 160, p. 45-66.

Roeder, P.L., Emslie, R.F., 1970, Olivine-liquid equilibrium. *Contributions to Mineralogy and Petrology 96, p. 1-23.*

Rutherford, M.J., Devine, J.D., 2003, Magmatic conditions and magma ascent as indicated by hornblende phase equilibria and reactions in the 1995-2002 Soufrière Hills magma. *Journal of Petrology* 44 (8), p. 1433-1454.

Rutherford, M.J., Devine, J.D., 2008, Magmatic conditions and processes in the storage zone of the 2004-2006 Mount St. Helens dacite, *in* Sherrod, D.R., Scott, W.E.,

Stauffer, P.H. (eds.), A volcano rekindled: The Renewed Eruption of Mount St. Helens, 2004-2006, eds USGS Professional Paper 1750, p. 703-726.

Venezky, D.Y., Rutherford, M.J., 1999, Petrology and Fe-Ti oxide reequilibration of the 1991 Mount Unzen mixed magma. Journal of Volcanology and Geothermal Research 89 (1-4), p. 213-230.

Walker, B.A., Miller, C.F., Claiborne, L.L., Wooden, J.L., and Miller, J.S., 2007, Geology and geochronology of the Spirit Mountain batholith, southern Nevada: Implications for timescales and physical processes of batholith construction: Journal of Volcanology and Geothermal Research, v. 167, p. 239-262.

Walker, B.A., Grunder, A.L., and Wooden, J.L., 2010, Organization and thermal maturation of long-lived arc systems: Evidence from zircons at the Aucanquilcha volcanic cluster, northern Chile: *Geology* 38 (10), p. 1007-1010.

Watson, E.B. and Harrison, T.M. (2005) Zircon thermometer reveals minimum melting conditions on earliest Earth. *Science* 308, 841-844.

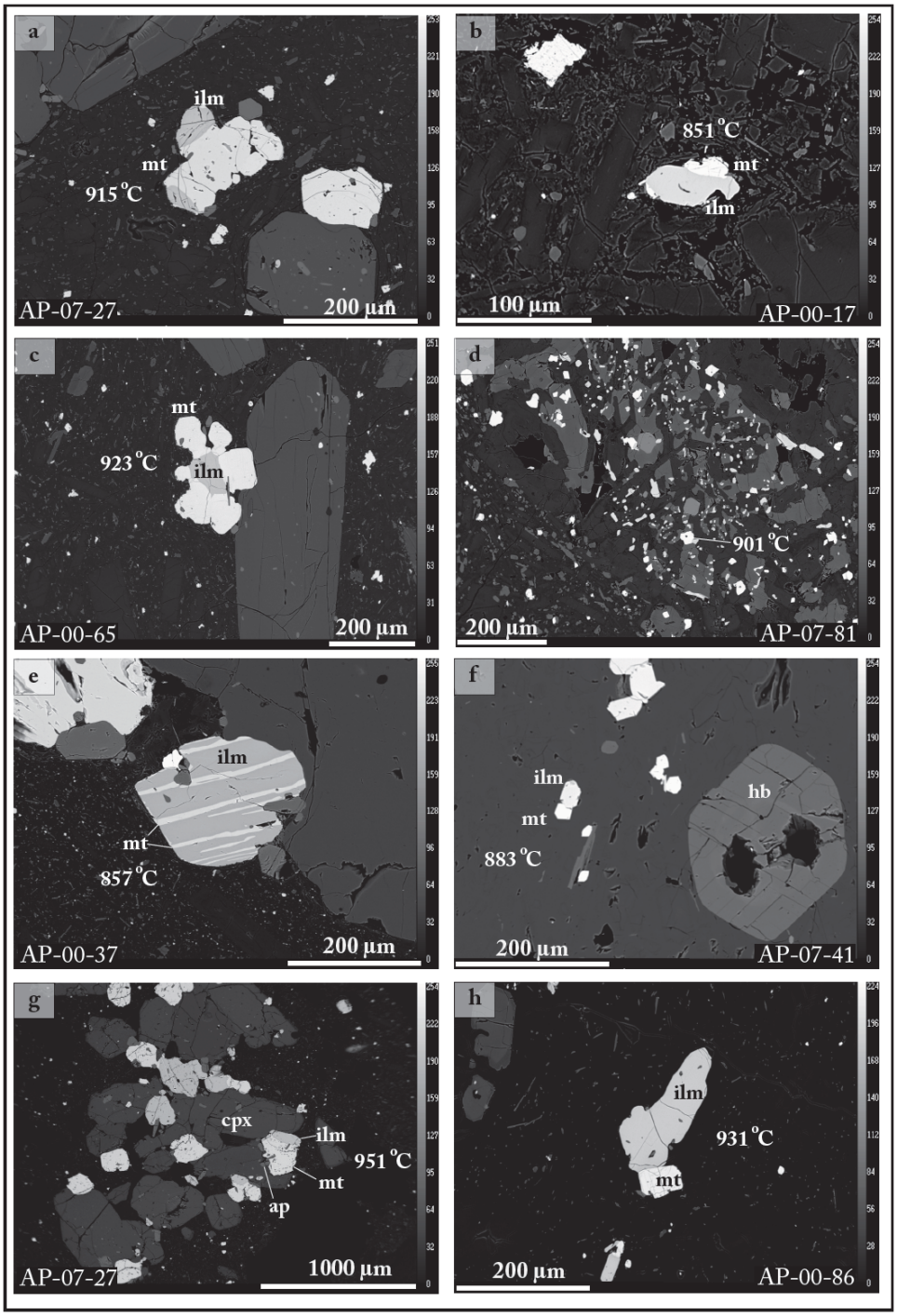

Figure 4.1: Backscattered electron images of selected Fe-Ti oxides. Various Fe-Ti oxide textures were observed in AVC lavas including: subhedral - euhedral grains in the groundmass (f, h); resorbed, composite grains (a,b); oxidation exsolution lamellae (e), complex graphic occurrences (d), and within large crystal clusters, generally containing pyroxene and apatite (g). Calculated equilibrium temperatures shown for each pair (thermometer of Andersen and Lindsley, 1985). Ilm = ilmenite; mt = magnetite; cpx = clinopyroxene; ap = apatite; hb = hornblende.

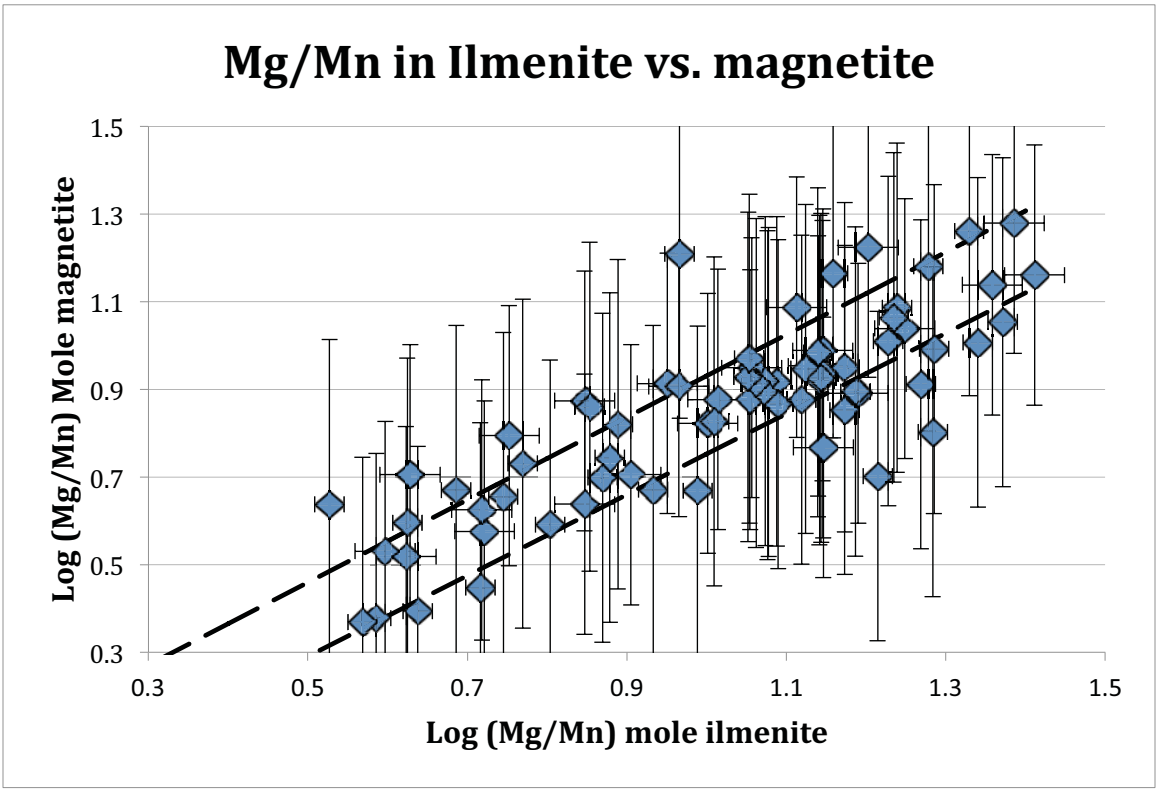

Figure 4.2: Equilibrium test for Fe-Ti oxide data, using the Mg/Mn ratios of each analyses. We kept pairs whose 2 sigma error overlapped with the line observed by Bacon and Hirschmann (1988). Error calculated from electron probe standard data reproducibility.

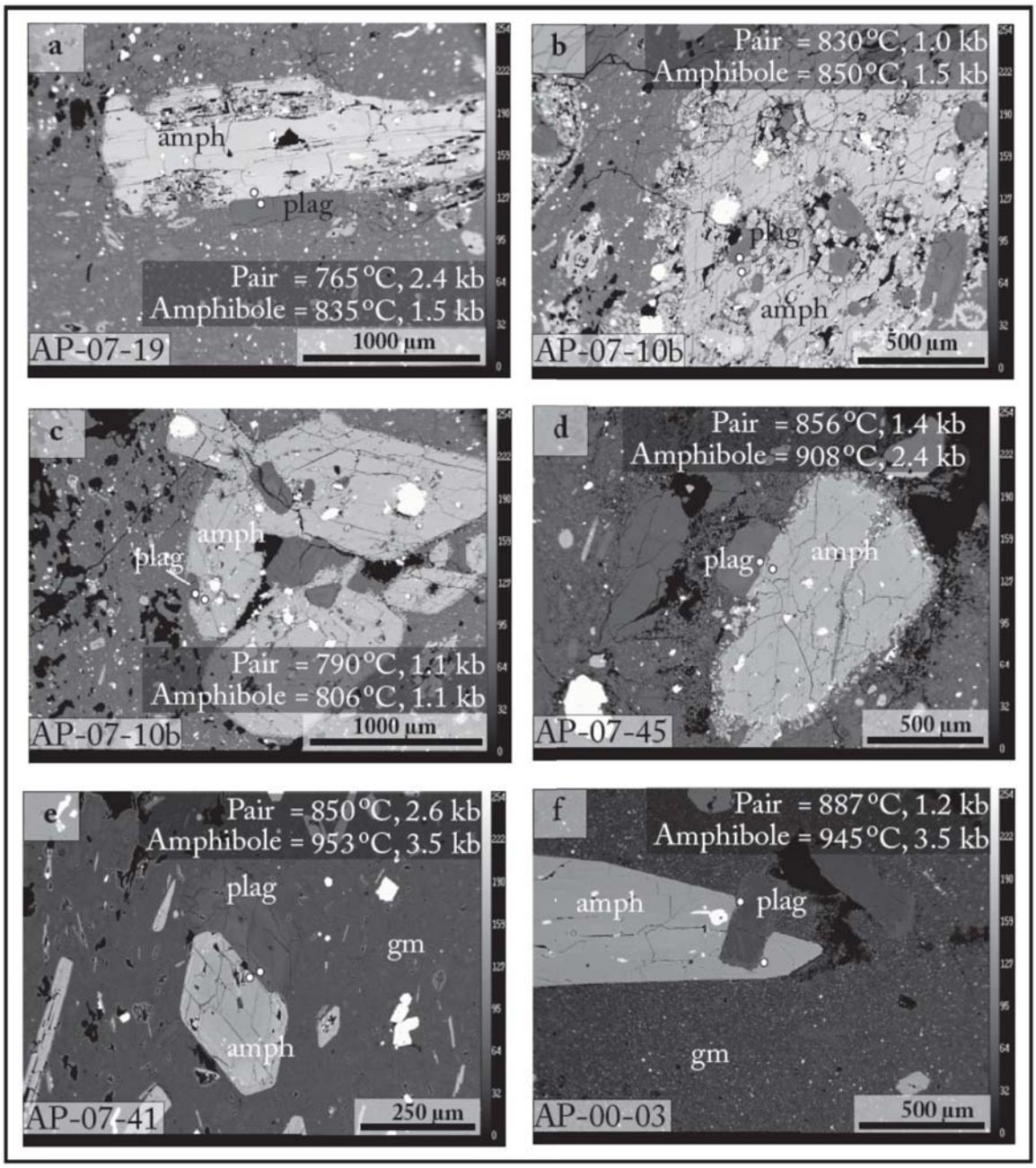

Figure 4.3: Backscattered electron images of selected amphiboles (with plagioclase pairs) from the Aucanquilcha volcanic cluster (see also Giles, 2009). Also shown are the temperatures and pressures calculated using amphibole-plagioclase (pair) thermobarometry (Holland and Blundy, 1994, Anderson and Smith, 1995) and amphibole thermobarometry (Ridolfi et al., 2010). For several pairs, the two methods provide very similar values. Amph = amphibole; plag = plagioclase; gm = groundmass.

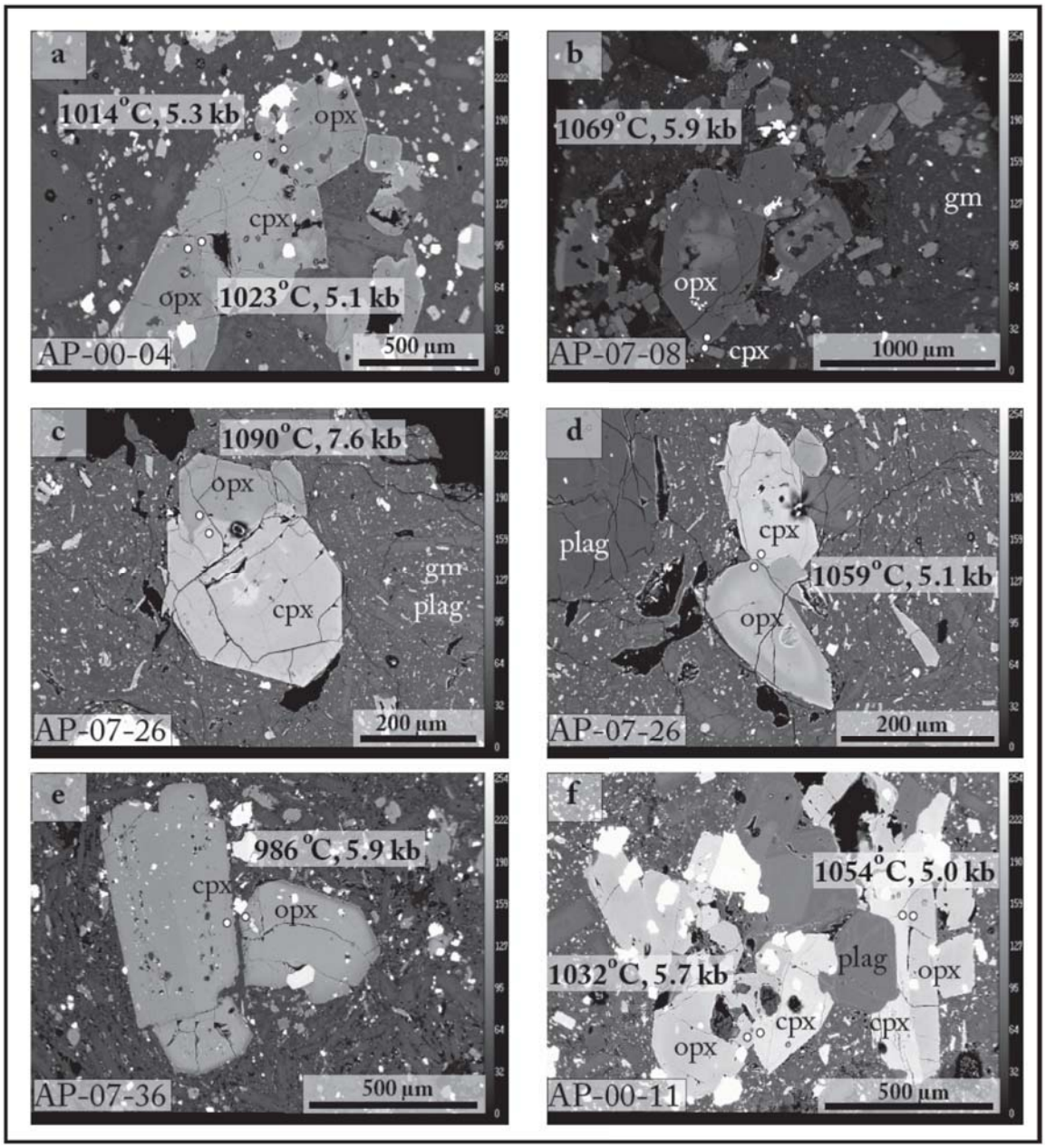

Figure 4.4: Backscattered electron image of selected clinopyroxene-orthopyroxene pairs, with calculated pressures and temperatures using the method of Putirka (2008). Note that while pressures are moderately variable, temperatures are very similar in all samples. Opx = orthopyroxene; cpx = clinopyroxene; plag = plag; gm = groundmass.

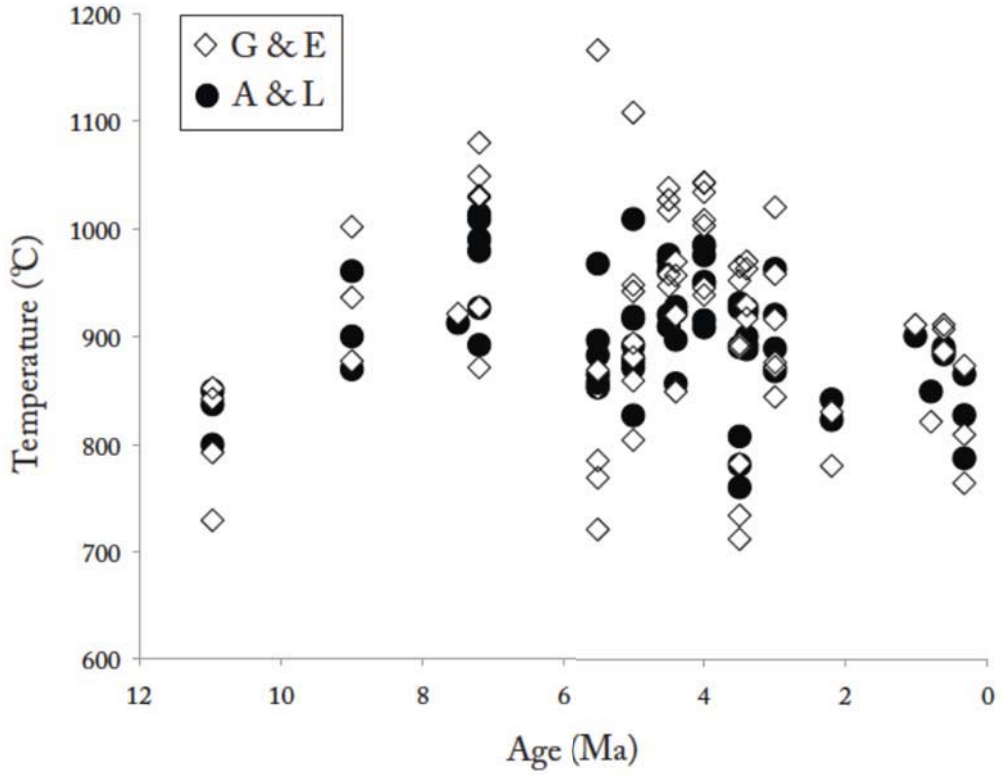

Figure 4.5: Fe-Ti oxide temperatures of AVC lavas plotted against eruption age. Shown are the temperatures calculated from two different thermometers: G & E = Ghiorso and Evans (2008); A & L= Andersen and Lindsley (1985). The two thermometers yield relatively similar temperatures, though those from the G & E thermometer are more variable. Note the generally higher temperatures from ~5 to 3 Ma, corresponding to the time of increased eruptive activity at the AVC.

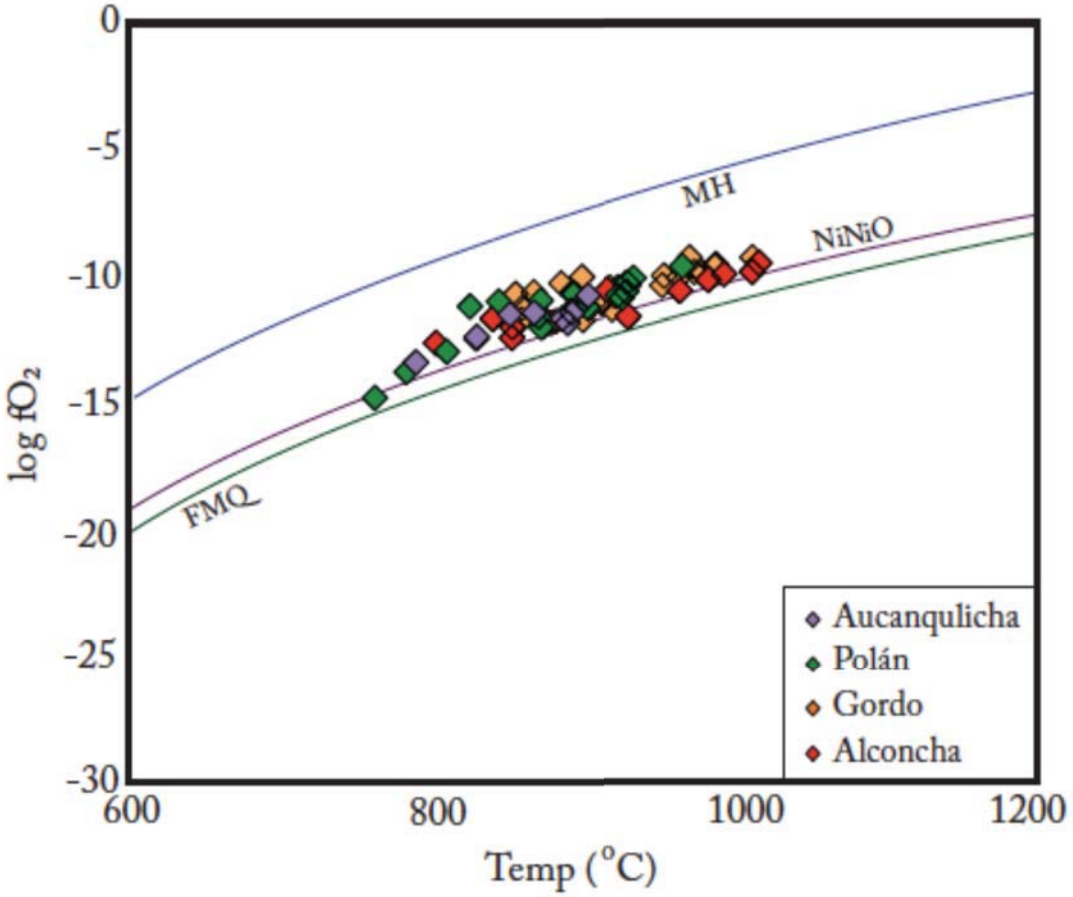

Figure 4.6: Oxygen fugacity vs. temperature of AVC lavas, as calculated from Fe-Ti oxide pairs using the thermobarometer of Andersen and Lindsley (1985). AVC lavas fall in the range of NNO to NNO+2, fairly oxidizing conditions.

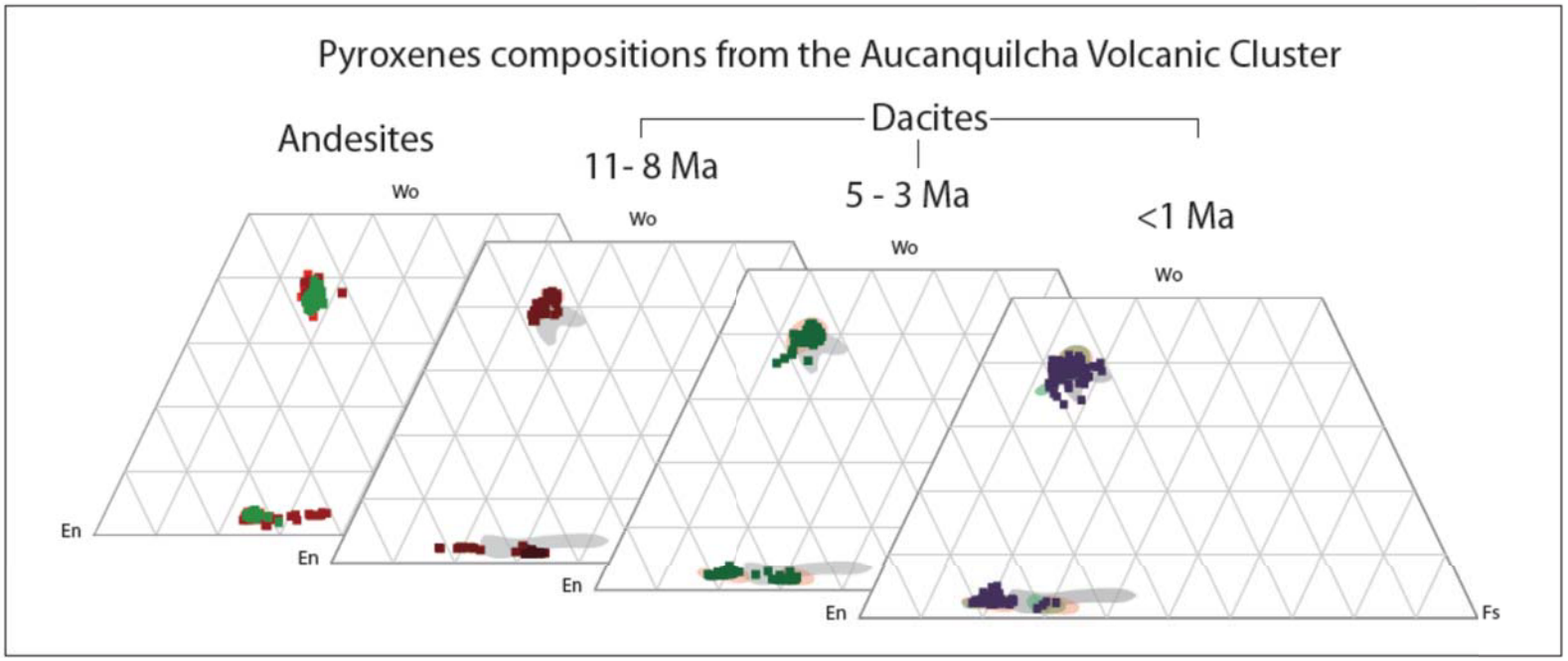

Figure 4.7: Compositions of AVC pyroxenes. Gray field on dacite plots indicates pyroxene compositions from AVC andesites. Note the bimodal orthopyroxene populations in the dacite lavas. En = enstatite; Wo= wollastonite; Fs = ferrosilite.

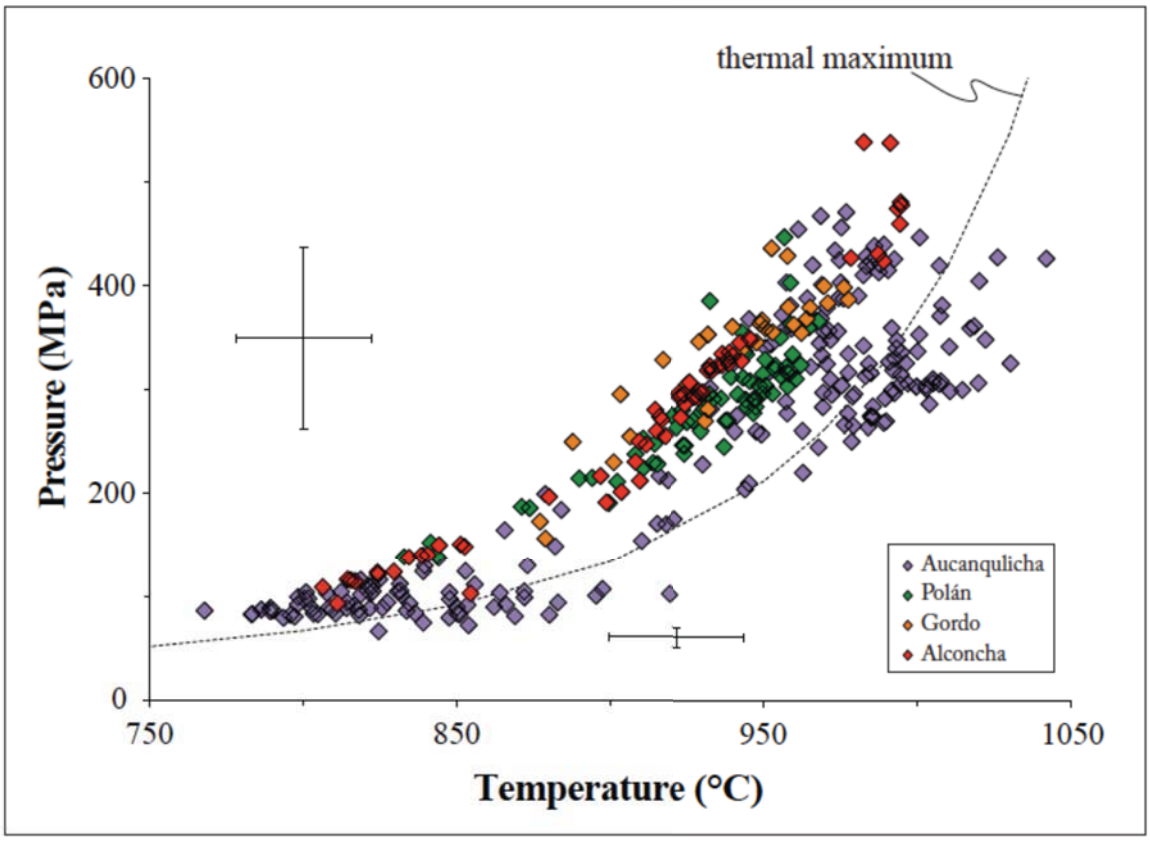

Figure 4.8: Pressure and temperatures for AVC amphibole crystallization as calculated by the Ridolfi model. Analyses are coded for eruptive phase. Error bars indicate the greater error for higher-pressure analyses. Note that several analyses yield a temperature higher than the maximum thermal stability curve defined by Ridolfi and others (2010).

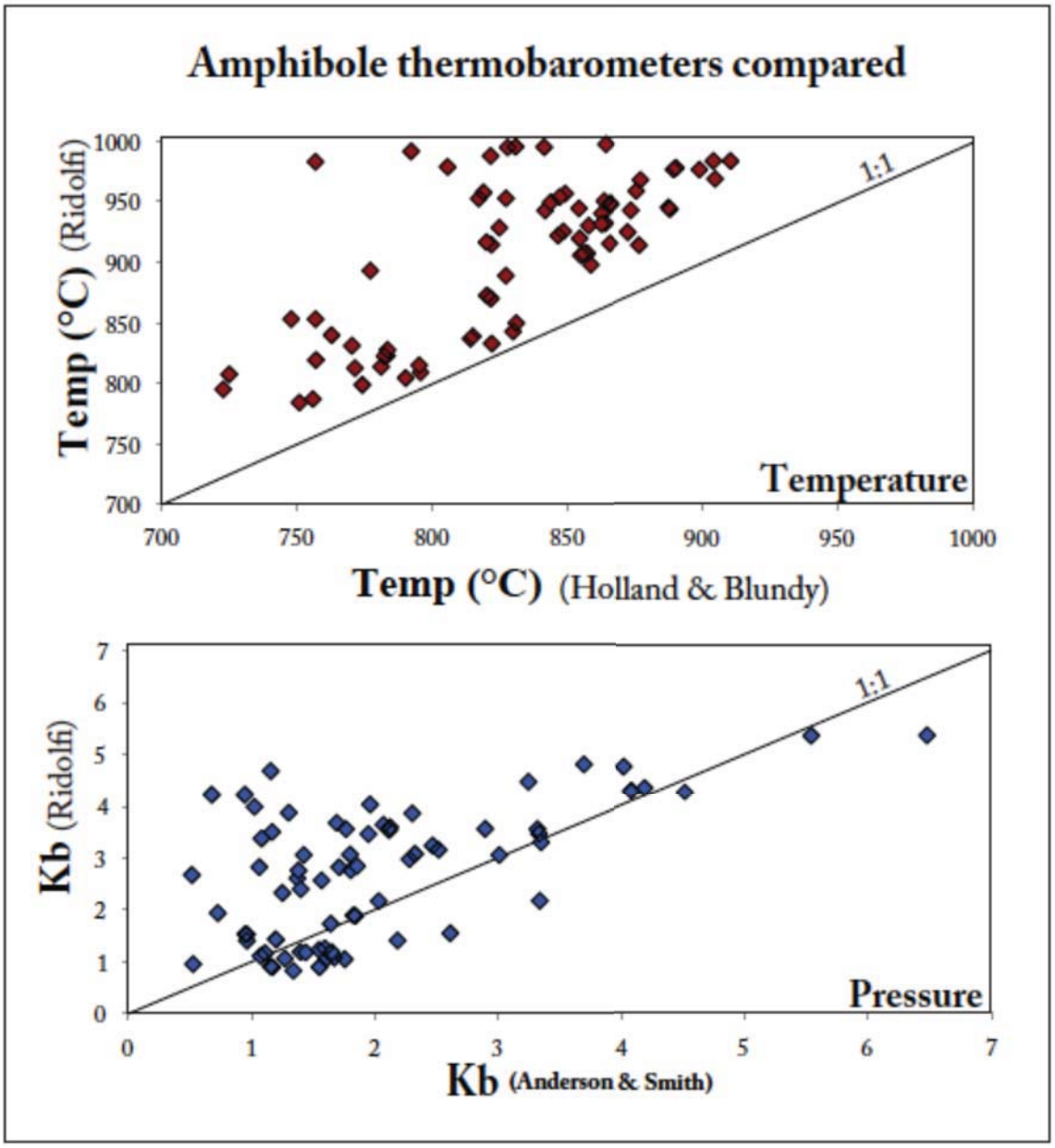

Figure 4.9: Pressure and temperature solutions calculated from Ridolfi et al., 2010 plotted against solutions calculated from Holland & Blundy (1994) and Anderson & Smith (1995). Temperature estimates for the Ridolfi model are consistently higher than those for the B&H equations. Pressure estimates are more consistent, but vary considerably for analyses yielding low pressures from the A&S equations. The H&S equations iteratively solve for P and T using amphibole/plagioclase pairs, while the Ridolfi equations use only amphibole compositions.

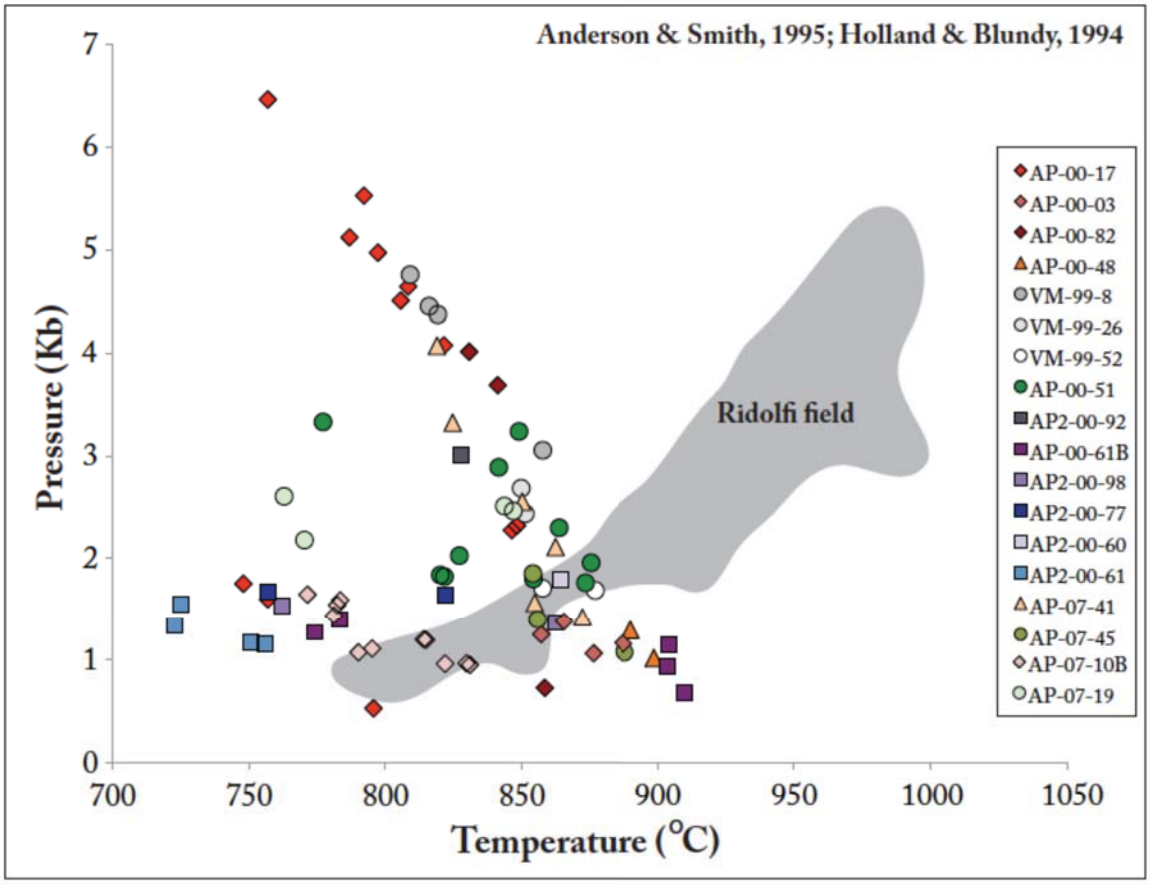

Figure 4.10: Pressure vs. temperature as calculated using amphibole-plagioclase pairs (Anderson & Smith, 1995 and Holland & Blundy, 1994) from AVC lavas. The "Ridolfi field" shows pressure/temperature estimates from the same amphibole data, but calculated with the model of Ridolfi and others (2010). Note the opposite trends in pressure/temperature space. See Figure 4.9 for all amphibole compositions and the corresponding pressure/temperature estimates from the Ridolfi model.

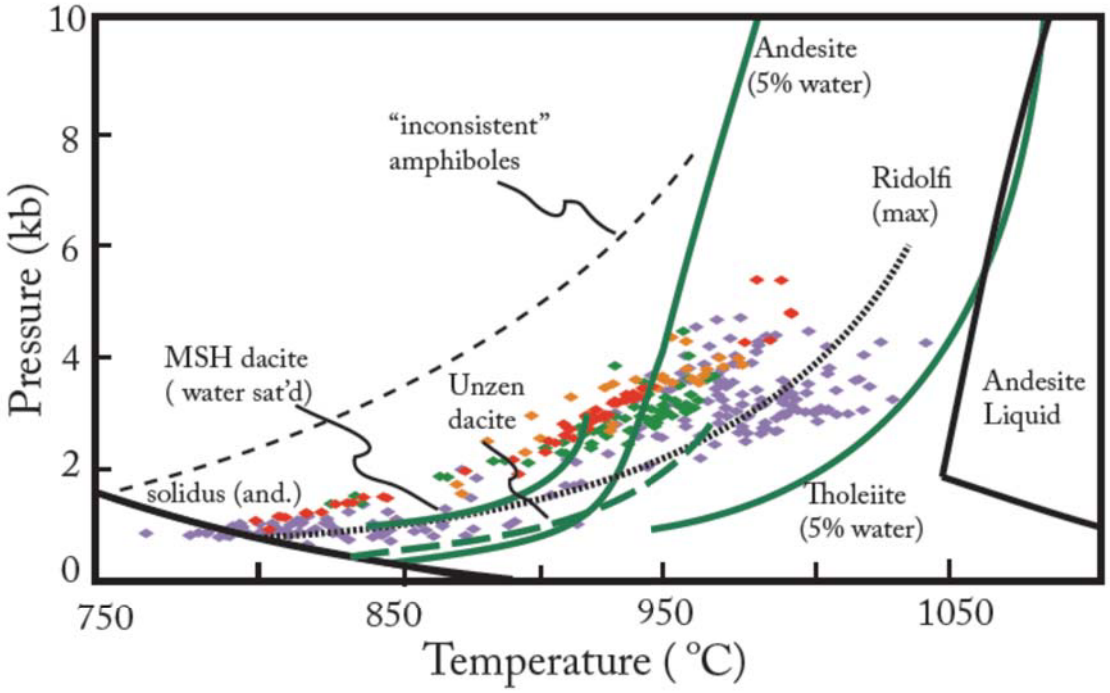

Figure 4.11. All crystallization pressures and temperatures (no "valid" amphiboles rejected) of AVC amphibole data as calculated from equations by Ridolfi and others (2010), shown together with amphibole stability curves for basalt (from Green et al., 1982), andesite (Eggler and Burnham, 1973), and dacite (Rutherford and Devine (2008). Also plotted is the "maximum thermal stability" curve shown by Ridolfi and others (2010), along with their line demarcating "inconsistent" amphibole P/T conditions. Note how many of the P/T conditions calculated for AVC amphiboles at temperatures well above amphibole stability for andesites at 5 wt% water. This discrepancy is likely attributable to the tendency of the equations of Ridolfi and others (2010) to calculate P/Ts along "maximum amphibole stability", rather than well inside the stability field. These amphibole temperatures are likely overestimated and pressures underestimated. Alternatively, these high temperature amphiboles could have crystallized from basaltic andesite melts. Colors for data points same as Figure 4.6.

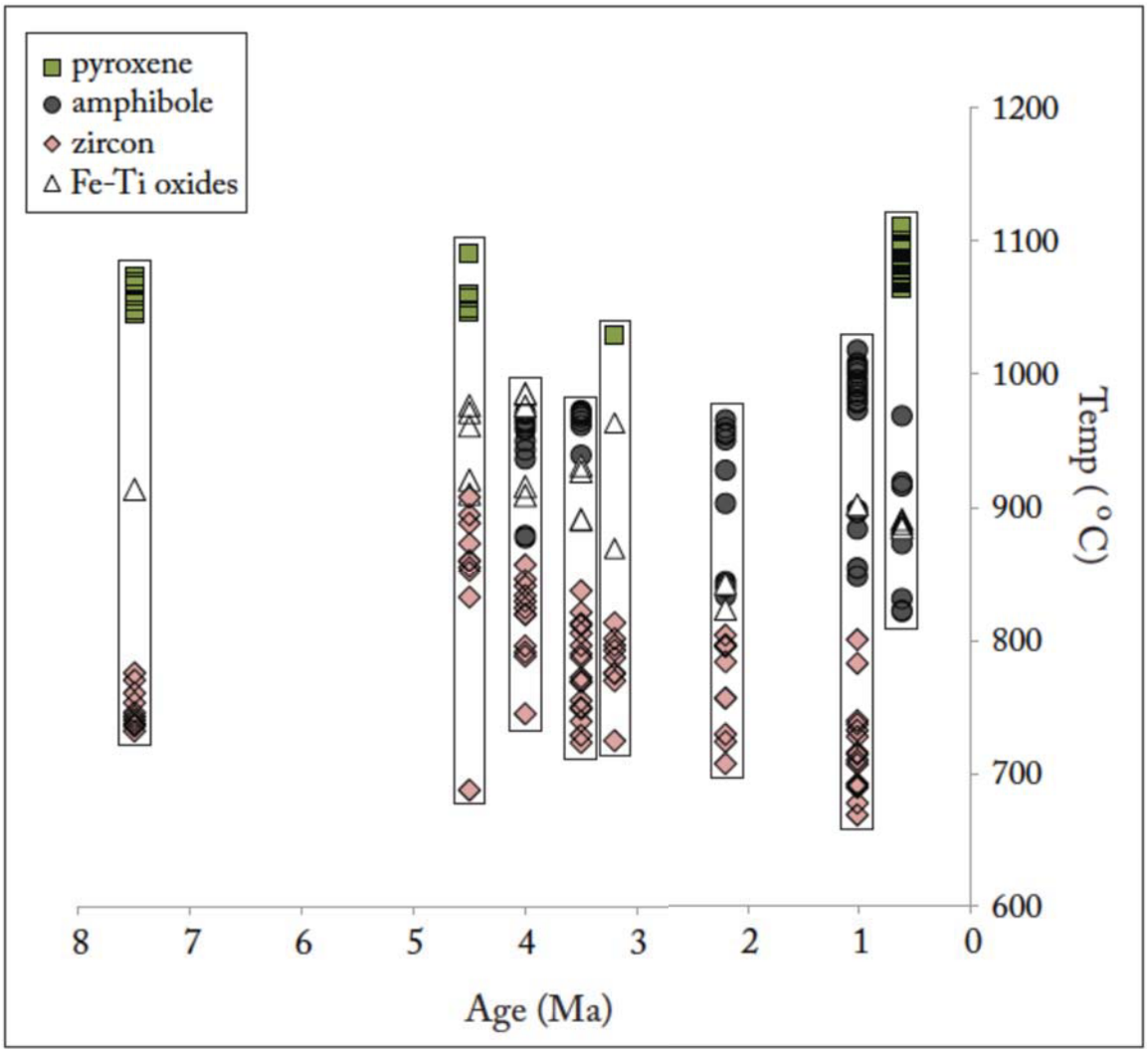

Figure 4.12: Individual AVC lavas with three thermometry constraints. Pyroxenes always yield the highest Ts and zircon the lowest. Amphibole and Fe-Ti oxides fall in the middle.

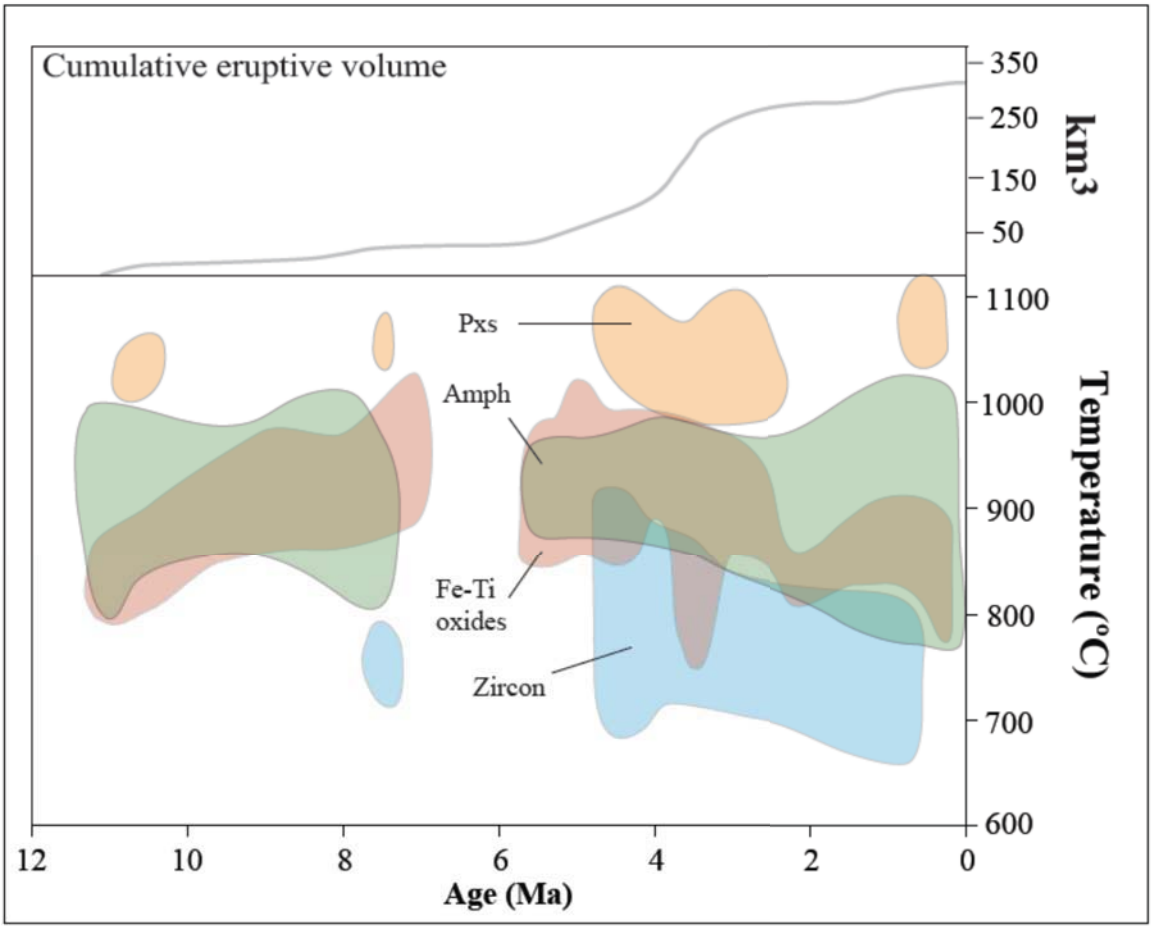

Figure 4.13: All thermometry data, through time, plotted with the cumulative volume curve for the AVC. Pyroxene temperatures are consistently the highest, and zircon temperatures the lowest. Amphiboles and Fe-Ti oxides fall in between. Temperatures for both zircon and Fe-Ti oxide pairs yield the highest Ts around 5 – 3 Ma, during the peak time of AVC volcanism. Amphibole Ts are the highest during the opposite times, the beginning and waning stages of magmatism.

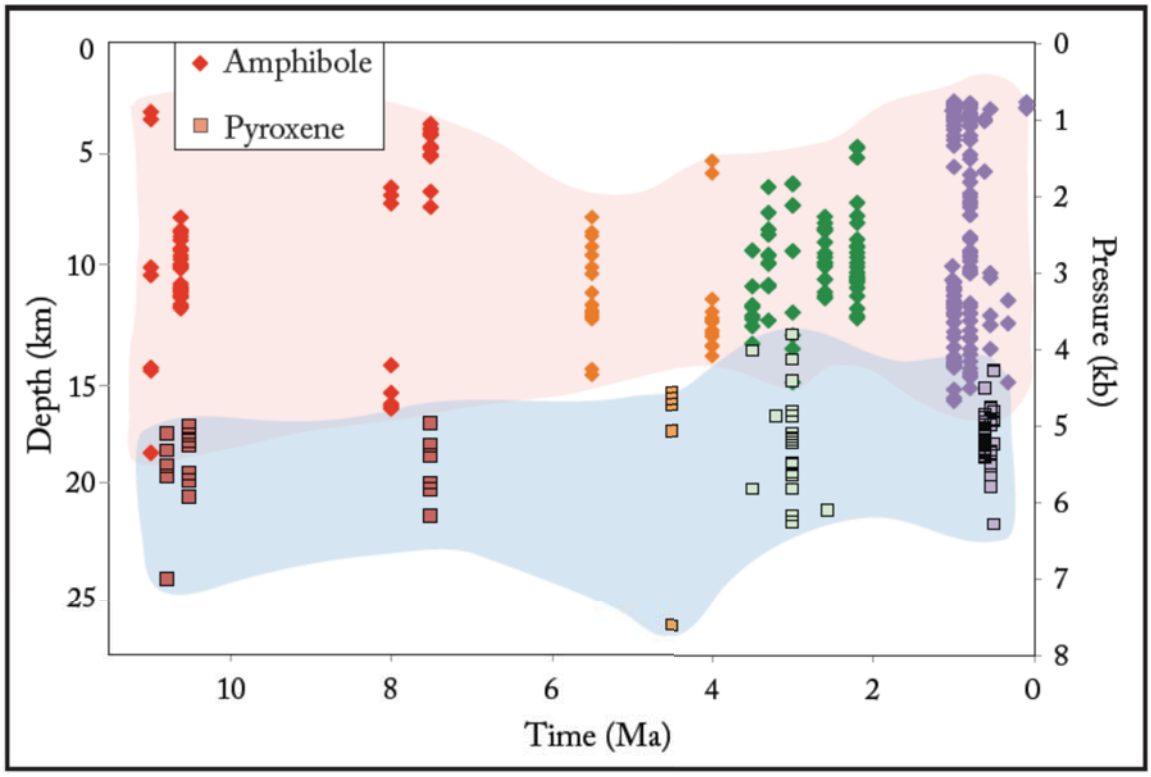

Figure 4.14: Barometric data for amphibole and pyroxene pairs from AVC lavas, through time. Amphiboles crystallized over a significant depth range (~1 - 5 kb). Pyroxenes crystallized deeper than amphibole, but over less of a range (~5 – 7 kb). During the time of peak volcanism (~5 to 2 Ma), amphibole pressures converge to some extent from 2 – 4 kb, suggestive of a consolidation of major amphibole growth reservoirs in the AVC underpinnings.

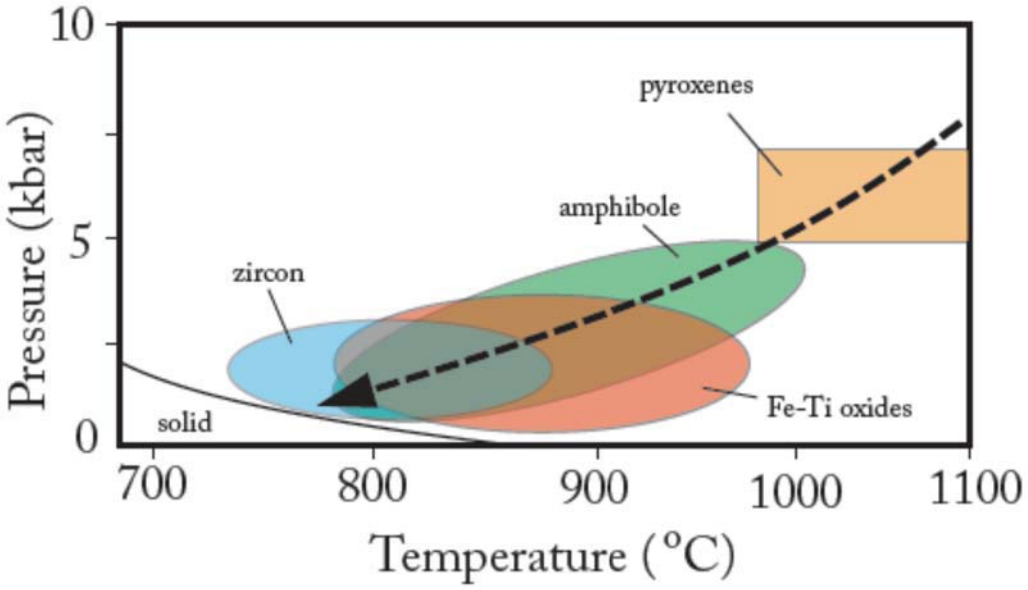

Figure 4.15: Schematic Pressure/Temperature trajectory for magmas of the AVC based on the intensive parameters reported here. Pressures for zircon crystallization and Fe-Ti oxide equilibrium are unknown, but estimated to be similar to amphibole crystallization pressures. Andesite solidus from Eggler and Burnham (1973).

Table 4.1: AVC samples and phases used in this study. Amph/plag pairs from Giles (2009); Amphibole with AP2-00 prefix and (*) ages (Klemetti, 2005); zircon data and (**) ages from Walker et al. (2010). Italicized ages estimated from stratigraphic position.

Sample	rock type	Age (Ma)	2-Px	Amph	Zircon	Fe-Ti ox	amph/plag
AP2-00-61	**dacite**	*0.5*		X			X
AP2-00-60	**dacite**	**0.33***		X		X	
AP2-00-73	**dacite**	*0.5*	X	X			
AP2-00-59	**dacite**	*0.5*	X				
AP2-00-77	inclusion	0.62*	X	X		X	X
AP-07-07	dacite	0.7**			X	X	
AP2-00-98	dacite	*0.8*		X			X
AP2-00-71	inclusion	*0.8*		X			
AP2-00-97	dacite	*1*		X			
AP-00-61B	inclusion	*1*		X			X
AP2-00-94	dacite	*1*		X			
AP2-00-92	dacite	1.02*		X	X	X	X
AP-07-19	dacite	2.2**		X	X	X	X
AP-07-62B	inculsion	*2.2*		X			
AP-00-52	dacite	*2.57*	X			X	
AP-07-51	dacite	3.2**	X		X	X	
AP-00-30	andesite	*3*	X				
AP-07-45	dacite	*2.6*		X		X	X
AP-00-51	dacite	*3*		X			X
VM99-52	dacite	*3.3*		X			
AP-00-65	dacite	3.4**			X	X	
AP-07-36	andesite	*3.5*	X			X	
AP-00-86	dacite	3.5**		X	X	X	
AP-00-48	dacite	*4*		X			X
AP-07-27	dacite	4**		X	X	X	
AP-00-37	dacite	4.4**			X	X	
AP-07-26	dacite	4.5**	X		X	X	
AP-00-69	dacite	*5*				X	
AP-07-41	dacite	*5.5*		X		X	X
AP-00-83	andesite	*5.5*				X	
AP-07-17	dacite	7.2**				X	
AP-07-08	dacite	7.5**	X		X	X	
AP-07-10B	inclusion	*7.5*		X			X
AP-00-82	dacite	7.99*		X		X	X
AP-07-81	andesite	*9*				X	
AP-00-11	andesite	*10.5*	X				
AP-00-03	dacite	*10.5*		X			X
AP-00-04	andesite	10.78*	X				
AP-00-17	dacite	10.97*		X		X	X

Table 4.2: Fe-Ti oxide compositions from AVC lavas. Data collected using the electron microprobe at Oregon State University. All Fe is reported here as FeO. Data reduction was accomplished using the ILMAT program (LePage, 2003). Intensive parameters shown here were calculated using the geothermombarometers of Andersen and Lindsley (A & L; 1985) and Ghiorso and Evans (G & E; 2008). Usp = ulvospinel; Ilm = ilmenite; The Mol % Usp and Ilm from Stormer (1983) are shown. Activity of TiO2 calculated from Ghirso and Evans (2008).

Sample	**AP-07-27**		**AP-07-27**		**AP-07-27**	
analysis	**1 / 20 .**	**1 / 5 .**	**1 / 28 .**	**1 / 24 .**	**1 / 26 .**	**1 / 25 .**
Wt% Oxides	**Magnetite**	**Ilmenite**	**Magnetite**	**Ilmenite**	**Magnetite**	**Ilmenite**
SiO2	0.07	0.02	0.05	0.02	0.01	0.01
TiO2	9.18	35.69	11.71	42.29	12.32	35.06
Al2O3	2.48	0.29	1.43	0.06	1.96	0.23
FeO(T)	78.30	56.12	77.61	51.03	77.02	58.42
MnO	0.38	0.29	0.30	0.33	0.32	0.17
MgO	1.69	1.96	2.08	3.20	2.07	2.23
CaO	0.01	0.04	0.01	0.05	0.00	0.01
Na2O	0.00	0.00	0.01	0.00	0.01	0.01
Cr2O3	0.22	0.10	0.11	0.03	0.10	0.06
V2O3	0.79	0.61	0.55	0.40	0.45	0.47
Sum:	93.17	95.13	93.87	97.40	94.34	96.66
Recalculated Total:	97.8	98.2	98.3	99.5	98.6	100.1
Log(Mg/Mn)	0.89	1.08	1.09	1.24	1.05	1.37
	Usp	***Ilm***	***Usp***	***Ilm***	***Usp***	***Ilm***
Mol %	0.28	0.68	0.34	0.79	0.36	0.65
Geothermobarometer:	***Temp (°C)***	***log10 fO2***	***Temp (°C)***	***log10 fO2***	***Temp (°C)***	***log10 fO2***
A & L (1985)	915.36	-10.53	908.64	-11.05	985.11	-9.60
G & E (2008)	938.5		945.2		1043.4	
NNO +	1.17		0.75		1.06	
TiO2 activity	0.73		0.66		0.67	

Table 4.2 continued

Sample	AP-07-26		AP-07-26		AP-07-26	
analysis	2 / 12 .	2 / 15 .	2 / 21 .	2 / 18 .	2 / 23 .	2 / 25 .
Wt% Oxides	Magnetite	Ilmenite	Magnetite	Ilmenite	Magnetite	Ilmenite
SiO2	0.06	0.04	0.05	0.01	0.05	0.02
TiO2	12.45	38.34	12.53	36.76	10.12	37.22
Al2O3	1.74	0.24	1.88	0.31	1.86	0.31
FeO(T)	76.24	54.57	77.59	56.30	78.37	55.71
MnO	0.35	0.36	0.39	0.27	0.36	0.23
MgO	1.70	2.31	1.85	2.13	1.99	2.49
CaO	0.03	0.11	0.00	0.02	0.01	0.02
Na2O	0.00	0.01	0.00	0.00	0.00	0.01
Cr2O3	0.08	0.04	0.19	0.07	0.21	0.05
V2O3	0.57	0.39	0.63	0.43	0.64	0.51
Sum:	93.23	96.44	95.17	96.35	93.61	96.58
Recalculated Total:	97.4	99.2	99.4	99.4	98.2	99.6
Log(Mg/Mn)	0.93	1.05	0.93	1.14	0.99	1.29
	Usp	*Ilm*	*Usp*	*Ilm*	*Usp*	*Ilm*
Mol %	0.37	0.72	0.37	0.69	0.30	0.70
Geothermobarometer:	*Temp (°C)*	*log10 fO2*	*Temp (°C)*	*log10 fO2*	*Temp (°C)*	*log10 fO2*
A & L (1985)	960.69	-10.14	970.91	-9.91	920.26	-10.52
G & E (2008)	1017		1027		958	
NNO +	0.89		0.96		1.11	
TiO2 activity	0.68		0.68		0.70	

Sample	AP-07-26		AP-07-41		AP-07-41	
analysis	1 / 32 .	1 / 30 .	1 / 1 .	1 / 3 .	1 / 8 .	1 / 6 .
Wt% Oxides	Magnetite	Ilmenite	Magnetite	Ilmenite	Magnetite	Ilmenite
SiO2	0.02	0.03	0.08	0.04	0.10	0.07
TiO2	3.22	37.37	8.94	27.98	5.34	26.71
Al2O3	0.70	0.17	1.28	0.38	1.62	0.31
FeO(T)	82.82	54.15	80.65	64.10	83.21	65.56
MnO	0.65	0.18	0.69	0.32	0.57	0.34
MgO	3.45	1.13	1.53	1.16	0.91	0.99
CaO	0.02	0.02	0.06	0.04	0.03	0.04
Na2O	0.01	0.00	0.02	0.01	0.01	0.00
Cr2O3	0.13	0.06	0.04	0.05	0.02	0.04
V2O3	0.58	0.72	0.25	0.55	0.34	0.45
Sum:	91.64	93.83	93.58	94.66	92.19	94.53
Recalculated Total:	97.8	96.4	98.5	99.3	97.7	99.4
Log(Mg/Mn)	0.97	1.05	0.59	0.80	0.45	0.72
	Usp	*Ilm*	*Usp*	*Ilm*	*Usp*	*Ilm*
Mol %	0.08	0.74	0.25	0.54	0.16	0.51
Geothermobarometer:	*Temp (°C)*	*log10 fO2*	*Temp (°C)*	*log10 fO2*	*Temp (°C)*	*log10 fO2*
A & L (1985)	768.06	-12.44	967.73	-9.34	896.51	-10.09
G & E (2008)	631		1166		852	
NNO +	2		1.93		1.67	
TiO2 activity	1.13		0.58		0.71	

Table 4.2 continued

Sample	AP-07-19		AP2-00-77		AP2-00-77	
analysis	29 / 3 .	29 / 4 .	17 / 2 .	17 / 1 .	23 / 1 .	22 / 1 .
Wt% Oxides	**Magnetite**	**Ilmenite**	**Magnetite**	**Ilmenite**	**Magnetite**	**Ilmenite**
SiO2	0.02	0.03	0.08	0.09	0.14	0.14
TiO2	4.10	33.17	10.70	44.00	12.38	44.78
Al2O3	2.43	0.34	2.51	0.15	2.05	0.18
FeO(T)	79.66	54.84	76.02	48.64	74.21	47.88
MnO	0.49	0.36	0.46	0.50	0.45	0.77
MgO	4.07	5.29	1.31	2.26	1.59	2.46
CaO	0.10	0.13	0.09	1.89	0.07	0.06
Na2O	0.00	-0.01	0.02	0.01	0.03	-0.01
Cr2O3	0.18	0.04	0.05	0.04	0.03	0.08
V2O3	0.65	0.33	0.62	0.27	0.33	0.27
Sum:	91.75	94.58	91.94	97.88	91.33	96.62
Recalculated Total:	97.54	98.46	**96.20**	**99.65**	**95.29**	**98.02**
Log(Mg/Mn)	1.16	1.41	0.70	0.91	0.79	0.75
	Usp	***Ilm***	***Usp***	***Ilm***	***Usp***	***Ilm***
Mol %	0.11	0.58	0.34	0.82	0.38	0.86
Geothermobarometer:	**Temp (°C)**	**log10 fO2**	**Temp (°C)**	**log10 fO2**	**Temp (°C)**	**log10 fO2**
A & L (1985)	822.70	-11.25	889.99	-11.51	887.03	-11.90
G & E (2008)	780					
NNO +	1.89		886		911	
TiO2 activity	0.73		0.45		0.26	

Sample	AP2-00-77		AP-07-36		AP-07-36	
analysis	25 / 3 .	25 / 1 .	1 / 3 .	1 / 1 .	1 / 4 .	1 / 2 .
Wt% Oxides	**Magnetite**	**Ilmenite**	**Magnetite**	**Ilmenite**	**Magnetite**	**Ilmenite**
SiO2	0.05	0.03	0.21	0.07	0.14	0.37
TiO2	10.58	44.30	6.96	46.48	7.04	45.05
Al2O3	2.88	0.13	2.49	0.24	3.22	0.41
FeO(T)	75.68	49.92	81.34	47.29	80.16	48.44
MnO	0.35	0.42	0.22	0.49	0.21	0.40
MgO	1.32	2.41	1.02	2.47	1.06	2.57
CaO	0.17	0.13	0.02	0.02	0.04	0.05
Na2O	0.02	-0.01	-0.02	0.01	0.02	0.05
Cr2O3	0.70	0.02	0.14	0.04	0.16	0.04
V2O3	0.51	0.32	0.66	0.43	0.57	0.37
Sum:	92.27	97.69	93.10	97.57	92.69	97.81
Recalculated Total:	**96.49**	**99.30**	98.15	98.72	97.64	99.20
Log(Mg/Mn)	0.82	1.00	0.91	0.95	0.95	1.06
	Usp	***Ilm***	***Usp***	***Ilm***	***Usp***	***Ilm***
Mol %	0.34	0.83	0.22	0.88	0.23	0.86
Geothermobarometer:	**Temp (°C)**	**log10 fO2**	**Temp (°C)**	**log10 fO2**	**Temp (°C)**	**log10 fO2**
A & L (1985)	883.59	-11.72	780.99	-13.83	807.38	-13.03
G & E (2008)			734		782	
NNO +	907		0.31		0.62	
TiO2 activity	0.56		0.62		0.68	

Table 4.2 continued

Sample	AP-07-27		AP-07-27		AP-07-27	
analysis	1 / 71 .	1 / 70 .	1 / 68 .	1 / 69 .	2 / 6 .	2 / 3 .
Wt% Oxides	Magnetite	Ilmenite	Magnetite	Ilmenite	Magnetite	Ilmenite
SiO2	0.10	0.02	0.09	0.01	0.05	0.17
TiO2	12.61	36.19	12.73	37.46	12.77	40.27
Al2O3	1.94	0.34	1.89	0.30	2.13	0.33
FeO(T)	76.85	57.77	76.90	56.72	76.04	52.20
MnO	0.38	0.27	0.40	0.25	0.39	0.39
MgO	1.82	2.12	1.78	2.21	1.84	2.68
CaO	0.03	0.01	0.02	0.01	0.04	0.03
Na2O	0.00	0.00	0.01	0.00	0.00	0.00
Cr2O3	0.07	0.07	0.06	0.08	0.06	0.03
V2O3	0.56	0.47	0.51	0.45	0.61	0.35
Sum:	94.41	97.27	94.42	97.53	93.95	96.44
Recalculated Total:	98.6	100.5	98.6	100.6	98.0	98.8
Log(Mg/Mn)	0.92	1.14	0.89	1.19	0.92	1.09
	Usp	*Ilm*	*Usp*	*Ilm*	*Usp*	*Ilm*
Mol %	0.37	0.68	0.38	0.70	0.38	0.76
Geothermobarometer:	*Temp (°C)*	*log10 fO2*	*Temp (°C)*	*log10 fO2*	*Temp (°C)*	*log10 fO2*
A & L (1985)	984.55	-9.69	975.51	-9.87	949.74	-10.43
G & E (2008)	1042.7		1034.1		1008.4	
NNO +	0.98		0.94		0.8	
TiO2 activity	0.67		0.68		0.68	

Sample	AP-07-27		AP-00-37		AP-00-37	
analysis	2 / 14 .	2 / 10 .	2 / 45 .	2 / 41 .	2 / 83 .	2 / 84 .
Wt% Oxides	Magnetite	Ilmenite	Magnetite	Ilmenite	Magnetite	Ilmenite
SiO2	0.01	0.01	0.02	0.00	0.04	0.00
TiO2	11.31	35.85	10.40	37.16	10.44	37.68
Al2O3	1.64	0.25	2.12	0.25	1.85	0.18
FeO(T)	78.22	56.97	78.96	55.94	79.92	55.77
MnO	0.36	0.26	0.32	0.21	0.30	0.26
MgO	2.07	2.50	1.87	2.56	1.52	2.23
CaO	0.01	0.01	0.00	0.00	0.03	0.02
Na2O	0.00	0.00	0.01	0.00	0.02	0.00
Cr2O3	0.11	0.08	0.12	0.07	0.10	0.05
V2O3	0.70	0.54	0.61	0.46	0.52	0.54
Sum:	94.48	96.49	94.51	96.66	94.73	96.75
Recalculated Total:	99.0	99.8	99.1	99.7	99.4	99.7
Log(Mg/Mn)	1.01	1.23	1.01	1.34	0.95	1.17
	Usp	*Ilm*	*Usp*	*Ilm*	*Usp*	*Ilm*
Mol %	0.33	0.67	0.31	0.69	0.31	0.71
Geothermobarometer:	*Temp (°C)*	*log10 fO2*	*Temp (°C)*	*log10 fO2*	*Temp (°C)*	*log10 fO2*
A & L (1985)	950.98	-10.05	927.73	-10.42	923.03	-10.53
G & E (2008)	1003		969.6		956.7	
NNO +	1.1		1.1		1.03	
TiO2 activity	0.67		0.69		0.70	

Table 4.2 continued

Sample	AP-07-41		AP-07-41		AP-07-41	
analysis	1 / 10 .	1 / 11 .	1 / 14 .	1 / 15 .	1 / 18 .	1 / 19 .
Wt% Oxides	Magnetite	Ilmenite	Magnetite	Ilmenite	Magnetite	Ilmenite
SiO2	0.12	0.04	0.07	0.10	0.10	0.03
TiO2	4.16	28.32	5.18	27.26	5.27	29.24
Al2O3	1.22	0.32	1.58	0.39	0.68	0.27
FeO(T)	84.97	62.84	82.13	62.74	83.23	60.87
MnO	0.15	0.38	0.67	0.46	0.80	0.63
MgO	0.38	1.21	0.94	1.14	1.09	1.38
CaO	0.04	0.03	0.01	0.03	0.02	0.02
Na2O	0.01	0.00	0.01	0.00	0.00	0.01
Cr2O3	0.03	0.05	0.02	0.06	0.02	0.05
V2O3	0.31	0.52	0.29	0.53	0.24	0.56
Sum:	91.43	93.71	90.89	92.82	91.44	93.05
Recalculated Total:	97.2	98.2	96.4	97.3	97.1	97.2
Log(Mg/Mn)	0.65	0.74	0.39	0.64	0.38	0.59
	Usp	*Ilm*	*Usp*	*Ilm*	*Usp*	*Ilm*
Mol %	0.13	0.55	0.16	0.53	0.15	0.57
Geothermobarometer:	*Temp (°C)*	*log10 fO2*	*Temp (°C)*	*log10 fO2*	*Temp (°C)*	*log10 fO2*
A & L (1985)	852.80	-10.76	882.83	-10.34	864.77	-10.69
G & E (2008)	721		785		769	
NNO +	1.5		1.45		1.45	
TiO2 activity	0.82		0.77		0.77	

Sample	AP-07-17		AP-07-17		AP-07-17	
analysis	2 / 4 .	2 / 2 .	2 / 5 .	2 / 9 .	2 / 8 .	2 / 11 .
Wt% Oxides	Magnetite	Ilmenite	Magnetite	Ilmenite	Magnetite	Ilmenite
SiO2	0.12	0.06	0.04	0.00	0.05	0.00
TiO2	13.76	39.90	14.74	39.39	14.75	42.10
Al2O3	1.70	0.06	0.96	0.08	1.77	0.09
FeO(T)	74.88	53.88	76.56	54.95	75.17	52.24
MnO	0.03	0.23	0.21	0.67	0.49	0.73
MgO	0.32	1.21	0.64	2.24	1.29	2.02
CaO	0.04	0.03	0.02	0.01	0.02	0.01
Na2O	0.00	0.00	0.01	0.01	0.00	0.01
Cr2O3	0.11	0.04	0.11	0.03	0.10	0.02
V2O3	0.57	0.46	0.57	0.20	0.56	0.25
Sum:	91.57	95.92	93.84	97.60	94.23	97.49
Recalculated Total:	95.2	98.2	97.6	100.3	97.9	99.6
Log(Mg/Mn)	1.21	0.97	0.73	0.77	0.67	0.69
	Usp	*Ilm*	*Usp*	*Ilm*	*Usp*	*Ilm*
Mol %	0.45	0.77	0.44	0.73	0.45	0.79
Geothermobarometer:	*Temp (°C)*	*log10 fO2*	*Temp (°C)*	*log10 fO2*	*Temp (°C)*	*log10 fO2*
A & L (1985)	990.53	-9.99	1013.52	-9.55	980.14	-10.21
G & E (2008)	1029		1080		1031	
NNO +	0.57		0.62		0.55	
TiO2 activity	0.68		0.62		0.67	

Table 4.2 continued

Sample	AP-07-36		AP-07-81		AP-07-81	
analysis	9 / 3 .	9 / 2 .	13 / 2 .	13 / 1 .	16 / 2 .	16 / 1 .
Wt% Oxides	**Magnetite**	**Ilmenite**	**Magnetite**	**Ilmenite**	**Magnetite**	**Ilmenite**
SiO2	0.07	0.05	0.08	0.09	0.14	0.06
TiO2	8.38	47.79	11.66	43.61	9.57	42.62
Al2O3	1.58	0.08	2.14	0.25	1.46	0.17
FeO(T)	80.06	44.98	75.23	48.63	78.41	50.49
MnO	0.25	0.50	0.35	0.36	0.33	0.41
MgO	1.07	2.95	2.15	3.64	1.42	2.64
CaO	0.03	0.03	0.14	0.16	0.05	0.05
Na2O	0.02	0.01	0.00	0.02	0.01	0.04
Cr2O3	0.10	0.03	0.12	0.05	0.13	0.03
V2O3	0.53	0.37	0.65	0.32	0.59	0.36
Sum:	92.15	96.82	92.53	97.16	92.14	96.88
Recalculated Total:	97.02	97.68	96.73	98.98	96.78	98.78
Log(Mg/Mn)	0.88	1.01	1.04	1.25	0.88	1.05
	Usp	***Ilm***	***Usp***	***Ilm***	***Usp***	***Ilm***
Mol %	0.25	0.91	0.35	0.81	0.29	0.81
Geothermobarometer:	**Temp (°C)**	**log10 fO2**	**Temp (°C)**	**log10 fO2**	**Temp (°C)**	**log10 fO2**
A & L (1985)	760.08	-14.85	900.88	-11.33	870.29	-11.66
G & E (2008)	712					
NNO +	-0.36		937		878	
TiO2 activity	0.50		0.59		0.74	

Sample	AP-07-81		AP-00-83		AP-00-17	
analysis	20 / 2 .	20 / 1 .	24 / 2 .	24 / 1 .	33 / 3 .	33 / 1 .
Wt% Oxides	**Magnetite**	**Ilmenite**	**Magnetite**	**Ilmenite**	**Magnetite**	**Ilmenite**
SiO2	0.09	0.08	0.05	0.03	0.65	0.02
TiO2	14.99	42.77	6.69	39.14	5.24	43.35
Al2O3	1.43	0.18	3.90	0.31	1.64	0.11
FeO(T)	72.30	49.63	79.04	51.73	79.95	49.60
MnO	0.41	0.40	0.37	0.35	0.19	0.60
MgO	1.90	2.09	2.88	4.48	0.80	2.41
CaO	0.06	0.09	0.11	0.20	0.06	0.04
Na2O	0.01	0.00	0.01	0.01	0.11	0.02
Cr2O3	0.33	0.05	0.16	0.06	0.04	0.01
V2O3	0.69	0.48	0.61	0.42	0.62	0.26
Sum:	92.25	95.77	93.85	96.72	89.37	96.43
Recalculated Total:	95.77	97.47	99.00	99.49	94.51	98.16
Log(Mg/Mn)	0.91	0.97	1.14	1.36	0.87	0.85
	Usp	***Ilm***	***Usp***	***Ilm***	***Usp***	***Ilm***
Mol %	0.45	0.83	0.20	0.71	0.17	0.82
Geothermobarometer:	**Temp (°C)**	**log10 fO2**	**Temp (°C)**	**log10 fO2**	**Temp (°C)**	**log10 fO2**
A & L (1985)	961.40	-10.65	857.20	-11.30	800.33	-12.69
G & E (2008)			869		730	
NNO +	1002		1.39		1	
TiO2 activity	0.43		0.73		0.74	

Table 4.2 continued

Sample	AP-00-37		AP-00-37		AP2-00-92	
analysis	2 / 60 .	2 / 64 .	2 / 10 .	2 / 12 .	1 / 18 .	1 / 17 .
Wt% Oxides	Magnetite	Ilmenite	Magnetite	Ilmenite	Magnetite	Ilmenite
SiO2	0.00	0.02	0.07	0.01	0.09	0.04
TiO2	8.59	43.00	13.26	45.83	9.58	38.14
Al2O3	1.38	0.04	1.98	0.04	1.29	0.11
FeO(T)	81.58	51.44	75.88	47.75	82.38	56.12
MnO	0.23	0.35	0.26	0.33	0.42	0.46
MgO	1.12	2.81	1.69	3.23	1.18	1.94
CaO	0.00	0.02	0.01	0.03	0.00	0.04
Na2O	0.01	0.00	0.02	0.00	0.02	0.00
Cr2O3	0.16	0.05	0.28	0.03	0.05	0.03
V2O3	0.84	0.36	0.77	0.33	0.43	0.37
Sum:	93.94	98.10	94.24	97.58	95.45	97.25
Recalculated Total:	98.9	100.1	98.2	99.0	100.4	100.1
Log(Mg/Mn)	0.94	1.15	1.06	1.23	0.70	0.87
	Usp	*Ilm*	*Usp*	*Ilm*	*Usp*	*Ilm*
Mol %	0.25	0.80	0.40	0.86	0.28	0.71
Geothermobarometer:	*Temp (°C)*	*log10 fO2*	*Temp (°C)*	*log10 fO2*	*Temp (°C)*	*log10 fO2*
A & L (1985)	856.59	-11.78	897.09	-11.78	900.57	-10.82
G & E (2008)	849		920		911	
NNO +	0.82		0.18		1.03	
TiO2 activity	0.68		0.60		0.70	

Sample	AP-07-07		AP-07-51		AP-07-51	
analysis	2 / 22 .	2 / 18 .	1 / 7 .	1 / 5 .	1 / 24 .	1 / 22 .
Wt% Oxides	Magnetite	Ilmenite	Magnetite	Ilmenite	Magnetite	Ilmenite
SiO2	0.03	0.03	0.08	0.02	0.05	0.00
TiO2	6.82	39.30	9.97	31.85	6.89	35.79
Al2O3	1.68	0.10	2.20	0.37	1.68	0.21
FeO(T)	81.25	54.02	78.08	60.27	81.84	57.61
MnO	0.48	0.42	0.38	0.17	0.30	0.28
MgO	1.28	2.04	1.75	1.80	1.66	2.16
CaO	0.00	0.00	0.08	0.03	0.01	0.01
Na2O	0.01	0.02	0.00	0.01	0.01	0.01
Cr2O3	0.12	0.02	0.18	0.10	0.25	0.05
V2O3	0.55	0.30	0.74	0.49	0.61	0.45
Sum:	92.23	96.25	93.46	95.10	93.40	96.58
Recalculated Total:	97.4	98.8	98.0	99.0	98.7	99.9
Log(Mg/Mn)	0.67	0.93	0.91	1.27	0.98	1.14
	Usp	*Ilm*	*Usp*	*Ilm*	*Usp*	*Ilm*
Mol %	0.20	0.75	0.30	0.61	0.20	0.67
Geothermobarometer:	*Temp (°C)*	*log10 fO2*	*Temp (°C)*	*log10 fO2*	*Temp (°C)*	*log10 fO2*
A & L (1985)	849.09	-11.56	962.95	-9.68	869.31	-11.01
G & E (2008)	821		1020		844	
NNO +	1.21		1.29		1.35	
TiO2 activity	0.77		0.67		0.76	

Table 4.2 continued

Sample	AP-07-17		AP-07-17		AP-07-17	
analysis	2 / 15 .	2 / 14 .	2 / 20 .	2 / 18 .	2 / 22 .	2 / 23 .
Wt% Oxides	Magnetite	Ilmenite	Magnetite	Ilmenite	Magnetite	Ilmenite
SiO2	1.99	0.08	0.14	0.06	0.07	0.05
TiO2	14.03	44.23	15.15	40.25	8.14	35.26
Al2O3	2.03	0.13	1.54	0.10	1.70	0.53
FeO(T)	71.67	48.33	72.69	50.69	83.80	57.63
MnO	0.33	0.37	0.38	0.61	0.17	0.45
MgO	0.73	0.88	0.50	1.28	0.42	0.86
CaO	0.06	0.05	0.04	0.05	0.01	0.03
Na2O	0.01	0.01	0.01	0.01	0.01	0.00
Cr2O3	0.10	0.04	0.14	0.03	0.09	0.03
V2O3	0.86	0.40	0.78	0.50	0.64	0.30
Sum:	91.85	94.50	91.40	93.56	95.14	95.15
Recalculated Total:	94.9	95.7	94.7	95.5	100.2	98.3
Log(Mg/Mn)	0.60	0.62	0.37	0.57	0.64	0.53
	Usp	*Ilm*	*Usp*	*Ilm*	*Usp*	*Ilm*
Mol %	0.49	0.88	0.49	0.80	0.25	0.69
Geothermobarometer:	*Temp (°C)*	*log10 fO2*	*Temp (°C)*	*log10 fO2*	*Temp (°C)*	*log10 fO2*
A & L (1985)	927.29	-11.65	1009.00	-9.90	892.87	-10.81
G & E (2008)	928		1049		872	
NNO +	0		0.42		1.09	
TiO2 activity	0.64		0.67		0.73	

Sample	AP-07-45		AP-07-45		AP-07-45	
analysis	3 / 2 .	3 / 4 .	3 / 9 .	3 / 6 .	3 / 10 .	3 / 13 .
Wt% Oxides	Magnetite	Ilmenite	Magnetite	Ilmenite	Magnetite	Ilmenite
SiO2	0.11	0.04	0.08	0.44	0.12	0.05
TiO2	9.13	42.52	10.98	41.80	11.18	42.38
Al2O3	1.39	0.04	1.18	0.12	1.16	0.11
FeO(T)	79.19	50.27	78.41	49.66	76.91	48.62
MnO	0.30	0.64	0.45	0.62	0.35	0.23
MgO	1.13	2.83	1.43	2.65	0.93	1.28
CaO	0.03	0.05	0.01	0.03	0.03	0.04
Na2O	0.00	0.00	0.01	0.00	0.00	0.00
Cr2O3	0.13	0.04	0.12	0.03	0.06	0.03
V2O3	0.74	0.40	0.86	0.31	0.67	0.33
Sum:	92.12	96.81	93.59	95.70	91.52	93.06
Recalculated Total:	96.8	98.8	98.1	97.6	95.8	94.5
Log(Mg/Mn)	0.82	0.89	0.74	0.88	0.67	0.99
	Usp	*Ilm*	*Usp*	*Ilm*	*Usp*	*Ilm*
Mol %	0.28	0.80	0.32	0.81	0.34	0.85
Geothermobarometer:	*Temp (°C)*	*log10 fO2*	*Temp (°C)*	*log10 fO2*	*Temp (°C)*	*log10 fO2*
A & L (1985)	867.84	-11.65	889.09	-11.43	869.63	-12.07
G & E (2008)	872		916		876	
NNO +	0.75		0.66		0.39	
TiO2 activity	0.66		0.65		0.66	

Table 4.2 continued

Sample	AP-07-08		AP-00-86		AP-00-86	
analysis	2 / 21 .	2 / 17 .	3 / 6 .	3 / 2 .	3 / 13 .	3 / 15 .
Wt% Oxides	Magnetite	Ilmenite	Magnetite	Ilmenite	Magnetite	Ilmenite
SiO2	0.51	0.02	0.06	0.00	0.10	0.01
TiO2	8.90	36.75	7.51	35.14	8.61	33.51
Al2O3	2.07	0.11	1.63	0.19	1.77	0.26
FeO(T)	77.12	57.32	82.91	57.52	78.83	58.84
MnO	0.29	0.15	0.14	0.34	0.25	0.24
MgO	1.03	1.59	1.15	2.78	0.72	2.23
CaO	0.14	0.01	0.00	0.01	0.02	0.02
Na2O	0.03	0.00	0.00	0.00	0.00	0.00
Cr2O3	0.11	0.05	0.23	0.08	0.24	0.09
V2O3	0.78	0.60	0.86	0.54	0.66	0.55
Sum:	91.05	96.60	94.61	96.68	91.28	95.81
Recalculated Total:	95.5	99.6	99.8	100.2	96.0	99.5
Log(Mg/Mn)	0.80	1.28	1.16	1.16	0.70	1.21
	Usp	*Ilm*	*Usp*	*Ilm*	*Usp*	*Ilm*
Mol %	0.29	0.70	0.22	0.65	0.27	0.63
Geothermobarometer:	*Temp (°C)*	*log10 fO2*	*Temp (°C)*	*log10 fO2*	*Temp (°C)*	*log10 fO2*
A & L (1985)	913.24	-10.61	890.26	-10.69	931.01	-10.14
G & E (2008)	922		890		952	
NNO +	1.09		1.25		1.13	
TiO2 activity	0.74		0.68		0.65	

Sample	AP-00-86		AP-00-86		AP-00-65	
analysis	3 / 18 .	3 / 22 .	3 / 7 .	3 / 10 .	4 / 2 .	4 / 3 .
Wt% Oxides	Magnetite	Ilmenite	Magnetite	Ilmenite	Magnetite	Ilmenite
SiO2	0.09	0.00	0.04	0.00	0.07	0.02
TiO2	7.63	35.86	9.85	35.55	11.09	43.07
Al2O3	1.76	0.19	1.60	0.21	1.28	0.03
FeO(T)	80.15	56.15	79.94	56.50	78.44	50.82
MnO	0.20	0.32	0.17	0.23	0.40	0.49
MgO	0.87	2.41	1.74	2.74	1.54	2.83
CaO	0.04	0.01	0.07	0.01	0.02	0.03
Na2O	0.02	0.00	0.00	0.00	0.00	0.00
Cr2O3	0.29	0.08	0.23	0.06	0.23	0.04
V2O3	0.93	0.50	0.72	0.52	0.57	0.42
Sum:	92.07	95.53	94.38	95.81	93.74	97.80
Recalculated Total:	97.0	98.7	99.1	99.1	98.2	99.8
Log(Mg/Mn)	0.88	1.12	1.26	1.33	0.83	1.01
	Usp	*Ilm*	*Usp*	*Ilm*	*Usp*	*Ilm*
Mol %	0.24	0.68	0.29	0.66	0.32	0.80
Geothermobarometer:	*Temp (°C)*	*log10 fO2*	*Temp (°C)*	*log10 fO2*	*Temp (°C)*	*log10 fO2*
A & L (1985)	890.82	-10.79	926.52	-10.32	892.11	-11.37
G & E (2008)	893		965		917	
NNO +	1.18		1.14		0.66	
TiO2 activity	0.70		0.67		0.65	

Table 4.2 continued

Sample	AP-07-45		AP-00-69		AP-00-69	
analysis	3 / 14 .	3 / 16 .	3 / 1 .	3 / 3 .	3 / 2 .	3 / 6 .
Wt% Oxides	Magnetite	Ilmenite	Magnetite	Ilmenite	Magnetite	Ilmenite
SiO2	0.12	0.24	0.12	0.26	0.13	0.00
TiO2	11.17	39.68	12.34	33.98	10.47	44.44
Al2O3	1.21	0.25	1.83	0.65	1.83	0.13
FeO(T)	77.38	51.03	73.25	54.05	74.48	48.11
MnO	0.17	0.56	0.28	0.39	0.26	0.34
MgO	0.69	2.25	1.45	3.05	0.87	2.69
CaO	0.03	0.04	0.02	0.02	0.03	0.06
Na2O	0.00	0.01	0.00	0.02	0.01	0.00
Cr2O3	0.07	0.03	0.08	0.06	0.12	0.03
V2O3	0.56	0.35	0.75	0.55	0.65	0.30
Sum:	91.49	94.43	90.11	93.03	88.95	96.11
Recalculated Total:	95.7	96.6	93.97	96.26	93.07	97.59
Log(Mg/Mn)	0.86	0.85	0.95	1.14	0.77	1.15
	Usp	*Ilm*	*Usp*	*Ilm*	*Usp*	*Ilm*
Mol %	0.35	0.77	0.39	0.66	0.34	0.85
Geothermobarometer:	*Temp (°C)*	*log10 fO2*	*Temp (°C)*	*log10 fO2*	Temp (°C)	log10 fO2
A & L (1985)	920.37	-10.84	1009.18	-9.33	871.04	-12.03
G & E (2008)	958		1108		881	
NNO +	0.68		0.95		0.3	
TiO2 activity	0.64		0.58		0.50	

Sample	AP-00-69		AP-00-69		AP-00-69	
analysis	4 / 4 .	4 / 3 .	8 / 4 .	8 / 2 .	9 / 1 .	9 / 3 .
Wt% Oxides	Magnetite	Ilmenite	Magnetite	Ilmenite	Magnetite	Ilmenite
SiO2	0.26	0.01	0.04	0.02	0.08	0.02
TiO2	12.80	44.44	10.29	44.41	11.00	44.69
Al2O3	1.87	0.14	5.42	0.29	2.30	0.13
FeO(T)	71.57	48.20	71.18	44.48	75.16	48.13
MnO	0.34	0.33	0.39	0.46	0.34	0.40
MgO	1.50	2.95	4.18	6.29	1.86	3.16
CaO	0.07	0.02	0.02	0.05	0.05	0.02
Na2O	0.10	0.01	-0.01	-0.01	0.01	0.00
Cr2O3	0.10	0.03	0.21	0.04	0.20	0.03
V2O3	0.54	0.24	0.75	0.37	0.84	0.28
Sum:	89.16	96.40	92.53	96.45	91.85	96.85
Recalculated Total:	92.83	97.94	96.68	98.25	96.06	98.41
Log(Mg/Mn)	0.89	1.19	1.28	1.39	0.99	1.15
	Usp	*Ilm*	*Usp*	*Ilm*	*Usp*	*Ilm*
Mol %	0.41	0.84	0.33	0.81	0.34	0.84
Geothermobarometer:	Temp (°C)	log10 fO2	Temp (°C)	log10 fO2	Temp (°C)	log10 fO2
A & L (1985)	916.60	-11.37	891.70	-11.39	876.06	-11.89
G & E (2008)	948		941.5		894	
NNO +	0.3		0.78		0.45	
TiO2 activity	0.62		0.63		0.64	

Table 4.2 continued

Sample	AP-00-65		AP-00-65		AP-00-65	
analysis	4 / 10 .	4 / 13 .	4 / 12 .	4 / 15 .	4 / 16 .	4 / 21 .
Wt% Oxides	Magnetite	Ilmenite	Magnetite	Ilmenite	Magnetite	Ilmenite
SiO2	0.06	0.00	0.05	0.02	0.06	0.01
TiO2	12.63	42.97	11.49	43.19	11.21	44.57
Al2O3	1.30	0.05	1.35	0.06	2.61	0.13
FeO(T)	76.79	51.46	77.89	50.93	77.11	48.48
MnO	0.37	0.42	0.36	0.42	0.29	0.39
MgO	1.72	2.85	1.58	2.88	2.47	4.19
CaO	0.02	0.02	0.01	0.01	0.03	0.01
Na2O	0.02	0.00	0.00	0.00	0.01	0.00
Cr2O3	0.22	0.05	0.21	0.04	0.11	0.03
V2O3	0.67	0.45	0.79	0.52	0.66	0.31
Sum:	93.91	98.31	93.76	98.07	94.64	98.15
Recalculated Total:	98.1	100.4	98.1	100.0	99.0	100.0
Log(Mg/Mn)	0.92	1.07	0.89	1.08	1.18	1.28
	Usp	*Ilm*	*Usp*	*Ilm*	*Usp*	*Ilm*
Mol %	0.37	0.80	0.34	0.80	0.33	0.82
Geothermobarometer:	*Temp (°C)*	*log10 fO2*	*Temp (°C)*	*log10 fO2*	*Temp (°C)*	*log10 fO2*
A & L (1985)	923.05	-10.94	899.94	-11.27	888.28	-11.51
G & E (2008)	963		929		917	
NNO +	0.63		0.64		0.62	
TiO2 activity	0.65		0.65		0.64	

Sample	AP-00-65		AP-07-26		AP-07-26	
analysis	4 / 26 .	4 / 25 .	2 / 1 .	2 / 2 .	2 / 11 .	2 / 14 .
Wt% Oxides	Magnetite	Ilmenite	Magnetite	Ilmenite	Magnetite	Ilmenite
SiO2	0.05	0.01	0.08	0.08	0.10	0.03
TiO2	11.72	40.26	12.25	42.98	13.24	38.84
Al2O3	1.54	0.13	1.68	0.09	1.72	0.22
FeO(T)	78.11	53.28	78.91	50.12	74.96	54.21
MnO	0.37	0.34	0.40	0.50	0.42	0.34
MgO	1.86	2.60	1.85	3.25	1.75	2.39
CaO	0.01	0.01	0.02	0.05	0.01	0.03
Na2O	0.02	0.00	0.02	0.01	0.00	0.01
Cr2O3	0.25	0.04	0.07	0.04	0.07	0.05
V2O3	0.70	0.40	0.57	0.43	0.61	0.44
Sum:	94.64	97.07	96.02	97.57	92.88	96.60
Recalculated Total:	99.0	99.5	100.4	99.5	96.8	99.3
Log(Mg/Mn)	0.95	1.12	0.91	1.06	0.87	1.09
	Usp	*Ilm*	*Usp*	*Ilm*	*Usp*	*Ilm*
Mol %	0.34	0.75	0.35	0.80	0.40	0.73
Geothermobarometer:	*Temp (°C)*	*log10 fO2*	*Temp (°C)*	*log10 fO2*	*Temp (°C)*	*log10 fO2*
A & L (1985)	926.10	-10.68	909.66	-11.13	976.05	-9.99
G & E (2008)	970		947		1038	
NNO +	0.87		0.63		0.84	
TiO2 activity	0.69		0.64		0.67	

Table 4.2 continued

Sample	AP-00-69		AP-00-69		AP2-00-60	
analysis	9 / 5 .	9 / 4 .	9 / 5 .		9 / 3 .	9 / 1 .
Wt% Oxides	**Magnetite**	**Ilmenite**	**Magnetite**	**Ilmenite**	**Magnetite**	**Ilmenite**
SiO2	0.06	0.04	0.06	0.04	0.07	0.03
TiO2	7.93	44.71	7.93	41.04	10.99	44.25
Al2O3	1.67	0.16	1.67	0.31	1.40	0.10
FeO(T)	80.68	48.44	80.68	51.66	76.96	48.51
MnO	0.47	0.43	0.47	0.43	0.51	0.69
MgO	0.99	3.14	0.99	2.93	1.08	2.07
CaO	0.02	0.02	0.02	0.02	0.02	0.08
Na2O	0.00	0.00	0.00	0.00	0.01	0.03
Cr2O3	0.07	0.02	0.07	0.02	0.03	0.01
V2O3	0.39	0.32	0.39	0.33	0.34	0.17
Sum:	91.35	97.34	92.31	96.84	91.45	95.99
Recalculated Total:	97.30	98.93	96.06	99.11	95.79	97.45
Log(Mg/Mn)	0.57	1.11	0.57	1.08	0.58	0.72
	Usp	***Ilm***	***Usp***	***Ilm***	***Usp***	***Ilm***
Mol %	0.24	0.84	0.34	0.77	0.33	0.85
Geothermobarometer:	**Temp (°C)**	**log10 fO2**	**Temp (°C)**	**log10 fO2**	**Temp (°C)**	**log10 fO2**
A & L (1985)	826.88	-12.52	918.71	-10.85	864.63	-12.15
G & E (2008)	804		859		873	
NNO +	0.58		0.96		0.33	
TiO2 activity	0.63		0.68		0.62	

Sample	AP2-00-60		AP2-00-60		AP-07-19	
analysis	9 / 4 .	9 / 2 .	11 / 1 .	10 / 1 .	29 / 2 .	29 / 1 .
Wt% Oxides	**Magnetite**	**Ilmenite**	**Magnetite**	**Ilmenite**	**Magnetite**	**Ilmenite**
SiO2	0.11	0.03	0.17	0.10	0.01	0.05
TiO2	8.94	44.72	7.76	45.54	5.19	33.78
Al2O3	1.60	0.09	1.97	0.09	2.30	0.36
FeO(T)	79.15	48.13	79.42	47.78	78.87	54.18
MnO	0.44	0.70	0.34	0.77	0.47	0.58
MgO	1.05	2.09	0.65	1.74	4.48	5.26
CaO	0.04	0.07	0.07	0.05	0.08	0.24
Na2O	0.01	0.01	0.01	0.01	0.00	0.01
Cr2O3	0.07	0.02	0.04	0.01	0.22	0.04
V2O3	0.42	0.21	0.35	0.11	0.59	0.15
Sum:	91.85	96.09	90.79	96.25	92.21	94.67
Recalculated Total:	96.58	97.43	95.61	97.44	97.86	98.46
Log(Mg/Mn)	0.62	0.72	0.53	0.60	1.22	1.20
	Usp	***Ilm***	***Usp***	***Ilm***	***Usp***	***Ilm***
Mol %	0.27	0.86	0.25	0.88	0.13	0.59
Geothermobarometer:	**Temp (°C)**	**log10 fO2**	**Temp (°C)**	**log10 fO2**	**Temp (°C)**	**log10 fO2**
A & L (1985)	827.08	-12.77	797.14	-13.51	841.75	-11.06
G & E (2008)	809		764		830	
NNO +	0.4		0.29		1.79	
TiO2 activity	0.64		0.63		0.70	

Table 4.2 continued

Sample	AP-00-17		AP-00-17		AP-00-17	
analysis	33 / 2 .	33 / 1 .	35 / 2 .	35 / 1 .	38 / 3 .	38 / 2 .
Wt% Oxides	**Magnetite**	**Ilmenite**	**Magnetite**	**Ilmenite**	**Magnetite**	**Ilmenite**
SiO2	0.20	0.02	0.05	0.01	0.13	0.06
TiO2	8.82	43.35	10.75	44.44	6.27	38.24
Al2O3	1.23	0.11	1.36	0.08	0.76	0.11
FeO(T)	78.24	49.60	77.12	45.82	80.69	50.73
MnO	0.39	0.60	0.58	1.13	0.34	0.88
MgO	0.97	2.41	1.09	2.69	0.98	2.12
CaO	0.16	0.04	0.03	0.03	0.05	0.02
Na2O	0.02	0.02	0.00	0.00	0.01	0.02
Cr2O3	0.04	0.01	0.05	0.01	0.05	0.01
V2O3	0.52	0.26	0.46	0.32	0.49	0.32
Sum:	90.59	96.43	91.53	94.54	89.86	92.54
Recalculated Total:	95.27	98.16	95.91	95.86	95.08	94.88
Log(Mg/Mn)	0.64	0.85	0.52	0.62	0.71	0.63
	Usp	***Ilm***	***Usp***	***Ilm***	***Usp***	***Ilm***
Mol %	0.27	0.82	0.33	0.86	0.19	0.75
Geothermobarometer:	**Temp (°C)**	**log10 fO2**	**Temp (°C)**	**log10 fO2**	**Temp (°C)**	**log10 fO2**
A & L (1985)	850.63	-12.06	850.39	-12.48	837.69	-11.73
G & E (2008)	843		853		793	
NNO +	0.63		0.16		1.16	
TiO2 activity	0.65		0.57		0.73	

Table 4.3: Pyroxene compositions from AVC lavas. Data collected with the electron microprobe at Oregon State University. Temperature, pressures, and equilibrium test values calculated using formulation of Putirka (2008). Two pressure estimates, from different equations in Putirka (2008), along with their average, are provided. The numbers reported in the text correspond to this average. The equilibrium test is based on the Fe-Mg exchange between orthopyroxene and clinopyroxene, and should be between 0.95 and 1.23 for pairs in equilibrium (see Putirka, 2008). All pairs presented here pass this equilibrium test.
Pyroxene components: En = Enstatie; Wo = Wollastonite; Fs = Ferrosilite.

sample	**AP-00-04**		**AP-00-04**		**AP-00-04**	
analysis	18 / 2 .	18 / 8 .	21 / 3 .	21 / 5 .	21 / 10 .	21 / 9 .
	opx	**cpx**	**opx**	**cpx**	**opx**	**cpx**
SiO2	54.26	52.50	55.50	51.69	55.19	51.32
TiO2	0.22	0.40	0.16	0.50	0.13	0.54
Al2O3	1.73	2.64	1.58	3.32	0.85	3.49
FeO	15.84	9.36	15.59	9.37	15.36	9.47
MnO	0.57	0.20	0.47	0.30	0.59	0.28
MgO	26.58	15.89	27.04	15.40	27.24	15.73
CaO	1.35	18.43	1.26	18.69	1.38	18.48
Na2O	0.01	0.36	0.00	0.37	0.03	0.33
K2O	0.01	0.01	0.00	0.00	0.01	0.00
Cr2O3	0.00	0.00	0.00	0.00	0.01	0.01
NiO	0.00	0.00	0.00	0.03	0.02	0.02
Total	100.57	99.78	101.60	99.66	100.80	99.67
En	72.94	46.20	73.70	45.18	73.92	45.82
Wo	2.66	38.52	2.46	39.40	2.70	38.70
Fs	24.40	15.28	23.84	15.42	23.38	15.48
Temp	1010		1014		1023	
Press (eq 38)	6.7		6.4		6.9	
Press (eq 39)	4.4		4.3		3.4	
avg Press	5.5		5.3		5.1	
Equilirium test	0.99		1.06		1.07	

Table 4.3 continued

sample	AP-00-30		AP-00-30		AP-00-30	
analysis	8 / 7 .	8 / 3 .	8 / 6 .	8 / 2 .	9 / 6 .	9 / 2 .
	opx	cpx	opx	cpx	opx	cpx
SiO2	54.34	52.83	55.42	50.97	54.23	52.23
TiO2	0.40	0.50	0.19	0.77	0.35	0.63
Al2O3	1.93	1.93	0.93	4.07	1.88	2.47
FeO	15.89	10.05	15.95	9.78	16.49	10.01
MnO	0.25	0.28	0.30	0.21	0.25	0.23
MgO	26.50	16.41	27.10	15.34	26.65	16.68
CaO	1.97	18.23	1.43	18.74	1.64	17.88
Na2O	0.03	0.36	0.03	0.38	0.06	0.35
K2O	0.02	0.00	0.01	0.00	0.00	0.02
Cr2O3	0.00	0.00	0.01	0.11	0.00	0.04
NiO	0.00	0.09	0.00	0.00	0.06	0.00
Total	101.32	100.68	101.37	100.37	101.61	100.53
En	71.96	46.67	73.10	44.74	71.87	47.47
Wo	3.84	16.05	2.77	16.00	3.18	15.98
Fs	24.21	37.28	24.13	39.27	24.94	36.56
Temp	1066		1053		1088	
Press (eq 38)	4.2		6.2		6.8	
Press (eq 39)	4.7		4.2		5.6	
avg Press	4.4		5.2		6.2	
Equilirium test	1.02		1.08		0.97	

sample	AP-00-30		AP-00-30		AP-00-30	
analysis	10 / 2 .	9 / 2 .	11 / 5 .	11 / 3 .	11 / 6 .	11 / 3 .
	opx	cpx	opx	cpx	opx	cpx
SiO2	54.37	52.23	54.23	51.16	53.57	51.16
TiO2	0.40	0.63	0.43	0.70	0.45	0.70
Al2O3	1.80	2.47	2.06	2.55	2.64	2.55
FeO	15.99	10.01	15.95	10.69	16.19	10.69
MnO	0.28	0.23	0.26	0.24	0.22	0.24
MgO	26.55	16.68	26.40	16.49	26.17	16.49
CaO	1.91	17.88	1.64	17.57	1.67	17.57
Na2O	0.02	0.35	0.05	0.37	0.06	0.37
K2O	0.00	0.02	0.00	0.00	0.00	0.00
Cr2O3	0.02	0.04	0.03	0.04	0.01	0.04
NiO	0.02	0.00	0.12	0.00	0.04	0.00
Total	101.35	100.53	101.19	99.81	101.02	99.81
En	71.96	47.47	72.27	46.96	71.78	46.96
Wo	3.72	15.98	3.24	17.08	3.30	17.08
Fs	24.31	36.56	24.49	35.96	24.92	35.96
Temp	1072		1093		1101	
Press (eq 38)	4.4		5.6		6.0	
Press (eq 39)	4.0		4.2		5.1	
avg Press	4.2		4.9		5.5	
Equilirium test	1.00		1.07		1.05	

Table 4.3 continued

sample	AP2-00-77		AP2-00-77		AP2-00-77	
analysis	35 / 2 .	35 / 4 .	35 / 6 .	37 / 1 .	38 / 4 .	38 / 5 .
	opx	cpx	opx	cpx	opx	cpx
SiO2	55.09	52.89	55.42	53.00	54.51	51.81
TiO2	0.24	0.40	0.28	0.51	0.26	0.60
Al2O3	2.12	2.16	2.16	3.23	2.08	3.26
FeO	12.32	7.80	12.40	7.67	12.15	7.69
MnO	0.17	0.11	0.11	0.12	0.16	0.10
MgO	29.79	17.79	29.76	16.67	30.00	16.75
CaO	1.35	18.56	1.32	17.76	1.22	18.72
Na2O	0.02	0.28	0.03	0.33	0.00	0.37
K2O	0.00	0.00	0.01	0.02	0.02	0.00
Cr2O3	0.34	0.30	0.30	0.31	0.27	0.50
NiO	0.04	0.00	0.02	0.00	0.00	0.05
Total	101.49	100.28	101.83	99.60	100.67	99.86
En	79.07	50.11	79.01	49.42	79.59	48.52
Wo	2.58	12.32	2.52	12.75	2.33	12.50
Fs	18.35	37.57	18.47	37.83	18.08	38.98
Temp	1095		1092		1083	
Press (eq 38)	5.3		6.0		4.9	
Press (eq 39)	5.2		4.7		4.9	
avg Press	5.3		5.3		4.9	
Equilirium test	1.06		1.10		1.13	

sample	AP2-00-77		AP2-00-77		AP2-00-77	
analysis	38 / 3 .	38 / 6 .	38 / 2 .	38 / 7 .	38 / 1 .	38 / 8 .
	opx	cpx	opx	cpx	opx	cpx
SiO2	54.76	51.39	55.60	52.41	54.26	52.34
TiO2	0.29	0.82	0.23	0.56	0.34	0.67
Al2O3	2.68	4.58	2.18	3.03	2.52	3.49
FeO	13.55	9.35	12.23	7.31	13.70	8.52
MnO	0.21	0.08	0.18	0.14	0.24	0.14
MgO	28.98	15.67	29.87	16.64	28.02	16.92
CaO	1.35	18.58	1.23	19.10	1.93	18.22
Na2O	0.04	0.42	0.03	0.41	0.03	0.34
K2O	0.01	0.00	0.01	0.00	0.01	0.00
Cr2O3	0.14	0.09	0.35	0.50	0.11	0.31
NiO	0.08	0.02	0.00	0.03	0.01	0.06
Total	102.10	101.01	101.92	100.14	101.18	101.00
En	77.16	45.73	79.41	48.28	75.54	48.63
Wo	2.59	15.30	2.35	11.90	3.74	13.73
Fs	20.25	38.97	18.24	39.83	20.72	37.63
Temp	1073		1070		1094	
Press (eq 38)	6.0		5.3		4.3	
Press (eq 39)	4.6		5.4		4.7	
avg Press	5.3		5.3		4.5	
Equilirium test	1.28		1.07		1.03	

Table 4.3 continued

sample	AP-00-04		AP-00-04		AP-07-08	
analysis	21 / 11 .	21 / 8 .	22 / 3 .	22 / 5 .	3 / 2 .	3 / 1 .
	opx	cpx	opx	cpx	opx	cpx
SiO2	54.58	51.69	53.96	52.53	54.90	51.97
TiO2	0.23	0.58	0.17	0.36	0.20	0.60
Al2O3	2.27	3.81	1.81	2.56	2.66	4.05
FeO	15.49	9.79	16.18	9.29	13.48	8.29
MnO	0.37	0.30	0.45	0.32	0.26	0.18
MgO	26.82	15.19	26.45	15.91	28.31	15.68
CaO	1.44	18.64	1.26	18.67	1.23	18.82
Na2O	0.03	0.35	0.04	0.35	0.02	0.44
K2O	0.00	0.02	0.02	0.01	0.00	0.00
Cr2O3	0.01	0.00	0.01	0.01	0.22	0.36
NiO	0.00	0.04	0.01	0.00	0.12	0.08
Total	101.24	100.40	100.36	100.02	101.40	100.47
En	73.40	44.57	72.60	46.07	**77.02**	46.31
Wo	2.83	39.32	2.49	38.85	**2.41**	39.96
Fs	23.77	16.12	24.92	15.08	**20.57**	13.73
Temp	1038		1030		1054	
Press (eq 38)	6.4		8.3		6.2	
Press (eq 39)	5.0		5.8		5.3	
avg Press	5.7		7.0		5.8	
Equilirium test	1.12		0.95		1.11	

sample	AP-07-08		AP-07-08		AP-07-08	
analysis	3 / 6 .	3 / 4 .	5 / 1 .	5 / 4 .	6 / 3 .	6 / 1 .
	opx	cpx	opx	cpx	opx	cpx
SiO2	55.54	50.69	55.24	52.47	55.82	52.61
TiO2	0.17	0.73	0.22	0.58	0.16	0.46
Al2O3	1.29	4.77	2.32	4.00	1.62	3.33
FeO	14.30	9.07	13.07	8.16	12.77	8.21
MnO	0.20	0.09	0.32	0.13	0.20	0.17
MgO	28.58	15.51	28.58	15.71	29.20	16.35
CaO	1.26	18.19	1.29	18.83	1.17	18.49
Na2O	0.02	0.55	0.01	0.44	0.04	0.40
K2O	0.03	0.01	0.00	0.00	0.00	0.00
Cr2O3	0.06	0.26	0.20	0.44	0.12	0.18
NiO	0.00	0.02	0.05	0.07	0.06	0.00
Total	101.46	99.87	101.32	100.84	101.14	100.20
En	76.19	46.07	77.57	46.44	78.49	47.75
Wo	2.42	38.82	2.52	40.02	2.26	38.81
Fs	21.39	15.11	19.91	13.54	19.25	13.44
Temp	1072		1045		1069	
Press (eq 38)	6.3		5.5		6.5	
Press (eq 39)	4.5		4.5		5.2	
avg Press	5.4		5.0		5.9	
Equilirium test	1.17		1.14		1.15	

Table 4.3 continued

sample	AP-00-30		AP-00-30		AP2-00-59	
analysis	12 / 7 .	12 / 5 .	12 / 8 .	12 / 3 .	14 / 4 .	14 / 2 .
	opx	cpx	opx	cpx	opx	cpx
SiO2	54.26	50.97	54.51	50.04	55.24	52.26
TiO2	0.35	0.75	0.36	0.93	0.29	0.45
Al2O3	1.49	3.52	1.79	4.82	2.34	2.82
FeO	16.04	10.45	15.39	10.05	12.71	7.15
MnO	0.33	0.29	0.19	0.17	0.16	0.13
MgO	27.18	15.66	27.49	15.38	29.53	16.68
CaO	1.54	18.13	1.64	18.68	1.51	19.40
Na2O	0.03	0.45	0.03	0.38	0.01	0.30
K2O	0.02	0.01	0.00	0.01	0.00	0.01
Cr2O3	0.01	0.10	0.02	0.08	0.27	0.29
NiO	0.05	0.02	0.00	0.01	0.03	0.00
Total	101.32	100.34	101.42	100.55	102.09	99.49
En	72.90	45.33	73.69	44.66	78.24	48.16
Wo	2.96	16.96	3.17	16.37	2.87	11.59
Fs	24.13	37.71	23.14	38.98	18.90	40.25
Temp	1061		1076		1057	
Press (eq 38)	5.7		4.5		3.6	
Press (eq 39)	3.9		3.2		5.0	
avg Press	4.8		3.8		4.3	
Equilirium test	1.13		1.17		1.00	

sample	AP2-00-59		AP2-00-59		AP2-00-59	
analysis	14 / 6 .	15 / 2 .	14 / 7 .	16 / 1 .	18 / 5 .	18 / 2 .
	opx	cpx	opx	cpx	opx	cpx
SiO2	54.48	51.30	54.75	53.35	54.75	53.67
TiO2	0.28	0.61	0.26	0.39	0.25	0.39
Al2O3	2.30	3.44	2.18	2.10	2.08	2.19
FeO	12.76	8.21	12.08	7.64	13.37	8.43
MnO	0.18	0.14	0.24	0.15	0.27	0.20
MgO	29.18	16.58	29.08	17.32	28.86	18.17
CaO	1.56	19.15	2.04	19.17	1.25	17.91
Na2O	0.06	0.37	0.03	0.30	0.04	0.39
K2O	0.03	0.00	0.00	0.00	0.00	0.02
Cr2O3	0.21	0.36	0.16	0.18	0.12	0.29
NiO	0.00	0.05	0.14	0.02	0.04	0.00
Total	101.02	100.20	100.98	100.60	101.04	101.65
En	77.90	47.45	77.91	48.95	77.45	50.79
Wo	2.99	13.18	3.93	12.12	2.42	13.22
Fs	19.11	39.38	18.16	38.94	20.13	35.99
Temp	1095		1078		1100	
Press (eq 38)	4.8		3.7		7.1	
Press (eq 39)	5.1		4.9		5.5	
avg Press	4.9		4.3		6.3	
Equilirium test	1.13		1.06		1.00	

Table 4.3 continued

sample	AP2-00-77		AP2-00-73		AP2-00-73	
analysis	39 / 3 .	39 / 1 .	40 / 6 .	40 / 2 .	40 / 8 .	40 / 5 .
	opx	cpx	opx	cpx	opx	cpx
SiO2	55.69	52.82	54.65	52.07	54.46	52.18
TiO2	0.26	0.61	0.21	0.67	0.30	0.63
Al2O3	2.27	3.21	1.72	3.63	2.19	3.22
FeO	12.17	7.71	14.22	8.56	14.02	8.73
MnO	0.21	0.22	0.31	0.14	0.25	0.13
MgO	29.77	16.78	28.53	16.11	28.54	16.09
CaO	1.35	18.72	1.48	19.36	1.36	19.42
Na2O	0.03	0.45	0.03	0.37	0.05	0.34
K2O	0.00	0.01	0.02	0.00	0.02	0.00
Cr2O3	0.35	0.53	0.08	0.17	0.10	0.16
NiO	0.03	0.00	0.00	0.04	0.01	0.03
Total	102.13	101.06	101.24	101.14	101.32	100.93
En	79.25	48.55	75.94	46.25	76.34	46.05
Wo	2.58	12.52	2.83	13.80	2.62	14.02
Fs	18.17	38.93	21.24	39.95	21.04	39.94
Temp	1081		1046		1054	
Press (eq 38)	5.3		5.1		5.2	
Press (eq 39)	5.6		4.5		4.8	
avg Press	5.4		4.8		5.0	
Equilirium test	1.12		1.07		1.10	

sample	AP2-00-73		AP2-00-73		AP2-00-73	
analysis	42 / 4 .	42 / 3 .	42 / 5 .	42 / 6 .	43 / 2 .	43 / 4 .
	opx	cpx	opx	cpx	opx	cpx
SiO2	54.55	52.36	55.07	51.96	54.26	51.05
TiO2	0.26	0.56	0.23	0.74	0.27	0.78
Al2O3	1.96	2.82	2.05	3.61	2.38	4.17
FeO	14.64	8.63	14.56	8.98	15.55	10.18
MnO	0.15	0.09	0.24	0.17	0.29	0.17
MgO	28.60	16.54	28.52	15.93	27.32	15.74
CaO	1.23	19.43	1.22	19.34	1.50	18.38
Na2O	0.02	0.32	0.05	0.37	0.02	0.36
K2O	0.01	0.00	0.01	0.00	0.00	0.01
Cr2O3	0.04	0.07	0.01	0.07	0.08	0.12
NiO	0.10	0.05	0.00	0.02	0.00	0.02
Total	101.56	100.86	101.95	101.18	101.68	100.98
En	75.87	46.80	75.93	45.69	73.60	45.40
Wo	2.34	13.70	2.33	14.45	2.90	16.48
Fs	21.79	39.51	21.74	39.86	23.50	38.12
Temp	1057		1056		1072	
Press (eq 38)	5.5		6.5		6.3	
Press (eq 39)	5.2		5.1		4.5	
avg Press	5.4		5.8		5.4	
Equilirium test	1.02		1.10		1.14	

Table 4.3 continued

sample	AP-07-08		AP-07-08		AP-00-11	
analysis	7 / 1 .	7 / 5 .	13 / 2 .	13 / 1 .	34 / 3 .	34 / 4 .
	opx	cpx	opx	cpx	opx	cpx
SiO2	54.22	51.80	54.87	51.35	54.74	51.05
TiO2	0.21	0.64	0.21	0.65	0.19	0.47
Al2O3	2.25	4.31	2.33	4.39	1.05	2.98
FeO	14.32	8.64	13.01	8.41	15.50	9.75
MnO	0.32	0.12	0.29	0.18	0.48	0.34
MgO	27.75	15.99	29.00	15.39	27.09	15.80
CaO	1.19	18.32	1.22	18.89	1.49	18.64
Na2O	0.03	0.47	0.03	0.45	0.05	0.35
K2O	0.01	0.02	0.01	0.03	0.00	0.03
Cr2O3	0.09	0.37	0.18	0.25	0.01	0.00
NiO	0.05	0.04	0.15	0.04	0.02	0.00
Total	100.45	100.72	101.30	100.03	100.63	99.42
En	75.73	47.02	78.01	45.69	65.66	45.58
Wo	2.34	38.72	2.36	40.31	1.47	38.65
Fs	21.93	14.26	19.63	14.01	32.87	15.77
Temp	1067		1048		1040	
Press (eq 38)	7.4		5.9		6.4	
Press (eq 39)	5.0		4.6		3.9	
avg Press	6.2		5.3		5.1	
Equilirium test	1.05		1.22		1.08	

sample	AP-00-11		AP-00-11		AP-00-11	
analysis	36 / 2 .	36 / 5 .	37 / 3 .	37 / 4 .	38 / 4 .	38 / 2 .
	opx	cpx	opx	cpx	opx	cpx
SiO2	54.66	52.55	55.94	53.25	53.99	53.11
TiO2	0.27	0.45	0.17	0.41	0.28	0.43
Al2O3	1.58	2.12	0.80	2.02	1.69	1.94
FeO	16.20	9.91	15.27	10.03	16.32	10.14
MnO	0.52	0.38	0.48	0.34	0.62	0.40
MgO	26.46	15.96	27.67	16.04	26.31	16.21
CaO	1.62	18.80	1.56	18.74	1.65	18.23
Na2O	0.08	0.36	0.03	0.45	0.04	0.34
K2O	0.02	0.02	0.03	0.00	0.01	0.00
Cr2O3	0.01	0.00	0.01	0.01	0.00	0.00
NiO	0.00	0.00	0.00	0.04	0.05	0.00
Total	101.42	100.55	101.95	101.33	100.97	100.81
En	72.07	45.56	74.08	45.66	71.79	46.32
Wo	3.18	38.57	2.99	38.33	3.23	37.43
Fs	24.75	15.87	22.93	16.01	24.98	16.25
Temp	1036		1025		1023	
Press (eq 38)	6.9		5.6		6.7	
Press (eq 39)	5.0		4.8		4.6	
avg Press	6.0		5.2		5.6	
Equilirium test	1.01		1.13		1.01	

Table 4.3 continued

sample	AP2-00-59		AP2-00-59		AP2-00-59	
analysis	20 / 6 .	20 / 2 .	20 / 8 .	20 / 5 .	21 / 3 .	21 / 1 .
	opx	cpx	opx	cpx	opx	cpx
SiO2	54.15	51.59	54.31	51.99	55.95	53.72
TiO2	0.31	0.61	0.28	0.60	0.15	0.36
Al2O3	3.16	3.33	2.68	3.10	1.03	1.89
FeO	12.66	8.42	12.91	8.68	11.74	8.10
MnO	0.26	0.13	0.21	0.17	0.31	0.19
MgO	27.87	16.92	28.35	17.40	29.98	17.83
CaO	1.93	17.92	2.02	17.70	1.40	17.99
Na2O	0.04	0.36	0.03	0.35	0.02	0.25
K2O	0.03	0.00	0.01	0.02	0.01	0.00
Cr2O3	0.21	0.42	0.24	0.20	0.11	0.14
NiO	0.09	0.12	0.07	0.00	0.00	0.06
Total	100.69	99.82	101.10	100.20	100.69	100.54
En	76.65	49.02	76.53	49.73	79.79	50.50
Wo	3.81	13.67	3.92	13.92	2.68	12.87
Fs	19.54	37.31	19.55	36.36	17.53	36.63
Temp	1110		1115		1077	
Press (eq 38)	4.7		4.8		5.6	
Press (eq 39)	5.3		4.9		5.0	
avg Press	5.0		4.8		5.3	
Equilirium test	1.09		1.10		1.16	

sample	AP2-00-77		AP2-00-77		AP2-00-77	
analysis	25 / 3 .	25 / 1 .	25 / 4 .	26 / 1 .	25 / 5 .	27 / 2 .
	opx	cpx	opx	cpx	opx	cpx
SiO2	54.00	51.75	55.17	52.12	55.31	51.13
TiO2	0.20	0.61	0.24	0.64	0.27	0.61
Al2O3	1.56	3.53	2.14	3.40	2.13	3.46
FeO	11.77	7.63	11.98	8.04	12.59	7.75
MnO	0.28	0.16	0.20	0.16	0.22	0.21
MgO	29.85	16.71	29.47	16.77	29.55	16.76
CaO	1.38	18.51	1.32	18.27	1.38	18.39
Na2O	0.03	0.38	0.03	0.38	0.03	0.36
K2O	0.00	0.00	0.02	0.01	0.01	0.00
Cr2O3	0.19	0.54	0.39	0.50	0.27	0.49
NiO	0.08	0.07	0.04	0.01	0.00	0.00
Total	99.33	99.88	100.99	100.29	101.76	99.15
En	79.72	48.74	79.35	48.74	78.59	48.82
Wo	2.64	12.48	2.55	13.10	2.64	12.67
Fs	17.64	38.78	18.10	38.16	18.78	38.51
Temp	1083		1097		1093	
Press (eq 38)	5.2		5.7		5.1	
Press (eq 39)	5.1		5.1		4.8	
avg Press	5.1		5.4		5.0	
Equilirium test	1.16		1.18		1.09	

Table 4.3 continued

sample	AP2-00-73		AP2-00-73		AP2-00-73	
analysis	43 / 1 .	43 / 5 .	47 / 1 .	47 / 2 .	47 / 5 .	47 / 2 .
	opx	cpx	opx	cpx	opx	cpx
SiO2	54.23	51.57	55.22	51.36	54.11	51.36
TiO2	0.31	0.73	0.29	0.75	0.30	0.75
Al2O3	2.66	4.12	2.67	4.18	3.09	4.18
FeO	15.64	11.00	14.28	9.81	14.37	9.81
MnO	0.24	0.15	0.20	0.12	0.23	0.12
MgO	27.40	15.98	28.38	15.85	28.19	15.85
CaO	1.35	17.82	1.43	18.97	1.47	18.97
Na2O	0.00	0.35	0.02	0.32	0.05	0.32
K2O	0.03	0.00	0.02	0.02	0.00	0.02
Cr2O3	0.07	0.11	0.13	0.18	0.16	0.18
NiO	0.07	0.06	0.06	0.00	0.00	0.00
Total	102.00	101.89	102.71	101.56	101.96	101.56
En	73.77	45.72	75.84	45.30	75.56	45.30
Wo	2.61	17.65	2.75	15.73	2.83	15.73
Fs	23.62	36.64	21.41	38.97	21.60	38.97
Temp	1085		1077		1085	
Press (eq 38)	7.0		5.2		6.2	
Press (eq 39)	4.4		4.4		5.0	
avg Press	5.7		4.8		5.6	
Equilirium test	1.21		1.23		1.21	

sample	AP-00-52		AP-07-26		AP-07-26	
analysis	32 / 1 .	32 / 2 .	16 / 2 .	16 / 1 .	17 / 1 .	17 / 2 .
	opx	cpx	opx	cpx	opx	cpx
SiO2	54.29	51.99	54.32	52.48	54.71	52.19
TiO2	0.23	0.58	0.17	0.38	0.26	0.46
Al2O3	1.45	3.30	2.87	3.75	2.32	2.83
FeO	17.03	10.02	13.38	7.89	14.11	8.41
MnO	0.42	0.14	0.19	0.22	0.24	0.17
MgO	25.59	15.68	28.45	16.44	27.51	16.49
CaO	1.45	18.43	1.23	18.34	1.40	18.82
Na2O	0.03	0.38	0.05	0.63	0.01	0.38
K2O	0.02	0.04	0.02	0.00	0.01	0.00
Cr2O3	0.00	0.01	0.17	0.46	0.15	0.25
NiO	0.00	0.00	0.02	0.00	0.05	0.03
Total	100.51	100.55	100.87	100.58	100.76	100.03
En	70.72	45.39	77.22	48.28	75.52	47.47
Wo	2.87	38.34	2.40	38.72	2.76	38.96
Fs	26.41	16.27	20.38	13.00	21.72	13.58
Temp	1040		1090		1059	
Press (eq 38)	7.5		7.9		4.9	
Press (eq 39)	4.7		7.4		5.2	
avg Press	6.1		7.6		5.1	
Equilirium test	0.96		1.02		0.99	

Table 4.3 continued

sample	AP-00-11		AP-00-11		AP-00-11	
analysis	39 / 3 .	39 / 2 .	40 / 4 .	40 / 2 .	41 / 4 .	41 / 3 .
	opx	cpx	opx	cpx	opx	cpx
SiO2	54.80	52.34	54.54	52.84	55.21	52.09
TiO2	0.24	0.50	0.24	0.43	0.19	0.51
Al2O3	1.53	2.34	1.59	2.07	1.00	2.76
FeO	16.30	10.04	15.17	10.01	15.71	9.84
MnO	0.50	0.31	0.52	0.30	0.50	0.31
MgO	26.85	16.03	27.09	16.71	27.18	15.85
CaO	1.48	18.22	1.89	17.73	1.44	18.68
Na2O	0.02	0.40	0.04	0.31	0.04	0.33
K2O	0.02	0.00	0.01	0.00	0.00	0.00
Cr2O3	0.01	0.01	5.00	0.00	0.00	0.00
NiO	0.00	0.05	0.02	0.01	0.00	0.01
Total	101.75	100.22	101.11	100.40	101.27	100.38
En	72.45	46.13	73.30	47.66	73.40	45.56
Wo	2.88	37.67	3.67	36.34	2.80	38.57
Fs	24.67	16.20	23.03	16.01	23.80	15.87
Temp	1032		1054		1030	
Press (eq 38)	6.7		5.7		6.5	
Press (eq 39)	4.8		4.3		4.1	
avg Press	5.7		5.0		5.3	
Equilirium test	1.03		1.07		1.07	

sample	AP-00-30		AP-00-30		AP-00-30	
analysis	1 / 5 .	1 / 4 .	1 / 6 .	1 / 7 .	2 / 4 .	2 / 5 .
	opx	cpx	opx	cpx	opx	cpx
SiO2	54.29	51.37	54.28	51.58	53.57	51.52
TiO2	0.34	0.80	0.29	0.83	0.34	0.82
Al2O3	2.32	3.12	1.53	3.03	1.96	3.48
FeO	15.53	10.48	15.77	11.12	16.22	11.22
MnO	0.25	0.20	0.34	0.19	0.23	0.20
MgO	26.79	16.13	27.24	15.98	26.56	16.15
CaO	1.58	17.87	1.49	17.77	1.67	17.36
Na2O	0.03	0.33	0.04	0.38	0.04	0.38
K2O	0.00	0.01	0.00	0.00	0.00	0.01
Cr2O3	0.06	0.03	0.02	0.00	0.00	0.01
NiO	0.05	0.07	0.00	0.01	0.02	0.00
Total	101.23	100.41	100.99	100.89	100.59	101.15
En	73.12	46.29	73.32	45.67	72.07	46.24
Wo	3.10	16.86	2.88	17.82	3.25	18.02
Fs	23.77	36.84	23.81	36.51	24.68	35.73
Temp	1081		1072		1097	
Press (eq 38)	5.7		6.7		6.7	
Press (eq 39)	4.6		4.3		5.0	
avg Press	5.2		5.5		5.9	
Equilirium test	1.12		1.20		1.14	

Table 4.3 continued

sample	AP2-00-77		AP2-00-77		AP2-00-77	
analysis	29 / 1 .	29 / 2 .	29 / 1 .	29 / 3 .	29 / 5 .	29 / 4 .
	opx	cpx	opx	cpx	opx	cpx
SiO2	54.61	52.21	54.61	53.26	55.67	53.11
TiO2	0.27	0.42	0.27	0.41	0.19	0.45
Al2O3	2.09	2.24	2.09	2.23	1.18	2.37
FeO	12.38	7.17	12.38	7.33	11.98	7.27
MnO	0.19	0.14	0.19	0.14	0.26	0.12
MgO	29.72	17.07	29.72	17.31	30.32	17.29
CaO	1.34	18.65	1.34	19.18	1.36	19.07
Na2O	0.03	0.29	0.03	0.39	0.04	0.36
K2O	0.00	0.00	0.00	0.00	0.00	0.01
Cr2O3	0.27	0.37	0.27	0.40	0.14	0.33
NiO	0.00	0.01	0.00	0.00	0.05	0.00
Total	100.90	98.57	100.90	100.65	101.19	100.38
En	78.99	49.49	78.99	49.16	79.75	49.30
Wo	2.57	11.66	2.57	11.68	2.58	11.63
Fs	18.45	38.85	18.45	39.16	17.68	39.06
Temp	1074		1069		1067	
Press (eq 38)	4.8		4.7		4.9	
Press (eq 39)	5.5		5.7		5.4	
avg Press	5.2		5.2		5.2	
Equilirium test	1.01		1.02		1.06	

sample	AP2-00-77		AP2-00-77		AP2-00-77	
analysis	30 / 4 .	30 / 3 .	30 / 5 .	30 / 3 .	31 / 3 .	31 / 4 .
	opx	cpx	opx	cpx	opx	cpx
SiO2	54.92	51.63	56.18	51.63	55.39	53.57
TiO2	0.26	0.78	0.25	0.78	0.28	0.45
Al2O3	1.93	3.93	1.96	3.93	2.25	2.25
FeO	12.44	8.71	12.44	8.71	12.96	7.56
MnO	0.23	0.18	0.18	0.18	0.19	0.13
MgO	29.89	16.79	29.85	16.79	29.18	17.33
CaO	1.33	17.95	1.36	17.95	1.33	18.93
Na2O	0.04	0.35	0.05	0.35	0.03	0.28
K2O	0.00	0.03	0.00	0.03	0.00	0.00
Cr2O3	0.26	0.31	0.24	0.31	0.17	0.29
NiO	0.02	0.00	0.05	0.00	0.01	0.00
Total	101.32	100.65	102.57	100.65	101.79	100.80
En	79.03	48.56	78.95	48.56	78.01	49.26
Wo	2.52	14.12	2.59	14.12	2.55	12.06
Fs	18.45	37.32	18.46	37.32	19.44	38.68
Temp	1099		1110		1071	
Press (eq 38)	6.0		6.0		5.1	
Press (eq 39)	4.2		4.7		5.5	
avg Press	5.1		5.4		5.3	
Equilirium test	1.25		1.24		0.98	

Table 4.3 continued

sample	AP-07-26		AP-07-26		AP-07-26	
analysis	18 / 1 .	18 / 4 .	20 / 1 .	20 / 2 .	24 / 1 .	24 / 2 .
	opx	**cpx**	**opx**	**cpx**	**opx**	**cpx**
SiO2	54.74	51.01	55.21	51.77	55.35	51.99
TiO2	0.22	0.55	0.19	0.45	0.18	0.57
Al2O3	2.08	3.27	1.15	2.99	1.40	3.30
FeO	13.74	8.38	13.87	8.31	13.30	8.21
MnO	0.29	0.17	0.27	0.22	0.26	0.20
MgO	28.43	16.05	28.51	16.37	28.92	16.06
CaO	1.28	19.17	1.39	18.86	1.44	19.08
Na2O	0.02	0.34	0.02	0.35	0.01	0.38
K2O	0.00	0.03	0.01	0.02	0.00	0.01
Cr2O3	0.14	0.18	0.06	0.28	0.16	0.29
NiO	0.06	0.07	0.00	0.01	0.01	0.05
Total	101.00	99.22	100.69	99.63	101.02	100.13
En	76.72	46.48	76.45	47.33	77.30	43.57
Wo	2.48	39.91	2.68	39.19	2.76	40.79
Fs	20.80	13.62	20.86	13.48	19.94	15.65
Temp	1046		1057		1048	
Press (eq 38)	5.0		4.8		4.5	
Press (eq 39)	4.3		4.7		4.7	
avg Press	4.7		4.8		4.6	
Equilirium test	1.08		1.04		1.11	

sample	AP-07-51		AP-07-36		AP-07-36	
analysis	9 / 2 .	9 / 4 .	2 / 1 .	2 / 3 .	4 / 6 .	4 / 2 .
	opx	**cpx**	**opx**	**cpx**	**opx**	**cpx**
SiO2	55.80	52.89	54.75	51.66	55.07	53.58
TiO2	0.20	0.47	0.30	0.86	0.23	0.23
Al2O3	2.07	3.39	2.29	3.83	0.73	1.30
FeO	12.91	8.49	12.78	8.70	16.24	10.06
MnO	0.18	0.04	0.30	0.18	0.50	0.23
MgO	29.14	15.54	29.03	16.08	27.06	15.15
CaO	1.16	19.41	1.53	18.93	1.20	19.57
Na2O	0.01	0.52	0.01	0.36	0.04	0.48
K2O	-0.01	0.00	0.02	0.00	0.03	0.02
Cr2O3	0.36	0.10	0.07	0.24	0.00	0.02
NiO	0.02	0.00	0.08	0.08	0.09	0.03
Total	101.85	100.84	101.17	100.92	101.19	100.65
En	78.30	45.38	77.83	46.53	73.07	43.46
Wo	2.24	40.72	2.95	39.35	2.33	40.35
Fs	19.47	13.90	19.22	14.12	24.60	16.19
Temp	1029		1056		986	
Press (eq 38)	5.2		3.9		6.6	
Press (eq 39)	4.6		4.2		5.1	
avg Press	4.9		4.0		5.9	
Equilirium test	1.23		1.23		1.11	

Table 4.3 continued

sample	AP-00-30		AP-00-30		AP-00-30	
analysis	3 / 3 .	3 / 2 .	4 / 1 .	3 / 5 .	5 / 6 .	5 / 3 .
	opx	cpx	opx	cpx	opx	cpx
SiO2	54.69	51.94	54.50	51.70	53.86	51.50
TiO2	0.34	0.71	0.31	0.78	0.32	0.95
Al2O3	1.81	2.86	1.86	2.98	1.65	3.71
FeO	15.63	11.19	16.04	10.77	16.00	11.22
MnO	0.34	0.15	0.25	0.25	0.34	0.16
MgO	26.78	15.66	26.74	16.27	26.98	15.61
CaO	1.61	17.98	1.52	17.71	1.63	18.32
Na2O	0.05	0.47	0.03	0.40	0.05	0.44
K2O	0.00	0.00	0.00	0.00	0.01	0.01
Cr2O3	0.00	0.00	0.01	0.00	0.03	0.01
NiO	0.08	0.00	0.06	0.00	0.09	0.04
Total	101.34	100.97	101.32	100.84	100.95	101.98
En	72.95	44.92	72.59	46.43	72.68	44.51
Wo	3.16	18.00	2.98	17.24	3.16	17.95
Fs	23.89	37.07	24.43	36.33	24.17	37.55
Temp	1064		1081		1070	
Press (eq 38)	5.7		6.4		6.4	
Press (eq 39)	4.5		4.9		4.1	
avg Press	5.1		5.6		5.2	
Equilirium test	1.22		1.10		1.21	

sample	AP-00-30		AP-00-30		AP-00-30	
analysis	6 / 1 .	5 / 3 .	7 / 3 .	7 / 4 .	8 / 4 .	8 / 3 .
	opx	cpx	opx	cpx	opx	cpx
SiO2	53.87	51.50	54.51	52.06	53.15	52.83
TiO2	0.40	0.95	0.31	0.57	0.32	0.50
Al2O3	2.46	3.71	1.36	2.24	2.26	1.93
FeO	16.35	11.22	16.06	11.06	16.41	10.05
MnO	0.38	0.16	0.29	0.18	0.39	0.28
MgO	26.95	15.61	27.25	16.68	26.37	16.41
CaO	1.58	18.32	1.60	17.18	1.40	18.23
Na2O	0.07	0.44	0.03	0.36	0.01	0.36
K2O	0.03	0.01	0.00	0.01	0.02	0.00
Cr2O3	0.03	0.01	0.02	0.02	0.02	0.00
NiO	0.11	0.04	0.07	0.04	0.02	0.09
Total	102.23	101.98	101.50	100.39	100.35	100.68
En	72.32	44.51	72.84	47.34	72.09	46.67
Wo	3.05	17.95	3.08	17.61	2.75	16.05
Fs	24.62	37.55	24.08	35.04	25.16	37.28
Temp	1070		1089		1043	
Press (eq 38)	7.0		6.6		7.0	
Press (eq 39)	4.4		4.7		5.6	
avg Press	5.7		5.6		6.3	
Equilirium test	1.18		1.13		0.98	

Table 4.3 continued

sample	AP2-00-77		AP2-00-77		AP2-00-77	
analysis	31 / 2 .	31 / 5 .	32 / 6 .	32 / 1 .	32 / 9 .	32 / 3 .
	opx	cpx	opx	cpx	opx	cpx
SiO2	54.59	52.06	54.93	52.11	55.81	52.32
TiO2	0.29	0.62	0.30	0.56	0.27	0.64
Al2O3	2.56	3.24	2.19	3.26	2.26	3.42
FeO	12.79	7.79	12.51	7.59	12.45	8.58
MnO	0.23	0.12	0.18	0.13	0.16	0.17
MgO	29.10	16.40	29.42	16.80	29.33	16.58
CaO	1.30	19.25	1.47	18.78	1.27	18.79
Na2O	0.05	0.36	0.05	0.36	0.02	0.37
K2O	0.01	0.00	0.02	0.01	0.00	0.00
Cr2O3	0.18	0.32	0.31	0.61	0.33	0.37
NiO	0.03	0.04	0.06	0.06	0.03	0.04
Total	101.14	100.20	101.44	100.25	101.94	101.28
En	78.19	47.39	78.47	48.62	78.79	47.51
Wo	2.52	12.63	2.81	12.32	2.45	13.79
Fs	19.29	39.98	18.72	39.07	18.76	38.70
Temp	1064		1097		1085	
Press (eq 38)	5.2		4.8		5.1	
Press (eq 39)	5.3		5.4		4.6	
avg Press	5.2		5.1		4.9	
Equilirium test	1.08		1.06		1.22	

sample	AP2-00-77		AP2-00-77		AP2-00-77	
analysis	32 / 10 .	32 / 3 .	33 / 3 .	33 / 2 .	34 / 2 .	34 / 3 .
	opx	cpx	opx	cpx	opx	cpx
SiO2	55.18	52.32	54.70	51.82	55.12	53.19
TiO2	0.22	0.64	0.25	0.61	0.28	0.43
Al2O3	2.31	3.42	2.03	3.36	2.12	2.21
FeO	12.30	8.58	12.59	7.94	12.11	7.39
MnO	0.14	0.17	0.34	0.09	0.18	0.08
MgO	29.60	16.58	29.62	16.71	29.62	17.32
CaO	1.42	18.79	1.32	18.72	1.36	19.05
Na2O	0.03	0.37	0.05	0.38	0.04	0.31
K2O	0.00	0.00	0.01	0.01	0.00	0.00
Cr2O3	0.36	0.37	0.28	0.51	0.28	0.33
NiO	0.03	0.04	0.00	0.04	0.08	0.10
Total	101.60	101.28	101.19	100.19	101.21	100.41
En	78.89	47.51	78.70	48.26	79.21	49.26
Wo	2.73	13.79	2.53	12.87	2.62	11.79
Fs	18.38	38.70	18.77	38.87	18.17	38.94
Temp	1096		1078		1077	
Press (eq 38)	5.4		5.7		4.7	
Press (eq 39)	5.5		4.5		5.4	
avg Press	5.4		5.1		5.1	
Equilirium test	1.25		1.12		1.04	

Table 4.4: Amphibole analyses for AVC lavas. All data from electron microprobe analysis at Oregon State University. All Fe reported as FeO. Temp and P (MPa) are the temperature and pressure calculated using the model of Ridolfi et al (2010). Temperature reported in degrees C, pressure in MPa. The error for each Ridolfi temperature is 22 degrees C. The error for each pressure calculation is shown. Al IV and Al VI calculated on the basis of 13 cations, after Leake et al (1997). Concentrations are in oxide weight percent.

Sample	**AP-07-19**	**AP-07-19**	**AP-07-19**	**AP-07-19**	**AP-07-19**	**AP-07-19**	**AP-07-19**
Analysis	**1 / 1 .**	**1 / 2 .**	**4 / 2 .**	**5 / 1 .**	**6 / 1 .**	**6 / 2 .**	**6 / 3 .**
SiO_2	47.28	47.12	44.21	44.77	42.88	42.94	43.58
TiO_2	1.47	1.54	2.60	2.43	2.07	2.51	2.12
Al_2O_3	8.33	8.28	10.93	9.88	12.21	12.15	12.19
FeO	13.35	13.24	12.00	12.26	12.18	11.47	11.76
MnO	0.33	0.26	0.25	0.30	0.14	0.16	0.08
MgO	15.28	15.27	14.67	14.74	15.08	15.09	15.49
CaO	11.07	11.29	11.41	11.26	11.28	11.47	11.30
Na_2O	1.71	1.73	2.15	2.15	2.26	2.31	2.35
K_2O	0.61	0.61	0.60	0.69	0.52	0.54	0.59
F	0.21	0.25	0.15	0.22	0.07	-0.02	0.13
Cl	0.11	0.10	0.04	0.05	0.02	0.02	0.02
total	99.74	99.69	99.03	98.74	98.70	98.64	99.61
Al IV	1.35	1.35	1.70	1.58	1.92	1.89	1.88
Al VI	0.03	0.03	0.14	0.08	0.13	0.15	0.14
Temp	839	843	927	902	959	965	955
P (MPa)	140	139	269	212	363	360	350
error	15	15	30	23	40	40	38

Table 4.4 continued

Sample	AP-00-03	AP-00-03	AP-07-41	AP-07-41	AP-07-41	AP-07-41	AP-07-41
Analysis	9 / 1 .	9 / 2 .	14 / 1 .	17 / 1 .	17 / 2 .	18 / 1 .	18 / 2 .
SiO_2	44.47	44.33	43.30	44.04	44.94	45.04	46.62
TiO_2	1.68	1.89	1.91	1.20	1.23	2.01	1.85
Al_2O_3	11.02	11.00	12.08	11.25	10.58	11.03	10.54
FeO	12.97	12.65	14.64	16.02	15.36	10.30	10.87
MnO	0.26	0.25	0.14	0.23	0.28	0.12	0.05
MgO	14.69	14.66	13.06	12.62	13.03	15.96	16.04
CaO	11.31	11.44	11.63	11.40	11.54	11.72	11.58
Na_2O	2.16	2.28	2.25	2.03	1.88	2.27	2.19
K_2O	0.59	0.58	0.55	0.56	0.62	0.58	0.50
F	0.02	-0.03	0.26	0.17	0.16	0.33	0.19
Cl	0.04	0.03	0.04	0.05	0.03	0.03	0.03
total	99.21	99.08	99.87	99.55	99.65	99.39	100.47
Al IV	1.69	1.69	1.80	1.68	1.57	1.64	1.52
Al VI	0.15	0.15	0.24	0.22	0.22	0.20	0.21
Temp (R)	917	923	940	903	888	931	901
Press (R)	272	273	360	296	250	269	230
error	30	30	40	74	28	30	25

Sample	AP-07-41	AP-07-62B	AP-07-62B	AP-07-62B	AP-07-62B	AP-07-62B	AP-07-62B
Analysis	18 / 3 .	20 / 1 .	20 / 2 .	21 / 1 .	21 / 2 .	22 / 1 .	22 / 2 .
SiO_2	44.91	44.78	44.51	43.25	44.07	43.21	43.43
TiO_2	2.04	2.47	2.85	2.91	2.69	2.99	2.62
Al_2O_3	11.26	11.06	11.77	11.76	11.32	11.66	11.26
FeO	11.26	11.67	11.97	12.02	11.44	11.77	11.85
MnO	0.06	0.14	0.17	0.17	0.17	0.18	0.17
MgO	15.66	15.28	15.07	14.96	15.26	15.20	15.19
CaO	11.61	11.49	11.43	11.46	11.64	11.40	11.28
Na_2O	2.35	3.02	2.37	2.70	2.48	2.39	2.53
K_2O	0.55	0.52	0.57	0.58	0.54	0.51	0.60
F	0.16	0.93	0.22	0.43	0.24	0.28	0.36
Cl	0.02	0.02	0.03	0.02	0.03	0.02	0.03
total	99.88	101.39	100.95	100.26	99.87	99.61	99.35
Al IV	1.69	1.69	1.79	1.87	1.77	1.88	1.82
Al VI	0.18	0.14	0.15	0.09	0.12	0.06	0.07
Temp (R)	932	938	943	962	947	958	948
Press (R)	280	269	311	323	290	315	290
error	31	30	34	36	32	35	32

Table 4.4 continued

Sample	AP-07-10B	AP-07-10B	AP-07-10B	AP-07-10B	AP-07-45	AP-07-45	AP-07-45
Analysis	8 / 4 .	8 / 5 .	9 / 1 .	9 / 2 .	13 / 1 .	13 / 2 .	13 / 3 .
SiO_2	46.03	47.27	45.03	44.13	44.18	43.75	44.32
TiO_2	1.77	1.44	2.23	2.39	2.20	2.08	2.18
Al_2O_3	8.42	7.65	9.58	9.94	11.40	11.65	11.37
FeO	14.05	13.57	14.31	14.91	12.57	13.07	12.42
MnO	0.37	0.39	0.28	0.28	0.20	0.23	0.23
MgO	14.27	14.67	13.72	13.36	14.77	14.72	14.91
CaO	11.48	11.40	11.25	11.39	11.30	11.29	11.39
Na_2O	1.52	1.37	1.74	1.79	2.36	2.39	2.63
K_2O	0.78	0.73	0.90	0.88	0.55	0.50	0.52
F	0.23	0.11	0.13	0.22	0.13	0.17	0.12
Cl	0.16	0.16	0.12	0.12	0.03	0.02	0.03
total	99.09	98.76	99.28	99.41	99.70	99.85	100.13
Al IV	1.40	1.24	1.54	1.64	1.76	1.82	1.75
Al VI	0.03	0.05	0.08	0.04	0.14	0.11	0.14
Temp (R)	852	824	880	897	932	939	936
Press (R)	149	123	197	217	295	312	291
error	16	14	22	24	32	34	32

Sample	AP-07-45	AP-07-45	AP-07-45	AP-07-45	AP-07-45	AP-07-45	AP-07-45
Analysis	14 / 1 .	14 / 2 .	14 / 3 .	14 / 4 .	14 / 5 .	15 / 3 .	16 / 1 .
SiO_2	43.63	43.39	43.85	44.14	44.21	44.89	43.98
TiO_2	2.16	2.12	2.18	2.16	2.06	1.96	2.20
Al_2O_3	11.26	11.80	11.97	11.39	11.19	10.69	10.56
FeO	12.96	12.32	12.84	12.25	13.06	12.29	12.68
MnO	0.26	0.20	0.18	0.23	0.26	0.25	0.22
MgO	14.64	14.91	14.69	14.91	14.91	15.12	15.03
CaO	11.33	11.44	11.32	11.34	11.24	11.29	11.27
Na_2O	3.02	2.43	2.42	2.96	2.53	2.34	2.43
K_2O	0.52	0.48	0.51	0.48	0.48	0.53	0.53
F	0.64	0.17	0.35	0.29	0.08	0.39	0.60
Cl	0.03	0.04	0.02	0.04	0.03	0.04	0.05
total	100.45	99.31	100.33	100.20	100.05	99.77	99.54
Al IV	1.79	1.84	1.83	1.75	1.77	1.66	1.74
Al VI	0.09	0.13	0.16	0.15	0.08	0.12	0.04
Temp (R)	944	951	944	942	930	914	924
Press (R)	290	328	333	295	278	248	246
error	32	36	37	32	31	27	27

Table 4.4 continued

Sample	AP-07-62B	AP-07-62B	AP-07-62B	AP-07-62B	AP-07-62B	AP-07-62B	AP-07-62B
Analysis	**22 / 3 .**	**23 / 1 .**	**23 / 2 .**	**24 / 1 .**	**24 / 2 .**	**25 / 1 .**	**25 / 2 .**
SiO_2	43.71	44.68	43.74	43.77	44.29	45.52	44.82
TiO_2	2.51	2.67	2.66	2.58	2.56	2.58	2.61
Al_2O_3	11.19	10.93	11.93	11.47	11.05	10.42	10.55
FeO	11.92	11.45	12.09	11.60	11.19	11.09	11.31
MnO	0.13	0.15	0.12	0.15	0.13	0.13	0.15
MgO	15.28	15.56	14.80	15.68	15.69	15.78	15.77
CaO	11.43	11.35	11.61	11.26	11.27	11.41	11.46
Na_2O	2.74	2.35	2.82	2.57	2.64	2.41	2.27
K_2O	0.52	0.52	0.58	0.50	0.46	0.49	0.48
F	1.09	0.31	0.61	0.57	0.55	0.46	0.29
Cl	0.03	0.02	0.04	0.02	0.03	0.03	0.03
total	100.54	99.97	101.00	100.17	99.86	100.31	99.74
Al IV	1.80	1.72	1.82	1.84	1.75	1.61	1.69
Al VI	0.07	0.09	0.16	0.06	0.09	0.11	0.06
Temp (R)	947	930	959	950	938	915	924
Press (R)	283	260	333	296	270	229	238
error	31	29	37	33	30	25	26

Sample	AP-07-62B	AP-07-62B	AP-07-62B	AP-07-62B	AP-07-62B	AP-07-62B	AP-07-62B
Analysis	**25 / 3 .**	**26 / 1 .**	**26 / 2 .**	**26 / 3 .**	**27 / 1 .**	**27 / 2 .**	**28 / 1 .**
SiO_2	43.79	43.51	43.22	43.59	43.59	44.57	43.47
TiO_2	2.65	2.90	2.77	2.60	2.92	2.54	2.86
Al_2O_3	11.51	11.47	11.61	11.06	11.72	11.08	11.50
FeO	11.77	11.95	11.71	11.63	12.19	12.74	11.78
MnO	0.16	0.20	0.15	0.20	0.18	0.19	0.14
MgO	15.17	15.46	15.08	15.34	15.17	14.91	15.26
CaO	11.36	11.38	11.51	11.29	11.43	11.20	11.42
Na_2O	2.55	2.38	2.43	2.75	2.48	2.38	2.79
K_2O	0.58	0.55	0.61	0.57	0.55	0.52	0.54
F	0.45	0.41	0.37	0.65	0.38	0.20	0.24
Cl	0.03	0.03	0.03	0.03	0.03	0.04	0.03
total	100.02	100.23	99.47	99.72	100.64	100.39	100.03
Al IV	1.81	1.88	1.85	1.80	1.88	1.74	1.85
Al VI	0.11	0.02	0.10	0.06	0.06	0.09	0.07
Temp (R)	949	953	958	947	956	925	958
Press (R)	303	296	316	277	313	268	302
error	33	33	35	30	34	29	33

Table 4.4 continued

Sample	AP-07-45	AP-07-45	AP-07-45	AP-00-03	AP-00-03	AP-00-03	AP-00-03
Analysis	16 / 2 .	17 / 1 .	17 / 2 .	1 / 1 .	1 / 2 .	2 / 1 .	2 / 2 .
SiO_2	43.95	45.07	44.62	43.59	44.68	44.47	44.60
TiO_2	2.08	2.19	2.08	2.15	2.03	1.98	1.90
Al_2O_3	10.65	10.36	10.96	11.82	11.55	11.40	10.82
FeO	13.37	12.89	12.62	13.49	12.94	12.96	12.93
MnO	0.26	0.27	0.27	0.22	0.21	0.25	0.21
MgO	15.26	14.79	14.98	14.24	14.85	14.44	14.98
CaO	11.17	11.32	11.25	11.46	11.50	11.42	11.52
Na_2O	2.49	2.88	2.46	2.28	2.23	2.10	2.05
K_2O	0.52	0.53	0.45	0.67	0.65	0.68	0.56
F	0.88	1.52	0.27	0.14	0.13	0.08	0.07
Cl	0.04	0.04	0.03	0.04	0.03	0.03	0.04
total	100.68	101.86	100.00	100.08	100.82	99.79	99.70
Al IV	1.77	1.63	1.71	1.83	1.75	1.71	1.71
Al VI	0.00	0.09	0.11	0.14	0.15	0.19	0.09
Temp (R)	937	914	922	943	930	924	918
Press (R)	245	230	263	327	297	295	256
error	27	25	29	36	33	32	28

Sample	AP-00-03	AP-00-03	AP-00-03	AP-00-03	AP-00-03	AP-00-03	AP-00-03
Analysis	2 / 3 .	2 / 4 .	3 / 2 .	4 / 1 .	4 / 2 .	5 / 1 .	5 / 2 .
SiO_2	43.83	44.37	43.41	43.81	44.54	43.89	43.70
TiO_2	2.04	2.04	1.67	2.08	2.04	1.95	2.05
Al_2O_3	11.40	11.34	11.67	11.76	11.44	11.85	11.86
FeO	13.30	13.31	14.07	13.09	13.06	13.65	13.63
MnO	0.30	0.26	0.19	0.18	0.20	0.23	0.19
MgO	14.39	14.20	13.94	14.28	14.73	14.14	13.93
CaO	11.22	11.33	11.51	11.50	11.55	11.58	11.46
Na_2O	2.12	2.15	2.15	2.19	2.17	2.18	2.11
K_2O	0.70	0.73	0.63	0.67	0.59	0.68	0.66
F	0.07	0.05	0.11	0.11	0.00	0.18	0.07
Cl	0.05	0.04	0.04	0.03	0.04	0.03	0.04
total	99.42	99.81	99.38	99.69	100.35	100.36	99.71
Al IV	1.78	1.72	1.81	1.78	1.75	1.80	1.79
Al VI	0.13	0.18	0.15	0.18	0.15	0.17	0.19
Temp (R)	929	923	935	939	929	938	937
Press (R)	298	292	323	325	292	328	334
error	33	32	36	36	32	36	37

Table 4.4 continued

Sample	AP-07-62B	AP-07-62B	AP-07-27	AP-07-27	AP-07-27	AP-07-27
Analysis	28 / 2 .	28 / 3 .	29 / 1 .	29 / 2 .	29 / 3 .	31 / 1 .
SiO_2	43.15	43.88	43.68	43.47	43.92	45.99
TiO_2	2.71	2.68	2.24	2.27	2.29	2.17
Al_2O_3	11.54	11.55	12.56	12.53	12.28	8.75
FeO	11.73	11.80	11.34	10.57	10.65	13.46
MnO	0.17	0.15	0.10	0.10	0.12	0.19
MgO	15.22	15.27	15.51	15.67	15.92	15.07
CaO	11.69	11.58	11.59	11.75	11.59	11.21
Na_2O	2.41	2.42	2.38	2.32	2.38	2.11
K_2O	0.57	0.60	0.45	0.47	0.47	0.78
F	0.27	0.54	0.10	-0.02	0.05	0.43
Cl	0.03	0.03	0.01	0.01	0.02	0.08
total	99.49	100.48	99.95	99.15	99.70	100.23
Al IV	1.87	1.82	1.89	1.87	1.85	1.46
Al VI	0.07	0.10	0.19	0.21	0.18	0.00
Temp (R)	960	951	965	971	962	879
Press (R)	310	303	379	383	354	157
error	34	33	42	42	39	17

Sample	AP-07-27	AP-07-27	AP-07-27	AP-07-27	AP-07-27	AP-07-27
Analysis	32 / 1 .	32 / 2 .	32 / 3 .	33 / 1 .	33 / 2 .	33 / 3 .
SiO_2	43.48	43.80	43.84	44.06	43.24	43.86
TiO_2	2.23	1.84	1.99	2.30	2.36	2.09
Al_2O_3	12.51	12.00	12.34	12.39	12.36	12.83
FeO	12.13	12.62	12.13	10.72	11.98	10.35
MnO	0.14	0.18	0.19	0.10	0.11	0.12
MgO	14.94	14.90	14.80	15.78	15.12	16.00
CaO	11.23	11.37	11.44	11.44	11.55	11.47
Na_2O	2.47	2.25	2.28	2.46	2.33	2.47
K_2O	0.49	0.48	0.47	0.49	0.51	0.51
F	0.08	0.12	0.15	0.14	0.26	0.05
Cl	0.02	0.02	0.01	0.01	0.02	0.02
total	99.73	99.56	99.64	99.88	99.83	99.75
Al IV	1.89	1.83	1.82	1.84	1.91	1.88
Al VI	0.19	0.17	0.23	0.20	0.15	0.23
Temp (R)	958	943	949	960	964	970
Press (R)	379	338	366	362	368	399
error	42	37	40	40	40	44

Table 4.4 continued

Sample	AP-00-03	AP-00-03	AP-00-03	AP-00-03	AP-00-03	AP-00-03	AP-00-03
Analysis	5 / 3 .	6 / 1 .	6 / 2 .	7 / 1 .	7 / 2 .	7 / 3 .	7 / 4 .
SiO_2	44.07	43.43	43.68	44.51	43.60	43.73	43.51
TiO_2	2.03	1.90	2.04	2.08	2.02	1.84	2.05
Al_2O_3	11.81	11.97	11.86	11.29	11.90	11.66	12.02
FeO	13.95	13.27	13.53	12.90	13.53	13.63	12.85
MnO	0.27	0.23	0.22	0.26	0.26	0.26	0.21
MgO	14.01	14.12	14.08	14.60	14.06	14.11	14.32
CaO	11.34	11.43	11.48	11.39	11.31	11.31	11.45
Na_2O	2.22	2.17	2.24	2.15	2.26	2.17	2.23
K_2O	0.76	0.66	0.64	0.68	0.64	0.65	0.61
F	0.13	0.11	0.15	0.13	0.04	0.25	-0.03
Cl	0.04	0.03	0.03	0.04	0.03	0.03	0.03
total	100.63	99.30	99.95	100.03	99.65	99.64	99.25
Al IV	1.79	1.82	1.81	1.72	1.81	1.79	1.82
Al VI	0.17	0.19	0.17	0.15	0.17	0.16	0.20
Temp (R)	932	942	940	924	939	932	946
Press (R)	322	345	332	285	335	318	348
error	35	38	37	31	37	35	38

Sample	AP-00-03	AP-00-03	AP-00-03	AP-00-03	AP-00-03	AP-00-03	AP-00-03
Analysis	7 / 5 .	8 / 1 .	8 / 2 .	8 / 3 .	8 / 4 .	8 / 5 .	8 / 7 .
SiO_2	44.00	44.00	44.74	44.70	44.93	43.59	43.86
TiO_2	2.00	2.09	2.00	1.79	1.91	2.12	2.03
Al_2O_3	11.34	11.65	10.84	10.62	10.73	11.69	11.32
FeO	13.47	12.91	12.30	12.68	12.68	13.11	12.93
MnO	0.24	0.22	0.21	0.26	0.28	0.21	0.21
MgO	14.40	14.20	14.85	14.87	14.89	14.18	14.43
CaO	11.31	11.42	11.38	11.42	11.30	11.31	11.34
Na_2O	2.14	2.16	2.08	2.13	2.07	2.20	2.14
K_2O	0.70	0.70	0.61	0.56	0.58	0.61	0.69
F	0.09	0.11	0.12	-0.03	0.14	0.15	0.02
Cl	0.03	0.04	0.05	0.04	0.04	0.04	0.04
total	99.74	99.50	99.18	99.05	99.56	99.21	99.02
Al IV	1.77	1.75	1.65	1.65	1.65	1.79	1.75
Al VI	0.12	0.21	0.16	0.12	0.13	0.17	0.15
Temp (R)	927	933	915	912	909	937	929
Press (R)	292	318	261	247	250	323	296
error	32	35	29	27	28	36	33

Table 4.5 : Amphibole analyses paired with plagioclase An contents for AVC lavas. All data from electron microprobe analysis at Oregon State University. All Fe reported as FeO. Plagioclase compositions shown as An content. Temp (R) and Press (R) are the temperature and pressure calculated using the model of Ridolfi et al (2010). Temp (H & B) is the temperature calculated using the formulation of Holland & Blundy (1994). Press (A & L) is the pressure calculated from Al-in-hornblende formulation of Anderson & Lindsley (1995). Temperature reported in degrees C, pressure in MPa. The error for each Ridolfi temperature 22 degrees C and for pressure is shown. Al IV and Al VI calculated on the basis of 13 cations, after Leake et al (1997).

Sample	**AP-07-19**	**AP-07-19**	**AP-07-19**	**AP-07-19**	**AP-07-10B**	**AP-07-10B**	**AP-07-10B**
Analysis	**2 / 1 .**	**2 / 2 .**	**7 / 1 .**	**7 / 2 .**	**8 / 1 .**	**8 / 2 .**	**8 / 3 .**
SiO_2	44.14	44.30	46.51	46.19	47.79	47.83	48.74
TiO_2	2.20	2.21	1.31	1.28	1.37	1.45	1.43
Al_2O_3	11.75	11.93	8.12	8.49	7.41	7.43	7.26
FeO	10.56	10.74	15.66	15.69	13.80	13.32	13.53
MnO	0.09	0.12	0.34	0.44	0.39	0.37	0.40
MgO	16.13	16.17	13.50	13.11	14.83	14.70	14.99
CaO	11.39	11.53	11.55	11.68	11.50	11.46	11.48
Na_2O	2.39	2.41	1.42	1.45	1.31	1.27	1.35
K_2O	0.46	0.53	0.90	0.92	0.76	0.74	0.69
F	0.03	0.15	0.22	0.15	0.15	0.16	0.16
Cl	0.01	0.01	0.18	0.16	0.14	0.14	0.13
total	99.17	100.10	99.73	99.56	99.44	98.86	100.15
Al IV	1.80	1.82	1.32	1.34	1.21	1.17	1.14
Al VI	0.14	0.14	0.05	0.10	0.03	0.08	0.06
Temp (R)	950	954	833	841	817	814	806
Press (R)	314	323	138	153	114	116	109
error	35	35	15	17	13	13	12
analysis (plag)	**2 / 1 .**	**2 / 2 .**	**7 / 1 .**	**7 / 2 .**	**8 / 1 .**	**8 / 2 .**	**8 / 1 .**
Xab (plag)	0.53	0.53	0.65	0.64	0.55	0.58	0.55
Xan (plag)	0.45	0.45	0.30	0.31	0.41	0.37	0.41
Temp (H & B)	843	847	770	762	795	771	790
Press (A & L)	251	247	218	261	111	165	107

Table 4.5 continued

Sample	AP-07-10B	AP-07-10B	AP-07-10B	AP-07-10B	AP-07-10B	AP-07-10B	AP-07-10B
Analysis	**10 / 1 .**	**10 / 2 .**	**10 / 3 .**	**11 / 1 .**	**11 / 2 .**	**11 / 3 .**	**12 / 1 .**
SiO_2	47.71	47.39	48.47	47.44	47.15	47.27	46.47
TiO_2	1.37	1.55	1.45	1.69	1.67	1.71	1.67
Al_2O_3	7.66	7.74	7.54	8.25	8.31	8.28	8.56
FeO	13.95	13.67	13.90	14.38	14.24	14.15	14.18
MnO	0.41	0.43	0.35	0.33	0.38	0.29	0.33
MgO	14.84	14.88	15.03	14.35	14.43	14.40	14.41
CaO	11.60	11.54	11.55	11.41	11.59	11.52	11.49
Na_2O	1.33	1.34	1.31	1.55	1.41	1.51	1.56
K_2O	0.79	0.73	0.78	0.83	0.86	0.87	0.84
F	0.16	0.14	0.24	0.13	0.09	0.14	0.16
Cl	0.15	0.15	0.16	0.14	0.15	0.14	0.14
total	99.98	99.55	100.78	100.50	100.29	100.27	99.79
Al IV	1.25	1.28	1.21	1.31	1.33	1.31	1.39
Al VI	0.03	0.02	0.04	0.07	0.05	0.07	0.04
Temp (R)	824	829	815	834	840	838	851
Press (R)	121	124	115	138	141	140	151
error	13	14	13	15	15	15	17
analysis (plag)	**10 / 1 .**	**10 / 1 .**	**10 / 1 .**	**11 / 2 .**	**11 / 3 .**	**11 / 3 .**	**12 / 1 .**
Xab (plag)	0.59	0.59	0.59	0.53	0.55	0.55	0.53
Xan (plag)	0.37	0.37	0.37	0.43	0.42	0.42	0.44
Temp (H & B)	782	783	781	822	815	814	831
Press (A & L)	154	159	144	96	119	119	95

Table 4.5 continued

Sample	AP-07-10B	AP-07-45	AP-07-45	AP-07-45	AP-00-03	AP-00-03	AP-00-03
Analysis	**12 / 2 .**	**15 / 1 .**	**15 / 2 .**	**16 / 3 .**	**3 / 1 .**	**7 / 6 .**	**8 / 6 .**
SiO_2	47.14	43.77	45.39	43.71	44.64	43.72	44.72
TiO_2	1.67	1.69	1.92	2.02	1.96	1.98	1.90
Al_2O_3	8.57	12.00	10.58	11.13	11.22	12.13	11.07
FeO	13.74	12.89	11.23	12.08	13.56	13.19	12.86
MnO	0.33	0.20	0.29	0.30	0.33	0.20	0.23
MgO	14.44	14.88	15.87	15.08	14.23	14.39	14.49
CaO	11.55	11.32	11.16	11.33	11.18	11.50	11.47
Na_2O	1.52	2.45	2.11	3.04	2.11	2.23	2.04
K_2O	0.74	0.49	0.50	0.51	0.67	0.59	0.62
F	0.23	0.25	0.08	1.22	0.14	0.07	0.04
Cl	0.11	0.02	0.03	0.05	0.05	0.02	0.03
total	100.03	99.95	99.15	100.48	100.09	100.01	99.49
Al IV	1.32	1.84	1.63	1.77	1.70	1.83	1.66
Al VI	0.11	0.15	0.12	0.10	0.16	0.18	0.18
Temp (R)	844	944	908	945	914	945	916
Press (R)	150	336	238	283	281	349	274
error	17	37	26	31	31	38	30
analysis (plag)	**12 / 2 .**	**15 / 3 .**	**15 / 1 .**	**16 / 3 .**	**3 / 1 .**	**7 / 6 .**	**8 / 6 .**
Xab (plag)	0.45	0.44	0.46	0.62	0.46	0.44	0.46
Xan (plag)	0.45	0.53	0.52	0.31	0.52	0.54	0.52
Temp (H & B)	829	888	856	854	876	887	865
Press (A & L)	96	108	140	185	106	116	138

Table 4.5 continued

Sample	AP-07-41	AP-07-41	AP-07-41	AP-07-41	AP-07-41	AP-07-41	AP-07-41
Analysis	**10 / 1 .**	**10 / 2 .**	**10 / 3 .**	**11 / 2 .**	**12 / 1 .**	**12 / 2 .**	**12 / 3 .**
SiO_2	43.39	43.15	44.23	43.74	43.82	42.90	42.35
TiO_2	2.25	2.37	1.53	2.10	2.04	1.97	1.88
Al_2O_3	12.12	12.00	11.72	11.45	12.06	12.83	12.75
FeO	12.56	12.49	14.32	13.49	12.22	14.47	14.87
MnO	0.11	0.06	0.20	0.17	0.12	0.11	0.17
MgO	14.27	14.14	13.13	14.14	14.84	12.98	12.50
CaO	11.43	11.56	11.41	10.98	11.41	11.65	11.40
Na_2O	2.38	2.36	2.08	2.24	2.38	2.34	2.18
K_2O	0.55	0.51	0.71	0.52	0.62	0.66	0.63
F	0.22	0.18	0.14	0.09	0.19	0.31	0.13
Cl	0.02	0.02	0.05	0.02	0.02	0.03	0.04
total	99.31	98.84	99.51	98.95	99.71	100.26	98.90
Al IV	1.82	1.81	1.67	1.77	1.81	1.88	1.88
Al VI	0.22	0.22	0.30	0.15	0.20	0.28	0.29
Temp (R)	951	953	917	925	948	958	953
Press (R)	359	355	329	305	345	428	436
error	39	39	82	33	38	47	48
analysis (plag)	**10 / 1 .**	**10 / 3 .**	**10 / 1 .**	**11 / 1 .**	**12 / 1 .**	**12 / 2 .**	**12 / 2 .**
Xab (plag)	0.51	0.60	0.51	0.50	0.50	0.60	0.60
Xan (plag)	0.47	0.37	0.47	0.48	0.49	0.38	0.38
Temp (H & B)	863	827	820	872	866	819	817
Press (A & L)	212	332	335	142	194	408	419

Table 4.5 continued

Sample	AP-07-41	AP-07-41	AP-07-41	AP-07-41	AP-07-62B
Analysis	**13 / 1 .**	**13 / 2 .**	**16 / 1 .**	**16 / 2 .**	**19 / 2 .**
SiO_2	43.41	43.57	43.64	45.26	44.27
TiO_2	2.12	1.66	1.66	1.75	2.55
Al_2O_3	12.18	11.91	12.04	10.80	11.63
FeO	12.85	14.77	14.77	12.93	11.64
MnO	0.05	0.19	0.15	0.11	0.14
MgO	14.17	13.02	13.17	14.58	15.18
CaO	11.43	11.52	11.52	11.59	11.54
Na_2O	2.44	2.13	2.17	2.12	2.43
K_2O	0.44	0.57	0.59	0.45	0.63
F	0.13	0.13	0.26	0.24	0.23
Cl	0.02	0.04	0.03	0.02	0.02
total	99.24	99.51	100.01	99.85	100.26
Al IV	1.82	1.76	1.78	1.60	1.77
Al VI	0.23	0.25	0.24	0.20	0.16
Temp (R)	949	929	932	906	946
Press (R)	363	346	353	255	308
error	40	38	39	28	34
analysis (plag)	**13 / 3 .**	**13 / 1 .**	**16 / 2 .**	**16 / 2 .**	**19 / 2 .**
Xab (plag)	0.50	0.56	0.47	0.47	0.60
Xan (plag)	0.48	0.42	0.52	0.52	0.38
Temp (H & B)	866	824	862	855	844
Press (A & L)	207	333	211	156	241

CHAPTER 5
General Conclusions

Erupted lavas at the Aucanquilcha Volcanic Cluster document eleven million years of stationary and relatively continuous arc volcanism in the central Andes. Bulk compositional trends of AVC lavas indicate that fractional crystallization and recycling of precursor magmas (magma mixing) are the most important processes generating compositional diversity observed in any given eruptive phase. Time transgressive trends suggest that the high flux period of AVC volcanism (5 – 2 Ma) was characterized by magma mixing and mush remobilization, likely leading to the development and homogenization of a large, upper crustal batholith. Lavas from the beginning and waning phases of AVC volcanism lack this strong mixing signal, suggesting these low-flux times were characterized by disparate, physically isolated magmatism.

The phenocryst assemblages of AVC lavas have been probed for various intensive parameters. Crystallization of pyroxene, amphibole, Fe-Ti oxide, and zircon is documented for over 7 kb (~24 km) of pressure and from ~1150 to 750°C in these lavas. The diversity of crystallization temperatures and pressures recorded by phases in individual AVC lavas suggests erupting magma batches accumulate phases from different levels within the upper crust. Many crystals in AVC lavas are likely to be true phenocrysts, but eruptions also extensively recycled crystals from the possibly multi-tiered, evolving reservoir. Age and compositional data from erupted zircons indicate that they are broadly cognate crystal cargo at the multi million-year scale, and that the plutonic underpinnings were episodically active in concert with the volcanic pulses. Most zircon recycling involved grains only a few hundred thousand years older than the eruption age. We take this to reflect the timescale of plutonic episodes. Antecrysts of older vintage document the magmatic cannibalism associated with batholith assembly—that is, the blending of discrete plutons into a patchwork body. Intensive parameters of AVC phases indicate a spatial focusing of the upper crustal subvolcanic system that accompanying increased volcanic output, and presumably system power. If intensive

parameters of erupted crystals are indicative of those left behind at similar conditions of formation, they imply the existence of a large, zoned batholith, ranging from at least ~3 to 25 km depth.

All AVC lavas are isotopically contaminated (high $^{87}Sr/^{86}Sr$ and $\delta^{18}O$, low εNd) with respect to primitive mantle and have pronounced garnet signatures (elevated Dy/Yb ratios). Though bulk compositions do not change appreciably, the baseline isotopic signature and the Dy/Yb ratios of AVC lavas increase through time, suggesting the site of the isotopic contamination and acquisition of garnet signature was likely the middle to deep crust where higher temperatures and pressures promote fusion of crustal material and/or reactions between crust and basaltic magma. Time-integrated basaltic underplating and an expanding zone of melting, assimilation, homogenization, and storage (MASH) likely influence, to a first order, this progressive evolution. With prolonged magmatism, successive basalt injections into such an expanding MASH zone would be increasingly intercepted, where prodigious crystallization of garnet is likely to occur. The large, blurred MOHO from ~50 – 80 km beneath the AVC is probably the result of such protracted MASH expansion.

Petrologic modeling of trace element and Sr, Nd, and O isotopic variation suggests that magmagenesis of AVC lavas involved the incorporation of 10 – 30 % pre-existing crust. Accompanying this assimilation was prodigious crystallization, which deposited thousands of cubic kilometers of unerupted, residual material in the crustal column. Though difficult to constrain precise volumes, it is a safe assumption that the crystal residue from this process is vast, accumulating both from the modeled AFC processes modeled and from the extra basalt crystallization that is necessary to thermally drive such assimilation (Grunder, 1995). Furthermore, estimates of intrusive:extrusive ratios from other continental subduction systems (cf. White et al., 2006; Dilles,1987) indicate that magma stalled in the crust could be equal to ten to one hundred times the amount of erupted material.

The eruptive flare-up from ~5 – 2 Ma at the AVC is characterized by a focusing of Sr and Nd isotopes, suggesting that the dramatic increase in eruptive output was not the result of peak rates of crustal addition, but rather the result of peak rates of mantle delivery and thermal modulation in the crust accompanied by modest crustal input. **A**lthough the history of central Andean magmatism is replete with large scale crustal recycling, compositions of AVC lavas suggest that the current magmatic phase is largely a crust formation event.

References

Dilles, J.D., 1987, Petrology of the Yerington Batholith, Nevada; evidence for evolution of porpyhyry copper ore fluids. *Economic Geology* 82 (7), p. 1750-1789.

Grunder, A.L., 1995, Material and thermal roles of basalt in crustal magmatism: case study from eastern Nevada. *Geology*, 23:952-956.

White, S.M., Crisp, J.A., Spera, F.J., 2006, Long-term volumetric eruption rates and magma budgets. *Geochemistry Geophysics Geosystems* 7 (1).

Bibliography

Aitcheson, S.J., Harmon, R.S., Moorbath, S., Schneider, A., Soler, P., Soria-Escalante, E., Steele, G., Swainbank, I., Wörner, G., 1995, Pb isotopes define basement domains of the Altiplano, central Andes. *Geology* 23 (6), 555-558.

Almendinger, R.W., Jordan, T.E., Kay, S.M., Isacks, B.L., 1997, The evolution of the Altiplano-Puna plateau of the central Andes. *Annual Review of Earth and Planetary Sciences* 25, 139-174.

Andersen, D.J., Lindsley, D.H., (1985). New (and final!) models for the Ti-magnetite/ilmenite geothermometer and oxygen barometer. Abstract AGU 1985 Spring Meeting Eos Transactions. *American Geophysical Union 66* (18), 416.

Anderson, J.L. and Smith, D.R. 1995. The effects of temperature and f (sub O2) on the Al-in-hornblende barometer. *American Mineralogist,* Issue 5-6, pp.559-549.

Anderson, J.L., Barth, A.P., Wooden, J.L, Mazdab, F., 2008, Thermometers and thermobarometers in granitic systems. Reviews in Mineralogy and Geochemistry 69, 121 – 142.

Annen, C., Blundy, J. D., Sparks, R. S. J., 2006, The genesis of intermediate and silicic magmas in deep crustal hot zones, *Journal of Petrology* 47 (3), 505-539.

Baby, P., Rochat, P., Mascle, G., Hérail, G., 1997, Neogene shortening contribution to crustal thickening in the back arc of the central Andes. *Geology* 25 (10), 883-886.

Bachmann, O. and Dungan, M., 2002. Temperature-induced Al-zoning in hornblendes of the Fish Canyon magma, Colorado. *American Mineralogist* 87 (8-9), pp. 1062-1076.

Bachmann, O., and Bergantz, G.W., 2004. On the origin of crystal-poor rhyolites: extracted from batholithic crystal mushes. *Journal of Petrology* 45 (8), 1565-1582.

Bachmann, O. B., L.A. Charlier and J.B. Lowenstern (2007) Zircon crystallization and recycling in the magma chamber of the rhyolitic Kos Plateau Tuff (Aegean arc): *Geology*, vol. 35, no. 1, pp. 73-76.

Bacon, C. R., Hirschmann, M. M., (1988). Mg/Mn partinitioning as a test for equilibrium between coestisting Fe-Ti oxides. *American Mineralogist 73*(1), 57-61.

Bacon, C.R., 1992, Partially melted granodiorite and related rocks ejected from Crater Lake caldera, Oregon. *Transactions of the Royal Society of Edinburgh, Earth Science* 83, p. 27-47.

Bacon, C.R., and Lowenstern, J.B., 2005, Late Pleistocene granodiorite source for recycled zircon and phenocrysts in rhyodacite lava at Crater Lake, Oregon: *Earth and Planetary Science Letters*, v. 233, p. 277-293.

Baker, M.C.W., Francis, P.W., 1978, Upper Cenozoic volcanism in the central Andes – ages and volumes. *Earth and Planetary Science Letters* 41, 175-187.

Bartley, J.M., Coleman, D.S., Glazner, A.F., 2006, Incremental pluton emplacement by magmatic crack-seal. *Earth and Environmental Transactions of the Royal Society of Edinburgh* 97, p. 383-396.

Beck, S.L., Zandt, G., Myers, S.C., Wallace, T.C., Silver, P.G., Drake, L., 1996, Crustal-thickness variations in the central Andes: *Geology*, v. 24, p. 407-410.

Beck, S.L., Zandt, G., 2002, The nature of the orogenic crust in the central Andes. *Journal of Geophysical Research* 107 (B10), doi:10.1029/2000JB000124

Bevis, M., E. C. Kendrick, R. Smalley Jr., T. Herring, J. Godoy, and F. Galban (1999), Crustal motion north and south of the Arica deflection: Comparing recent geodetic results from the central Andes, *Geochem. Geophys. Geosyst.*, *1*(12), 1005, doi:10.1029/1999GC000011.

Bindeman, I.N., Valley, J.W., 2001, Low-$\delta^{18}O$ rhyolites from Yellowstone: Magmatic evolution based on analyses of zircons and individual phenocrysts. *Journal of Petrology* 42 (8), p. 1491-1517.

Bindeman, I.N., Ponomareva, V.V., Bailey, J.C., Valley, J.W., 2004, Volcanic arc of Kamchatka: a province with high-δ18O magma sources and large-scale 18O/16O depletion of the upper crust. *Geochimica et Cosmochimica Acta* 68, 841–865.

Bindeman, I.N., Schmitt, A.K., Valley, J.W., 2006, U-Pb zircon geochronology of silicic tuffs from the Timber Mountain/Oasis Valley caldera complex, Nevada: rapid generation of large volume magmas by shallow-level remelting: *Contributions to*

Mineralogy and Petrology, v.152, n.6.

Blundy, J., Cashman, K., 2008, Petrologic reconstruction of magmatic systems variables and processes, Reviews in Mineralogy and Geochemistry 69, p. 179-239.

Bohrson,, W.A., Spera, F.J., 2001, Energy-constrained open-system magmatic processes II: Application of Energy-Constrained Assimilation-Fractional Crystallization (EC-AFC) model to magmatic systems. *Journal of Petrology* 42 (5), p. 1019-1041.

Brady, J.B., McCallister, R.H., 1983, Diffusion data for clinopyroxenes from homogenization and self-diffusion experiments. *American Mineralogist* 68, p. 95-105.

Brey, G.P., Kohler, T., 1990, Geothermobarometry in four-phase lherzolites II. New thermobarometers, and practical assessment of existing thermobarometers. *Journal of Petrology* 31, p. 1,353-1,378.

Cherniak, D.J., Dimanov, A., 2010, Diffusion in Pyroxene, Mica and Amphibole, *in* Zhang, Y., Cherniak, D.J., (eds.), Diffusion in minerals and melts. *Reviews in Mineralogy and Geochemistry* 72, p. 641-690.

Cherniak, D.J., Watson, E.B., 2003, Diffusion in zircon, *in* Hanchar, J.M., Hoskin, P.W.O., (eds.) Zircon. *Reviews in Mineralogy and Geochemistry* 53, p. 113-143.

Chmielowski, J., Zandt, G., and Haberland, C., 1999, The central Andean Altiplano-Puna magma body: *Geophysical Research Letters*, v. 26, p. 783-786.

Claiborne, L.L., Miller, C.F., Walker, B.A., Wooden, J.L., Mazdab, F.K., and Bea, F., 2006, Tracking magmatic processes through Zr/Hf ratios in rocks and Hf and Ti zoning in zircons: An example from the Spirit Mountain batholith, Nevada: Mineralogical Magazine, v. 70, p. 517-543.

Claiborne, L.L., Miller, C.F., Flanagan, D.M., Clynne, M.A., Wooden, J.L., 2010, Zircon reveals protracted magma storage and recycling beneath Mount St. Helens, *Geology* 38 (11), p. 1011-1014.

Coleman, D.S., Gray, W., and Glazner, A.F., 2004, Rethinking the emplacement and evolution of zoned plutons: Geochronologic evidence for incremental assembly of the Tuolumne Intrusive Suite, California: Geology, v. 32, p. 433-436.

Coney, P., Evenchick, C., 1994, Consolidation of the American Cordilleras. *Journal of South American Earth Science* 7, 241–262, 1994.

Conrad, W.K., Kay, S.M., Kay, R.W., 1983, Magma mixing in the Aleutian arc: evidence from cognate inclusions and composite xenoliths. *Journal of Volcanology and Geothermal Research* 18 (1-4), p. 279-295.

Crowley, J.L., Schoene, B., and Bowring, S.A., 2007, U-Pb dating of zircon in the Bishop Tuff at the millennial scale: Geology, v. 35, p. 1123-1126.

Davidson, J.P., McMillan, N.J., Moorbath, S., Wörner, G., Harmon, R.S., Lopez-Escobar, L., 1990, The Nevados de Payachata volcanic region (18°S/69°W Chile) II. Evidence for widespread crustal involvement in Andean magmatism. *Contributions to Mineralogy and Petrology* 105, p. 412-432.

Davidson, J.P. , Harmon, R.S, and Worner, G., 1991. The source of central Andean magmas: Some considerations. In: Andean Magmatism and its Tectonic Setting, eds. R.S. Harmon and C.W. Rapella, *GSA Special Paper* 265; 233-244

Davidson, J.P., and de Silva, S.L., 1995, Late Cenezoic magmatism of the Bolivian Altiplano. *Contributions to Mineralogy and Petrology* 119, 387-408.

Davidson, J.P., Hora, J.M., Garrison, J.M., Dungan, M.A., 2005, Crustal forensics in arc magmas. *Journal of Volcanology and Geothermal Research* 140, pp. 157-170.

de Silva, S.L., Francis, P.W., 1989, *Volcanoes of the Central Andes*. Springer-Verlag, 216 p.

de Silva, S.L., 1989, Altiplano-Puna volcanic complex of the central Andes: Geology, v. 17, p. 1102-1106.

de Silva, S.L., and Gosnold, W.D., 2007, Episodic construction of batholiths: Insights from the spatiotemporal development of an ignimbrite flare-up: Journal of Volcanology and Geothermal Research, v. 167, p. 320-335.

DeCelles, P.G., Ducea, M.N., Kapp, P., Zandt, G., 2009, Cyclicity in Cordilleran orogenic systems. *Nature Geoscienes* 2, 251 -257.

Deering, C.D., Bachmann, O., 2010, Trace element indicators of crystal accumulation in silicic rocks. *Earth and Planetary Science Letters* 297, p. 324-331.

Delacour, A., Gerbe, M.C., Thouret, J.C., Wörner, G., Paquereau-Lebti, P., 2007, Magma

evolution of Quaternary minor volcanic centres in southern Peru, central Andes. *Bulletin of Volcanology* 69, p. 581-608.

DePaolo, D.J., 1981, Trace element and isotopic effects of combined wallrock assimilation and fractional crystallization. *Earth and Planetary Science Letters* 53 (2), p. 189-202.

Dilles, J.D., 1987, Petrology of the Yerington Batholith, Nevada; evidence for evolution of porpyhyry copper ore fluids. *Economic Geology* 82 (7), p. 1750-1789.

Dilles, J.H., Wright, J.E., 1988, The chronology of early Mesozoic arc magmatism in the Yerington district of western Nevada and its regional implications. *GSA Bulletin* 11 (5), p. 644-652.

Ducea, M.N., Barton, M.D., 2007, Igniting flare-up events in Cordilleran arcs, *Geology* 35 (11), 1047-1050.

Dufek, J., and Bergantz, G.W., 2005, Lower crustal magma genesis and preservation: a stochiastic framework for the evaluation of basalt – crust interaction, *Journal of Petrology* 46 (11), 2167-2195.

Eggler, D.H., Burnham, C.W., 1973, Crystallization and fractionation trends in the system Andesite-H_2O-CO_2-O_2 at Pressures to 10 Kb. *GSA Bulletin* 84 (8), p. 2517-2532.

Farmer, G.L., Broxton, D.E., Warren, R.G., Pickthorn, W., 1991, Nd, Sr, and O isotopic variations in metaluminous ashflow tuffs and related volcanic rocks at the Timber Mountain/Oasis Valley Caldera Complex, SW Nevada: implications for the origin and evolution of large-volume silicic magma bodies, *Contrib. Mineral. Petrol.* 109, 53-68.

Feeley, T.C., Davidson, J.P., and Armendia, A., 1993. The volcanic and magmatic evolution of Volcan Ollague, a high-K, late Quaternary stratovolcano in the Andean Central Volcani Zone.. *J. of Volcanology and Geothermal Res*., v. 54, p. 221-245.

Feeley, T.C., and Davidson, J.P., 1994. Petrology of calcalkaline lavas at Volcan Ollague and the origin of compositional diversity at the Central Andean stratovolcanoes. *J. Petrol.* V. 53(5), p. 1295-1340.

Feeley, T.C., Sharp, Z.D., 1995, $^{18}O/^{16}O$ isotope geochemistry of silicic lava flows erupted from Volcán Ollagüe, Andean Central Volcanic Zone, *Earth and Planetary Science Letters* 133 (3-4), ps. 239 – 254.

Ferriss, E.D.A., Essene, E.J., Becker, U., 2008, Computational study of the effect of pressure on the Ti-in-zircon geothermometer; European Journal of Mineralogy, v. 20, p. 745-755.

Ferry, J.M., and Watson, E.B., 2007, New thermodynamic models and revised calibrations for the Ti-in-zircon and Zr-in-rutile thermometers: Contributions to Mineralogy and Petrology, v. 154, p. 429-437.

Francis, P.W., Thorpe, R.S., Moorbath, S., Kretzschmar, G.A., Hammill, M., 1980, Strontium isotope evidence for crustal contamination of calc-alkaline volcanic rocks from Cerro Galan, northwest Argentina. *Earth and Planetary Science Letter* 48, p. 257-267.

Friedman, I., Lipman, P.W., Obradovich, J.D., Gleason, J.D., Christiansen, R.L., 1974, Meteoric water in magmas. *Science* 184 (4141), p. 1069-1072.

Fu B, Page FZ, Cavosie AJ, Fournelle J, Kita NK, Lackey JS, Wilde SA, Valley JW (2008) Ti-in-zircon thermometry: applications and limitations. *Contrib Mineral Petrol* 156:197–215. doi: 10.1007/s00410-008-0281-5

Ghiorso, M.S., Evans B.W., 2008, Thermodynamics of Rhombohedral Oxide Solid Solutions and a Revision of the Fe-Ti Two-oxide Geothermometer and Oxygen-barometer. *American Journal of Science* 308, p. 957-1039.

Giese, P., Scheuber, E., Schilling, F.R., Schmitz, M. and Wigger, P., 1999. Crustal thickening processes in the Central Andes and the different natures of the Moho-discontinuity. *Journal of South American Earth Sciences* 12: 201-220.

Giles, D., 2009, Dynamics of a long-lived magmatic system as indicated by variations in amphibole composition and textures in dacites erupted over 11 m.y. at the Aucanquilcha Volcanic Cluster, Central Andes, Chile. MS thesis.

Glazner, A.F., J.M. Bartley, D.S. Coleman, W. Gray and R.Z. Taylor (2004) Are plutons assembled over millions of years by amalgamation from small magma chambers? *GSA Today*, v. 14, no. 4-5, p. 4-11.

Graeber, F.M., Asch, G., 1999, Three-dimensional models of *P* wave velocity and *P*-to-*S* velocity ratio in the southern central Andes by simultaneous inversion of local earthquake data. *Journal of Geophysical Research* 194 (B9), 20,237-20,256.

Green, T.H., 1982, Anatexis of mafic crust and high pressure crystallization of andesite. *In* R.S. Thorpe, ed., *Andesites*. John Wiley & Sons, p. 465-487.

Grunder, A.L., 1987, Low $\delta^{18}O$ silicic volcanic rocks at the Calabozos caldera complex, southern Andes. *Contributions to Mineralogy and Petrology* 95 (1), p. 71-81.

Grunder, A.L., Mahood, G.A., 1988, Physical and chemical models of zoned silicic magmas: the Loma Seca Tuff and Calabozos Caldera, southern Andes. *Journal of Petrology* 29 (4), p. 831-867.

Grunder, A. L. 1997. Report on the Miocene to Recent volcanic rocks from the eastern margin of the project area. *In* Tomlinson, A. *et al*. (eds) *Proyecto de Estudio Geológico de la Franja Longitudinal entre Quebrada Blanca y Chuquicamata, Fase I*. SERNAGEOMIN de Chile report to Coldelco.

Grunder, A.L., 1992, Two-stage contamination during crustal assimilation: isotopic evidence from volcanic rocks in eastern Nevada. *Contributions to Mineralogy and Petrology* 112 (2-3), p. 219-229.

Grunder, A.L., 1995, Material and thermal roles of basalt in crustal magmatism: case study from eastern Nevada. *Geology*, 23:952-956.

Grunder, A.L., Klemetti, E.W., Feeley, T.C., and McKee, C.M., 2008 (for 2006), Eleven million years of arc volcanism at the Aucanquilcha Volcanic Cluster, Northern Chilean Andes: implications for the life span and emplacement of plutons: *Transactions of the Royal Society of Edinburgh-Earth Sciences*, v. 97, p. 415-436.

Grunder, A.L., de Silva, S.L., 2007, Patterns in Long-lived Continental Magmatism; Crustal Modulation of Mantle-Derived Input, *Eos Trans. AGU*, 88 (52), Fall Meet. Suppl., Abstract V41F-05.

Haggerty, S.E., 1991, Oxide Textures – A Mini-atlas. In D.H. Lindsley, *Ed.*, Oxide Minerals: Petrologic and Magnetic Significance. *Mineralogical Society of America*, vol. 25, p. 129-219.

Harmon, R.S., Hoefs, J., 1995, Oxygen isotope heterogeneity of the mantle deduced from global 18O systematics of basalts from different geotectonic settings. *Contributions to Mineralogy and Petrology* 120 (1), p. 95-114.

Harmon, R.S., Thorpe, R.S., Francis, P.W., 1981, Petrogenesis of Andean andesites from combined O-Sr isotope relationships. *Nature* 290, p. 396-399.

Harrison, T.M., Watson, E.B., and Aikman, A.B., 2007, Temperature spectra of zircon crystallization in plutonic rocks: Geology, v. 35, p. 635-638.

Haschke, M., Gunther, A., 2003, Balancing crustal thickening in arcs by tectonic vs. magmatic means. *Geology* 31 (11), 933-936.

Haschke, M., Siebel, W., Günther, A., Scheuber, E., 2002, Repeated crustal thickening and recycling during the Andean orogeny in north Chile (21° -26° S). Journal of Geophysical Reearch 107 (B1),

Hawkesworth, C.J., Hammill, M., Gledhill, A.R., van Calsteren, P., Rogers, G., 1982, Isotope and trace element evidence for late-stage intra-crustal melting in the High Andes. *Earth and Planetary Science Letter* 58, p. 240-254.

Hayden, L.A., and Watson, E.B., 2007, Rutile saturation in hydrous siliceous melts and its bearing on Ti-thermometry of quartz and zircon: Earth and Planetary Science Letters, v. 258, p. 561-568.

Heit, B., Sodoudi, F., Yuan, X., Bianchi, M., Kind, R., 2007, An S receiver function analysis of the lithospheric structure in South America. American Geophysical Research Letters 34, L14307. 5 p., doi:10.1029/2007GL030317.

Hildreth, W., 1981, Gradients in silicic magma chambers: implications for lithospheric magmatism. *Journal of Geophysical Research* 86 (B11), p. 10,153 – 10,192.

Hildreth, W., and Moorbath, S., 1988, Crustal contributions to arc magmatism in the Andes of Central Chile, *Contributions to Mineralogy and Petrology* 98, 455-489.

Hildreth, W., 2004, Volcanological perspectives on Long Valley, Mammoth Mountain and Mono Craters: several contiguous but discreet systems. *Journal of Volcanology and Geothermal Research* 136, 169-198.

Hofmann, A.E., Valley, J.W., Watson, E.B., Cavosie, A.J., and Eiler, J.M., 2009, Sub-micron scale distributions of trace elements in ziron: Contributions to Mineralogy

and Petrology, v.158, n.3, 317-335.

Hoke, L., Lamb, S., 2007, Cenozoic behind-arc volcanism in the Bolivian Andes, South America: implications for mantle melt generation and lithospheric structure. *Journal of the Geological Society of London* 164, 795-814.

Holland, T.J.B. and Blundy, J.D., 1994. Non-ideal interactions in calcic amphiboles and their bearing on amphibole-plagioclase thermometry. *Contributions to Mineralogy and Petrology,* v.116, pp.433-447.

Holtz, F., Sato, H., Lewis, J., Behrens, H., Nakada, S., 2005, Experimental petrology of the 1991-1995 Unzen dacite, Japan. Part I: Phase relations, phase composition and pre-eruptive conditions. *Journal of Petrology* 46 (2), p. 319-337.

Hora, J.M., Singer, B.S., and Wörner, G., 2007, Volcano evolution and eruptive flux on the thick crust of the Andean Central Volcanic Zone: $^{40}Ar/^{39}Ar$ constraints from Volcán Parinacota, Chile: GSA Bulletin, v. 119, no. 3-4, p. 343-362.

Isacks, B.L., 1988, Uplift of the central Andean plateau and bending of the Bolivian orocline. *Journal of Geophysical Research* 93 (B4), 3211-3231.

James, D.E., 1982, A combined O, Sr, Nd, and Pb isotopic and trace element study of crustal contamination in central Andean lavas, I. Local geochemical variations. *Earth and Planetary Science Letters* 57, p. 47-62.

James, D.E., Brooks, C., Cuyubamba, A., 1976, Andean Cenozoic volcanism: Magma genesis in the light of strontium isotopic composition and trace-element geochemistry. *GSA Bulletin* 87, p. 592-600.

Johnson, C.M., Lipman, P.W., Czamankse, G.K., 1990, H, O, Sr, Nd, and Pg isotope geochemistry of the Latir volcanic field and cogenetic intrusions, New Mexico, and relations between evolution of a continental magmatic center and modifications of the lithosphere. *Contributions to Mineralogy and Petrology* 104, p. 99-124.

Johnson, D.M., Hooper, P.R., and Conrey, R.M., 1999, XRF analysis of rocks and minerals for major and trace elements on a single low-dilution Li-tetraborate fused bead: Advances in X-Ray Analysis, v. 41, p. 117–132.

Karlstrom, L., Dufek, J., Manga, M., 2009, Organization of volcanic plumbing through

magmatic lensing by magma chambers and volcanic loads. *Journal of Geophysical Research* 114, 16p.

Karlstrom., L., Dufek, J., Manga, M., 2010, Magma chamber stability in arc and continental crust. *Journal of Volcanology and Geothermal Research* 190 (3-4), p. 249-270.

Kay, R.M., and Kay, S.M., 1993, Delamination and delamination magmatism: Tectonophysics, v. 219, no. 1–3, p. 177–189.

Kay, S.M., Mpodozis, C., Coira, B., 1999, Neogene magmatism, tectonism, and mineral deposits of the central Andes (22° to 33°S Latitude), *in* Skinner, B.J., ed., Geology and Ore Deposits of the Central Andes: *Society of Economic Geology Special Publication* 7, p. 27-59.

Kay, S.M., Godoy, E., Kurtz, A., 2005, Episodic arc migration, crustal thickening, subduction erosion, and magmatism in the south-central Andes. *GSA Bulletin* 117 (1/2), p. 67-88.

Kay, S.M., and Coira, B.L., 2009, Shallowing and steepening subduction zones, continental lithospheric loss, magmatism, and crustal flow under the Central Andean Altiplano-Puna plateau, in Kay, S.M., Ramos, V.A., and Dickinson, W.R., eds., Backbone of the Americas: Shallow Subduction, Plateau Uplift, and Ridge and Terrane Collision: Geological Society of America Memoir 204, p. 229–259.

Kendrick, E., Bevis, M., Smalley, R., Brooks, B., 2001, An integrated crustal velocity field for the central Andes, Geochemistry Geophysics Geosystems 2, 11 p, DOI: 10.1029/2001GC000191

Kennan, L., Lamb, S.H., Hoke, L., 1997, High-altitude paleosurfaces in the Bolivian Andes: evidence for late Cenozoic surface uplift, *in Palaeosurfaces: Reconstruction and Palaeoenvironmental Interpretation,* ed. Widdowson, M., Geological Society Special Publications No. 120, 307 – 323.

Klemetti, E.W., 2005, Constraining the magmatic evolution of the Andean arc at 21°S using the volcanic and petrologic history of Volcán Aucanquilcha, Central Volcanic Zone, northern Chile. Ph.D. Thesis.

Klemetti, E.W., and Grunder, A.L., 2008, Volcanic evolution of Volcán Aucanquilcha: a long-lived dacite volcano in the Central Andes of northern Chile. *Bulletin of Volcanology*, v. 70, p. 633-650.

Koleszar, A.M., Kent, A.J., Cooper, K.M., Eppich, G.R., 2010, Conditions of magma mixing as recorded in amphiboles from Mount Hood, Oregon. *American Geophysical Union*, Fall Meeting 2010, abstract #V43C2387

Leake, B.E., Woolley, A.R., Arps, C.E.S., Birch, W.D., Gilbert, M.C., Grice J.D., Hawthorne, F.C., Katio, A., Kisch, H.J., Krivovichev, V.G., Linthout, K., Laird, J., Mandarino, J.A., Maresch, W.V., Nickel, E.H., Rock, N.M.S., Schumacher, J.C., Smith, D.C., Stephenson, N.C.N., Ungaretti, L., Whittaker, E.J.W., Youzhi, G. 1997. Nomenclature of amphiboles: report of the subcommittee on amphiboles of the International Mineralogical Association, Commission on new minerals and mineral names. *The Canadian Mineralogist,* v. 35, pp. 219-246.

Leidig, M., Zandt,G., 2003, Modeling of highly anisotropic crust and application to the Altiplano-Puna volcanic complex of the central Andes. Journal of Geophysical Research 108 (B1) doi:10.1029/2001JB000649.

Leonard, G.S., Cole, J.W., Nairn, I.A., Self, S., 2002, Basalt triggering of the c. AD 1305 Kaharoa rhyolite eruption, Tarawera Volcanic Complex, New Zealand. *Journal of Volcanology and Geothermal Research* 115 (3-4), p. 461-486.

LePage, L.D., 2003, ILMAT: an excel worksheet for ilmenite-magnetite geothermotery and barometry. *Computers & Geosciences* 29 (5), pp. 673-678. doi: 10.1016/S0098-3004(03)00042-6

Lipman, P.W., 2007, Incremental assembly and prolonged consolidation of Cordilleran magma chambers: Evidence from the Southern Rocky Mountain volcanic field: *Geosphere*, v. 3, p. 42-70.

Loewy, S.L., Connelly, J.N., Dalziel, I.W.D., 2004, An orphaned basement block: The Arequipa-Antofalla Basement of the central Andean margin of South America, *GSA Bulletin* 116 (1/2), pp. 171-187.

Longo, A.A., Dilles, J.H., Grunder, A.L., Duncan, R., 2010, Evolution of Calc-alkaline volcanism and associated hydrothermal gold deposits at Yanacocha, Peru.

Economic Geology 105 (7), p. 1191-1241.

Lucassen, F., Becchio, R., Wilke, H. G., Franz, G., Thirlwall, M. F., Viramonte, J., Wemmer, K., 2000, Proterozoic-Paleozoic development of the basement of the Central Andes (18-26 degrees S)- a mobile belt of the South American craton, *Journal of South American Earth* Sciences 13 (8), 697-715.

Lucassen, F., Becchio, R., Harmon, R.S., Kasemann, S., Franz, G., Trunbull, R., Wilke, H.G., Romer, R.L., Dulski, P., 2001, Composition and density model of the continental crust at an active continental margin—the Central Andes between 21° and 27°S. *Tectonophysics* 341, 195-223.

Lucassen, F., Kramer, W., Bartsch, V., Wilke, H., Franz, G., Romer, R.L., Dulski, P., 2006, Nd, Pb, and Sr isotope composition of juvenile magmatism in the Mesozoic large magmatic province of northern Chile (18 – 27 °S): indications for a uniform subarc mantle. Contributions to Mineralogy and Petrology 152, p. 571-589.

Ludwig, K.R., 2003. Isoplot 3.00: A geochronological toolkit for Microsoft Excel. Berkeley, CA: Berkeley Chronological Center.

Macfarlane, A.W., Marcet, P., LeHuray, A.P., and Petersen, U., 1990, Lead isotope provinces of the Central Andes inferred from ores and crustal rocks. *Economic Geology* 85 (8), p. 1857-1880.

Mamani, M., Tassara, A., and Woerner, G., 2008, Composition and structural control of crustal domains in the central Andes: *Geochemistry Geophysics Geosystems*, v. 9.

Mamani, M., Worner, G., and Sempere, T., 2010, Geochemical variations in igneous rocks of the Central Andean orocline (13ºS to 18ºS): Tracing crustal thickening and magma generation through time and space, *GSA Bulletin*, v. 122, no. 1/2, p. 162-182.

Matzel, J., Bowring, S., Miller, R., 2006, Time scales of pluton construction at differing crustal levels: Examples from the Mount Stuart and Tenpeak intrusions, North Cascades, WA, GSA Bulletin, v. 118, p. 1412 - 1430

McKee, C. M. 2001, Volcanology and petrology of Volcán Miño,; Andean central volcanic zone‘. Master’s Thesis, Oregon State University, USA.

McQuarrie, N., Horton, B.K., Zandt, G., Beck, S., DeCelles, P.G., 2005, Lithospheric evolution of the Andean fold-thurst belt, Bolivia, and the origin of the central Andean plateau. *Tectonophysics* 399, p. 15-37.

Mercier, J-C., Beoit, V., Girardeau, J., 1984, Equilibrium state of diopside-bearing harzburgites from ophiolites: geobarometric and geodynamic implications. *Contributions to Mineralogy and Petrology* 85, p. 391-403.

Miller, C.F., McDowell, S.M., and Mapes, R.W., 2003, Hot and cold granites? Implications of zircon saturation temperatures and preservation of inheritance: Geology, v. 31, p. 529-532.

Miller, J.F., Harris, N.B.W., 1989, Evolution of continental crust in the Central Andes; constraints from Nd isotope systematics. *Geology* 17, p. 615 – 617.

Miller, J.S., and Wooden, J.L., 2004, Residence, resorption and recycling of zircons in Devils Kitchen rhyolite, Coso Volcanic field, California: Journal of Petrology, v. 45, p. 2155-2170.

Miller, J.S., Matzel, J.E.P., Miller, C.F., Burgess, S.D., and Miller, R.B., 2007, Zircon growth and recycling during the assembly of large, composite arc plutons: Journal of Volcanology and Geothermal Research, v. 167, p. 282-299.

Nakamura, M., 1995, Continuous mixing of crystal mush and replenished magma in the ongoing Unzen eruption. *Geology* 23 (9), p. 807-910.

Putirka, K.D., 2008, Thermometers and barometers for volcanic systems. *Reviews of Mineralogy and Geochemistry* 69. P. 61-120.

Reid, M.R., Vazquez, J.A., Schmitt, A.K., 2011, Zircon-scale insights in the history of a Supervolcano, Bishop Tuff, Long Valley, California, with implications for the Ti-in zircon geothermometer. *Contributions to Mineralogy and Petrology* 161, p. 293-311.

Reiners, P.W., Nelson, B.K., 1998, Temporal-compositional-isotopic trends in rejuvenated-stage magmas of Kauai, Hawaii, and implications for mantle melting processes. *Geochimica et Cosmochimica Acta* 62 (13), p. 2,347-2,368.

Reiners, P.W., Nelson, B.K., Ghiorso, M.S., 1995, Assimilation of felsic crust by basaltic magma: Thermal limits and extents of crustal contamination of mantle-derived magmas. *Geology* 23 (6), p. 563-566.

Reubi, O., Blundy, J., 2009, A dearth of intermediate melts at subduction zone volcanoes and the petrogenesis of arc andesites. *Nature* 461, p. 1269 – 1273.

Riciputi, L.R., Johnson, C. M., Sawyer, D. A., Lipman, P. W., 1995, Crustal and magmatic evolution in a large multicyclic caldera complex: isotopic evidence from the central San Juan volcanic field, *Journal of Volcanology and Geothermal Research* 67, 1-28.

Ridolfi, F., Renzulli, A., Puerini, M., 2010, Stability and chemical equilibrium of amphibole in calc-alkaline magmas: an overview, new thermobarometric forumulations and application to subduction-related volcanoes, *Contributions to Mineralogy and Petrology* 160, p. 45-66.

Roeder, P.L., Emslie, R.F., 1970, Olivine-liquid equilibrium. *Contributions to Mineralogy and Petrology 96, p. 1-23.*

Rogers, G., Hawkesworth, C.J., 1989, A geochemical traverse across the north Chilean Andes: evidence for crust generation from the mantle wedge. *Earth and Planetary Science Letters* 91, p. 271-285.

Rutherford, M.J., Devine, J.D., 2003, Magmatic conditions and magma ascent as indicated by hornblende phase equilibria and reactions in the 1995-2002 Soufrière Hills magma. *Journal of Petrology* 44 (8), p. 1433-1454.

Rutherford, M.J., Devine, J.D., 2008, Magmatic conditions and processes in the storage zone of the 2004-2006 Mount St. Helens dacite, *in* Sherrod, D.R., Scott, W.E., Stauffer, P.H. (eds.), A volcano rekindled: The Renewed Eruption of Mount St. Helens, 2004-2006, eds USGS Professional Paper 1750, p. 703-726.

Salisbury, M.J. Jicha, B.R., de Silva, S.L., Singer, B.S., Jiménez, N.C., and Ort, M.H., 2011, $^{40}Ar/^{39}Ar$ chronostratigraphy of Altiplano-Puna volcanic complex ignimbrites reveals the development of a major magmatic province: *GSA Bulletin*, v. 123, no. 5-6, p. 821-840.

Salisbury, M.J., 2011, Convergent margin magmatism in the central Andes and its near antipodes in western Indonesia: spatiotemporal and geochemical considerations. Ph.D. dissertation. 147p.

Sambridge, M.S., and Compston, W., 1994, Mixture Modeling of Multicomponent Data Sets with Application to Ion-Probe Zircon Ages: Earth and Planetary Science Letters, v. 128, p. 373-390.

Scheuber, E., Giese, P., 1999, Architecture of the Central Andes—a compilation of geoscientific data along a transect at 21°S. *Journal of South American Earth Sciences* 12, p. 103-107.

Schilling, F.R., Partzsch, G.M., Brasse, H., Schwarz, G., 1997, Partial melting below the magmatic arc in the central Andes deduced from geoelectromagnetic field experiments and laboratory data. *Physics Earth Planet. Interiors* 103, p. 17-31.

Schnurr, W.B.W., Trumbull, R.B., Clavero, J., Hahne, K., Sibel, W., Gardeweg, M., 2007, Twenty-five million years of silicic volcanism in the southern central volcanic zone of the Andes: Geochemistry and magma genesis of ignimbrites from 25 to 27 °S, 67 to 72 °W, *Journal of Volcanology and Geothermal Reasearch* 166, pp. 17-46.

Schmitz, M. et al., 1999. The crustal structure beneath the Central Andean forearc and magmatic arc as derived from seismic studies--the PISCO 94 experiment in northern Chile (21-23S). *Journal of South American Earth Sciences* 12: 237-260.

Schmitz, M., Heinsohn, W.D. and Schilling, F.R., 1997. Seismic, graviy and petrological evidence for partial melt beneath the thickened Central Andean crust (21-23S). *Tectonophysics*, 270: 313-326.

Sempere, T., Butler, R.F., Richards, D.R., Marshall, L.G., Sharp, W., Swisher, C.C., 1997, Stratigraphy and chronology of late Cretaceous-early Miocene major tectonic crisis and related basins in Bolivia and northern Argentina. *Geological Society of America Bulletin* 109, p. 709-727.

Siebel, W., Schnurr, W., Hahne, K., Kraemer, B., Trumbull, R.B., van den Bogaard, P., Emmermann, R., 2001, Geochemistry and isotope systematics of small- to medium-volume Neogene-Quaternary ignimbrites in the southern central Andes:

evidence for derivation from andesitic magma sources. *Chemical Geology* 171 (3-4), p. 213-237.

Simon, J.I., and Reid, M.R., 2005, The pace of rhyolite differentiation and storage in an 'archetypical' silicic magma system, Long Valley, California: Earth and Planetary Science Letters, v. 235, p. 123-140.

Streck, M.J., 2008, Mineral textures and zoning as evidence for open system processes. In: *Minerals, Inclusions, and Volcanic Processes, Reviews of Mineralogy & Geochemistry*, 69: 595-619

Tepley, F. J., III, Davidson, J. P., Tilling, R. I. & Arth, J. G. (2000). Magma mixing, recharge, and eruption histories recorded in plagioclase phenocrysts from El Chichón Volcano, Mexico. *Journal of Petrology*, 41, 1397-1411.

Thorpe, R.S., Francis, P.W., 1979, Variations in Andean andesite compositions and their petrogenetic significance. *Tectonophysics* 57 (1), p. 53-70.

Tilton, G.R., 1979, Isotopic studies of Cenozoic Andean calc-alkaline rocks. *Carnegie Institution of Washigton Yearbook* 78, p. 298-304.

Vazquez, J.A., and Reid, M.R., 2002, Time scales of magma storage and differentiation of voluminous high-silica rhyolites at Yellowstone caldera, Wyoming: Contributions to Mineralogy and Petrology, v. 144, p. 274-285.

Venezky, D.Y., Rutherford, M.J., 1999, Petrology and Fe-Ti oxide reequilibration of the 1991 Mount Unzen mixed magma. Journal of Volcanology and Geothermal Research 89 (1-4), p. 213-230.

Walker, B.A., Miller, C.F., Claiborne, L.L., Wooden, J.L., and Miller, J.S., 2007, Geology and geochronology of the Spirit Mountain batholith, southern Nevada: Implications for timescales and physical processes of batholith construction: *Journal of Volcanology and Geothermal Research*, v. 167, p. 239-262.

Walker, B.A., Grunder, A.L., and Wooden, J.L., 2010, Organization and thermal maturation of long-lived arc systems: Evidence from zircons at the Aucanquilcha volcanic cluster, northern Chile: *Geology* 38 (10), p. 1007-1010.

Watson, E.B., and Harrison, T.M., 1983, Zircon Saturation Revisited - Temperature and Composition Effects in a Variety of Crustal Magma Types. *Earth and Planetary*

Science Letters, v. 64, p. 295-304.

Watson, E.B. and Harrison, T.M., 2005, Zircon thermometer reveals minimum melting conditions on earliest Earth. *Science* 308, 841-844.

White, S.M., Crisp, J.A., Spera, F.J., 2006, Long-term volumetric eruption rates and magma budgets. *Geochemistry Geophysics Geosystems* 7 (1).

Wigger et al., Schmitz, M., Asch, G., Baldzuhn, S., Giese, P., Heinsohn, W., Martinez, E., Ricaldi, E., Röwer, P., Viramonte, J., 1994. In: Reutter, K, J., Scheuber, E., Wigger, P.J. (Eds.), Variation of the crustal structure of the southern central Andes deduced from seismic refraction investigations, Tectonics of the southern central Andes. Springer-Verlag, New york, pp. 23-48.

Wörner, G., Moorbath, S., Harmon, R.S., 1992a, Andean Cenozoic volcanic centers reflect basement isotopic domains: Geology, v.20, p.1103-1106.

Wörner, G., Moorbath, S., Horn, S., Entenmann, J., Harmon, R.S., Davidson, J.P., Lopez-Escobar, L., 1994. Large- and fine-scale variations along the Andean arc of Northern Chile (17.5° - 22°S). In: Reutter, K.J., Scheuber, E., Wigger, P.J. (Eds.). Tectonics of the Southern Central Andes. Springer, Heidelberg, Germany, pp. 77-92.

Yuan, X., Sobolev, S.V., and Kind, R., 2002, Moho topography in the central Andes and its geodynamic implications: Earth and Planetary Science Letters, v. 199, p. 389-402.

Zandt, G., Leidig, M., Chmielowski, J., Baumont, D., and Yuan, X.H., 2003, Seismic detection and characterization of the Altiplano-Puna magma body, central Andes: Pure and Applied Geophysics, v. 160, p. 789-807.